The synthesis and characterisation of novel precursors for the chemical vapour deposition of silver

Harker, Robert Martin

Award date:
1996

Awarding institution:
University of Bath

THE SYNTHESIS AND CHARACTERISATION OF NOVEL PRECURSORS FOR THE CHEMICAL VAPOUR DEPOSITION OF SILVER

submitted by Robert Martin Harker

for the degree of PhD

of the University of Bath

1996.

ProQuest LLC
789 East Eisenhower Parkway
P.O. Box 1346
Ann Arbor, MI 48106-1346

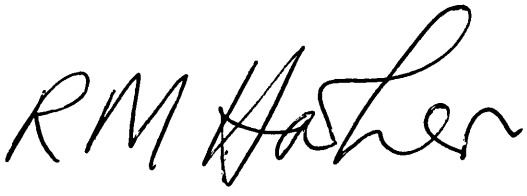

R.M. Harker.

ABSTRACT

The work described in this thesis has been concerned with the synthesis and characterisation of novel precursors for the growth of thin silver films via aerosol assisted chemical vapour deposition. Four classes of compounds have been investigated; silver carboxylates and their phosphine adducts, silver fluorocarboxylates and their phosphine adducts, silver β-diketonate phosphine adducts and organometallic silver compounds.

Chapter One - INTRODUCTION - provides a discussion of both the applications of thin silver films and current fabrication techniques. The chapter subsequently introduces chemical vapour deposition (CVD) with particular reference to metal CVD, followed by a survey of reports of silver CVD in the literature. A brief summary of silver(I) chemistry is also included to provide a basis for the structural discussions of later chapters.

Chapter Two - SILVER CARBOXYLATES - details the synthesis and characterisation of a range of silver carboxylates and their phosphine adducts, the strategy being to influence the molecular structure by variation of both the carboxylate and phosphine ligands. Compounds have been characterised by IR, ^{1}H, ^{13}C, ^{31}P and ^{109}Ag NMR, thermal analysis techniques (TGA) and mass spectrometry [FAB(LSIMS)]. The structure of $[AgO_2CMe(PPh_3)_2]$ as determined by single crystal XRD is also described. These compounds have been screened for use as precursors for the CVD of silver by aerosol assisted techniques, films grown have been characterised with respect to SEM, EDXS, reflectivity and conductivity.

Chapter Three - SILVER FLUOROCARBOXYLATES - describes the synthesis of a number of silver fluorocarboxylates with an increasing chain length and the preparation of their bis(triphenylphosphine) adducts. These compounds have been characterised using IR, ^{1}H, ^{13}C, ^{19}F, ^{31}P and ^{109}Ag NMR, thermal analysis techniques (TGA, DSC) and mass spectrometry [FAB(LSIMS)]. The molecular structure of $[AgO_2CC_3F_7(PPh_3)_2]$ as determined by single crystal XRD is also described. Films grown from these precursors have been characterised with respect to SEM, EDXS, reflectivity and conductivity.

Chapter Four - SILVER β-DIKETONATES - describes the synthesis and characterisation of a range of silver β-diketonate phosphine adducts. Additionally two silver β-ketoiminate phosphine adducts have also been prepared. Compounds have been subject to characterisation by IR, ^{1}H, ^{13}C, ^{19}F, ^{31}P and ^{109}Ag NMR, thermal analysis (TGA, DSC) and mass spectrometry [FAB(LSIMS)]. The molecular structure of $[Ag(hfac)(PPh_3)]$ as determined by single crystal XRD is also discussed. Coatings grown from these precursors have been characterised by SEM, EDXS, reflectivity and conductivity. A number have been additionally characterised by High Resolution SEM and Auger depth profiling analysis.

Chapter Five - ORGANOMETALLIC SILVER COMPOUNDS - details the synthesis of {2-dimethylaminomethyl)phenyl}silver(I) and its characterisation by IR, ^{1}H and ^{13}C NMR, mass spectrometry [FAB(LSIMS)] and single crystal XRD. Its molecular structure is discussed and its film growth properties are reported. This compound was found to react with trace quantities of dimethylsiloxane polymer in the presence of triphenylphosphine to yield a unique silver siloxide cluster. This novel decomposition product has been characterised by IR, ^{1}H, ^{13}C, ^{29}Si and ^{31}P NMR, mass spectrometry [FAB(LSIMS)] and its structure elucidated by single crystal XRD.

A brief conclusion is included to draw comparisons between the four classes of compounds with respect to their potential as CVD precursors, comparisons include film growth properties, ease of preparation and stability considerations.

Appendices provided contain brief summaries of some of the techniques widely used in this work, namely ^{109}Ag NMR, FAB mass spectrometry and EDXS. X-ray crystallographic data tables are collected in Appendix Four A4.1 to A4.5. Details concerning instrumentation, film growth equipment and procedures are provided in Appendices Five and Six. Appendix Seven lists further reflectivity data. A numerical list of compounds is provided in Appendix Eight.

ACKNOWLEDGMENTS

I would like to thank my supervisors Dr Kieran Molloy and Dr Dennis Edwards for their encouragement and help during the course of this project. I am particularly grateful to Kieran and Dennis for initially finding the funding to enable me to study for this PhD, for their guidance and support through the duration of this project and their advice while in the advanced (terminal?) stages of 'writing-up'. I am also indebted to Dr Mary Mahon who has conducted the single crystal XRD studies with skill and wit, and provided me with the excellent structural diagrams and data contained in this thesis.

From the technical staff I would like to thank Alan Carver for microanalysis, Dr Richard Kinsman for his help with the silver NMR studies and Dave Wood and Harry for the bulk of NMR results contained in this thesis. Mass spectrometry studies were performed at the EPSRC Mass Spectrometry service at the University of Wales, Swansea. Thanks are also due to Dr Glyn Love and Mr Hugh Perrott for their assistance with the SEM and EDXS analysis of samples. For the help and advice given to me during the assembly of the CVD reactor system (Bob), I am grateful to the staff from the Science Schools Workshop, particularly Les Steele and Mike Lock, and helpful discussions with a number of industrial contacts. Mike Bailes is gratefully acknowledged as a world authority on the resuscitation of very ill nebuliser driver circuits, my thanks are due to him for this and his help in setting up the electrical systems required for 'Bob'. I should also like to thank Morgan-Matroc in Southampton for their advice on nebulisation and their kind donation of several ultrasonic transducers.

I would like to extend my gratitude to friend and flatmate Dr Kim 'it'll never work' Wong for his moral support and advice throughout the period of this write-up, particularly concerning photographic plates and crashing computer systems. I am also very grateful my good friend Yuan-Yao Li for his help with scanning diagrams for this thesis.

My thanks are due to the technical staff from Inorganic Chemistry at Bath University, Shiela, Robert and Ahmad. Further, I should like to thank all of the members of the Molloy, Edwards and Brisdon research groups throughout my time at Bath 1992-1996, in particular Paul Deacon, John 'Quickfit Cassidy' McGinley, Mike Hill, Nathalie Devylder, Dave Smith, Tim 'Grandpa' Paget, Dele Omatowa, Chris Rainford, Joanne Hill, Sonali Bhandari, Virginie Ogrodnik, Phil Wright and Mike Maxwell without whom tea-breaks will never be the same again.

Finally I would like to thank my family for their encouragement and support throughout the last four years, a period which has seen its fair share of up's and down's. My appreciation to Jack, as always, for being around.

Financial support for this project from the EPSRC is gratefully acknowledged.

DEDICATION

This thesis is dedicated to my father, who taught me to ask difficult questions,

and to my son, Jack, whom I have still to teach.

CONTENTS

ABBREVIATIONS

AACVD	Aerosol Assisted Chemical Vapour Deposition
AES	Auger Electron Spectroscopy
acac	pentane-2,4-dionate
bipy	2,2′-bipyridyl
br	broad
bzac	benzoylacetonate
BPSCCO	Bi-Pb-Sr-Ca-Cu-O
BSCCO	Ba-Sr-Ca-Cu-O
^{t}Bu	tertiary butyl i.e. $-C(CH_3)_3$
CI	Chemical Ionisation
cod	cycloocta-1,5-diene
CVD	Chemical Vapour Deposition
d	doublet
dd	doublet of doublets
DEPT	Distortionless Enhancement by Polarisation Transfer
dmcod	1,5-dimethylcycloocta-1,5-diene
DMSO	dimethylsulphoxide, i.e. $(CH_3)_2S=O$
dpm	dipivaloylmethanate
dppe	bis(diphenylphosphino)ethane
dppf	bis(diphenylphosphino)ferrocene
dppm	dis(diphenylphosphino)methane
DSC	Differential Scanning Calorimetry

DTA	Differential Thermal Analysis
ED	Energy Dispersive X-ray Spectroscopy
EDXS	Energy Dispersive X-ray Spectroscopy
EI	Electron Ionisation
ES	Electrospray
eV	electron volt
FAB	Fast Atom Bombardment
fod	2,2-dimethyl-6,6,7,7,8,8,8-heptafluoroocta-3,5-dionate
hfac	1,1,1,5,5,5-hexafluoropentane-2,4-dionate
hfacNhex	4-(hexyl)imino-1,1,1,5,5,5-hexafluoropentan-2-onate
hfacNchex	4-(cyclohexyl)imino-1,1,1,5,5,5-hexafluoropentan-2-onate
IBAD	Ion Beam Assisted Deposition
IC	Integrated Circuit
INEPT	Insensitive Nuclei Enhancement by Polarisation Transfer
IPA	Isopropyl alcohol
IR	Infra-Red
KeV	thousand electron volts
LACVD	Laser Assisted Chemical Vapour Deposition
LPCVD	Low Pressure Chemical Vapour Deposition
LSIMS	Liquid Secondary Ion Mass Spectrometry
m	multiplet
Me	Methyl i.e. $-CH_3$
nbd	norbornadiene
NMR	Nuclear Magnetic Resonance
NOE	nuclear Overhauser enhancement

NP_3	tris[2-(diphenylphosphino)ethyl]amine
PECVD	Plasma Enhanced Chemical Vapour Deposition
PVD	Physical Vapour Deposition
pyr	pyridine (C_5H_5N)
s	strong
sh	sharp
SEM	Scanning Electron Microscopy
SIM	Scanning Ion Microscopy
SIMS	Secondary Ion Mass Spectrometry
t	triplet
TBCCO	Tl-Ba-Ca-Cu-O
terpy	2,2′:6′,2′′ terpyridine
tfac	1,1,1-trifluoropentan-2,4-dionate
TGA	Thermal Gravimetric Analysis
THF	tetrahydrofuran
THT	tetrahydrothiophene
w	weak
XPS	X-Ray Photoelectron Spectroscopy
XRD	X-Ray Diffraction
YBCO	Y-Ba-Cu-O

CHAPTER ONE

INTRODUCTION

1.1 APPLICATIONS FOR THIN FILMS OF SILVER

Thin films of silver have a variety of useful properties and a corresponding range of potential industrial applications (Figure 1-1). The specular properties give rise not only to mirror applications, but also the ability to optically tailor glass by means of transparent films. As the most conductive metal, silver has obvious potential uses in the microelectronics industry as electrical contacts. Soft metal films, including silver, are seen as potential lubricants for high temperature ceramic engines, and there has been recent research regarding the use of silver films as permeable membranes in gas separation processes.

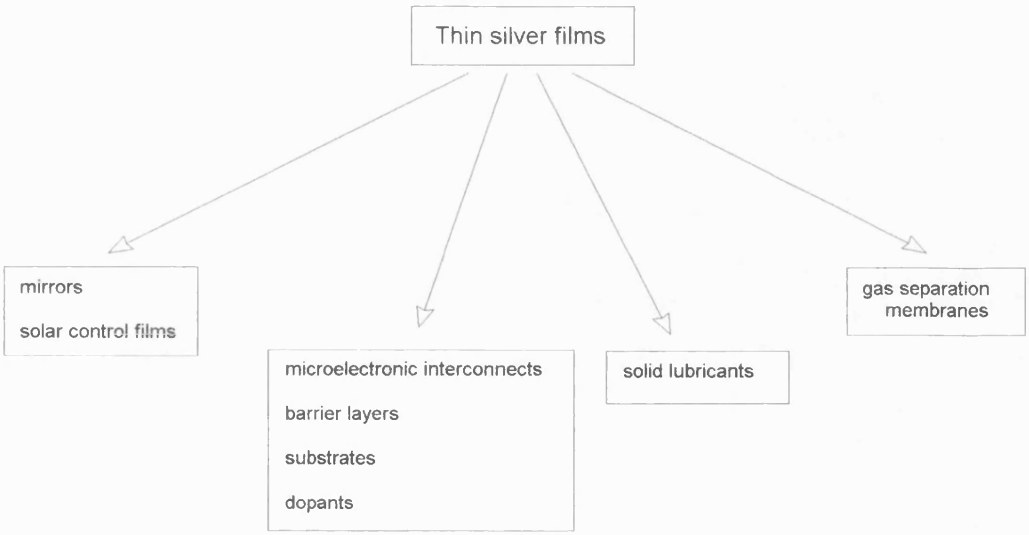

Figure 1-1 Applications for thin films of silver

Each of these applications involves an emphasis on particular film properties. Each may also impose constraints in the fabrication process, for example the film may need to be formed within a particular temperature range, or on a particular substrate. The ability to grow thin

silver films with tailored properties within these imposed constraints will be the key factor in utilising this technology.

1.1.1 Optical applications

Thin metal films were probably first systematically prepared by Faraday using wet electrochemical methods. Until the 1960's research was driven primarily by an interest in the optical applications of thin metal films including mirrors, anti-reflection coatings for lenses, multi-layer interference filters, car headlights and decorative coatings. In the production of silver mirrors, wet chemical techniques - chemical reduction, electroless plating (autocatalytic chemical reduction) and electrodeposition - have long been the chosen fabrication method. A brief description of these methods is given here because of their current importance in the production of silver mirrors, where wet methods are invariably used. For a more detailed discussion the reader is directed to references given. [1, 2]

In the chemical reduction process, the substrate is contacted by a mixture of solutions, containing a silver salt and a reducing agent, chemical reduction of the silver salt to silver metal resulting in a coating formed on the substrate. This method is many years old and a large number of suitable reducing agents are known including sucrose, Rochelle's salt [KNa(tartrate).$4H_2O$], formaldehyde and hydrazine. The electroless plating method similarly relies on the reaction of a metallic salt with a reducing agent, but in this case the deposition only occurs at catalytic sites on the substrate. Once underway, previously deposited metal acts as a catalyst to further plate the substrate, and this is the basis for the description as 'autocatalytic'. The process of depositing a metal film upon an electrode by electrolysis is

known as electrodeposition. By applying a potential difference across a solution containing the silver salt, metal is deposited on the cathode, the rate of deposition being directly proportional to the current that passes through the system.

In the higher technology area of solar energy applications, the very high reflectivity of silver makes it a prime candidate for concentrating solar energy. Silver has a solar weighted reflectance of approximately 97%, aluminium about 92% (in vacuum), all other materials have a reflectivity of less than 83%. [3] There is a considerable loss in optical properties when mirrors are formed using the conventional wet chemical electroless method, degradation occurring in some cases after a few months. [1] In addition, in a terrestrial environment, the reflectivity can degrade due to agglomeration and the formation of sulphides and chlorides. Problems also exist with diffusion between component layers and delamination from the substrate. Since the lifetime of these mirrors may be limited by the fabrication techniques employed and their reflectivity by trace impurities and surface morphology, novel processes for producing silver mirrors are of interest.

There has been considerable recent interest in the development of non-glass supported mirrors. Metallized flexible polymer based reflectors are potentially much lighter and cheaper than the silver-glass combination. [4, 5] Such materials are very important in the aerospace industry, where they have the added advantage of ease of fabrication as curved objects.

Thin films are known to have a number of useful properties when fabricated onto a glass substrate. [6, 7] The ability to effectively control reflection and transmission of light from or through a glass sheet is an attractive prospect, with considerable economic gains. A thin film that allows visible light to transmit through glass while reflecting infra-red radiation can

dramatically reduce air conditioning costs for large buildings in hot climates. For example, IROX ® TiO_2/Pd coated architectural glass is often quoted as state of the art in this respect, TiO_2 controlling the reflectivity and the palladium providing the desired absorption control. [8] Recent patents describe the use of very thin silver films (~10 nm) between ITO or Ta_2O_5 films (35-80 nm) on glass for optical tailoring. This combination is reflective to IR (Infra-red) and microwave radiation but transparent to electromagnetic radiation in the visible light region. [9-11]

1.1.2 Microelectronics applications

Interconnects in semiconductor devices provide a conductive path within a three dimensional architecture (Figure 1-2), between components at the first level, and for power distribution at succeeding levels.

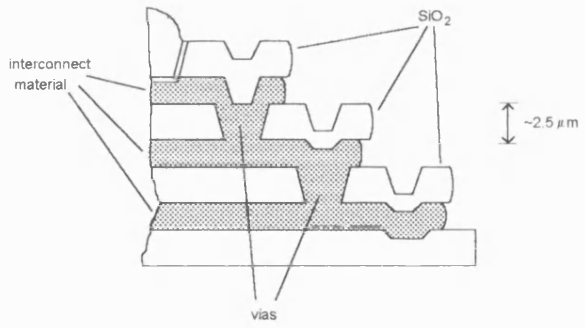

Figure 1-2 Simplified schematic representation of Integrated Circuit (IC) architecture

An aluminium alloy (4% wt Cu, 1.7% wt Si) is used as the workhorse material for current interconnect schemes in silicon devices. These designs are fabricated using a sputtering process, where the metallisation occurs when the interconnect material is ballistically projected

at the substrate. A physical line-of-sight process such as this has inherent limitations, incomplete step coverage and difficulty in filling high aspect ratio contact and via holes.

Interconnect dimensions are constantly being reduced due to the pressure for higher speed devices in a smaller volume at a lower cost. It has been estimated that by the year 2001, devices of 0.25 μm dimensions will be wired with five or more layers. [12] Such a massive reduction in device size and consequently interconnect size has compounded limitations with aluminium metallisation schemes. Electromigration and hillock formation are particular problems at high current densities. [13] Additionally, with an alloy resistance of ~3-4 μΩcm, interconnects are prone to crosstalk, interference, capacitance resistance and heat generation.

Among possible replacements for aluminium alloy, are tungsten (~5.7 μΩcm) which has a high resistance to electromigration and copper (~1.7 μΩcm), consequently a considerable level of CVD technology has been developed with regard to these metals. [14] Tungsten is already used in particular roles within silicon devices, notably as vertical interconnects (vias) and copper is widely regarded as the successor to aluminium in next-generation semiconductors. Gold (~2.2 μΩcm) is already used as a complete substitute for aluminium in the more expensive GaAs devices.

With such a low resistivity (1.59 μΩcm) silver is potentially very useful in high-speed and specialist applications in semiconductor devices. With respect to silicon devices however, rapid diffusion of silver into a variety of materials (significantly Si and SiO_2) and its ability to be corroded [15] has limited its applications but advances in barrier technology have already alleviated similar problems with copper interconnect schemes. Silver, silver-palladium and

silver-platinum thick film conductors have found a variety of uses in electronics packaging [16] and sputtered silver electrical contacts have been discussed in the literature. [17]

The disadvantages suffered by silver deposited by physical techniques has resulted in interest in being able to develop fabrication methods where surfaces can be metallized irrespective of orientation. Deposition from a volatile precursor in the vapour phase will simultaneously coat all surfaces where conditions for film growth are satisfied, this technique being widely referred to as Chemical Vapour Deposition (CVD). Silver films grown for interconnect schemes via CVD will require a high degree of conformal coverage (i.e. films of uniform thickness that follow the contours of the surface of the substrate), with very low levels of impurities. Such a scheme would have to deposit silver within constraints of the fabrication process, ideally at temperatures below 350°C.

Silver has also found several specific applications in superconducting devices where it remains highly attractive as a substrate for the growth of superconducting films via CVD, as electrical contacts, passivation barriers, and as a beneficial dopant in many materials. There are significant problems in finding a substrate for superconducting devices grown by CVD. This is largely due to a destructive chemical interaction between substrate and film, and the migration of substrate atoms into the superconductor (particularly at the required high processing temperatures). Such interaction inevitably leads to a reduction in device performance.

Metallic silver however appears unique in this respect, having excellent compatibility with high T_c materials with good bonding properties [18] and excellent conductivity both thermal and electrical. Recent research has shown the feasibility of fabricating superconducting wires using this technology. [19] Firstly, a deposited silver film acts as a passivation layer to limit interactions

between the flexible ceramic fibre support and superconductor, and to act as a substrate for the superconducting element. A second silver film is deposited over the superconductor to act as an electrical contact. The passivation layer was found to successfully limit interactions between the Al_2O_3 and superconducting YBCO (Y-Ba-Cu-O) components where barium aluminate has been found to form.

Contamination of the superconducting material itself by silver is not problematic, in contrast to gold or the platinum group metals. [20] Indeed silver has been found to be an attractive dopant in high T_c superconductors because it promotes crystallisation and c-axis orientation, strengthens intergranular coupling and improves surface morphology. [21] Compared to undoped materials, doping of both YBCO [22, 23] and BSCCO (Ba-Sr-Ca-Cu-O) [20] materials results in greatly reduced normal resistivities and enhanced T_c and J_c (the critical current density). With ~10% wt Ag in YBCO ceramics J_c enhancement is of the order of 50%, from J_c~450 to 700 A cm^{-2} at 77 K. It is suggested that Ag fills the intergranular space without substituting Cu within the YBaCuO grains. [24] A similar doping technique has recently been attempted using the TBCCO (Tl-Ba-Ca-Cu-O) [25, 26] and the BPSCCO (Bi-Pb-Sr-Ca-Cu-O) [27] superconductor materials.

As with interconnect applications, purity of the silver film is likely to prove very important. Phosphorus and sulphur impurities are particularly undesirable, as they may be prone to oxidation, if migration of phosphate and sulphate into the superconductor occurs then superconducting properties are likely to be diminished.

1.1.3 Other applications

Soft metal films (including silver) are seen as possible lubricants for high temperature, high efficiency and ceramic engines. In advanced transport systems, advanced heat engines and space technology there is a need for lubrication systems that can operate in high temperature, corrosive or vacuum environments. Conventional liquid oil based systems are limited by the thermal stability of the oils and have a relatively low operating temperature (less than 350°C). [28]

Solid silver films have a low shear strength, high chemical inertness, high thermal conductivity and a moderately high melting point (962°C). Silver is ideally placed to provide solid film based lubrication systems, either as a metal film or part of a multi-component system. Silver - alkaline earth metal fluoride composites can act as lubricants from room temperature to 900°C. [29]

As lubricants, critical properties of the films are surface quality, porosity, tribological (wear, friction and lubricant) properties and substrate adhesion. Coating life in these applications is largely determined by delamination, but it is known that film adhesion may be increased by the use of ion bombardment during deposition, [30] or by the use of intermediate bond layers such as Cu, Cr, Ti. [31]

Silver films used in lubrication studies have been grown by physical methods, ion-beam assisted deposition (IBAD), [30] sputtering, [31, 32] and laser surface cladding. [33] Chemical vapour deposition is an ideal method for producing uniform films on three dimensional substrates with complex topographies, an advantage over physical deposition methods. Deposition

temperatures for these applications need not be low as the substrates themselves will have a high thermal stability.

Silver is well known to be more permeable to oxygen than other gases and this has led to recent research into its use in gas permeable membranes. [34] The transport of oxygen through silver in such a system is thought to proceed through a sequence of steps; dissociative adsorption of molecular oxygen on a higher pressure upstream surface, dissolution of the silver into the bulk and its migration through octahedral sites or defects, and finally recombination and desorption at a very low pressure downstream surface. The rate of transfer of oxygen can be increased by glow discharge technology and the permeation of gases through membranes is known to be increased by reducing film thickness. [35]

Similarly a commercial hydrogen purification process using palladium-silver alloy tubes has been in use for many years at the small to medium scale level. [36] Permeation rates can be increased by decreasing the film thickness, and forming films on an inorganic porous substrate. Recent work has shown the feasibility of spray pyrolysis, to grow such thin films [35] on a porous alumina hollow fibre support. A chemical vapour deposition method for producing these films is ideally placed to provide a thin uniform coating to such supports.

1.2 VAPOUR DEPOSITION ROUTES TO THIN METAL FILMS

Thin metal films have traditionally been grown by a range of different techniques. Wet chemical and electrochemical deposition solution methods have long been important in the manufacture of mirrors (Section 1.1.1), however there also exists interest in the formation of silver films from other solution [3, 37, 38] and solid techniques, [39-41] and vapour techniques in cases where more subtle control is required. These vapour techniques can be subdivided according to whether the film growth is based on a physical or chemical process; i.e. Physical Vapour Deposition (PVD) or Chemical Vapour Deposition (CVD).

1.2.1 Physical Vapour Deposition

The PVD of silver is relatively well developed, being generally accomplished by evaporation [42] or sputtering. [43, 44] In the evaporation process, material to be deposited is heated in a high vacuum (typically 10^{-7} Torr). Heating is carried out using an electron beam or by induction to create an area of molten metal in a crucible near the substrate. Metal atoms condense on the substrate to form high purity films. In the past, evaporation has been used as a major method for aluminium PVD in integrated-circuit fabrication, however this technique cannot easily be adapted for alloys and this has been the main reason for interest in sputtering.

In sputtering a target of the material to be deposited is bombarded by high energy ions created from a glow discharge. This bombardment results in the dislodging of atoms which ballistically transport to the substrate where they condense to form the film. Various additional techniques

have been developed to increase growth rates for sputtering, the basic principle however remains the same. Sputtering has enjoyed large scale use in the semiconductor industry where many materials (including Al alloy interconnects) are deposited by the technique.

Sputtering and to some extent evaporation are limited in many applications due to their inability to cover a three dimensional surface with a uniform thickness of film. As essentially line-of-sight processes, PVD techniques are inefficient at providing conformal step coverage, at filling high aspect ratio (deep and narrow) trenches and vias. Bias sputtering has in recent years been used to significantly enhance step coverage, the process resputters material that has already been deposited and via a number of routes enhances step coverage.

1.2.2 Chemical Vapour Deposition

The CVD technique differs from PVD in that it relies on a chemical reaction to produce the target material *in situ*, either at or near a substrate interface. At its simplest CVD requires the transport of a volatile precursor (containing the target element) to a reaction zone where deposition takes place. Deposition occurs when a reaction allows the precursor to decompose to yield the target element. The decomposition is brought about by the use of thermal energy in a variety of forms, generally by heating the substrate, or in a few cases by heating the gas. The chemical reactions involved are often of a complex mixture and may be based on pyrolysis, reduction, oxidation, disproportionation or hydrolysis pathways.

CVD was used as early as the 1880's for the production of carbon filaments for the incandescent lamp industry. [45] The Mond process is however the best known early example of

CVD technology used in industry. The discovery of nickel tetracarbonyl in 1890 by Langer and Mond led to its use as a precursor in the refining of nickel on an industrial scale. [46] In the Mond process, nickel ore is reacted with CO at 50°C and vaporised. After transportation to a deposition zone, decomposition at 180°C occurs to give pure nickel metal (Eqn 1-1).

$$Ni(CO)_4 \rightleftharpoons Ni(s) + 4CO \qquad (1\text{-}1)$$

1.2.2.1 CVD mechanisms

Figure 1-3 schematically represents a minimum number of steps required to describe a fundamental thermal CVD process for a metal deposited from a metal-organic precursor.

a) *mass transport of precursor to the deposition zone*
b) *possible gas phase reactions which may lead to species more involved or less involved in the deposition process.*
c) *transport of precursors to the substrate surface where adsorption occurs.*
d) *reaction of the adsorbed species to generate the desired material and organic by-products.*
e) *desorption of organic species away from the surface.*
f) *surface diffusion of the adsorbed metal to growth sites and incorporation into the film.*
g) *mass transport of by-products and unreacted precursor material from the deposition zone.*

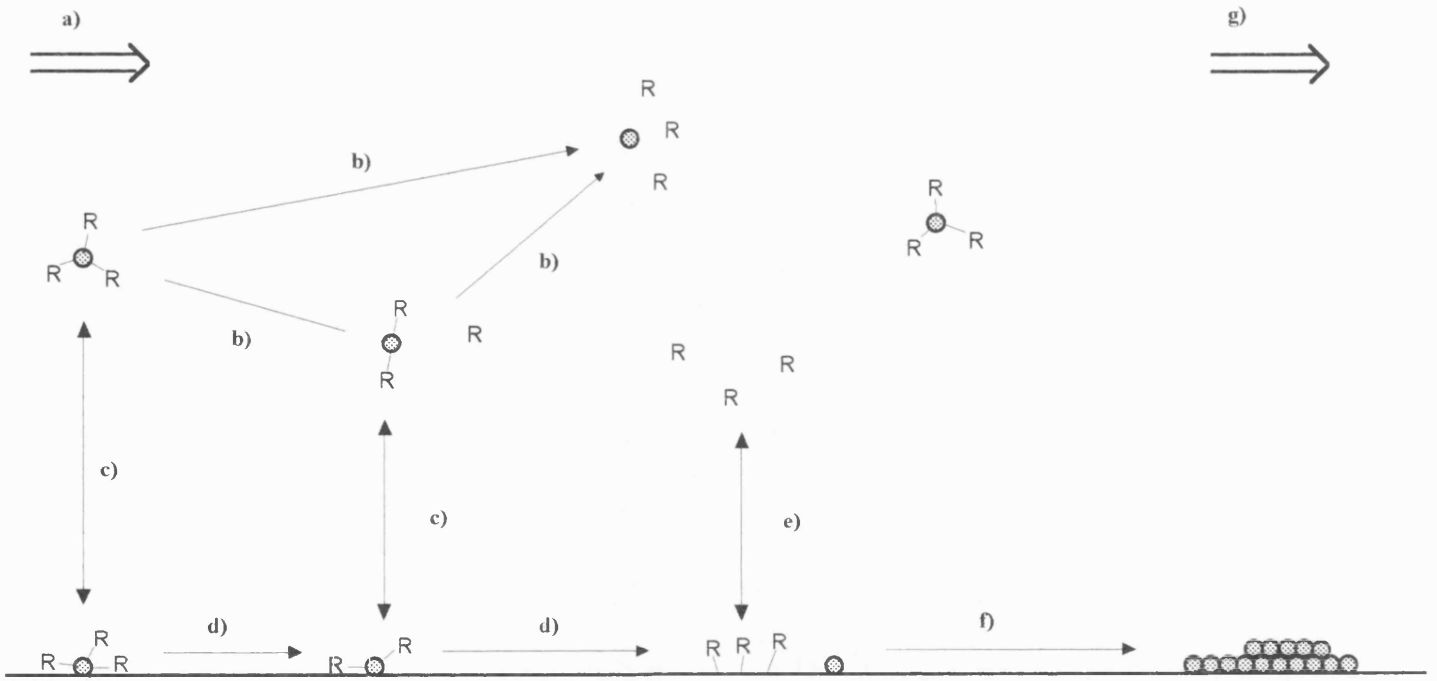

Figure 1-3 Schematic representation of the thermal CVD of metals

At or near atmospheric pressures, a gaseous boundary layer forms across the film growth area where physical conditions differ dramatically from the bulk vapour. [47] Species diffuse through this boundary layer in order to take part in the deposition **(c)**. Similarly by-products have to transverse the boundary layer before being pumped or swept out of the deposition zone **(e)**.

The relative rates of gas mass-transport and surface reactions are important because either can be rate limiting. At a high enough temperature, surface reaction rates exceed the rate at which material is delivered. This results in a mass-transport limited process. If the mass-transport is sufficiently fast then the growth rate is dictated by surface reaction kinetics, these kinetics increasing with temperature according to the Arrhenius expression. In particular cases, the point at which CVD schemes become mass-transport or surface reaction limited depends on parameters peculiar to each individual system, dependent on precursor delivery system type, gas flow conditions, and the activation energies for the decomposition.

Gas phase reactions have a direct influence on the growth and quality of the film **(b)**. The precursor may decompose to give active species *in situ* that are responsible for the film growth, or inactive species retarding the film growth (pre-reaction) and sometimes contaminating the growing film. As the deposition temperature and the partial pressure of precursor are increased, these problems are exaggerated, gas phase reactions can predominate resulting in poor film quality, primarily due to nucleation in the gas-phase. Such problems are further compounded in cases where more than one precursor is involved, for example in the formation of TiN using $TiCl_4$ and NH_3. Very little is currently understood about pre-reaction in the gas-phase. A significant amount of work has been carried out on SiO_2 systems for semi-conductor CVD [48-50] but relatively little involving the pre-reaction of organometallic species. [51-52] It is

probably the case that there is a complex set of interacting pathways with competing reaction schemes involved.

Adsorption-desorption processes may be regarded as dynamic in equilibrium. If reaction of adsorbed species **(d)** is incomplete or if desorption of by-products **(e)** is incomplete, impurities will be trapped inside the growing film. This can have serious consequences for film quality. Metal-organic precursors should ideally have facile and clean decomposition pathways to enable stable by-products to leave the surface without further decomposition **(e)**. If a clean decomposition pathway is not available, complex mixtures of hydrocarbons or organic species will find themselves at the surface. Of particular problems are individual atoms, for example elemental carbon which will not be so readily desorbed.

1.2.2.2 Film growth mechanisms

Film growth takes place when adsorbed atoms agglomerate together on the substrate surface [Figure 1-3, **(f)**], individual atoms can be fairly mobile upon the surface and this mobility is dependent on a number of factors including substrate temperature. The mechanism of film growth can be of three principal types (Figure 1-4). The type that occurs within a particular system will depend on thermodynamic and kinetic considerations in decomposition and crystal growth, and by the interaction between the film and the substrate.

In layer-by-layer or Franck-van der Merwe film growth, a complete monolayer forms across the substrate which is then covered by succeeding layers. In some cases subsequent layers can begin to grow before lower layers are complete. This layer-by-layer growth can be promoted

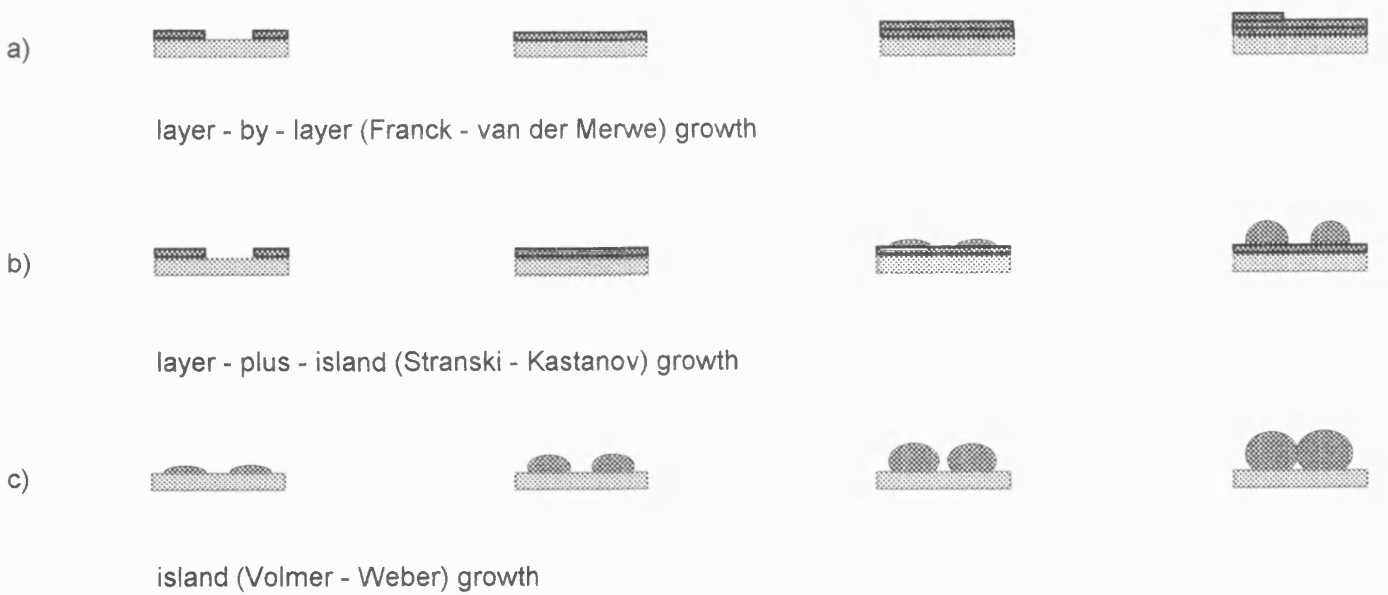

Figure 1-4 Modes of film growth in CVD

where growth rates are low at a high temperature (growth is mass-transport limited). In this case surface diffusion rates are far higher than the incoming flux of atoms, thus allowing metal atoms to diffuse quickly through to the growth site and incorporate into the film to give crystalline growth. Examples of layer-by-layer growth include that of the PVD of silver on gold surfaces.

Island growth normally occurs when film atoms are more strongly bound to each other than to the substrate. In this island or Volmer-Weber growth, initial nucleation occurs at nucleation sites on the substrate and subsequent deposition occurs at these sites forming islands. These islands eventually coalesce to give at best a microcrystalline and at worst an amorphous film. In addition this growth mode will result in a very rough surface as well as voids and pockets inside the film where islands have coalesced.

A final growth mode is the Stranski-Kastanov or layer-plus-island. In this case initially layer growth occurs, however at a certain point - after several layers - island growth starts to predominate. The reasons for this are still not very clear, although it is known that an important factor in determining the mode of film growth is the molecular orientation of adsorbed precursor molecules. The layer-plus-island growth mode is highly dependent on the substrate and often forms highly strained intermediate monolayers, on which islands start to form. This mode of growth has been investigated in the case of silver on tungsten surfaces by a consideration of adsorption energies involved in the growth process. The work suggests that island growth predominates at around the third monolayer and this has been confirmed by scanning electron microscopy (SEM) and Auger electron spectroscopy (AES). [53] Similarly epitaxial grown films of silver on Si, GaAs and Pt are believed to grow via layer-by-layer or layer-plus-island modes. [54, 55]

For more detailed discussions of film growth processes, the reader is directed to further references.[56, 57] Recent work outlines an attempt to model the morphology of film growth by means of competing processes of film growth and surface diffusion to determine surface morphology quality.[58]

1.2.2.3 Advantages of CVD

Chemical vapour deposition has significant advantages over traditional deposition techniques. High purity, superior quality uniform films can be formed easily. In contrast to PVD, CVD does not suffer from line-of-sight limitations. Film growth on the substrate is restricted only by the diffusion of precursors to the substrate. As an illustration, blanket copper CVD carried out on overhanging test structures (Figure 1-5) showed outstanding conformality with no apparent thinning on the inside of the polysilicon structure.[59] SEM work revealed that copper deposition occurred even in the deepest corners of the structure, at growth rates as high as 1200 Å min^{-1}. Such film growth on complex structures would not be possible with conventional methods.

CVD technology exhibits a great deal of kinetic deposition control. As deposition can be controlled by the surface chemistry of the substrate-precursor pair, selective area and pattern deposition becomes a possibility. In advanced systems this may reduce the potential number of steps required in fabricating complex electronic structures.

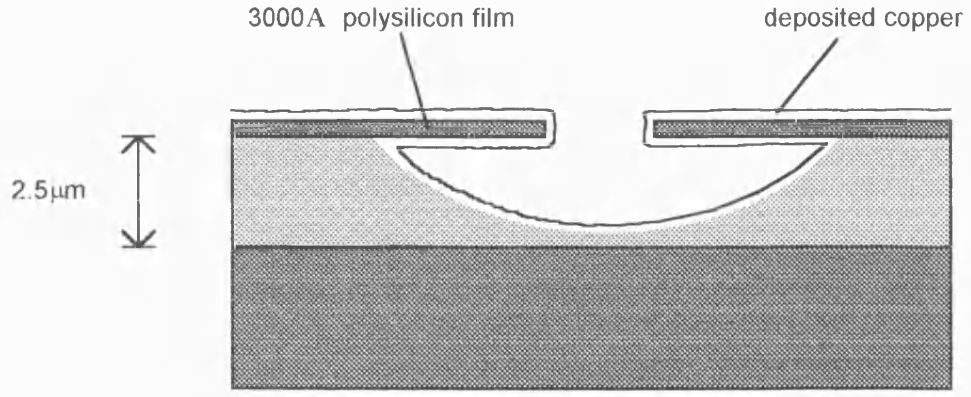

Figure 1-5 Overhanging test structure for blanket Cu CVD. [59]

In contrast to PVD, CVD processes are found at much reduced deposition temperatures. This has major advantages in electronics where many steps are involved in the fabrication process. At high processing temperatures, migration of materials becomes a serious problem, indeed barrier layers are often needed. The use of lower temperature CVD methods increases the control at interfaces, reduces migration and leaves sharp boundary features. CVD also has the advantage of no radiation damage to previously fabricated layers. Finally CVD has been successfully scaled up to industrial levels in many cases. All surfaces may be coated simultaneously where the substrate is in a region of sufficient partial pressure, increasing industrial throughput.

1.2.2.4 Pre-requisites for CVD precursors

Given the advantages of CVD over other techniques, interest in developing these processes is now at a high level. However, with quality limitations of the film, purity, morphology, reflectivity, crystallinity, etc. CVD can only provide the desired end product if a suitable precursor can be found. This provides the synthetic chemist with a challenge to develop potential precursor chemistries and provide precursor molecules with the desired properties.

In order for a precursor to be practical for thermal CVD, precursor decomposition pathways should proceed both cleanly and at reasonable rates. This imposes fundamental constraints on precursor design. It should have reasonable volatility at temperatures within limits imposed by the substrate and the fabrication process, a vapour pressure of ~10 Torr at 20-50°C being generally considered sufficient. In thermal CVD, precursor volatilisation generally occurs in a heated bubbler assembly where diluent gases are passed over or through precursor material. The precursor needs to be thermally stable over extended periods in the temperature range at which it exhibits reasonable volatility. In addition, precursors which achieve a liquid phase at this temperature are often favoured due to the potential of keeping the surface area constant within the bubbler.

Once in the gas-phase, the molecules should be stable at elevated temperatures, and not pre-react or decompose until the deposition zone is reached as this may result in particle formation and surface contamination. Decomposition routes should be clean and facile, the metal-ligand bonds being cleaved readily and the free ligand relatively stable. The organic by-products themselves should ideally be chemically unreactive, thermally stable, volatile and desorb readily following surface reactions.

1.2.2.5 Specialised CVD techniques

For practical thermal CVD, precursors are sometimes not readily identifiable (this is the case for silver). In these instances, a number of techniques have been developed that can exploit less than perfect precursors. These techniques can alter the mode of activation of the decomposition, as in Laser Assisted CVD (LACVD) and Plasma Enhanced CVD (PECVD), or alternatively can utilise precursors with limited volatility, as in Low Pressure CVD (LPCVD) or Aerosol Assisted CVD (AACVD).

In *Laser Assisted Chemical Vapour Deposition* (LACVD), the substrate is heated by means of a laser beam. Deposition will only take place in the vicinity of the laser beam heating the substrate. By moving the laser, fine lines can be written directly to the substrate, thus allowing the possibility of selective area deposition. The writing of lines using LACVD has obvious applications in the microelectronics industry. As a potentially low temperature deposition method, complex temperature sensitive substrates may be used. In addition, lithographic steps may be avoided as this becomes an essentially selective deposition technique. Using this method the repair of interconnects on integrated circuits (IC) becomes possible and indeed, the LACVD of gold for circuit repair has already been incorporated into fabrication processes.[15]

The laser can promote deposition in a number of ways. 1) Photons may activate the precursor molecules in the gas phase (gas-phase photolysis). 2) Precursor molecules may be activated by photons while in an adsorbed state. 3) Photons may activate growth sites on the surface of the substrate. 4) The laser beam may act in the same way as a thermal heat source localised in a small region.

Plasma Enhanced Chemical Vapour Deposition (PECVD) is another example of a potentially low temperature deposition method. PECVD techniques in general operate at around 200-300°C or below. High energy electrons are produced (usually) by a glow discharge in the vapour above the substrate. These high energy electrons collide inelastically with precursor molecules to produce active radical and ionic species. The electrons can activate almost any reaction without the need for subjecting the bulk of the vapour to high temperatures. Therefore this again becomes significant for temperature sensitive substrates and substrate-film combinations with mismatched thermal expansion coefficients.

Another effect of the glow discharge is to bathe the substrate in a flux of high energy particles, having the effect of radically altering the surface chemistry during deposition. Because of this, films grown by PECVD may be very different to those grown by thermal CVD and may possess special properties. However PECVD, despite high growth rates, also possesses disadvantages. Pure films are difficult to obtain, desorption of by-products is particularly slow (due in part to lower temperatures) and impurities can therefore be significant. A number of references include more detailed discussions. [60, 61]

Normal thermal CVD is generally carried out at atmospheric pressures but by decreasing the total pressure in the system however, partial pressures of relatively involatile precursors may become more significant. In *Low Pressure Chemical Vapour Deposition* (LPCVD) different physical processes become significant. Diffusion of precursor to the surface becomes far easier as the boundary-layer effect is less important. Growth rates become limited by the rate of the surface reaction rather than mass-transfer. Desorption of by-products becomes much easier. Films have improved uniform thickness and properties, better step coverage and conformality,

and superior structural integrity. A good example of this on an industrial scale is the deposition of Si from silane (SiH_4) at 600-650 °C.

Large areas of substrate can be coated simultaneously with good uniformity due to the large diffusion coefficient where the mean free path of molecules is increased. Similarly, because inter-molecular collisions are reduced, so is the extent of pre-reaction. In low pressure reactors, dilution gases are not required, hence reaction rates are generally only an order of magnitude less than atmospheric pressure CVD.

A recent development in the field of CVD, and one of particular importance to this work is that of *Aerosol Assisted Chemical Vapour Deposition* (AACVD). AACVD differs from conventional CVD in that precursor delivery is by means of an aerosol of solvent droplets containing the precursor in solution. Soluble precursors with limited volatility or thermal stability can be introduced directly into the gas phase in the form of an aerosol mist by a number of relatively straightforward routes. Once in the gas stream, the mist of fine droplets is transported to the deposition zone by means of the diluting sweep gas. During this transport, solvent evaporates from the mist, either completely or partially (sometimes by means of heated gas lines), to deliver precursor in the vapour phase. Chemical vapour deposition can then take place in a conventional manner with the added complication of solvent molecules. AACVD can be readily distinguished from spray pyrolysis (another similar form of liquid droplet delivery) where a precursor dissolved in solvent is sprayed onto a heated substrate. In this case solvent evaporation and reaction occurs on the surface. This is distinct from CVD where gas-phase molecules are responsible for the deposition (Figure 1-6).

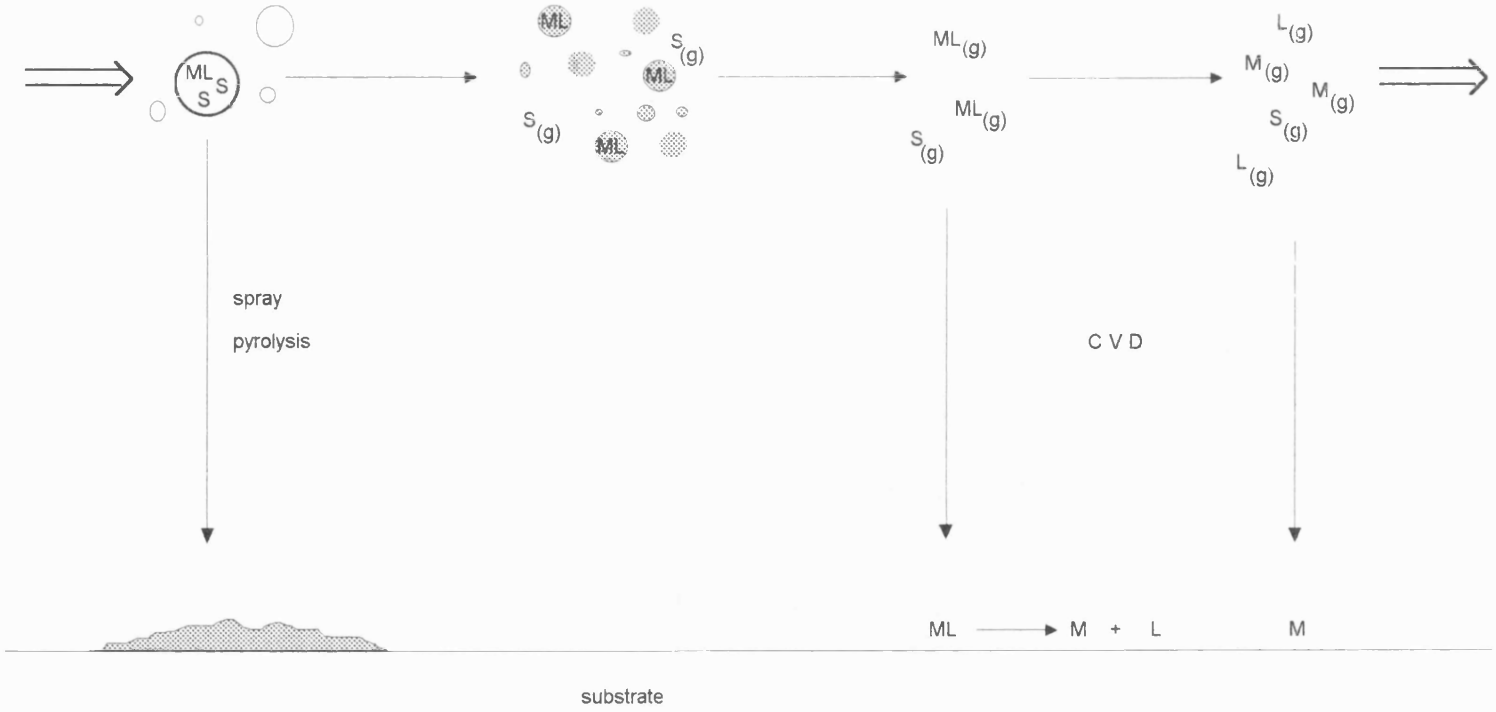

Figure 1-6 Film formation from aerosol routes; spray pyrolysis and aerosol assisted CVD, ML - precursor, containing metal (M) and ligand (L), S - solvent.

The method of nebulisation (atomisation) is an important step. Several techniques exist with individual advantages and disadvantages. The method employed will determine the production rate, size of droplets and the particle size distribution. Three types of aerosol will be discussed here, those of pneumatic jet, electrospray and ultrasonic based generators. The three methods require differing amounts of development to attain successful industrial scale-up. The latter technique was used in this study, construction details being given in Appendix 6-2.

In *pneumatic jet nebulisation*, a stream of gas is used to atomise the solution into an aerosol. The gas also performs the role of carrier-diluent gas, sweeping the aerosol to the reaction zone. These generators have been largely developed for medicinal applications where aerosol delivery of drugs is an attractive prospect. The units themselves are inexpensive, small plastic assemblies, each capable of generating 0.5 cm^3 min^{-1}. Plastic units although functional for aqueous solutions are however unsuitable for many organic solvents. The droplet size (approximately 1-5μm) can be dependent on gas flow conditions and solution viscosity, the polydispersity (a measure of the range of aerosol droplet sizes) can be relatively high (>1.6 geometric standard deviations) [62] in comparison with other techniques.

The *electrospray* technique uses an electrostatic field to produce droplets. When the surface tension of a liquid placed in an electric field balances the electrical force a stable 'Taylor' cone is formed and this cone emits a stream of droplets. The method was originally developed as a 'soft' mass spectrometry tool ES (Electrospray Ionisation). As with other atomisation processes, a major obstacle is the need to scale up throughput to a feasible industrial scale. [63] Finally there remains problems in atomising solvents with high electrical conductivities (e.g. aqueous solvent mixtures).

In *ultrasonic nebulisation*, the solution is atomised by means of a piezo-electric transducer vibrating at very high frequencies (typically 1-2 MHz). The high frequency ultrasonic sound waves cause the solution to fountain, and at the tip nebulisation occurs propelling droplets into the vapour phase. This technology has been reasonably well developed at small scales for humidifiers and drug delivery systems. The equipment can be relatively inexpensive and easy to set up in the laboratory. Droplet generation is very uniform with a low polydispersity (1.4 geometric standard deviations). [62]

A significant amount of work has been carried out with aerosols for the generation of advanced materials and an excellent recent review is available. [64] However much of the CVD related work has been concerned with metal oxides and thin film formation via metal AACVD has yet to be fully exploited. [65]

1.3 THE CHEMISTRY OF SILVER

The elements of the Group 11 triad, copper, silver and gold, share the same electronic ground state with a single s electron outside a completed d shell. Ionisation energies apart this is where, to a large extent, group similarities and trends end. Although silver chemistry can be compared in places to copper(I) chemistry, and to a lesser extent gold(I) chemistry, the chemistries are in general quite distinct. There is no obvious reason for the lack of group trends, although some silver-gold differences have been traced to relativistic effects of 6s electrons in gold.

The differences in the chemistry go a long way to explaining why the development of gold CVD and the incredible advances of copper CVD have, to a large extent, not been mirrored in silver CVD. Further, the chemistry of silver has hindered the development of precursors suitable for CVD work. Inorganic silver compounds are polymeric and involatile except under extreme conditions. Metal-organic and in particular organometallic compounds are generally too thermally unstable to achieve efficient vaporisation and are susceptible to decomposition at room temperature via photolysis, hydrolysis and oxidation.

Loss of the single s electron from silver metal atoms leads to the stable Ag(I) oxidation state with a d^{10} electronic configuration. Silver(I) is the most common and widely studied oxidation state and has been observed in geometries from two to six. Loss of further electrons from the d shell requires more energy and Ag(II) (d^9) and Ag(III) (d^8) oxidation states are considerably less common. These higher oxidation states can be reached by chemical or electrochemical oxidation but are thermodynamically and kinetically unstable in aqueous solutions.

Some stability may be imposed on the compounds of higher oxidation states where N-donor ligands or fluorine are present and this has led to some discussion in characterising the Ag(II) and Ag(III) ions as class A or 'hard' Lewis acids. Examples of Ag(II) include $[Ag(py)_4]^{2+}$ [66] and AgF_2, [67] and Ag(III) species can be found in various oxides, [68, 69] the $[AgF_4]^-$ anion [70] and a variety of compounds containing N-containing macrocycles and cryptates. [71, 72] Silver(II) and (III) compounds are often found as either four coordinate (square planar) or six coordinate (octahedral and distorted octahedral) complexes. A number of reviews concerning silver in its higher oxidation states are available. [72-75]

Silver(I) has been classified as a class B or 'soft' Lewis acid due to its reactivity and enhanced stability with 'soft' Lewis bases. With main group donor atoms, better stability is noted with phosphorus and sulphur than with nitrogen and oxygen donors. Within Group 15, stabilities observed are N<<P>As>Sb, and in Group 16, O<<S-Se-Te. Comparative studies suggest Group 15 donors achieve more stability than Group 16 donors i.e. P>S>N>O. With halides, greater affinity is again seen with softer donors; I>Br>Cl>F. [76]

The stabilities of Ag(I) and Ag(II) can be reversed with N_4-macrocycles in non-aqueous solvents. In such cases Ag(I) compounds disproportionate to Ag(II) and Ag(0) (Eqn 1-2). Disproportionation reactions have become an important facile deposition pathway in copper CVD, for example copper (I) hexafluoroacetylacetonate disproportionates to copper metal and stable, volatile copper (II) hexafluoroacetylacetonate (Eqn 1-3), limiting the incorporation of organic by-products into the film. The variety of compounds containing higher oxidation states of silver is however modest in comparison to silver(I) chemistry and the use of disproportionation decomposition pathways for silver CVD may remain impractical and unrealised for some time.

$$2Ag(I) \longrightarrow Ag(0) + Ag(II) \qquad (1\text{-}2)$$

$$2Cu(hfac) \xrightarrow{\Delta} Cu(0) + Cu(hfac)_2 \qquad (1\text{-}3)$$

Historically the co-ordination chemistry of silver has been more extensively developed than organometallic chemistry due to the relative instability of the Ag-C bond. Silver chemistry has been the basis of photography since the 1800's, and this led to much early research with N-donor ligand adducts of silver halides. A short review of the geometries adopted by silver coordination compounds is given here to provide a framework for structural discussions found in later chapters. Organosilver chemistry is discussed in depth in Chapter Five.

Structurally, silver is known to exist in range of geometries with coordination numbers two through six. These geometries rarely exist in the classical 'text book' fashion but, and particularly for high coordination numbers, often as distorted or indeed heavily distorted coordination spheres. Aqueous silver species (particularly with N-donor ligands) of linear geometry were first studied in the 1930's. For example, the structure of the $[NH_3\text{-}Ag\text{-}NH_3]^+$ ion was first elucidated in 1934. [77] At that time such linear arrangements were thought to be characteristic of silver(I) in general, however since then the chemistry has developed with the realisation of more complex structures. Silver(I) structures are in general linear, trigonal or (pseudo)tetrahedral, but may be found as highly distorted five- or six- coordinate complexes. Typical coordination environments for silver in the +1 oxidation state are listed in Table 1-1.

Molecular orbital studies have attempted to explain linear geometries of copper, silver, gold and mercury. [78] In these cases it has been suggested that involvement of d electrons is the chief cause for such structural features. Hybridisation of the doubly filled d_{z^2} with unoccupied 5s and $5p_z$ orbitals results in molecular orbitals suitable for linear geometry (Figure 1-7).

Table 1-1 Typical coordination environments for silver in the +1 oxidation state.

Coordination Number	Geometry around Silver	Examples [a]
2	linear	$[NH_3\text{-}Ag\text{-}NH_3]^+$, $[Ag(CN)_2]^-$, $Ag(PR_3)Br$
3	trigonal	$Ag(NP_3)^+$, $[Ag(PPh_3)_2Br]$
	distorted trigonal	half of Ag atoms in $[Ag(PPh_3)I]_4$ ('step')
4	tetrahedral	$[Ag(PPh_3)_2Br.CHCl_3]_2$, $Ag(dppe)_2^+$
	distorted tetrahedral	$[Ag(PPh_3)I]_4$ ('cubane'),
		half of Ag atoms in $[Ag(PPh_3)I]_4$ ('step')
5	distorted bipyramidal	$Ag(PPh_3)_2(terpy)^+$
6	octahedral	AgF, AgCl, AgBr (NaCl structure)
	highly distorted octahedral	$[Ag([15]aneS_2O_3)]^+$

[a] PR_3 = tris(2,4,6-trimethoxyphenyl)phosphine, NP_3 = tris{2-(diphenylphosphino)ethyl}amine, dppe = bis(diphenylphosphino)ethane, terpy = 2,2':6'2"-terpyridine, [15]aneS_2O_3 = 1,4,7-trioxa-10,13-dithiacyclopentadecane

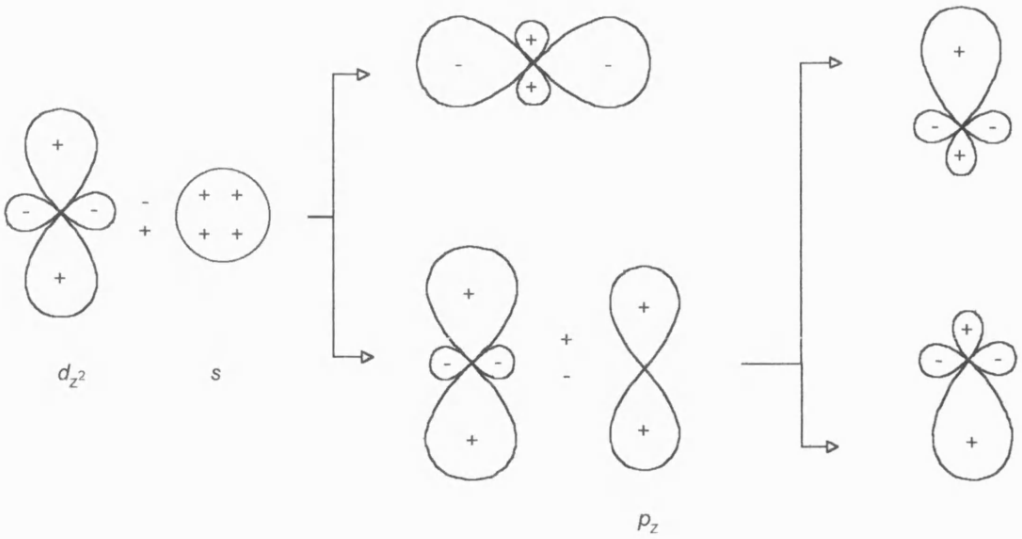

Figure 1-7 Hybridisation of d_{z2}, s and p_z orbitals resulting in molecular orbitals suitable for linear geometry. [78]

Linear geometry was prevalent in the early structural studies of silver compounds, examples including silver cyanide [79, 80] and $[Ag(SCN)_2]^-$. [81] In more complex coordination compounds, molecules tend to aggregate and linearity is less favoured, although the use of bulky ligands will hinder oligomerisation. For example 1:1 phosphine adducts of silver halides LAgX (L = PR_3, X = Cl, Br) generally form 'cubane' or 'step' type tetramers with halide bridges, however the use of the bulky ligand [tris (2,4,6-trimethoxyphenyl)phosphine] favours formation of a monomer (Figure 1-8). [82] The P-Ag-X angle (θ) in each case deviates slightly from linearity (X = Cl, θ = 175.0°; X = Br, θ = 174.4°), and this has been attributed to interactions between silver and nearby *ortho*-methoxy oxygens.

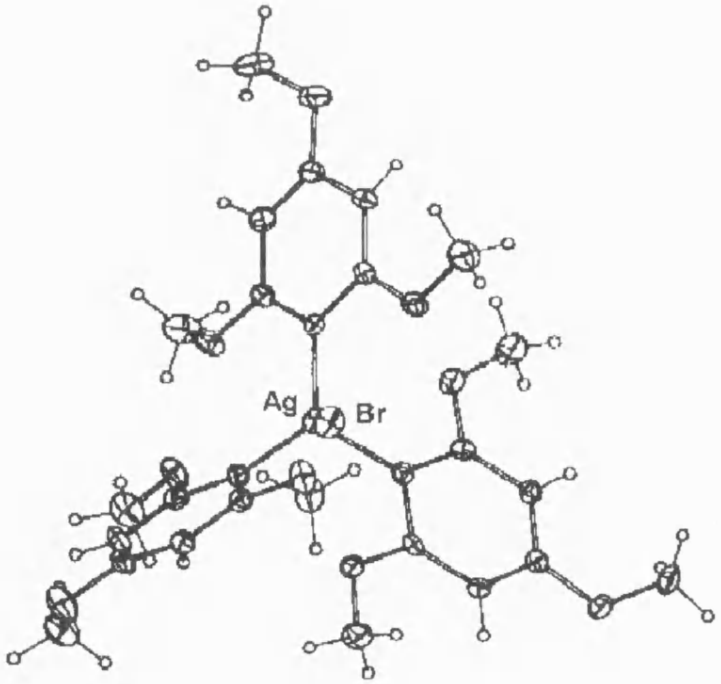

Figure 1-8 The structure of the 1:1 tris(2,4,6-trimethoxyphenyl)phosphine-silver bromide adduct as projected down the P-Ag bond. [82]

With large multidentate ligands silver(I) can be readily found in trigonal planar geometry, particularly when ligand bulk sterically hinders approach of other coordinating species. An example here the complex $[Ag(NP_3)]PF_6$ the cation of which contains the potentially tetradentate ligand, tris[2-(diphenylphosphino)ethyl]amine (NP_3). It is interesting to note that there is no interaction with either the PF_6^- or the central nitrogen atom, the silver preferentially bonding to phosphorus(III) (Figure 1-9). [84] This contrasts with the nitrate analogue where a silver-nitrate interaction is present. [84]

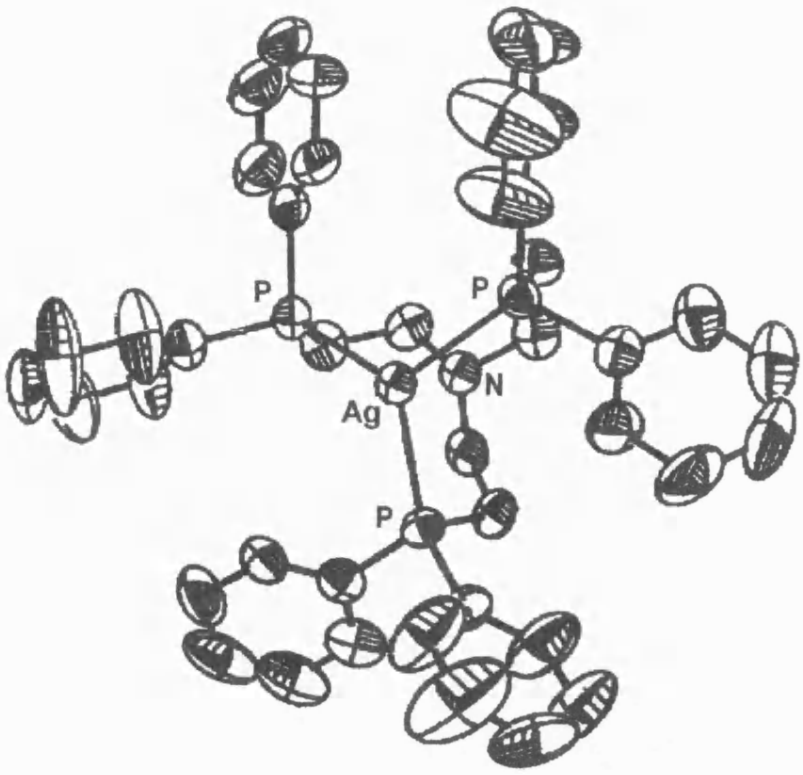

Figure 1-9 Structure of the $Ag(NP_3)^+$ cation in $[Ag(NP_3)]PF_6$. [84]

A further example of trigonal geometry is that found in the bis(triphenylphosphine) adduct of silver bromide (Figure 1-10a), [85] which forms a monomer in the unsolvated complex (with a P_2Br coordination sphere), similar to the $(PPh_3)_2CuBr$ analogue. However recrystallisation from chloroform results in a dimeric bridged complex where silver atoms are in tetrahedral (P_2Br_2) environments (Figure 1-10b). [85] The dimeric form is as found in the bis(triphenylphosphine) adduct of silver chloride. [86]

(a)

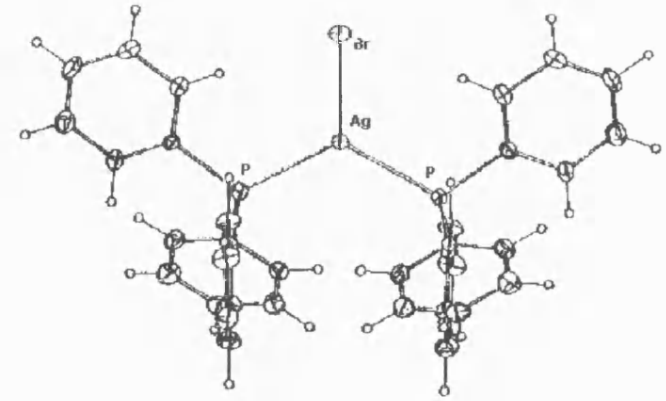

(b)

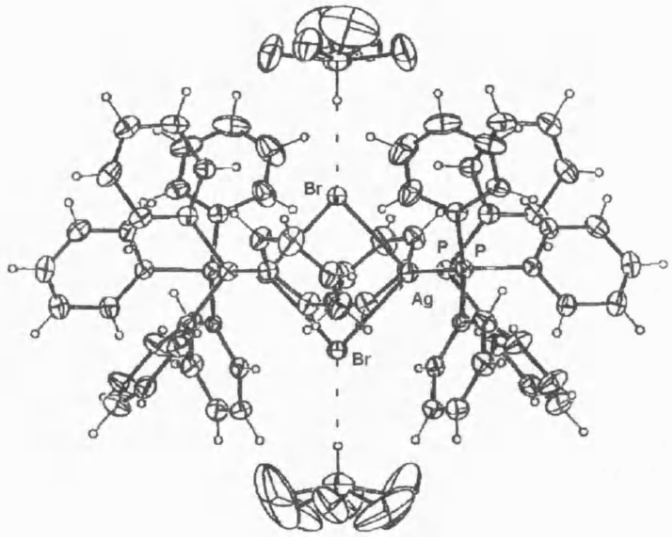

Figure 1-10 Structures of bis(triphenylphosphine) silver(I) bromide, (a) - unsolvated, (b) - chloroform solvate. [85]

Four-coordinate complexes are very common for silver(I), both as tetrahedral or, more commonly in sterically demanding situations, distorted tetrahedral geometries. 1:1 phosphine adducts of silver halides generally take the form of tetrameric 'cubane' or 'step' type complexes. Indeed with triphenylphosphine, the silver iodide complex can exist in either

structural form (Figure 1-11). [87] In the highly distorted 'cubane' structure, each of the four silver atoms is tetracoordinate, in the 'step' complex two are four coordinate, the remaining two trigonal. Reported results indicate that these two forms are fairly close in energy, the difference being of the order of van der Waals interactions.

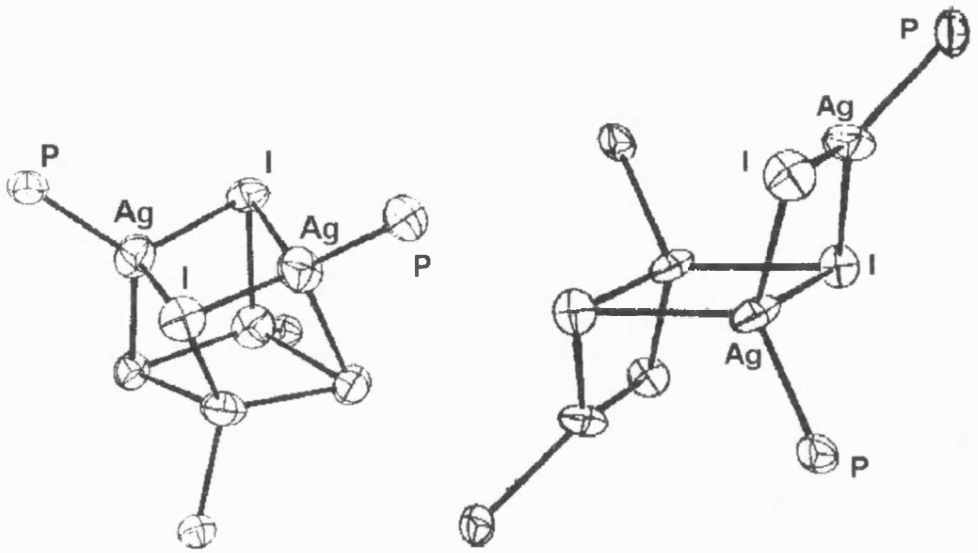

(a) (b)

Figure 1-11 Structures of (triphenylphosphine)silver(I) iodide, (a) - 'cubane' form, (b) - 'step' form. [87]

A central silver atom may be surrounded with four large donor ligands or, as in the case of $[Ag(dppe)_2]NO_3$ [dppe = 1,2-bis(diphenylphosphino)ethane, $Ph_2PCH_2CH_2PPh_2$] two bidentate ligands (Figure 1-12). [88] The Ag atom is coordinated by all four P atoms in a distorted tetrahedral geometry.

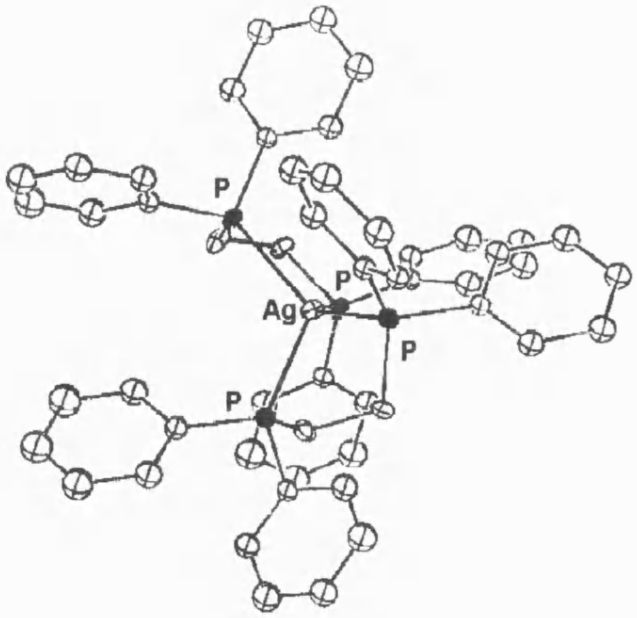

Figure 1-12 Structure of the cation of bis[1,2-bis(diphenylphosphino)ethane]silver(I) nitrate. [88]

Examples of five- and six- coordinate complexes are much less common, generally distorted and achieved with multidentate ligands. Five-coordinate silver, for example, was achieved after crystallising silver(I) perchlorate in the presence of 2,2':6',2" terpyridine and triphenyl-phosphine (Figure 1-13). [89] The silver achieves a distorted trigonal bipyramidal coordination with a N_3P_2 set of donor atoms. Other examples of penta-coordinate silver can be found in Schiff-base chemistry where N-containing macrocycles can fold to present several coordination sites for metal ions, for example $[Ag(BF_4)]_2L$ where L is a tetraimine Schiff-base macrocycle with N-isopropylidine bearing pendant arms. [90] These large macrocycles can hold two silver atoms, each forming five Ag-N bonds and in cases such as this the geometry around silver does not resemble any simple descriptive shape.

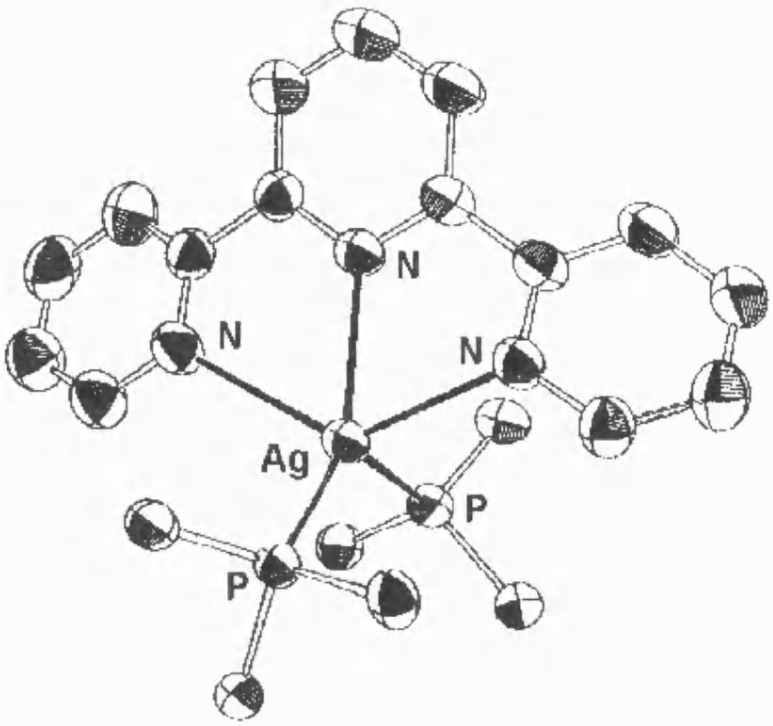

Figure 1-13 Structure of the cation of $[Ag(PPh_3)_2(terpy)]ClO_4$. [89]

The highest coordination number known for silver is six. In a complex of silver(I) perchlorate with the hexadentate podand tris[3-(2-pyridyl)-pyrazol-1-yl]borate, three silver atoms are found as a triangular cationic cluster within the environment of two ligands. [91] The silver coordination spheres are highly disordered and might loosely be described as octahedral. A similar geometry is found in the cation $[Ag([15]aneS_2O_3)]^+$ ([15]aneS_2O_3 = 1, 4, 7-trioxa-10, 13-dithiacyclopentadecane) where silver ions are bound within mixed thioether oxa crown molecules (Figure 1-14). [92] In this case the silver is bound to all potential donor atoms within the crown and an additional sulphur (S' in Figure 1-14) bridges from a second molecule to give a distorted octahedral S_3O_3 donor set.

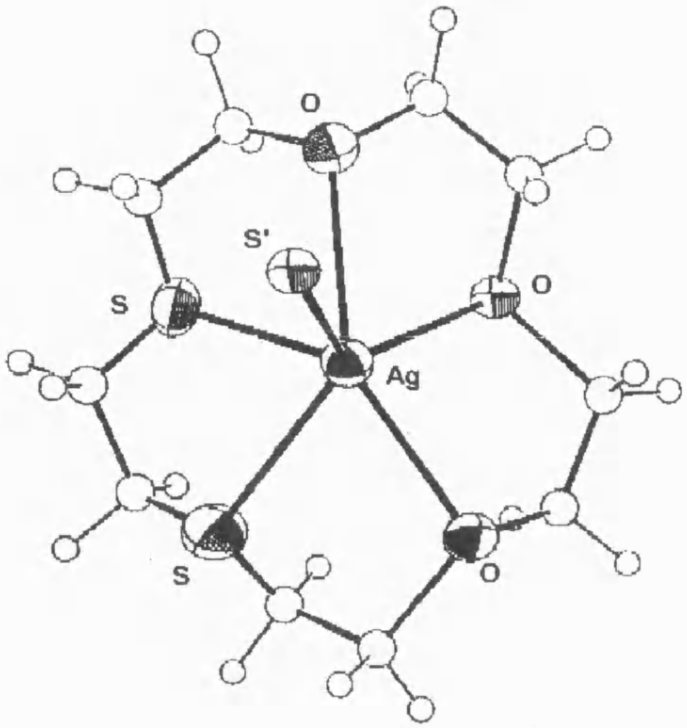

Figure 1-14 Structure of the cation $[Ag([15]aneS_2O_3)]^+$ in $[Ag([15]aneS_2O_3)]PF_6$.[92]

1.4 THE CHEMICAL VAPOUR DEPOSITION OF SILVER

Precursors for the CVD of silver currently fall into four groups of compounds halides: carboxylates, β-diketonates and organometallics (Figure 1-15). There are relatively few examples in the literature of the CVD of silver using halides, carboxylates and organometallics, and these are collected in Table 1-2. At present adducts of silver β-diketonates at present represent state of the art precursors for silver CVD and are the largest number of tested precursors. These are listed in Table 1-3. Examples in both tables are limited to cases where details of film growth conditions are reported.

Inorganic precursors were first studied in 1972 when silver deposition was achieved selectively on silicon with AgF vapour. [93] Deposition was found to occur over a wide temperature range (80-600°C) but very low pressures (10^{-6} Torr) were required. The reaction was thought to proceed via etching of the silicon substrate to form SiF_4 after formation of the initial silver layer. This would necessitate diffusion of silicon through the silver to react at the surface. The silver film was found to adhere well to the substrate and this might indicate significant diffusion of silicon into the silver film.

More recently, commercially available silver halides were tested at 300-900°C in an argon-hydrogen atmosphere at 30 Torr. [19] Deposition was carried out onto Al_2O_3 substrates using a powder feed delivery system. AgI was found to achieve the most complete deposition of silver at rates of up to 5000 nm min^{-1} at 800°C, the deposition being smooth and continuous under these conditions. The overall pressure and partial pressure of hydrogen in the reactor were found to be critical to the film growth.

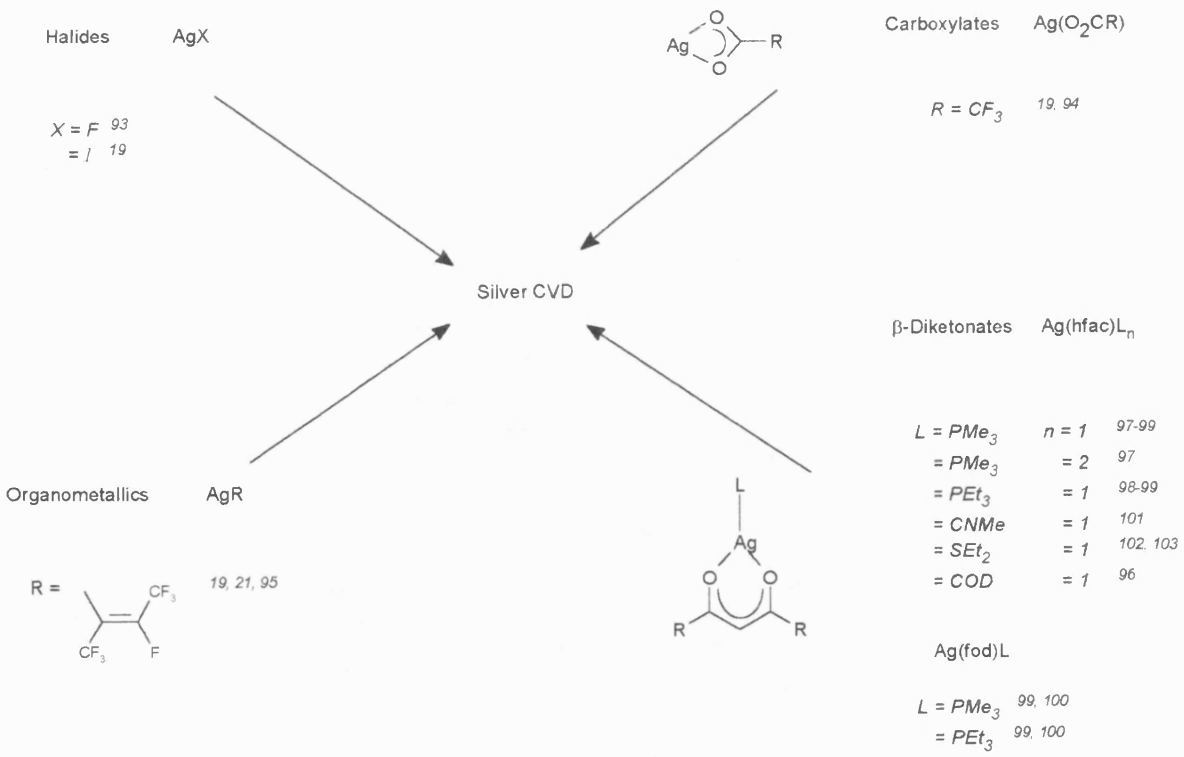

Figure 1-15 Precursors used for the Chemical Vapour Deposition of Silver

Table 1-2 Literature reported silver CVD experiments involving silver halide, carboxylate or organometallic precursors.

Precursor	Substrate	Technique [a]	Temperature (°C)	Pressure (Torr)	H_2 present ?	Growth rate (nm min^{-1})	Ref
AgF	Si	LPCVD	80-600	10^{-6}	no	50-500	93
AgI	Al_2O_3	thermal	800	30	yes	5000	19
AgO_2CCF_3	Si, SiO_2, ceramics	LACVD	NA [b]	vacuum	no	NA [b]	94
AgO_2CCF_3	Al_2O_3	thermal	600	30	yes	100	19
$[CF_3CF=C(CF_3)Ag]_4$	various	PECVD	120	0.2	yes	5.5	95
$[CF_3CF=C(CF_3)Ag]_4$	Al_2O_3	thermal	300-700	30	yes	90-110	19
$[CF_3CF=C(CF_3)Ag]_4$	borosilicate glass	LPCVD	275	10^{-4}	no	2.8	21

[a] LPCVD = low pressure CVD, LACVD = laser assisted CVD, PECVD = plasma enhanced CVD [b] NA - not available

A number of silver carboxylates are also commercially available precursors and are reported as limited by low volatility. To date silver trifluoroacetate has been the only carboxylate investigated, by two independent studies. In 1986, in an anonymous brief report, it was disclosed that silver films could be deposited using a laser-assisted technique (LACVD). [94] Silver films were grown under vacuum onto Si, SiO_2 and ceramic substrates, though no growth data were given. It was postulated that the mechanism involved pyrolysis at the heated surface (rather than gas-phase or active site excitation). More recently CVD of silver trifluoroacetate has been achieved thermally onto Al_2O_3. [19] The most uniform films were deposited at 600°C, at 30 Torr in the presence of H_2, with growth rates of approximately 100 nm min^{-1}. Again H_2 was found to be significant, film thickness increasing with H_2 partial pressures and films became insulating at low P_{H_2}. XRD and AES did not detect impurities in the film, although computational studies predicted carbon would be present.

For organometallics, precursors generally quoted are adducts of silver cyclopentadienyl compounds (for which no film growth details have been published) or the compound perfluoro-1-methylpropenyl silver (I) $\{[CF_3CF=C(CF_3)Ag]_4\}$. Perfluoro-1-methylpropenyl silver (I) was initially used as a precursor with plasma enhanced deposition (PECVD). [95] In an argon-hydrogen atmosphere at 0.2 Torr films could be deposited between 40-150°C on a number of different substrates such as glass, quartz, Si (100), copper, aluminium, aluminium oxide and polyimide. Control experiments showed that the thermal CVD contribution was negligible under these conditions. Hydrogen was again important, although only small amounts were required (e.g. >20%), high resistance coatings being obtained if hydrogen was not present. Films examined by XPS showed small amounts of carbon and oxygen, though only at the surface, fluorine not being identified in the film.

The same precursor has been used for thermal CVD experiments. [19] At 700°C in the presence of an Ar/H_2 atmosphere at 30 Torr, silver films were deposited on Al_2O_3 at rates of up to 110 nm min^{-1}. At lower temperatures, growth rates were still appreciable, i.e. at 300°C, deposition rates were 90 nm min^{-1}. The content of H_2 in the atmosphere was found not to be critical, films being uniform with little or no porosity irrespective of H_2 flow. No chemical impurities were found by AES, although silver oxide was identified by XRD when little or no H_2 was used. In other thermal CVD deposition experiments using the same precursor [21] silver films were deposited onto borosilicate glass. At 275°C, 10^{-4} Torr, rates were up to 2.8 nm min^{-1}. Apparently hydrogen was not used in these experiments. XPS indicated trace fluorine and oxygen but no carbon. The oxygen was also found to be depth related which might indicate post-experiment oxidation of the film. XRD experiments indicated that films were amorphous and made up of agglomerations of particles and voids.

By far the largest source of precursors, particularly since 1992, has been the various adducts of silver β-diketonates [Ag(β-diketonate)L, where L is a neutral donor ligand]. Of note are the olefin, phosphine, isocyanide and thioether adducts. These precursors have been used to grow films by conventional thermal techniques, with aerosol delivery being used most recently.

The earliest silver β-diketonate CVD example (1992) used the Ag(hfac)COD (hfac = 1,1,1,5,5,5-hexafluoroacetylacetonate, COD = 1,5-cyclooctadiene) olefin adduct as a precursor. [96] The precursor was heated to 60°C and with a carrier gas of H_2/He, films were grown at 250°C. Films were of shiny appearance and had total impurities of less than 5%. β-Diketonate-olefin adducts can be sublimed (and hence volatilised), however the sublimation is accompanied by some decomposition. At higher temperatures this is due to olefin loss to give the relatively involatile $[Ag(hfac)]_n$ compound.

It was suggested in the literature that adducts with stronger metal-ligand interactions would prove more stable to volatilisation and a number of phosphine adducts of the same β-diketonate were synthesised and tested. The mono- and bis- trimethylphosphine adducts were prepared and proved to be reasonably volatile (both sublimed easily in vacuo at 20-50°C). [97] Silver films were grown from these precursors in the presence of H_2 in the temperature range 200-425°C. Films could be grown on glass, silicon, copper, tungsten, aluminium and nickel. Under vacuum these same precursors would only deposit on copper. It was suggested that this was due to the etching of the copper to produce the volatile and stable $Cu(hfac)_2$. Auger Electron Spectroscopy established the interior of the films to contain less than 1% C, O and F contaminants.

In similar studies the complexes Ag(β-diketonate)L [β-diketonate = hfac, [98, 99] fod (2,2-dimethyl-6,6,7,7,8,8,8-heptafluoroocta-3,5-dionate), [99, 100] L = PMe_3, PEt_3] were prepared and tested. These compounds were found to be low melting point solids and volatile enough to be used for conventional thermal CVD. Conditions were optimised for the precursors with regard to carrier gas, pressures and temperature, for decomposition on glass, silicon and copper. It was found that hfac compounds were capable of producing films with 5-10% C at 310-350°C at 10^{-2} Torr without the presence of H_2. Growth rates for $Ag(hfac)PMe_3$ were as high as 33 nm min^{-1}, but the use of H_2 under these conditions caused premature reaction within the precursor reservoir.

Adducts of Ag(fod) were found to have increased stability and required more extreme conditions to allow for film growth (10^{-4} Torr, 370-380°C). Under these conditions film quality was poor, with 16-34% C, and 4-5 % O contamination. In addition trace fluorine was found in films grown with the PMe_3 adduct, and trace phosphorus with the PEt_3 adduct. The trace

Table 1-3 Literature reported silver CVD experiments involving silver β-diketonate adducts as precursors

Precursor	Substrate	Technique [a]	Temperature (°C)	Pressure (Torr)	H_2 present ?	Growth rate (nm min^{-1}) [b]	Ref
Ag(hfac)COD	various	thermal	250	atmospheric	yes	NA	96
$Ag(hfac)(PMe_3)_n$ [c]	various	thermal	200-425	atmospheric	yes	NA	97
$Ag(hfac)PMe_3$	glass	thermal	310	0.05	no	33	98
$Ag(hfac)PEt_3$	glass	thermal	250-350	0.05	no	NA	98
$Ag(fod)PMe_3$	glass / Si / Cu	thermal	300	0.1	yes [d]	NA [e]	99
$Ag(fod)PEt_3$	glass / Si / Cu	thermal	230-260	0.1	yes [d]	NA	99
Ag(hfac)CNMe	glass / Si	thermal	250	0.1	yes	NA	101
$Ag(hfac)SEt_2$	Cu coated Si	AACVD	200	atmospheric	no	40	102

[a] AACVD - aerosol assisted CVD [b] NA = not available [c] n = 1, 2 [d] H_2 was passed through a water bubbler before entering the CVD chamber [e] at 310°C, 10^{-4} Torr in the absence of H_2 this precursor is reported to have a growth rate of up to 33 nm min^{-1}

phosphorus was suggested to be due to β-elimination on PEt_3 to give ethylene, H_2 and phosphido groups, the latter not being so readily be desorbed from the growing film. These Ag(fod) adducts could be deposited in the presence of H_2 or moist H_2 (H_2 bubbled through water) to give better films at less extreme conditions (10^{-1} Torr, 230-300°C, 0-9% C, 0-5% O). [99]

Since alkyl isocyanide adducts of platinum, gold and copper are known to be successful precursors for metal CVD, this argument was extrapolated to silver and Ag(hfac)(CNMe) was prepared and examined as a potential thermal CVD precursor. [101] Using this compound, films could be deposited on silicon or glass in the range 250-320°C, under vacuum (10^{-4} Torr). Impurities were significant (16% C, 7% O by XPS), although in the presence of H_2 (at 10^{-1} Torr) films could be grown at 250°C with no detectable impurities.

Recently aerosol-assisted techniques have been used to grow silver [102] and silver alloy (Ag-Pd, Ag-Cu) [103] films using the precursor $Ag(hfac)SEt_2$. This compound was chosen to demonstrate this technique because of its insignificant volatility, which precludes its use with conventional vaporisation techniques. In the first study [102] the precursor was dissolved in toluene and nebulised at room temperature. The carrier gas (N_2) swept the aerosol through a heated tube at 80°C to allow vaporisation to take place, to a copper coated silicon substrate at 120-250°C. Growth rates at 200°C were of the order of 40 nm min^{-1}. Impurities could not be detected by XPS and electrical conductivities were good. In more recent work the same precursor was used to grow alloy films at 250-275°C. [103] The precursors were again dissolved in toluene, nebulised and carried to the reaction zone through a preheat zone at 70-80°C. In this study however the argon carrier gas contained 10 % H_2 and deposition rates were 18-22 nm min^{-1} on SiO_2 substrates.

1.5 SPECIFIC AIMS AND SYNTHETIC STRATEGIES

The specific aim of this study was to prepare and characterise compounds which might be useful as precursors for the CVD of silver. Compounds have been screened and tested to examine film growth qualities using purpose-built apparatus in order to evaluate the relationship between molecular structure and film growth. The work also aims to identify areas of silver chemistry which might prove useful for further synthesis.

Compounds prepared and reported in this thesis fall into four main categories: silver carboxylates, silver fluorocarboxylates, silver β-diketonates and organosilver compounds. While the chemistry of these compounds varies from case to case, synthetic strategies used to promote stability and increase volatility are general in nature and will be discussed briefly here.

As outlined in preceding sections, silver compounds have a tendency to aggregate. Where silver compounds exist in polymeric arrays, volatility is very low. Additionally volatilisation may require significantly high temperatures to break intermolecular interactions and this can cause decomposition of the precursor due to the concomitant breaking of intramolecular bonds.

The strategy adopted involves preparing compounds which do not oligomerise but ideally exist in the molecular form as discrete monomers or low molecular weight oligomers (typically tetramers or less). Thus energy to break intermolecular/interoligomer attractions will be low, volatility will be high and at temperatures normally required for volatilisation, molecular stability will be increased. Additionally, problems of stability in general need to be addressed. For ease of handling, precursor compounds ideally should be thermally stable, as well as resistant to oxidation, hydrolysis and photolysis. The solutions to these two major problems

largely coincide, as the break up of aggregates and increase in molecular stability can be achieved in a number of ways, such as the use of steric hindrance and coordinatively saturating the metal centre.

The monovalent character of silver has a large impact on the oligomerisation properties of silver. Coordination compounds containing unsaturated silver centres may oligomerise readily by the formation of additional metal-ligand bonds, the extra ligands arising from neighbouring molecules. Organometallic silver compounds are also prone to remove coordinative unsaturation by this method although the generation of multi-silver atom species is also common. Strategies employed to inhibit oligomerisation are summarised schematically in Figure 1-16.

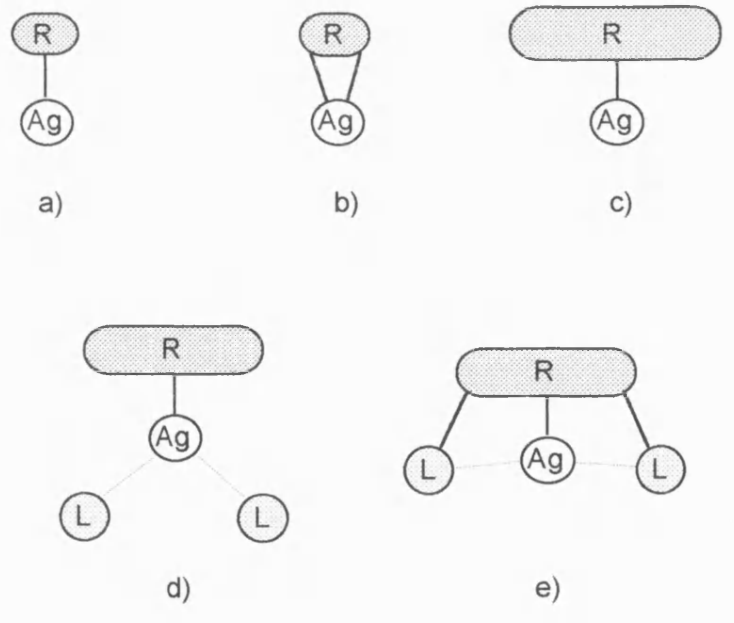

Figure 1-16 Schematic representation of strategies employed in this study.

- The use of potentially multidentate anions (such as carboxylates and β-diketonates) [Figure 1-16 (b)] will help to intramolecularly fully coordinate the metal, silver being in most cases tetra-coordinate or less. In addition, this will strengthen intramolecular bonding with respect to intermolecular attractions [as compared to ligands bound through only one bond Figure 1-16 (a)].

- Large organic groups can be incorporated into the precursor to cause maximum disruption to potential intermolecular metal-ligand interactions. The design of ligands and prediction of the structure of precursors can be more straightforward where rigid structures (e.g. a phenyl ring) allow for more topographical control of other potential pendant donor groups attached to them, in relation to the position of the metal.

- The use of fluorinated organic groups is well known to reduce melting points of compounds. Ligands partially or completely fluorinated are often used in CVD. Their beneficial effect is thought to be due to a decrease in van der Waals attractions.

- The use of neutral donor molecules to form adducts [Figure 1-16 (d)], will favour a reduction in oligomerisation through coordinative saturation and in the case of large donor ligands, through steric hindrance. Typical donor molecules might include olefins, phosphines and thiols.

- The use of neutral donor species might be extended if additional donor atoms are found within the anionic ligand [Figure 1-16 (e)]. In this way intramolecular bonding will be further increased and smaller oligomers will be favoured.

These strategies have been employed throughout this study, often in combination. However, several points should be borne in mind. Clearly there exists a point at which advantages gained reducing aggregation by adding more molecular weight of the precursor, will not overcome the disadvantages of increasing the mass of the precursor molecule. At this point addition of further ligands will reduce volatility. Additional molecular weight particularly in rigid systems will however allow for greater crystallinity. This is useful with respect to characterisation, ease of purification and topographic control, but it will however have a detrimental effect on volatility (although the extent of this is difficult to quantify). Similarly use of long chains will bring disorder to the molecule, decreasing crystallinity, decreasing the melting point and increasing the volatility, although this possibility has not been fully explored in this thesis.

CHAPTER TWO

SYNTHESIS, CHARACTERISATION AND CVD PROPERTIES OF SILVER(I) CARBOXYLATES AND THEIR PHOSPHINE ADDUCTS

2.1 INTRODUCTION

Silver carboxylate chemistry has been stimulated by the number of areas where these compounds find application. Historically they have found use in organic chemistry where their degradation by halogens provides a convenient method for the preparation of alkyl halides (the Hunsdieker reaction) and esters (Simonini reaction). [104, 105] They have also found extensive use as catalysts in the polymerisation of urethane [106] and in recent years there has been interest in the biocidal activity of phenoxycarboxylates and their silver salts. [107]

Silver carboxylates were considered to be a primary class of precursors for silver CVD. Known to be light sensitive and largely insoluble in all but the most polar solvents (e.g. H_2NR, DMSO), this class of compounds was considered worthy of investigation for a number of reasons. The carboxylate groups are potentially multidentate ligands, allowing for greater stability and coordinative saturation around the metal. These compounds are known to be thermally stable at low temperatures (below several hundred degrees Centigrade), and are thought to decompose like many metal carboxylates via a decarboxylation mechanism (Eqn. 2-1). [108] Such a mechanism would yield unstable organometallic species *in situ*, thus these compounds have the capability of use as 'masked' organosilver precursors.

$$RCO_2Ag \xrightarrow{\triangle} R\text{-}Ag + CO_2 \qquad \textbf{(2-1)}$$

Decarboxylation has been implicated in thermal decomposition, [109, 110] and mass-spectrometry studies. [111-113] The Hunsdieker reaction, which is essentially the thermal decarboxylation of a silver carboxylate in the presence of halogen and mercuric oxide, (Eqn. 2-2) is thought to

proceed via a free radical mechanism and formation of small quantities of the alkane R-R supports this view. Mass-spectrometry studies have explored parallels with thermal decomposition of silver carboxylates. [112]

$$R\text{-}CO_2Ag + Br_2 \xrightarrow{\triangle\ /\ HgO} R\text{-}Br + CO_2 + AgBr \qquad \textbf{(2-2)}$$

Decarboxylation may occur readily, only to be followed by a fast decomposition of transient organosilver species. Thermal analysis studies would not be expected to support such mechanistic proposals. Mass spectrometry however has identified organosilver fragments from the decomposition of silver carboxylates and these experiments show that such organometallic species are found in greater abundance where R is aromatic or fluorinated.

2.1.1 Synthetic Routes

Silver carboxylates are extremely easy to prepare owing largely to their insoluble nature in aqueous solutions. Preparation can be effected by a number of routes.

I) If the acid is available as a water soluble salt, the simplest preparation involves precipitation by addition of solutions of silver nitrate and the carboxylate salt. (Eqn. 2-3) The resulting precipitate can be filtered, washed with distilled water to remove by-products and dried.

$$AgNO_3 + NaO_2CR \longrightarrow AgO_2CR + NaNO_3 \qquad \textbf{(2-3)}$$

II) The silver salt may be prepared by reaction of the free acid and silver oxide (Eqn 2-4). This method requires some solubility of the acid in aqueous solution and only the stronger acids will react quantitatively. The yield may be enhanced by the use of freshly prepared silver oxide (a dark brown suspension of silver hydroxides precipitated by addition of alkali to Ag^+ aqueous solutions).

$$Ag_2O + 2HO_2C\text{-}R \longrightarrow H_2O + AgO_2CR \qquad \textbf{(2-4)}$$

This method has found greatest use in cases where the salt was found to be soluble in water. In such cases, the mixture was filtered (to remove excess Ag_2O) and the solvent and excess acid allowed to evaporate. The route also requires a relatively low boiling acid (less than 120°C).

III) By far the most useful preparative method used in this study involved the reaction between ammonium salts of the carboxylic acids and silver nitrate. Free carboxylic acids suspended in water may be solubilised with a few drops of concentrated ammonia solution, to form the ammonium salt *in situ*. At this stage unreacted acid may be filtered off, and stirring with gentle warming will remove excess ammonia. Reaction of this ammonium salt *in situ* with silver nitrate will result in an immediate precipitate in most cases (Eqn. 2-5).

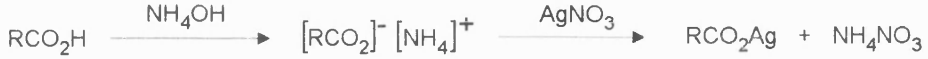

$$RCO_2H \xrightarrow{NH_4OH} [RCO_2]^- [NH_4]^+ \xrightarrow{AgNO_3} RCO_2Ag + NH_4NO_3 \qquad \textbf{(2-5)}$$

2.1.2 Structural chemistry

A variety of silver carboxylates have been isolated, and a number have been structurally characterised. With a range of these compounds now crystallographically determined, a number of structural features have become apparent. These are summarised in Table 2-1 and Figure 2-1. Silver carboxylates and the related silver-betaine complexes can be classified as typically belonging one of seven structural types (see Figure 2.1). [114] Silver-betaine structures will not be discussed here, for more information the reader is directed to a number of references. [114-119]

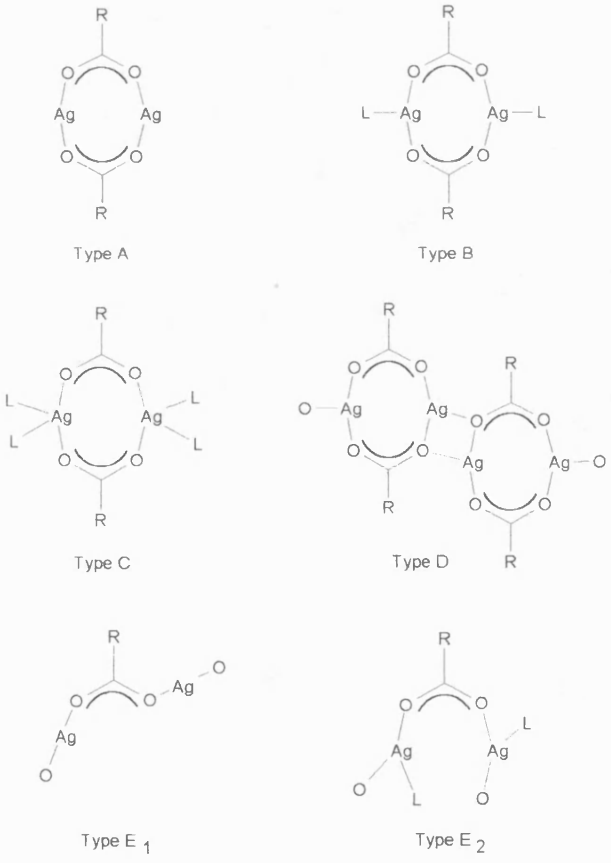

Figure 2-1 Principal structural types of silver(I) carboxylates and related compounds.

(L represents a donor atom from an adjacent sub-unit, typically oxygen from O_2CR, $OCNH_2$, H_2O)

Table 2-1 Continued

2-chlorophenoxyacetate	$0.5(AgClO_4)$	---	½	1	0	0	0	polymeric	2.809	134
phenylthioacetate	---	---	0	1	0	0	0	polymeric	---	135
2-carbomoylphenoxyacetate			0	1	0	0	0	polymeric (B)	3.001	124
glutarate	---	---	0	1	0	0	0	polymeric (D)	2.804	145
sulphoacetate	---	H_2O	0	0	1	0	1	polymeric	3.071	129
glycolate	---	---	0	1	1	0	0	polymeric	2.881	146
furanoate	---	---	0	0	1	0	0	polymeric (D)	2.881	133
oxalate	---	---	0	0	1	0	0	polymeric (C)	2.945	126
malonate[b]	---	---	0	0	1	0	0	polymeric (C)	2.851	127
glycine nitrate	---	---	1	0	0	0	0	dimeric (A)	2.877	123
citrate	$0.5(NH_4^+)$	H_2O	0	0	2	0	0	polymeric	2.845	107
tartrate	Sb^{3+}	H_2O	0	0	2	1	1	linked tetramers	2.992	130
citrate	Sb^{3+}	---	0	1	0	0	0	tetranuclear dimers	3.221	147
cyclohexane carboxylate [c]	---	---	1	0	1	0	0	OH bridged dimers	2.778	141

[a] in cases where more than one significant Ag-Ag distance was determined, the smaller is given [b] the structure also exhibits univalent silver atoms [c] 3-hydroxy-4-phenyl-2,2,3-trimethylcyclohexanecarboxylate

Table 2-1 Structural data for silver(I) carboxylates and related compounds

Carboxylate	Other species present		CN of silver atoms					Structural Type (A-E)	Ag-Ag	Reference
	anions	ligands	2	3	4	5	6		distance (Å) [a]	
benzoate	---	---	1	0	0	0	0	dimeric (A)	2.902	120
4-hydroxybenzoate	---	---	1	0	0	0	0	dimeric (A)	2.915	120
2-hydroxybenzoate	---	---	1	0	0	0	0	dimeric (A)	2.861	143
2,6-dihydroxybenzoate	---	---	1	0	0	0	0	dimeric (A)	2.910	143
4-aminobenzoate	---	---	0	1	0	0	0	polymeric	2.92	132
2-nitrobenzoate	---	---	0	0	2	1	0	polymeric	2.804	140
4-nitrobenzoate	---	$0.5(NH_3)$	1	1	0	0	0	polymeric no rings	3.151	144
phenoxyacetate	---	---	0	1	0	0	0	polymeric (D)	2.866	128
4-fluorophenoxyacetate	---	H_2O	0	1	1	0	0	tetramers (D)	2.836	128
perfluorophenoxyacetate	---	---	1	0	0	0	0	dimeric (A)	2.943	121
4-chloro-2-methyl phenoxyacetate	---	---	2	0	0	0	0	zig-zag polymer (E_1)	---	134
2,4-dichlorophenoxyacetate	---	---	2	0	0	0	0	zig-zag polymer (E_1)	---	134

The vast majority of silver carboxylate structures are based around linkage of dimeric sub-units made up of 8-membered bis(carboxylato-*O,O'*)bis(silver) rings. These rings are in most cases essentially flat, with OCO bond angles typically much less than the OAgO angles which tend to approach linearity (160-170°). Differences within this class of compounds are derived in the main from the way these sub-units are assembled, either as discrete dimers (Type A - Figure 2-1) or as a variety of polymeric structures (Types B-E - Figure 2-1). Polymerisation is achieved through additional bonds to silver atoms of individual dimers using other donors (carboxylate or otherwise) originating from adjacent sub-units.

Type A structures have no additional donors on the silver, examples being the benzoate, [120] *p*-hydroxybenzoate, [120] perfluorophenoxyacetate [121] and the related silver glycylglycine nitrate [122] and glycine nitrate. [123] Silver-oxygen bond lengths in type A structures are of the order of 2.2 Å. Type B structures are distinct from type A in that the silver centres accept donors parallel to the Ag-Ag vector to form a polymer of bridged dimeric sub-units. An example of this structure can be found with silver carbamoylphenoxyacetate where the silver atoms are additionally bonded to oxygen atoms on the carbamoyl ($OC-NH_2$) group (Figure 2-2). [124] The silver-carbamoyl oxygen bonds in this case are of the order of 2.49 Å, the ring Ag-O bonds found in the range of 2.23-2.27 Å.

Type C structures have two additional donors perpendicular to the O-Ag-O vector. In cases where oxygen bridges to other sub-units are found, Ag-O bond lengths range 2.5-2.7 Å. Examples include silver oxalate [125, 126] and malonate. [127] Additional long range interactions can often be identified which are not formally recognised as bonds. In the citrate structure two individual Type C dimer units exist, one with silver bonded additionally to carboxylate oxygen

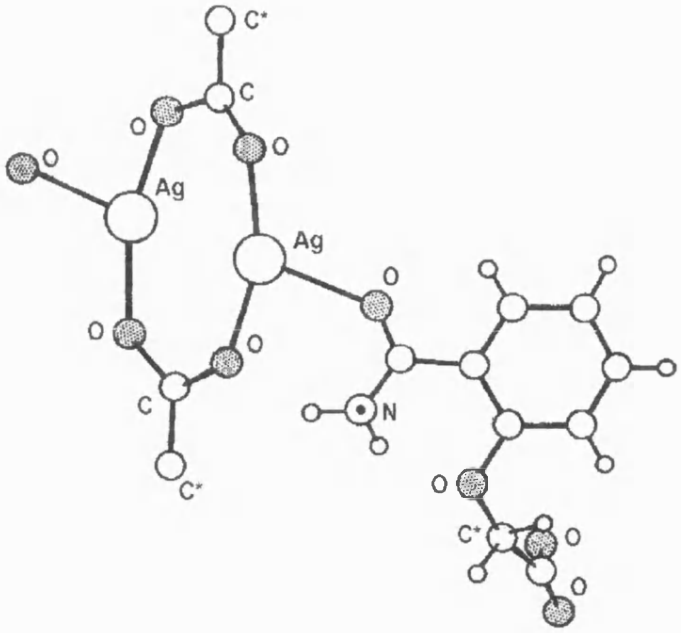

Figure 2-2 Crystal structure of silver(I) carbamoylphenoxyacetate, [124] (Type B).

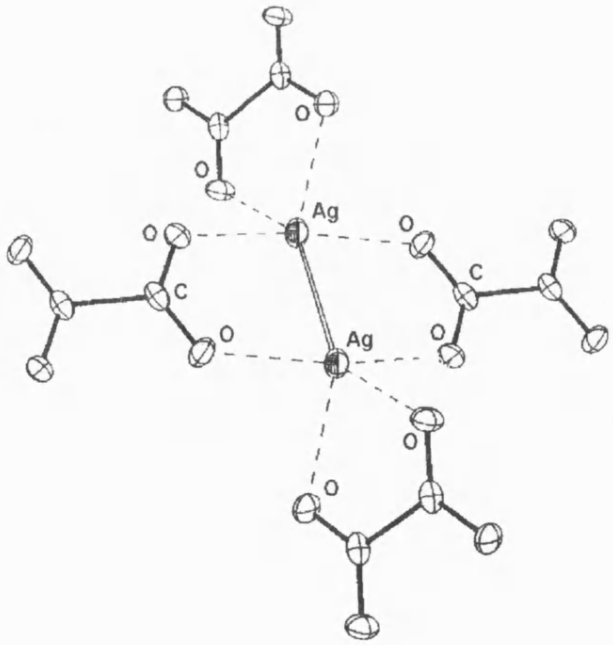

Figure 2-3 Crystal structure of silver(I) oxalate, [126] (Type C).

atoms, the other with silver bonded additionally to carboxylates and water molecules. [107] Although silver carboxylates are invariably prepared in aqueous environments and hydrates and hemihydrates are common, water co-ordination to silver atoms as shown in the citrate is rare. Other examples where water coordination occurs include the 4-fluorophenoxyacetate, [128] sulphoacetate, [129] and the antimony(III) silver(I) (+)-tartrate. [130]

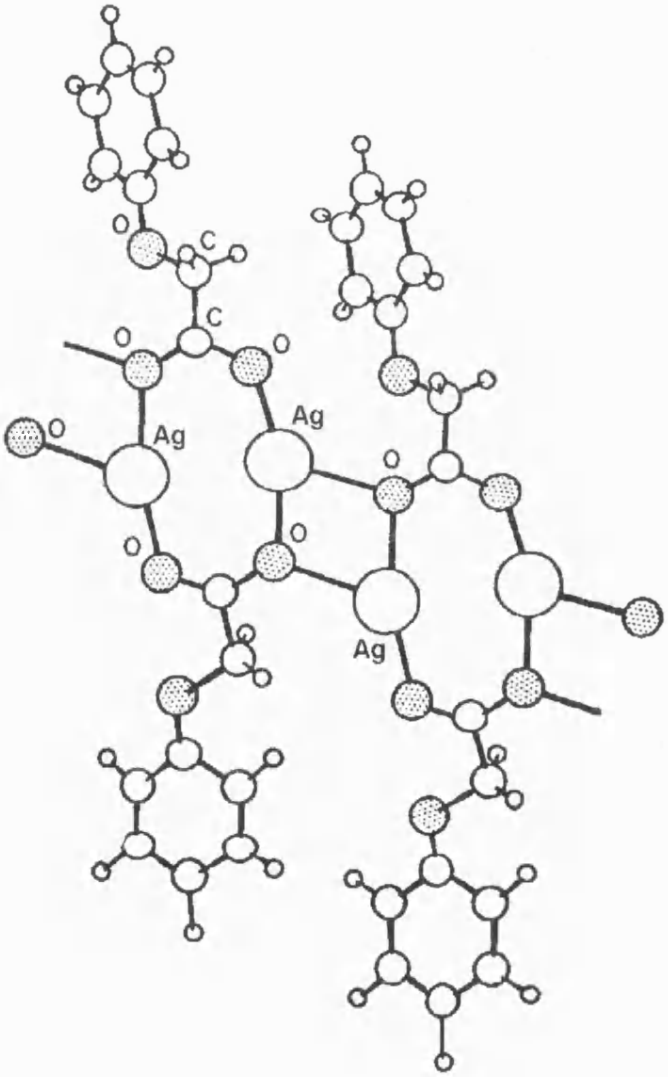

Figure 2-4 Crystal structure of silver(I) phenoxyacetate, [128] (Type D).

The type D step polymer is very common with the smaller and functionally simpler carboxylates. Dimeric sub-units are found to line up in a ladder type formation to allow oxygen and silver atoms to bond to silver and oxygen on adjacent dimers, thus forming four-membered AgOAgO rings. Typical examples include the 4-aminobenzoate, [132] phenoxyacetate [128] and the furoate (furan-2-carboxylate). [133] The latter compound exhibits an interesting structure where *every* oxygen within the carboxylate groups is bridging to another dimer, in other cases of type D structures only half of the oxygens bridge to other dimers. A further variation of this type is found with the 4-fluorophenoxyacetate, [128] which has structural similarities with type D.

Only a few examples of these compounds not taking up structures based on the bis (carboxylato-*O,O'*) dimer are known, these have been classified as types E_1 and E_2, both of which are polymeric. Structures of the type E_1 are found with 2,4-dichlorophenoxyacetate and 4-chloro-2-methylphenoxyacetate [134] which form zig-zag chains. The E_2 type structure is shown in the (pyridinebetaine)silver(I) system, which is the only known example of a *syn-syn* bridged one-dimensional polymer. [114]

When additional donors can be found in the molecule, particularly where multidentate coordination is possible, such as the (phenylthio)acetate, [135] or the pyridinecarboxylates, [136-138] the basic dimeric structure for these compounds is less common. In the Ag-Gd complex with 2,6-pyridinedicarboxylic acid, silver is not found in dimeric sub-units but takes up a bridging role itself between monomeric $Gd(dipic)_2$ molecules (H_2dipic = 2,6-pyridine dicarboxylic acid), in the form of 4-membered AgOAgO rings (common to type D). [139]

The prevalence of bis(carboxylato-*O,O'*)disilver(I) dimers in silver carboxylate structures has lead to some discussion of the extent of Ag-Ag bonding in such species. In cases where Ag-Ag distances are significantly less than that found in the metal (2.89 Å), for instance such as the 2-nitrobenzoate (2.809 Å) [140] and the 3-hydroxy-4-phenyl-2,2,3-trimethylcyclohexanecarboxylate (2.778, 2.834 Å), [141] silver-silver bonds have been formally recognised. In general, Ag-Ag distances range from 2.78-3.22 Å and have been seen in the main as indicative of possible silver-silver interactions, although some authors have held other views. [142]

The structural nature of silver carboxylates changes as other possible donor groups are incorporated into the system. In the case of the thiophenoxyacetate [135] and the pyridine-2-carboxylate, [136] structural classifications previously discussed become obsolete as chelate effects break up dimeric based structures. The addition of neutral donor molecules to silver carboxylates is thought to have a similar effect due to a combination of steric and electronic effects. A wide variety of adducts of silver carboxylates (the majority involving phosphine ligands) have been isolated and characterised. [148, 149] These adducts are significantly more soluble in organic solvents and, particularly with triphenylphosphine as the additional ligand, are thermally and light stable solids. Their solution chemistry has also been investigated. [150] Adducts of silver carboxylates whose structures have been elucidated are summarised in Table 2-2.

The 1:1 pyridine adduct of silver benzoate which can be isolated from recrystallisation of the silver salt from neat pyridine, [151] forms a one-dimensional chain similar to that found in type D. In this case each silver is four-coordinate to three oxygens and a nitrogen (Figure 2-5), pyridine ligands bonding from above and below the chain. This is an unexpected result when viewed in comparison to the structure of silver benzoate, the latter being an unbridged type A dimer.

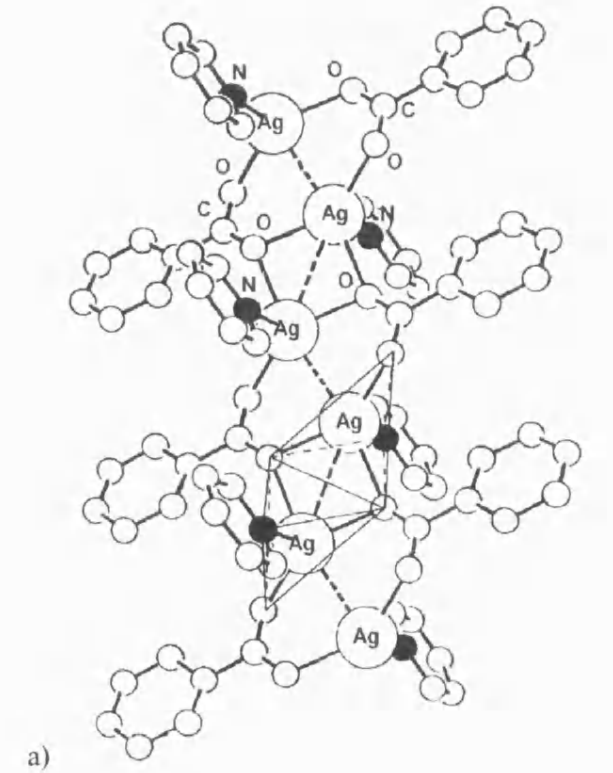

a)

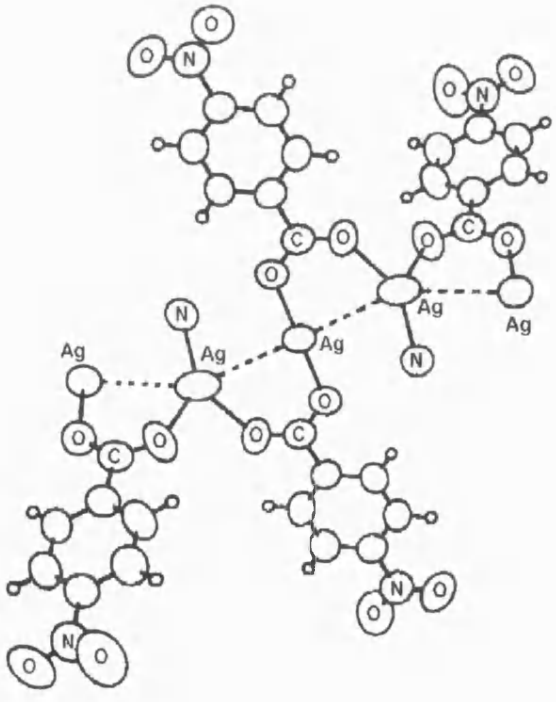

b)

Figure 2-5 Structures of silver(I) benzoate pyridine adduct [151] (a) (nitrogen atoms are shaded) and ammine silver(I) *p*-nitrobenzoate [144] (b).

Addition of ligands would be expected to reduce oligomerisation due to steric effects, however in this example this appears not to be the case. Similarly, the formation of the benzene adduct of silver trifluoroacetate is also known not to cause a reduction in aggregation. [142]

A similar N-donor adduct of silver(I) 4-nitrobenzoate was isolated from a concentrated ammoniacal solution. [144] A structure determination shows the presence of one ammonia molecule per two silver atoms. The $(AgOCO)_2$ rings are broken, though the carboxylates remained bridging in the *syn-syn* configuration, leaving a polymeric backbone based around a silver 'chain' (Figure 2-5). Silver-silver distances in this structure are 3.151 Å suggesting no formal bonding.

More extensive investigations have been carried out on adducts containing either mono- or bi-dentate phosphines, no doubt due to their stable crystalline nature. The 1:1 $Ag:PPh_3$ adduct of bis(1,8-napthalenedicarboxylato)silver(I) was found to exist as a tetranuclear cluster. [152] The four independent silver atoms were surrounded by one phosphorus and three or four oxygen atoms. The carboxylato groups are bound to silver in both chelating and monodentate modes. In this adduct there are no dimeric sub-units, although there is no reason to assume that the carboxylate itself would assume that configuration.

The structure of the 1:1 triphenylphosphine adduct of silver acetate has also been determined as a tetranuclear cluster [153] (Figure 2-6). Dimeric sub-units are found in this structure, although puckered into boat conformations. Two dimers are bonded together via Ag-O bonds from the carboxylate, much the same as in structural type D. There are two silver environments, one trigonal three-coordinate, the other tetrahedral in nature, made up of one phosphorus and two or three oxygens respectively.

Table 2-2 Structural data for adducts of silver(I) carboxylates.

Compound	Ligand	Ag:L	Structural type	Ag coordination sphere [a]	Ref
AgO_2CH	PPh_3	1:2	monomer	tetrahedral (O_2P_2)	154
AgO_2CH	dppf [b]	2:3	dimer	tetrahedral (OP_3)	157
AgO_2CCH_3	PPh_3	1:1	tetramer	trigonal (O_2P), tetrahedral (O_3P)	153
AgO_2CCH_3	dppm [c]	2:1	tetramer	trigonal (O_2P)	156
AgO_2CCH_3	dppm [c]	1:1	dimer	distorted tetrahedral (O_2P_2)	156
AgO_2CCH_3	dppf [b]	2:1	tetramer	tetrahedral (O_3P)	157
AgO_2CCH_3	N_2S_2-macrocyle	1:1	monomer	square pyramidal (ON_2S_2)	158
$AgO_2CC_6H_5$	C_5H_5N	1:1	polymer	distorted tetrahedral (O_3N)	151
$AgO_2CC_6H_5$	dppf [b]	2:1	dimer	trigonal (O_2P)	157
$Ag_2(O_2C)_2C_{12}H_6$	PPh_3	1:2	tetranuclear dimer	tetrahedral (O_3P), sqr-pyramidal (O_4P)	152
AgO_2CCCl_3	IC_6H_5	2:1	polymeric	tetrahedral (O_3I)	159
AgO_2CCCl_3	$I_2C_6H_4$	2:1	polymeric	tetrahedral (O_3I)	159

[a] geometric terms should only be taken as approximations of geometry [b] dppf = 1,1'-bis(diphenylphosphino)ferrocene

[c] dppm = bis(diphenylphosphino)methane

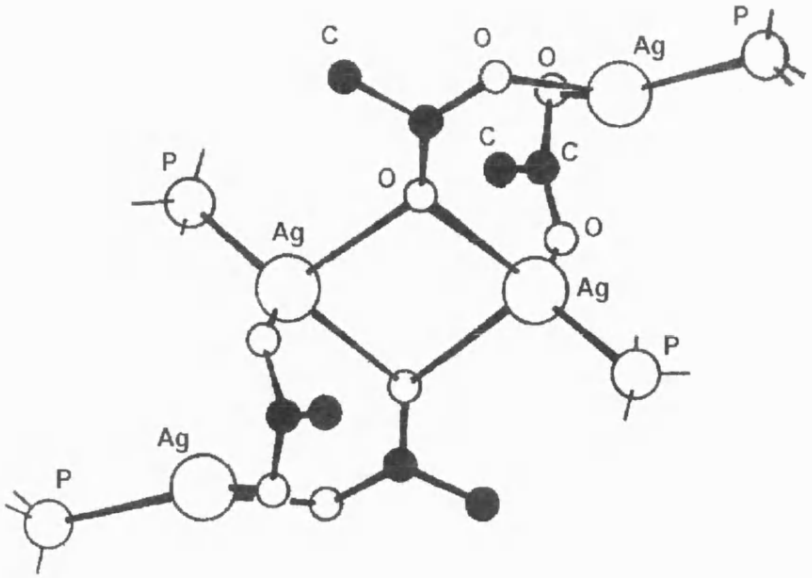

a)

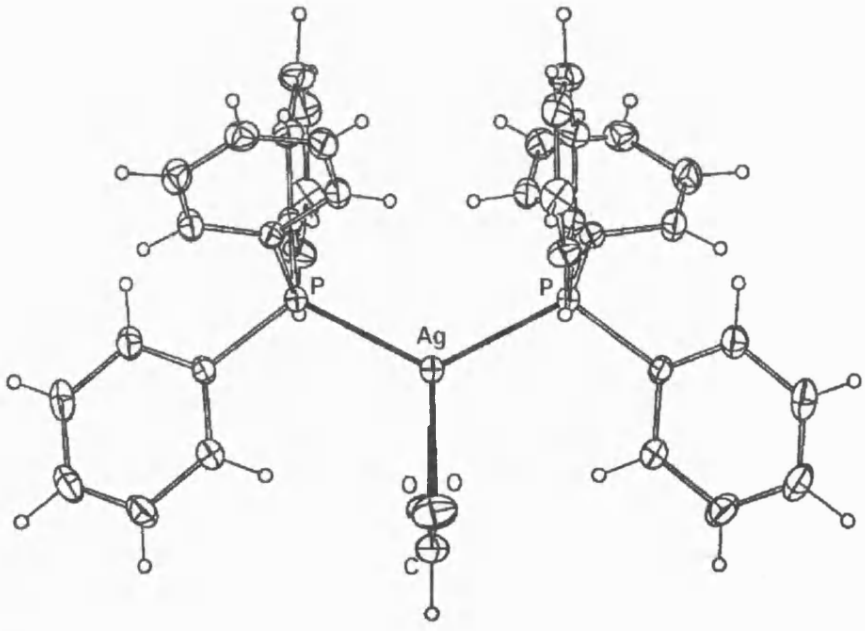

b)

Figure 2-6 Structures of $[Ag(O_2CCH_3).(PPh_3)]_4$ [153] (a) and $Ag(O_2CH)(PPh_3)_2$ [154](b), (some incidental atoms are omitted for clarity).

Other adducts of silver carboxylates with triphenylphosphine include the Ag:PPh_3 1:2 adducts of silver formate [154] and acetate [155] (although only a preliminary study of the acetate has been carried out). The silver formate species exists as a monomer with a bidentate formate ligand completing an O_2P_2 coordination sphere around the silver (Figure 2-6). This structure is discussed in more depth later in the Chapter.

A number of adducts of silver carboxylates with bidentate phosphines have been isolated and their structures determined. The bidentate phosphines used include bis(diphenylphosphino) methane (dppm) and 1,1'-bis(diphenylphosphino)ferrocene (dppf). Conformations in the dppm ligand generally prohibit chelation to a single metal atom, it being most often found as a bridging ligand in oligomeric structures. In contrast, the flexibility of the dppf ligand caused in part by rotational freedom around the Cp-Fe-Cp unit means that structural conformations for this ligand are wide, varied and very difficult to predict.

Two dppm adducts of silver acetate have been structurally investigated, those of 2:1 and 1:1 Ag:dppm ratios. Dppm will react with two equivalents of silver acetate to give a tetranuclear species [156] which differs from the dinuclear species proposed in solution. [152] The solid state structure of the 2:1 adduct, $[Ag_2(\mu\text{-}O_2CCH_3\text{-}O,O')(\mu\text{-}O_2CCH_3\text{-}O)(\mu\text{-dppm})]_2$, consists of a central 12 membered ring made up of four silvers, two bridging oxygens (from monodentate acetates) and two bridging acetate groups. Each silver is bridged by a dppm and an acetate group in an *anti-syn* fashion, each silver atom being three-coordinate. This complex reacts rapidly with more dppm to give dimeric $[Ag(\eta^2\text{-}O_2CCH_3)(\mu\text{-dppm})]_2.2CHCl_3$. [156] The addition of the additional dppm molecule causes the adduct to take up a dimeric arrangement with silver atoms doubly bridged by diphosphines (Figure 2-7). Acetate groups chelate to individual silver atoms which take up a distorted P_2O_2 tetrahedral configuration.

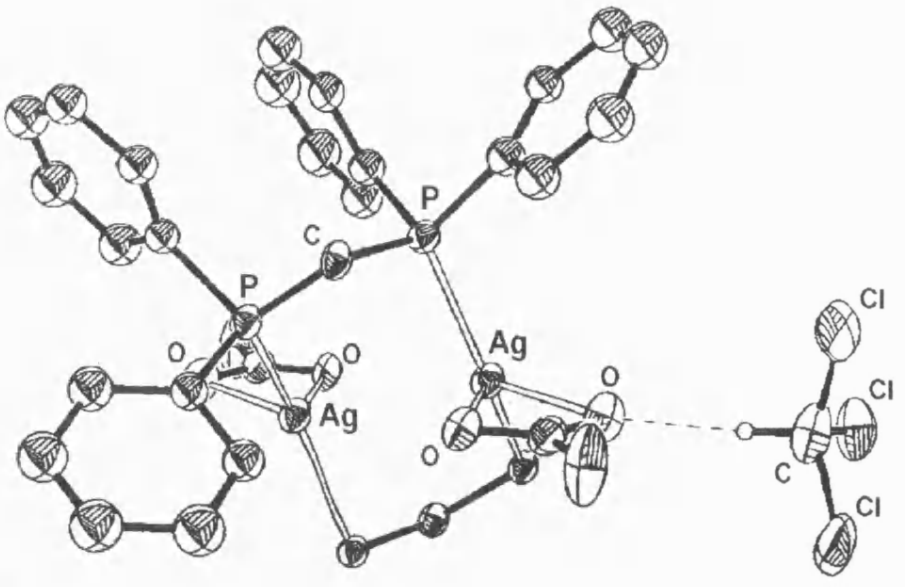

a)

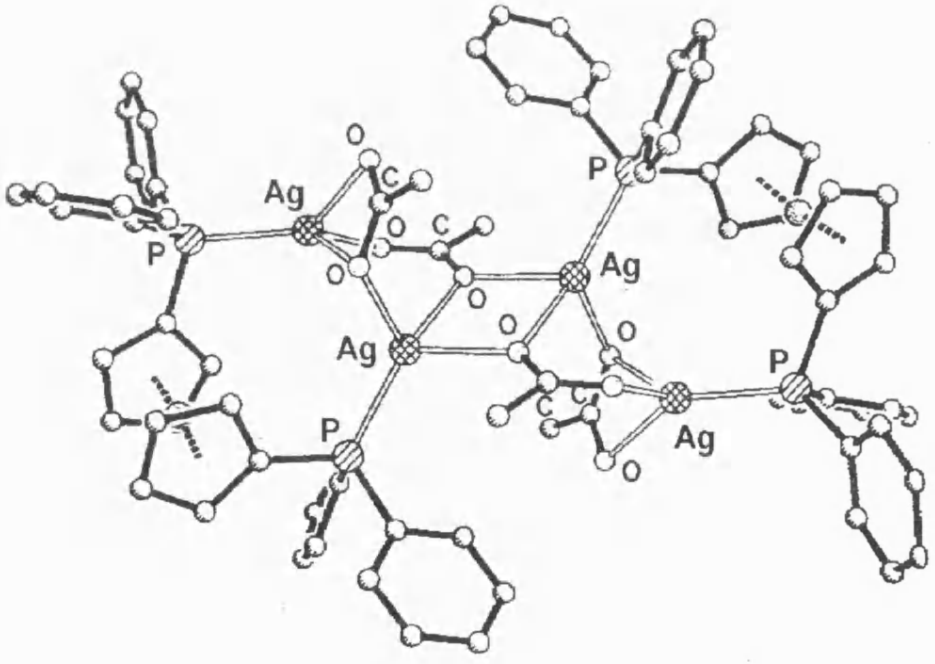

b)

Figure 2-7 Structures of silver(I) carboxylate adducts of diphosphine ligands; $|Ag(O_2CCH_3)(dppm)|_2.2CHCl_3$ [156] (a), $|Ag_2(O_2CCH_3)_2(dppf)|_2$ [157] (b), (some incidental atoms are omitted for clarity).

Complexes with dppf ligands have been studied with silver formate, acetate and benzoate. [157] The formate adduct $[Ag_2(O_2CH)_2(dppf)_3].2CH_2Cl_2$, can be described as a dppf ligand symmetrically bridging two $Ag(dppf)(HCO_2)$ species. Such co-existence of bridging and chelating modes of the dppf is rare, as is the unidentate bonding of the formato ligand. In the acetate adduct $[Ag_2(O_2CCH_3)_2(dppf)]_2$, the core consists of a tetranuclear framework made up of two adjacent 8 membered bis(carboxylato-*O,O'*) dimers (Figure 2-7), similar to the triphenylphosphine adduct of silver acetate (Figure 2-6). A number of important differences exist, though all the acetato ligands are three-coordinate, two are in a chelate-bridge coordination mode, the remainder in a triply-bridging coordination mode. Thus, in contrast to the $[Ag(O_2CCH_3)PPh_3]_4$ structure previously described, all silver atoms are four coordinate with an O_3P coordination sphere. The benzoate adduct $Ag_2(C_6H_5CO_2)_2(dppf)$ incorporates a dppf ligand bridging silvers across a puckered eight membered $Ag_2(O_2C)_2$ ring. The silver atoms are brought into close proximity by the puckered conformation (3.346 Å), although this is not indicative of a metal-metal bonding interaction.

A number of other adducts of silver carboxylates are worthy of note. Reaction between silver acetate and the dithia-diaza-macrocycle (3,3,7,7,11,11,15,15-octamethyl-1,9-dithia-5,13-diazacyclohexadecane) results in a monomeric silver complex [158] with the central metal atom in a square pyramidal arrangement with all donor atoms bonding from the macrocycle and unidentate coordination from the acetate. The silver-oxygen distance is 2.686 Å, fairly long in comparison to other acetates. In addition iodobenzene adducts have recently been reported for the trichloroacetate silver salt. [159] In a similar way to the pyridine adduct, these 'soft' donor ligand molecules IC_6H_5 and *m*-$I_2C_6H_4$ have not broken the polymeric nature of the trichloroacetate. The structure is however significantly distorted by addition of these ligands, which in both cases bridge across dimeric sub-units.

From the structural information found in the literature, it was considered that in forming adducts of silver carboxylates, if the polymeric nature of these compounds could be inhibited, the formation of higher volatility monomers might be favoured. A patent in the literature [160] outlines pyrolysis of silver carboxylates solubilised with amines and this initially lead to attempts to isolate adducts of silver carboxylates with amines and other nitrogen donors. Although the carboxylates were solubilised easily with amines, adducts were not isolable and these attempts to isolate discrete compounds containing N-donors met with little success except in the case of 2,2'-bipyridyl.

This study has therefore focused on phosphine adducts using R_3P (R = Me, Ph) with a range of carboxylates with increasing R′ group size (R′ = CH_3, ^tBu, 2,4,6-trimethylphenyl). These adducts have been characterised structurally and their use as precursors for silver film formation explored.

2.2 RESULTS AND DISCUSSION

2.2.1 Synthesis

A series of silver carboxylates have been prepared in which the organic group of the carboxylate (R) has been used to vary the steric crowding in any resulting complex, these were prepared using several routes (Scheme 2-1) to give yields 64-96 %.

2:1 adducts of each of these carboxylates were prepared with trimethylphosphine by the addition of excess phosphine (Scheme 2-1), in all cases only the bis adduct was isolated. Preparative yields for these reactions were found to be high (70-96 %). Decomposition

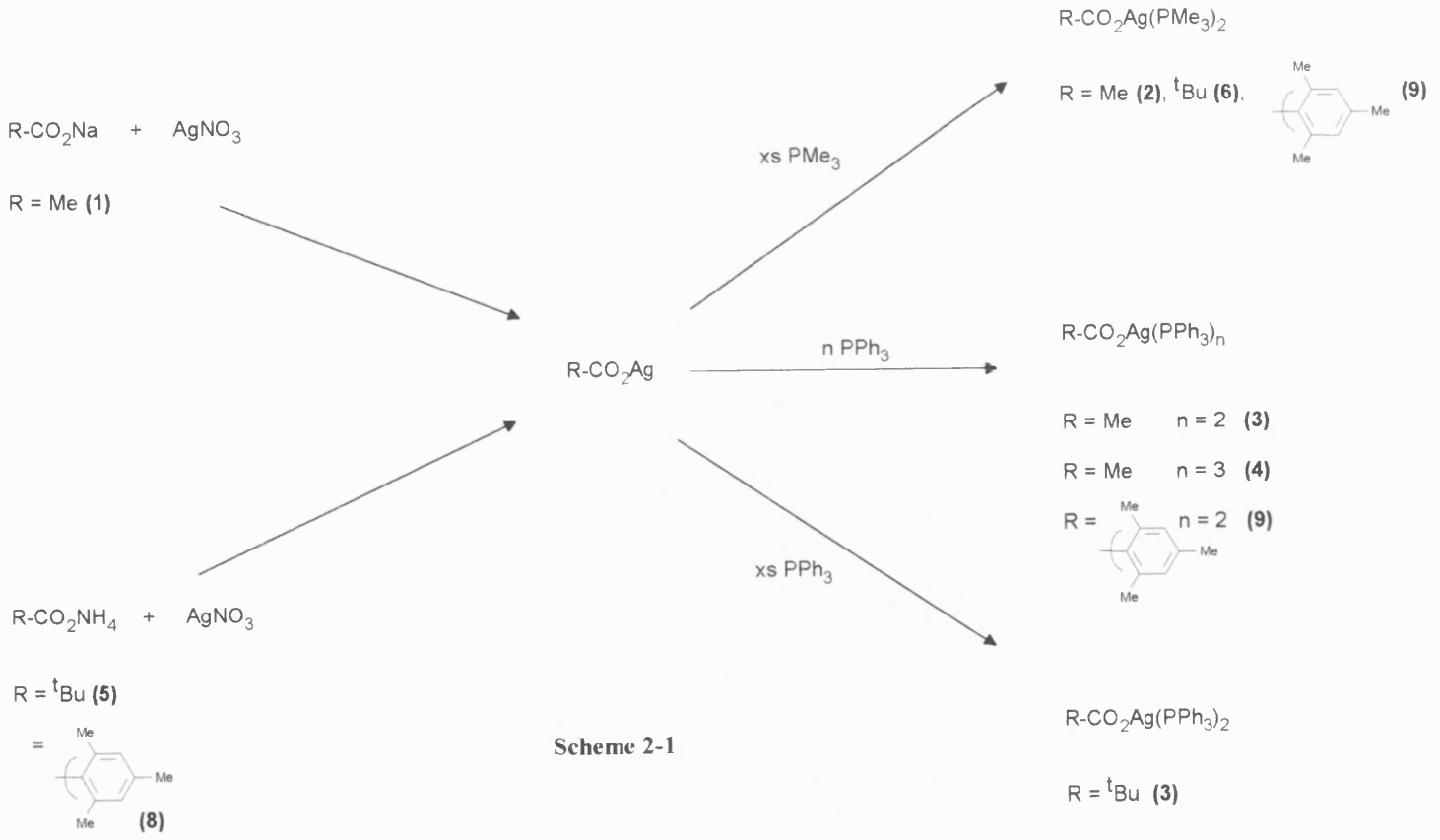
R-CO2Na + AgNO3
R = Me (1)
R-CO2NH4 + AgNO3
R = tBu (5)
=
(8)
R-CO2Ag
xs PMe3
n PPh3
xs PPh3
R-CO2Ag(PMe3)2
R = Me (2), tBu (6),
(9)
R-CO2Ag(PPh3)n
R = Me n = 2 (3)
R = Me n = 3 (4)
R = n = 2 (9)
R-CO2Ag(PPh3)2
R = tBu (3)

Scheme 2-1

temperatures, as measured by TGA, were influenced by the size of R group on the carboxylate; 25°C **(2)**, 70°C **(6)**, 76°C **(9)**.

Adducts were also prepared with triphenylphosphine (Scheme 2-1) to give 2:1 and 3:1 complexes. Where two equivalents of phosphine were added, the bis adduct was always isolated. Where excess phosphine was used, the tris(triphenylphosphine) adduct of silver acetate was isolated **(4)**, the analogous adduct of silver pivalate was not. Preparative yields were relatively high (52-94%). Decomposition points were found to be higher than the analogous trimethylphosphine adducts but appeared to be less influenced by the size of the R group; 208°C **(3)**, 150°C **(4)**, 200°C **(7)**, 85°C **(10)**.

The triphenylphosphine adducts were, as expected, easier to recrystallise and purify, the trimethylphosphine adducts suffering slightly from the lability and volatility of the donor ligand.

2.2.2 Infra-red Spectroscopy

The infra-red spectra of carboxylic acids reveals five frequency bands characteristic of the carboxylic acid group. [161] i) 2500-2700 cm^{-1} ν(OH), ii) ~1700 cm^{-1} ν(C=O), iii) and iv) ~1400, 1200-1300 cm^{-1} ν(C-O), δ(O-H), v) ~900 cm^{-1} δ(O-H) non-planar to the CO_2. On forming the carboxylate anion, the loss of the proton removes the presence of O-H stretches and deformations. Metal-oxygen bond stretches are found in their place at much lower frequencies, for example in silver acetate ν(Ag-O) is reported at 284 cm^{-1}. [111] Such frequencies are beyond

the range of the instrumentation used in this study, consequently ν(M-O) was not used to aid structural investigations.

The carboxylate group itself is a useful diagnostic 'handle' to indicate structural changes. Four distinct modes of coordination of the carboxylate group have been characterised in terms of infra-red analysis, namely ; ionic carboxylates (I), unidentate carboxylates (II), (bidentate) chelating carboxylates (III) and (bidentate) bridging carboxylates (IV) (Figure 2-8).

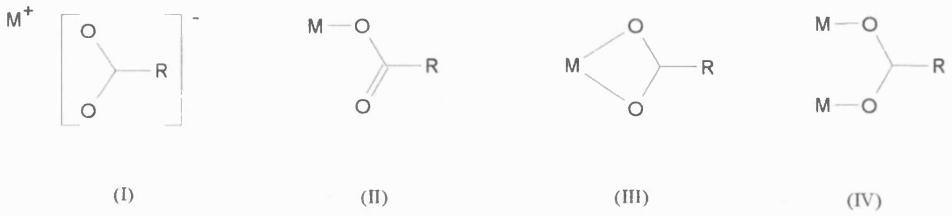

Figure 2-8 Modes of coordination of the carboxylate group.

Of the structural forms given above, I, III and IV have basic C_{2v} symmetry and many of their spectral features are quite similar. The unidentate carboxylate mode (II) is markedly less symmetrical (C_s) and this has consequences for its infra-red spectrum. Changes in the carboxylate group vibrational frequencies are normally compared to those of the free ion (I), where the carboxylate group is completely symmetrical and the metal atom associated equally with both oxygen atoms.

Ionic carboxylates have been studied extensively and while they show no carbonyl group stretch there are characteristic bands in the range 1510-1650 cm^{-1} and 1280-1400 cm^{-1} denoted as the asymmetric stretch $\nu_a(CO_2^-)$ and symmetric stretch $\nu_s(CO_2^-)$ respectively. A reduction in frequency of the asymmetric stretch is due to the mixing of C=O and C-O character in the

symmetrical ion. The difference between the asymmetric and symmetric stretches is given by $\Delta\nu$ [where $\Delta\nu = \nu_a(CO_2^-)-\nu_s(CO_2^-)$] and when compared to that found in the free ion gives a value typical of the coordination mode.

In the free acetate ion $\nu_a(CO_2^-)$ and $\nu_s(CO_2^-)$ are found at about 1560 and 1416 cm^{-1} respectively, $\Delta\nu$ = 144 cm^{-1}. By comparison, in unidentate bonding (II), the two carbon-oxygen bonds are less equivalent, ν(C=O) is higher than $\nu_a(CO_2^-)$ and ν(C-O) is lower than $\nu_s(CO_2^-)$. As a result the separation between the two is much larger, examples of unidentate acetate bonding giving $\Delta\nu$ in the range 230-315 cm^{-1}.

According to Nakamoto [162] the opposite trend is generally observed in a (bidentate) chelate complex where the separation $\Delta\nu$ is much smaller than in the free ion. This is supported by the work of Grigorev, [163] whose conclusions are based both on theoretical considerations and empirical data. In the (bidentate) bridging complex, the separation is said to be approximately that of the free ion. In summary :

$$\Delta\nu(\text{chelate}) < \Delta\nu\,(\text{bridging}) \sim \Delta\nu\,(\text{free anion}) \leq \Delta\nu\,(\text{unidentate})$$

Other workers have pointed to the unreliability of using IR band frequencies to assign structural modes of coordination. [164, 165] The carbon-oxygen stretching vibrations may be affected by hydrogen bonding or interactions with metal lone-pairs. In addition, the C-H bending modes are found in the same region and although weak for alkyl C-H modes, some confusion may be experienced with the in plane C-H vibrations of aryl groups.

On the above basis, tentative assignments have been made for $\nu_a(CO_2^-)$ and $\nu_s(CO_2^-)$ (Table 2-3). The sharp, strong, bands found with the triphenylphosphine adducts at 1435, 1477-1482 cm^{-1} have been assigned to C-H vibrations, as have the bands at 1283-1287 cm^{-1} found in the trimethylphosphine adducts. The values of $\Delta\nu$ found for silver acetate **(1)** and pivalate **(5)** are much lower than those of the sodium salts (143 cm^{-1} and 135 cm^{-1} respectively). In line with previous observations, this is consistent with a chelating carboxylate structure, although this conflicts with the general structural trend for silver carboxylates which are known to prefer bridging structures. Although no structural studies on these particular carboxylates have been published, mass spectral evidence for the acetate points to an oligomeric or polymeric (and therefore bridging) structure. [111] The presence of oxygen-silver bridges between dimeric sub-units could well have an effect on C-O bond character. In contrast the infra-red spectrum of the mesitylate shows a much larger $\Delta\nu$, changing only slightly on forming adducts, indicating only a small change of structure on adduct formation.

Single crystal X-ray diffraction studies of compound **(3)** have revealed a chelating acetate group, monomeric ($^tBu_3P)Ag(O_2CCH_3$) is reported to have $\Delta\nu$ of 164 cm^{-1} [166] and other chelating acetate groups have shown a $\Delta\nu$ of 162 cm^{-1}. [156] On this basis, the data of Table 2-3 suggest that the remaining bis adducts also incorporate chelating carboxylates around a four coordinate silver. It should be stressed that these results are not unambiguous, as bridging benzoate and acetate groups are reported to have $\Delta\nu$ values of 169 cm^{-1} and 177 cm^{-1}, respectively. [157, 156] A final point worthy of note is the lack of a much larger $\Delta\nu$ splitting in compound **(4)** which might be expected to involve a unidentate structure due to the presence of three equivalents of phosphine. The data are, however, consistent with previously published IR data for this compound, the authors suggesting values of $\Delta\nu$ of 185 cm^{-1} [148] or 190 cm^{-1} [149] support the presence of unidentate bonding.

Table 2-3 Selected IR data for silver(I) carboxylates and their adducts.

Compound		$\nu_a(CO_2^-)$ (cm^{-1})	$\nu_s(CO_2^-)$ (cm^{-1})	$\Delta\nu$ (cm^{-1})
AgO_2CCH_3	**(1)**	1514	1422	92
$AgO_2CCH_3.(PMe_3)_2$	**(2)**	1574	1404	170
$AgO_2CCH_3.(PPh_3)_2$	**(3)**	1553	1396	157
$AgO_2CCH_3.(PPh_3)_3$	**(4)**	1565	1406 [a]	159 [a]
AgO_2C^tBu	**(5)**	1512	1399	113
$AgO_2C^tBu.(PMe_3)_2$	**(6)**	1557	1401	156
$AgO_2C^tBu.(PPh_3)_2$	**(7)**	1562	1402	160
$AgO_2C\text{-}Me_3C_6H_2$	**(8)**	1557	1393	164
$AgO_2C\text{-}Me_3C_6H_2.(PMe_3)_2$	**(9)**	1564	1387	177
$AgO_2C\text{-}Me_3C_6H_2.(PPh_3)_2$	**(10)**	1545	1385	160

[a] assignment in this case is complicated by a nearby peak at 1381 cm^{-1}, assignment of $\nu_s(CO_2^-)$ to this would suggest a $\Delta\nu$ of 184 cm^{-1}

2.2.3 ^{1}H and ^{13}C NMR Spectroscopy

Proton and carbon-13 NMR results, as shown in Tables 2-4 and 2-5 respectively, gave expected results. ^{13}C carboxylate resonances were found to be affected by the formation of adducts, as a rule shifting downfield some 2-3 ppm, although this could be due to solvent effects. Silver carboxylate NMR experiments were conducted in d^6-DMSO, experiments with their adducts were carried out in $CDCl_3$. The only adduct having an unchanged ^{13}C carboxylate resonance from the carboxylate, was the silver acetate tris(triphenylphosphine) adduct.

2.2.4 ^{31}P and ^{109}Ag Multinuclear NMR Spectroscopy

Compounds **(1)** to **(10)** were also investigated using ^{31}P and ^{109}Ag NMR techniques both at room temperature and at low temperature (-80°C). All room temperature ^{31}P NMR spectra exhibited broad unresolved peaks indicating a degree of lability in solution. This is consistent with most such solution studies in the literature, [148-150] though some have been resolved at room temperature. [166] The shift of the phosphorus resonances in the adducts as compared to the free ligand PR_3 (R = Me, Ph) (denoted $\Delta\delta$), is largely characteristic of the phosphine and not the carboxylate. $\Delta\delta$ for trimethylphosphine and triphenylphosphine adducts were 22.4-25.6 ppm and 10.8-13.8 ppm downfield respectively. The tris(triphenylphosphine)acetate complex $Ag(O_2CCH_3)(PPh_3)_3$ **(4)** did not appear different in any respect.

At lower temperatures (-80°C) the dynamic solution behaviour was found to be inhibited and the dissociation of ligands was slowed sufficiently to allow resolution in a number of cases. Bis triphenylphosphine complexes **(3)**, **(7)** and **(10)** resolved readily to give resonances apparent as

a doublet of doublets at 7.6-8.0 ppm. An example given in Figure 2-9 was that observed for compound **(3)**. Inner doublets due to $^{1}J(^{107}Ag\text{-}^{31}P)$ one bond coupling and outer (quoted) due to $^{1}J(^{109}Ag\text{-}^{31}P)$ coupling were found in the expected range (480-497 Hz).

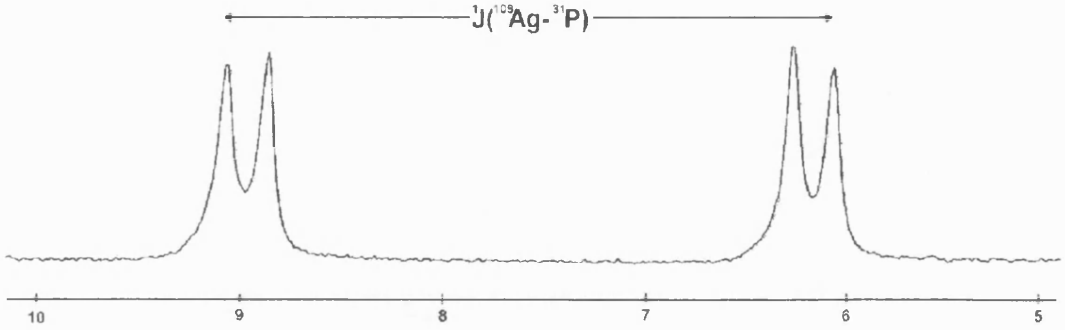

Figure 2-9 ^{31}P NMR spectra for $Ag(O_2CCH_3)(PPh_3)_2$ **(3)**.

A number of spectra of the trimethylphosphine adducts - compounds **(2)** and **(6)** - were found to contain unresolved resonances at this temperature. Compound **(9)** was found to be partially resolved allowing for an estimate of one bond coupling to silver. The spectrum of the tris (triphenylphosphine) complex **(4)** was also found to be partially resolved (in contrast to resolved spectra for the bis triphenylphosphine adducts). The spectrum appeared to show two species in solution, the major peaks (an unresolved doublet) close to those found in the corresponding bis adduct **(3)**.

In the silver NMR studies, a number of resonances were not detected at all, i.e. those of compounds **(1)**, **(4)** and **(6)**. For silver pivalate **(5)** and mesitylate **(8)** ^{109}Ag resonances were detected in the expected region (303 and 266 ppm respectively). These values compare well with other silver carboxylate resonances observed during the period of this study (AgO_2CPh at 278 ppm, *p*-$AgO_2CC_6H_4\text{-}NH_2$ at 180 ppm). Resolved ^{109}Ag resonances of bis(triphenyl-

phosphine) adducts - compounds **(3)**, **(7)** and **(10)** - appeared as 1:2:1 triplets in the region 895-931 ppm. One bond coupling to phosphorus-31 atoms is consistent with values found in the ^{31}P NMR spectra. An example is shown in Figure 2-10, namely that of $Ag(O_2CCH_3)(PPh_3)_2$ **(3)**. Resonances for trimethylphosphine adducts were either not detected **(6)** or unresolved **(2)**, **(9)** (772, 834 ppm respectively), indicating dynamic equilibria still operating at -80°C. Similarly no resonance was found for the tris(triphenylphosphine) complex **(4)**.

On formation of the adducts silver-109 resonances were shifted downfield by around 550-650 ppm. Bis(triphenylphosphine) adducts were detected at lower field (shifts of 627, 628 ppm for compounds **(7)** and **(10)**), than bis(trimethylphosphine) adducts (shift of 568 ppm for compound **(9)**) as compared to the silver carboxylates themselves. Collected data for phosphorus and silver NMR experiments are summarised in Table 2-4.

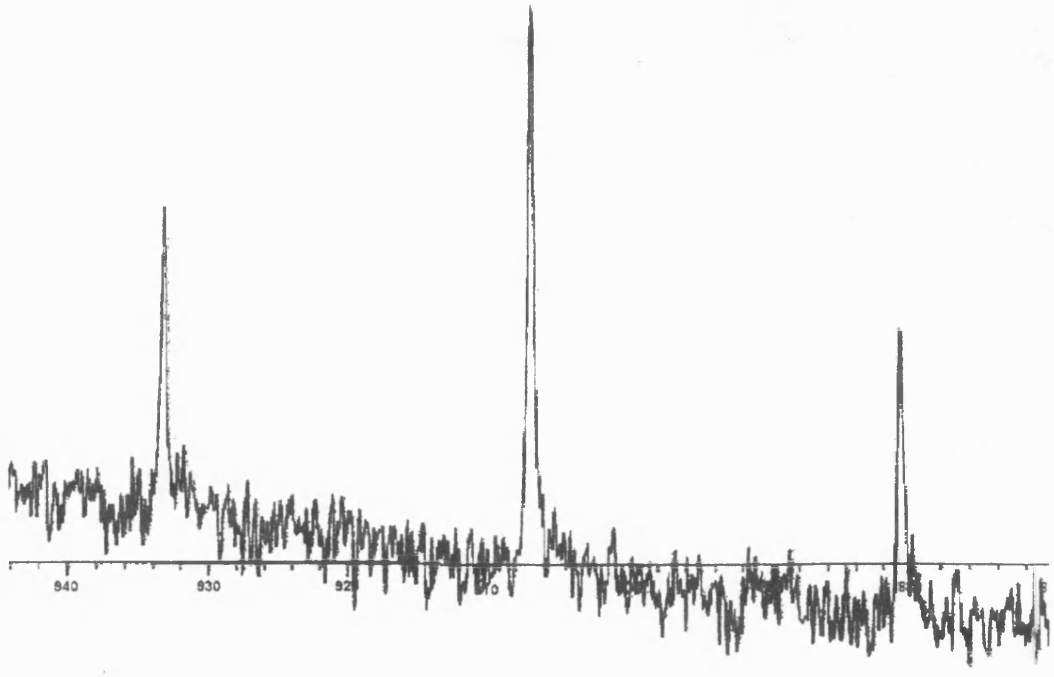

Figure 2-10 ^{109}Ag NMR spectra for $Ag(O_2CCH_3)(PPh_3)_2$ **(3)**

Table 2-4 ^{31}P and ^{109}Ag NMR data for silver(I) carboxylates and their phosphine adducts.

Compound		Room temp ^{31}P data [a]			Low temp ^{31}P data [b]			^{109}Ag data [c]	
		δ	δ free ligand	Δδ	^{31}P	$^{1}J(^{31}P\text{-}Ag)$	Δδ	^{109}Ag	$^{1}J\ (^{109}Ag\text{-}^{31}P)$
AgO_2CCH_3	**(1)**	------	------	------	------	-------	------	no [d]	------
$AgO_2CCH_3.(PMe_3)_2$	**(2)**	-36.4	-62	25.6	-38.8 (br) [e]	-------	23.2	772	no [d]
		------	------	------	-43.4 (dd) [f]	268	18.6	------	------
$AgO_2CCH_3.(PPh_3)_2$	**(3)**	8.01	-5.24	13.25	7.6 (dd) [f]	490	12.84	907 (t) [g]	489
$AgO_2CCH_3.(PPh_3)_3$	**(4)**	5.79	-5.24	11.03	7.4 (ud) [h]	~450+	12.64	no [d]	------
					4.9 (dd) [f]	256	10.14	------	------
AgO_2C^tBu	**(5)**	------	------	------	------	------	------	303 (s) [i]	------
$AgO_2C^tBu.(PMe_3)_2$	**(6)**	-39.1	-62	22.9	-38.2 (br) [e]	------	23.8	no [d]	------
$AgO_2C^tBu.(PPh_3)_2$	**(7)**	8.51	-5.24	13.75	7.75 (dd) [f]	480	12.99	931 (t) [g]	484
$AgO_2C\text{-}Me_3C_6H_2$	**(8)**	------	------	------	------	------	------	266 (s) [i]	------
$AgO_2C\text{-}Me_3C_6H_2.(PMe_3)_2$	**(9)**	-39.6	-62	22.4	-38.0 (d) [j]	~500+	24.0	834	------
$AgO_2C\text{-}Me_3C_6H_2.(PPh_3)_2$	**(10)**	5.56	-5.24	10.8	7.98 (dd) [f]	497	13.22	895 (t) [g]	503

[a] experiments recorded as $CDCl_3$ solutions at 20°C [b] experiments recorded as $CH_2Cl_2/CDCl_3$ solutions at -80°C [c] experiments recorded as $CH_2Cl_2/CDCl_3$ solutions at -80°C except **(1)**, **(5)** and **(8)** which were recorded as d^6-DMSO solutions at 20°C [d] no = not observed [e] br = broad [f] dd = doublet of doublets [g] t = triplet [h] ud = unresolved doublet [i] s = singlet [j] d = doublet

2.2.5 Mass Spectrometry

In order to determine the extent of oligomerisation and to provide preliminary data for potential decomposition routes, a selection of compounds were examined using fast atom bombardment [FAB(LSIMS)] mass spectrometry. Of particular interest were silver-containing fragments, easily identified due to the abundance of the two isotopes, silver-107 and silver-109 (Appendix 2).

No silver fragments were identified in the spectra for the silver carboxylates even with the sensitive techniques employed, presumably either due to their very low volatility or their limited solubility in the LSIMS solution matrix (see Appendix 2). Some studies have however shown the presence of silver containing fragments using EI techniques [111, 112] and studies using SIMS techniques show increased abundances of silver containing fragments. [112]

The mass spectrometry data for the phosphine adducts are summarised in Table 2-5 (trimethylphosphine adducts) and Table 2-6 (triphenylphosphine adducts). For the trimethylphosphine adducts **(2)**, **(6)** and **(9)**, the spectra are dominated by monosilver fragments also incorporating phosphine ligands and in these cases M^+ (100%) was $Ag(PMe_3)_n$ (n = 1, 2). Often these peaks were followed by minor peaks of oxidised fragments, $AgOL_2$, AgO_2L_2 but not AgOL. A number of dinuclear species were also identified, particularly for compound **(2)**. The fragment $Ag_2(O_2CR)L_2$ was common to **(2)**, **(6)** and **(9)**, $Ag_2(O_2CR)L$ was identified in **(2)** and **(9)**, $Ag_2(O_2CR)(O_2C)L_n$ (n = 3, 4) was identified in **(2)**. Such dinuclear species might be taken to indicate a dimeric based structure although similar fragments are observed in compound **(3)** which is known to take up a monomeric structure.

Table 2-5 Selected mass spectrometric data, silver(I) carboxylate - trimethylphosphine adducts. [a]

	(2) [b]		(6) [c]		(9) [d]	
Fragment ions [e]	**m/z**	**%**	**m/z**	**%**	**m/z**	**%**
	109	13	109	32	109	5
	149	22	---	---	147	8
AgL	183	82	183	100	183	84
AgL_2	259	96	259	79	259	100
$AgOL_2$	275	5	275	7	275	3
AgO_2L_2	291	2.5	---	---	---	---
$Ag_2(O_2CR)L$	349	4	---	---	453	3
Ag_2OHL_2	383	8	---	---	---	---
$Ag_2(O_2CR)L_2$	425	55	467	5	529	21
$Ag_2(O_2CR)(O_2C)L_3$	545	5	---	---	---	---
$Ag_2(O_2CR)(O_2C)L_4$	621	1.6	---	---	---	---
Other Ag containing	401 [f]	16	197 [f]	11	479 [f]	5
fragments (Ag_n)	497 [f]	3.6	323 [g]	12	---	---
	567 [g]	2.4	---	---	---	---
	643 [g]	1.4	---	---	---	---

[a] based on ^{107}Ag [b] R = CH_3 [c] R = ^tBu [d] R = 2,4,6-$Me_3C_6H_2$ [e] L = PMe_3 [f] recognised by isotopic pattern as containing one silver atom [g] recognised by isotopic pattern as containing a number of silver atoms

Table 2-6 Selected mass spectrometric data, silver(I) carboxylates - triphenylphosphine adducts. [a]

	(3) [b]		(4) [b]		(7) [c]		(10) [d]	
Fragment [e]	**m/z**	**%**	**m/z**	**%**	**m/z**	**%**	**m/z**	**%**
							185	21
L	262	13	262	31	262	24	262	36
AgL	369	62	369	89	369	100	369	100
AgO_L	385	2	385	5	385	4	385	4
AgL_2	631	100	631	99	631	92	631	50
$AgOL_2$	647	4	647	7	647	4.4	647	2
AgO_2L_2	---	---	---	---	---	---	663	1
AgL_3-H	892	0.7	892	1.9	892	6.2	---	---
$Ag_2O(O_2CR)L$	---	---	---	---	---	---	655	1
Ag_2L_2-H	737	0.3	737	0.6	---	---	---	---
Ag_2OHL_2	755	0.8	755	1.3	---	---	---	---
$Ag_2(O_2CR)L_2$	797	1.2	797	4.4	839	0.4	901	1
$Ag_2O(O_2CR)L_2$	---	---	---	---	---	---	917	1
Ag_2RL_3	1015	0.3	1015	0.4	---	---	---	---
$Ag_2OR(O_2CR)$-H	---	---	---	---	---	---	511	1
$Ag_2OR(O_2CR)L$-H	---	---	---	---	---	---	733	5
Other Ag	764 [f]	23	764 [f]	1.1	739 [g]	0.5	---	---
containing	773 [f]	0.6	773 [f]	1.2	755 [g]	0.8	---	---
fragments	865 [f]	1.1	923 [h]	0.3	855 [g]	1.1	---	---
	923 [f]	0.2	1061 [h]	0.5	---	---	---	---
	1127 [f]	0.2	1125 [g]	0.5	---	---	---	---

[a] based on ^{107}Ag [b] R = CH_3 [c] R = ^tBu [d] R = 2,4,6-$Me_3C_6H_2$ [e] L = PPh_3 [f] recognised by isotopic pattern as containing two silver atoms [g] recognised by isotopic pattern as containing a single silver atom [h] recognised by isotopic pattern as containing a number of silver atoms

For the triphenylphosphine adducts, results were similar with both mononuclear and dinuclear fragments identified. The bis and tris complexes of silver acetate **(3)** and **(4)** gave almost identical spectra with no significant differences. This may indicate a shared decomposition pathway between the two, or perhaps that one complex is a decomposition product of the other. General comparisons of the spectra for compounds **(3)**, **(4)**, **(7)** and **(10)** reveal that AgL_n (n = 1, 2, 3) and AgO_mL_2 (m = 1, 2) are common fragments and in all cases AgOL was found (in contrast to PMe_3 adducts). Additionally dinuclear fragments Ag_2L_2-1, Ag_2OHL_2, $Ag_2(O_2CR)L_2$, Ag_2RL_3 were found in several spectra, the latter fragment perhaps indicating a decarboxylation pathway. Finally, aryloxide fragments $Ag_2OR(O_2CR)L_n$-1 (n = 0, 1) were identified within the spectrum of **(10)**.

2.2.6 Thermal Analysis Studies

Compounds **(2)**, **(3)**, **(4)**, **(6)**, **(7)**, **(9)** and **(10)** were investigated using thermal analysis studies (Table 2-7) to give an indication of the temperatures at which decomposition may be expected to start. In this regard, the data may also suggest information concerning the relative stability of the compounds. The mass of residue remaining at the completion of the experiment may also indicate that the compound exhibits a measure of volatility if the observed mass of residue is less than would be expected.

In general, the trimethylphosphine adducts started to decompose at lower temperatures than triphenylphosphine adducts. Typically starting at 25 to 75°C and complete by 235-270°C, in the case of compounds **(2)** and **(6)**, decomposition was stepwise with loss of some ligand before loss of carboxylate and the remaining ligand, no doubt due to the high volatility of PMe_3. In the triphenylphosphine complexes, decomposition started at higher temperatures but was

Table 2-7 Thermal analysis data, silver(I) carboxylate adducts.

Compound		Decomposition temperature (°C) start [a]	maxima [b]	end [c]	Wt loss (%) at each stage calculated	found	Residue remaining (%) calculated	found	Liberated organic species [d]
$AgO_2CCH_3.(PMe_3)_2$	**(2)**	25	74	148	47.69	34.36	-----	-----	PMe_3
		148	221	235	18.50	35.15	33.81	29.72	O_2CR
$AgO_2CCH_3.(PPh_3)_2$	**(3)**	186	193	200	-----	-----	-----	-----	none [e]
		208	288	300	84.4	87.57	15.6	12.43	everything
$AgO_2CCH_3.(PPh_3)_3$	**(4)**	150	289	300	88.69	86.25	11.31	13.75	everything
$AgO_2C^tBu.(PMe_3)_2$	**(6)**	70	117	140	21.1	13.51	-----	-----	PMe_3
		140	163	186	21.1	14.30	-----	-----	PMe_3
		186	233	250	27.99	42.56	29.81	29.63	O_2CR
$AgO_2C^tBu.(PPh_3)_2$	**(7)**	200	308	332	85.3	84.37	14.7	15.63	everything
$AgO_2C\text{-}Me_3C_6H_2.(PMe_3)_2$	**(9)**	76	254	271	73.11	73.74	26.89	26.26	everything
$AgO_2C\text{-}Me_3C_6H_2.(PPh_3)_2$	**(10)**	85	120	163	9.6	13.20	-----	-----	CH_2Cl_2 solvent
		250	280	300	59.5	65.48	30.9	21.32	everything

[a] temperature corresponding to the onset of decomposition [b] temperature at which the rate of weight loss at a given stage was at a maximum

[c] temperature at which decomposition was complete [d] suspected organic species liberated during the decomposition [e] endothermic change with no weight loss

completed in a narrower temperature range, typically beginning in the range 200-250°C and completed by 330°C. The tris complex **(4)** started decomposing at a lower temperature (150°C) but the characteristics of the weight loss are very similar to those found with the related bis complex **(3)**. Finally, an endothermic change was observed with compound **(3)** before the onset of decomposition, which may be due to melting.

2.3 SINGLE CRYSTAL X-RAY STRUCTURE DETERMINATION OF $Ag(O_2CCH_3)(PPh_3)_2$ (3)

Crystallographic quality crystals of compound **(3)** $AgO_2CCH_3.(PPh_3)_2$, were obtained from a saturated solution of **(3)** in toluene at room temperature. The crystals were found to be stable both to light and to atmosphere; data collection was carried out at room temperature. A short note has reported the preliminary single crystal X-ray investigation of compound **(3)**, [155] although the full crystal structure has never been published. Unit cell dimensions and other crystal parameters are comparable with those already reported.

The crystal structure as determined by single crystal X-ray diffraction consists of independent monomeric molecules, two of which make up the asymmetric unit. The two molecules found in the asymmetric unit are essentially the same with only a small number of differences apparent, presumably due to packing effects. Silver atoms are found in a pseudo-tetrahedral arrangement with two triphenylphosphine ligands and chelating acetate groups (Figure 2-11). One phenyl group in the molecule containing Ag(2) exhibited a 39% disorder. This compound is iso-structural with the copper(I) analogue previously reported. [167] Chelating (non-bridging) carboxylate groups bound to silver in the presence of phosphines have only been described

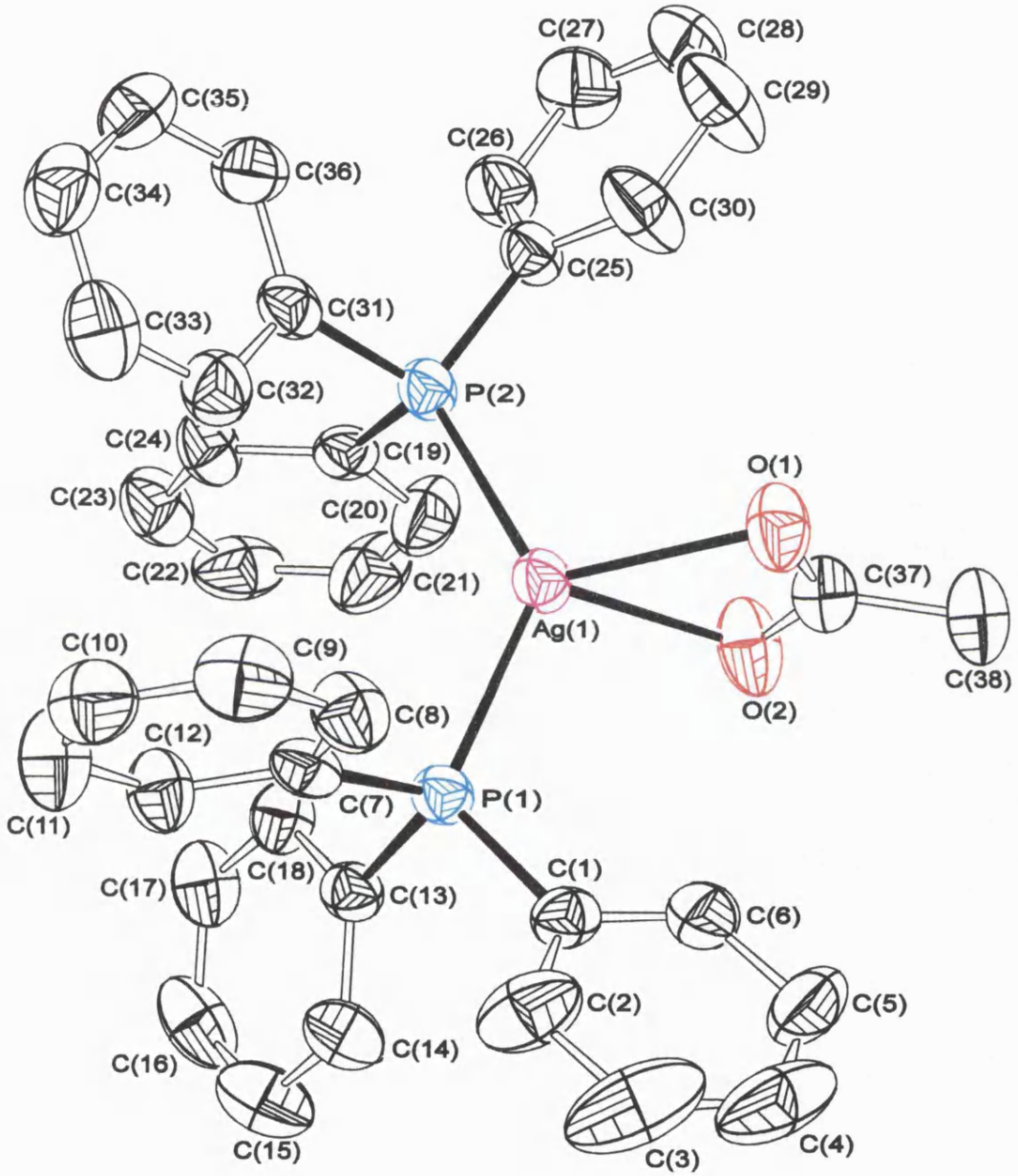

Figure 2-11 Structure of molecule 1 of complex **(3)**, $Ag(O_2CCH_3)(PPh_3)_2$

previously in three reported structures, those of; $[Ag(O_2CH)(PPh_3)_2]$, [154] $[Ag(O_2CH)(PPh_3)_2].2HCO_2H$ [154] and $[Ag(O_2CCH_3)(dppm)]_2.2CHCl_3$ (dppm = $Ph_2PCH_2PPh_2$). [156] Other silver carboxylate phosphine adducts generally have carboxylate groups in bridging [152, 153, 156, 157] or unidentate [156-158] bonding modes.

Silver-phosphorus bond lengths (2.429-2.464 Å) are comparable to other Ag-P bonds found in phosphine adducts of silver carboxylates (2.35-2.52 Å). Similarly C-O bond lengths (1.233-1.251 Å) are also in the expected range for chelating carboxylates (1.21-1.28 Å). Variations occur between the silver-oxygen bond lengths for the two molecules of the asymmetric unit.

Silver-oxygen distances for Ag(1), are found to be very similar (2.416 and 2.437 Å) indicating a symmetrical chelate. The differences between silver-oxygen bonds bound to Ag(2) are found to be more pronounced (2.378 and 2.512 Å), indicating a less symmetrical chelating acetate group. There appears no obvious crystallographic reason for this difference. These Ag-O distances however are all comparable with those found in the formate complex $[Ag(O_2CH)(PPh_3)_2]$ (2.425 Å) but less than those found in $[Ag(O_2CH)(PPh_3)_2].2HCO_2H$ and $[Ag(O_2CCH_3)(dppm)]_2.2CHCl_3$. In these cases a carboxylate oxygen also interacts with HCO_2H or $CHCl_3$ molecules via hydrogen bonds, reducing electron density at the oxygen and increasing Ag-O to 2.55-2.71 Å.

Comparing the geometry around silver, a decrease in the OAgO bond angle is accompanied by consequent increase in other angles, particularly the largest angle PAgP. Complex **(3)** in this respect is similar to $[Ag(O_2CH)(PPh_3)_2]$ where the OAgO angle is 53.1° and the PAgP angle 126.9°. Relevant bond distances and angles are summarised in Table 2-8, further data are provided in Appendix A4-1.

Table 2-8 Complex **(3)**, relevant bond lengths (Å) and angles (°).

Molecule 1		Molecule 2	
Ag(1)-P(1)	2.452(4)	Ag(2)-P(3)	2.429(3)
Ag(1)-P(2)	2.433(3)	Ag(2)-P(4)	2.464(4)
Ag(1)-O(1)	2.437(6)	Ag(2)-O(3)	2.378(7)
Ag(1)-O(2)	2.416(6)	Ag(2)-O(4)	2.518(9)
C(37)-O(1)	1.233(9)	C(75)-O(3)	1.246(11)
C(37)-O(2)	1.251(8)	C(75)-O(4)	1.239(10)
P(1)-Ag(1)-P(2)	129.7(2)	P(3)-Ag(2)-P(4)	124.0(2)
O(1)-Ag(1)-O(2)	53.4(2)	O(3)-Ag(2)-O(4)	52.7(3)
O(1)-C(37)-O(2)	122.7(7)	O(3)-C(75)-O(4)	122.2(8)

2.4 FILM GROWTH RESULTS

Compounds **(2)** - **(7)**, **(9)** and **(10)** were tested for potential use as CVD precursors, the compounds being screened using purpose-built equipment at the University of Bath. For a full description of the apparatus and procedures, the reader is directed to Appendix 6. This section includes a brief summary of results obtained from the characterisation of grown films. The results are collected into Tables 2-9 and 2-10.

The films were grown under fixed conditions at 310°C and 1 bar pressure in a nitrogen atmosphere. Samples were dissolved in THF, nebulised and passed over the heated substrate (glass). Typically 0.4-0.8 g of sample was dissolved in 25-40 cm^3 of THF, experimental growth times were dependent on N_2 (carrier) flow rates (typically 0.7-1.2 $Lmin^{-1}$) and varied between 10-30 minutes. The resulting films were found to be soft and although well adhered to the substrate, could be scratched or damaged relatively easily by touching. Films were examined using a number of techniques; visual inspection, scanning electron microscopy (SEM), conductivity and reflectance measurements. Additionally Energy Dispersive X-ray Spectroscopy (EDXS) was used to identify elements in the film and to estimate film thickness.

Silver pivalate **(5)** was shown not to grow films, either by itself or in the presence of an excess of 1,5-cod to allow solubilisation to occur. All of the phosphine adducts of silver(I) carboxylates showed an ability to generate films although film thickness and quality was variable between precursors. All of the trimethylphosphine adducts [**(2)**, **(6)** and **(9)**] were capable of producing films of measurable thickness, triphenylphosphine adducts with the exception of **(7)** did not.

Compounds **(2)** and **(6)** produced the thickest films at the highest growth rates (14.4, 13.7 $Åmin^{-1}$) although these films were not reflective on the coating side (1.1 and 0.7%). Compounds **(7)** and **(9)** produced thinner coatings at much reduced growth rates (5.7, 4.1 $Åmin^{-1}$) but these were significantly more reflective (22.2, 46.6%). This suggests a correlation between growth rates and reflectance under these conditions. Remaining compounds generated thin, discontinuous or non-conducting films for which thickness estimates could not be made. Films grown with precursor **(4)** gave a thin but reflective (49.7%) coating, remaining films [**(3)** and **(10)**] were of poor reflectivity (17.5, 17.6%).

Films grown from (2) and (6), i.e. the thickest films grown at the highest growth rates, appeared to be comprised of a thick mat of crystalline material (Plates 2-1 to 2-4). A significant fraction of these coatings appears to be made up of voids and pockets and this no doubt contributes to its poor reflectivity. The films grown from other precursors did not exhibit these surface features, coatings grown from (7) appeared very uniform in comparison (Plates 2-5, 2-6).

EDXS techniques could not provide accurate quantitative analysis of impurities although this technique has the ability to highlight possible contaminants. Carbon impurities were detected in all of the films where films were thick or conducting enough for analysis. In addition trace phosphorus was detected in films grown from **(2)** and **(6)**, those grown at the highest growth rates (both PMe_3 adducts). Trace phosphorus impurities reported in the literature have been detected in films grown from PEt_3 adducts of silver β-diketonates, although not PMe_3 adducts. There remains some difficulty in confirming the presence of oxygen in the films, due to their thin nature. The EDXS technique detected appreciable levels of Si and O (among others) from the glass substrate, thus the presence of O in the film was neither proved or disproved.

Sheet resistance measurements could only be obtained from films grown with precursors **(2)** and **(6)**, i.e. the thickest films. Sheet resistance per 25 mm square were measured as 17×10^6 and 168 Ω/□ respectively. The resistance of remaining films could not be measured, these can be described as having infinite resistance.

Table 2-9 Appearance of silver films grown from silver(I) carboxylate adducts.

Compound		visual appearance	SEM appearance	Detected Impurities [a, b] (EDXS)	Plate
$AgO_2CCH_3(PMe_3)_2$	**(2)**	thick greyish film, reflective in places	even film consisting of a thick mat of crystals	C, P (trace)	2-1, 2-2
$AgO_2CCH_3(PPh_3)_2$	**(3)**	transparent dark grey film	non-conducting film	---	
$AgO_2CCH_3(PPh_3)_3$	**(4)**	transparent but reflective silver film over a small area	thin, discontinuous or non-conducting film	---	
$AgO_2C^tBu(PMe_3)_2$	**(6)**	thick whitish film, grey in some areas, reflective in others, notably downstream	level film comprised of a thick mat of crystals	C, P (trace)	2-3, 2-4
$AgO_2C^tBu(PPh_3)_2$	**(7)**	silver reflective film, partially transparent	very smooth film	C	2-5, 2-6
$AgO_2C\text{-}C_6H_2Me_3(PMe_3)_2$	**(9)**	silver reflective film on entire substrate	rough undulating surface	C	
$AgO_2C\text{-}C_6H_2Me_3(PPh_3)_2$	**(10)**	transparent brown film	thin, discontinuous or non-conducting film	C	

[a] the presence of oxygen in the films was masked by oxygen detected in the glass [b] trace quantities were at the limits of detection of this instrumentation

Table 2-10 Properties of silver films grown from silver(I) carboxylate adducts.

Compound		Estimated film thickness (Å)	Deposition time (minutes)	Estimated deposition rate ($Åmin^{-1}$)	% Reflectance [a] coating	% Reflectance [a] glass	Sheet Resistance [b] ($\Omega/\square$)
$AgO_2CCH_3(PMe_3)_2$	**(2)**	288	20	14.4	1.1	20.7	17×10^6
$AgO_2CCH_3(PPh_3)_2$	**(3)**	---	37	---	17.5	6.5	∞
$AgO_2CCH_3(PPh_3)_3$	**(4)**	---	23	---	49.7	30.6	∞
$AgO_2C^tBu(PMe_3)_2$	**(6)**	273	20	13.7	0.7	42.8	168
$AgO_2C^tBu(PPh_3)_2$	**(7)**	80	14	5.7	22.2	9.7	∞
$AgO_2C\text{-}C_6H_2Me_3(PMe_3)_2$	**(9)**	91	22	4.1	46.6	31.1	∞
$AgO_2C\text{-}C_6H_2Me_3(PPh_3)_2$	**(10)**	---	20	---	17.6	7.3	∞

[a] λ = 550 nm corresponding to the peak in the eye response curve [b] sheet resistance was measured over a 25 mm square

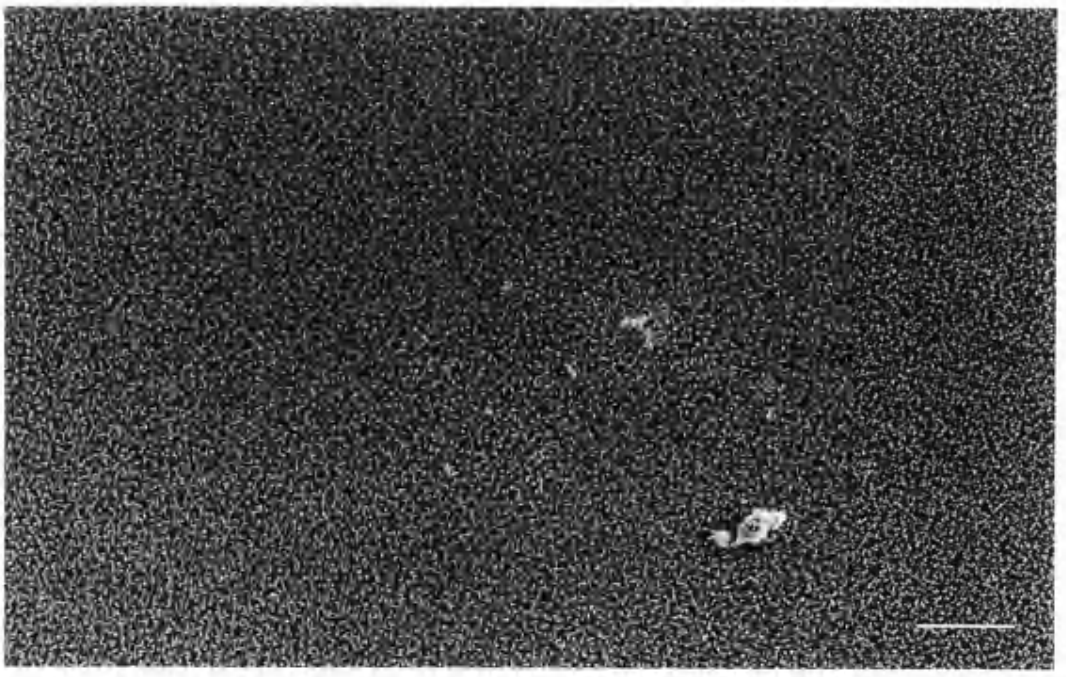

Plate 2-1 Scanning Electron Micrograph at 10kV of a silver film obtained from the AACVD of $AgO_2CMe(PMe_3)_2$ **(2)**, bar = 10 μm.

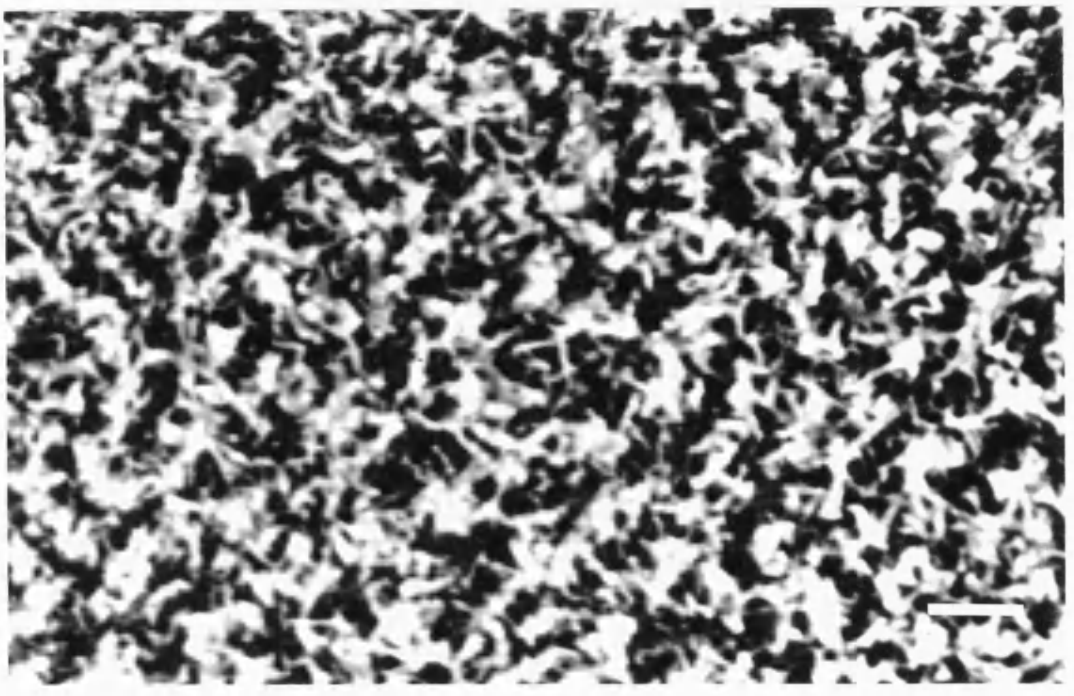

Plate 2-2 Scanning Electron Micrograph at 10kV of a silver film obtained from the AACVD of $AgO_2CMe(PMe_3)_2$ **(2)**, bar = 1 μm.

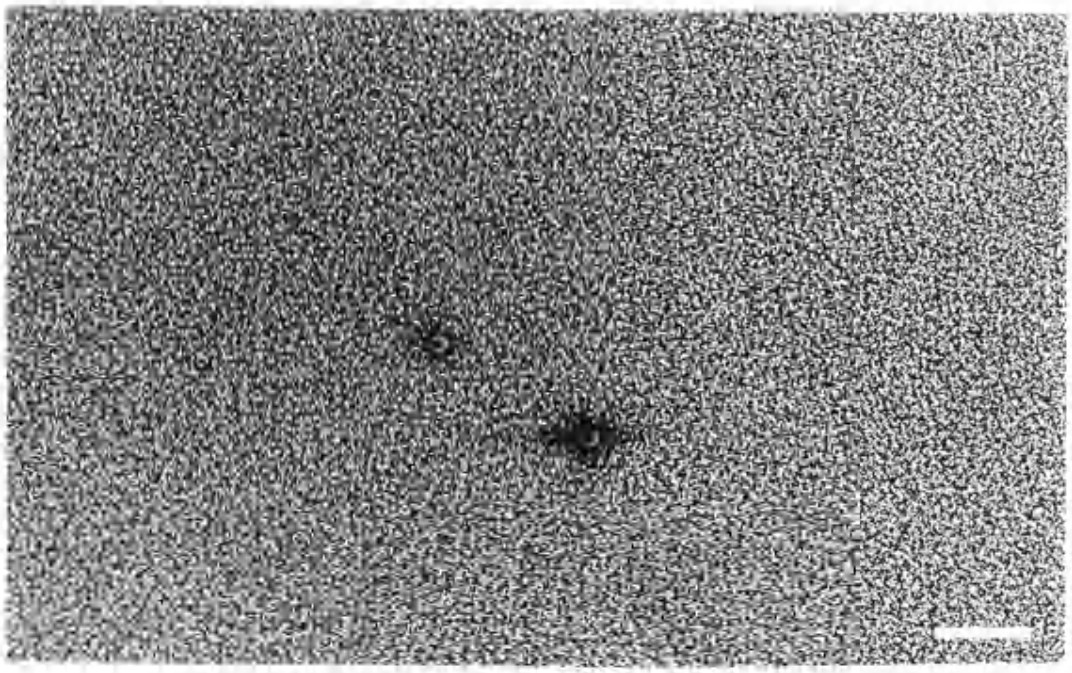

Plate 2-3 Scanning Electron Micrograph at 10kV of a silver film obtained from the AACVD of $AgO_2C^tBu(PMe_3)_2$ **(6)**, bar = 10 μm.

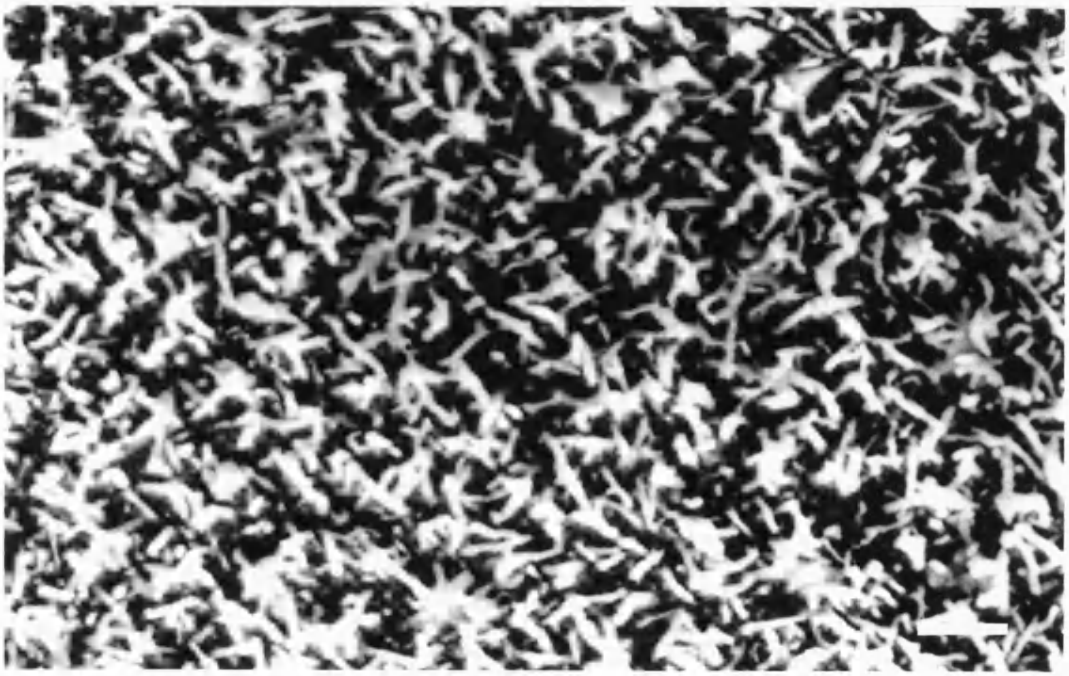

Plate 2-4 Scanning Electron Micrograph at 10kV of a silver film obtained from the AACVD of $AgO_2C^tBu(PMe_3)_2$ **(6)**, bar = 1 μm.

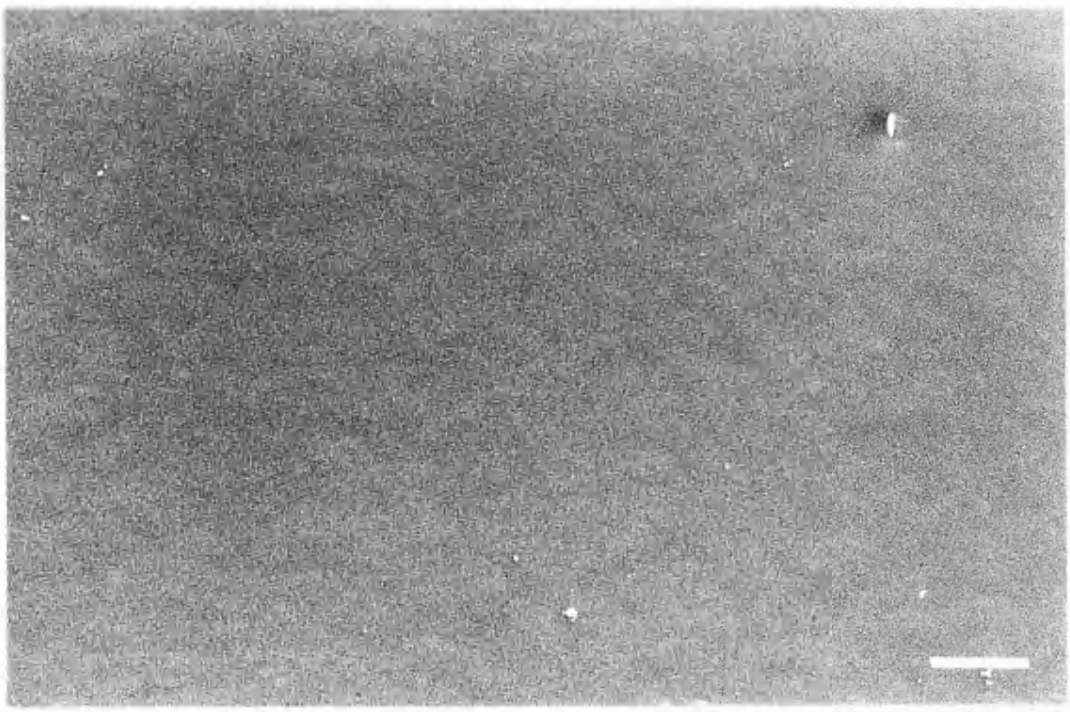

Plate 2-5 Scanning Electron Micrograph at 10kV of a silver film obtained from the AACVD of $AgO_2C^tBu(PPh_3)_2$ **(7)**, bar = 10 μm.

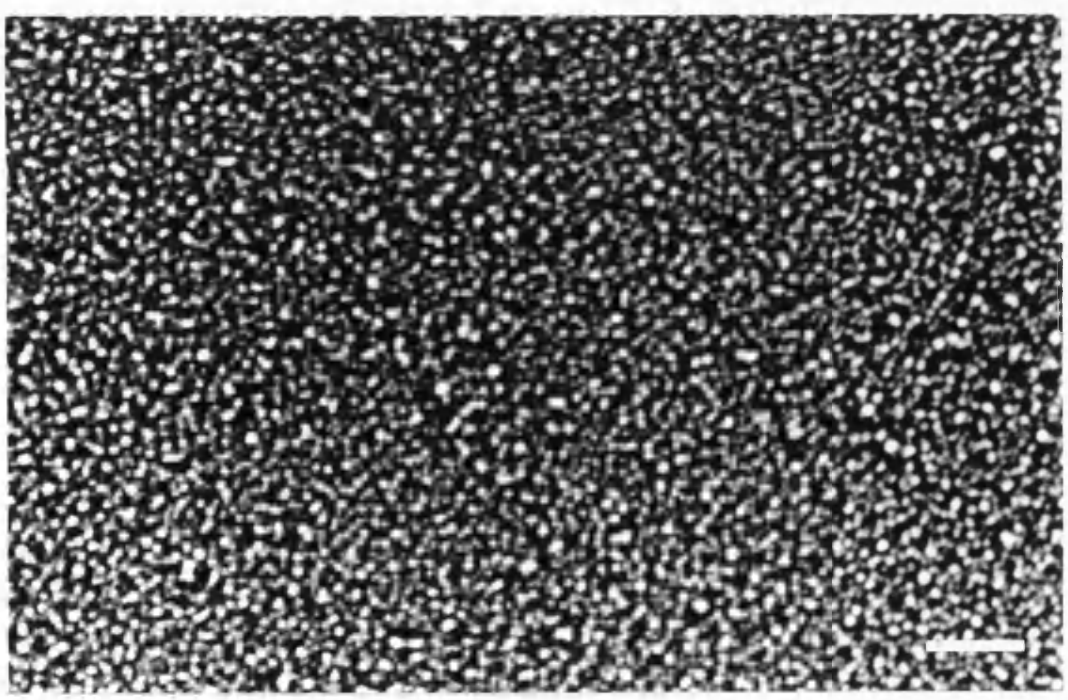

Plate 2-6 Scanning Electron Micrograph at 10kV of a silver film obtained from the AACVD of $AgO_2C^tBu(PPh_3)_2$ **(7)**, bar = 1 μm.

2.5 EXPERIMENTAL

The synthesis of silver(I) acetate - AgO_2CCH_3 (1)

A solution of silver nitrate (3.7 g, 21.8 mmol) in 20 cm^3 of distilled water was added to a solution of sodium acetate (1.7 g, 21.1 mmol) in 20 cm^3 of distilled water. The precipitate was filtered immediately in air, washed with distilled water, ethanol and diethyl ether, and dried *in vacuo*. Yield 2.26 g, 64 %.

Analysis : found (calculated for $C_2H_3O_2Ag$) C, 14.3 (14.4); H, 1.76 (1.81); Ag, 66.7 (64.6) %. IR (Nujol mull) 1200-1800 cm^{-1}: 1345w, 1422sh, 1514b. ^1H NMR (d^6-DMSO) δ; 1.8 (s, $-CH_3$). ^{13}C NMR (d^6-DMSO) δ; 174.8 (O_2C-), 22.2 ($-CH_3$).

The synthesis of O,O'-acetatobis(trimethylphosphine)silver(I) - $AgO_2CCH_3(PMe_3)_2$ (2)

Silver acetate (1) (0.4 g, 2.3 mmol) was suspended in benzene (15 cm^3) and stirred. To this was added 3.5 equivalents of trimethylphosphine as a solution in toluene (1M soln., 8 cm^3, 8 mmol). The solution cleared immediately on addition of the phosphine. The solvent and excess phosphine were removed *in vacuo* to give a brown precipitate in quantitative yield. On contact with air the compound reverted to a slightly brown - clear oil.

Analysis : found (calculated for $C_8H_{21}O_2AgP_2$) C, 30.8 (30.1); H, 6.46 (6.63) %. IR (Nujol mull) 1200-1800 cm^{-1}: 1261w, 1283, 1339w, 1404sb, 1574sb. ^1H NMR ($CDCl_3$) δ; 1.78 (s,

3H, $O_2CC\underline{H}_3$), 1.25 (s, 18H, $P\underline{Me}_3$). ^{13}C NMR ($CDCl_3$) δ; 180.8 (O_2C-), 15.8 (d, 11.1 Hz, $P\underline{Me}_3$). ^{31}P NMR (20°C, $CDCl_3$) δ; -36.4. ^{31}P NMR (-80°C, $CDCl_3/CH_2Cl_2$) δ; -43.4 (dd, 268 Hz), -38.8 (br). ^{109}Ag NMR (-80°C, $CDCl_3/CH_2Cl_2$) δ; 772.

The synthesis of O,O'-acetatobis(triphenylphosphine)silver(I) - $AgO_2CCH_3(PPh_3)_2$ (3)

Silver acetate (1) (1.7 g, 10.3 mmol) and triphenylphosphine (5.4 g, 20.6 mmol) were suspended in 35 cm^3 of toluene. The mixture was stirred for 18 hours, filtered in air and dried *in vacuo.* Yield 6.1 g, 85 %.

Analysis : found (calculated for $C_{38}H_{33}O_2AgP_2$) C,65.9 (66.0); H, 4.78 (4.81) %. IR (Nujol mull) 1200-1800 cm^{-1}: 1308w, 1331w, 1396w, 1553s. IR (hexachlorobutadiene mull) 1200-1800 cm^{-1}: 1283w, 1310w, 1333w, 1399w, 1435sh, 1480sh, 1561. ^1H NMR ($CDCl_3$) δ; 7.41-7.22 (m, 30H, $C_6\underline{H}_5$), 2.01 (s, 3H, $O_2CC\underline{H}_3$). ^{13}C NMR ($CDCl_3$) δ; 177.6 (O_2C-), 133.6 (d, 8.3 Hz, PPh_3), 132.4 (d, 11.9 Hz, PPh_3), 129.7 (PPh_3), 128.5 (d, 4.6 Hz, PPh_3). ^{31}P NMR (20°C, $CDCl_3$) δ; 8.01. ^{31}P NMR (-80°C, $CDCl_3/CH_2Cl_2$) δ; 7.6 (dd, 490 Hz). ^{109}Ag NMR (-80°C, $CDCl_3/CH_2Cl_2$) δ; 907 (t, 489 Hz).

The synthesis of O,O'-acetatotris(triphenylphosphine)silver(I) - $AgO_2CCH_3(PPh_3)_3$ (4)

Silver acetate (1) (1.67 g, 10 mmol) was added to a solution of triphenylphosphine (9.18 g, 35 mmol) in 50 cm^3 of toluene. The silver acetate was washed in with a further 5 cm^3 of toluene.

The flask was stoppered and the contents stirred in the absence of light for 24 hours. The pale cream precipitate was filtered in air, sucked dry and further dried *in vacuo.* Yield 7.82 g, 82 %.

Analysis : found (calculated for $C_{56}H_{48}O_2AgP_3$) C, 68.7 (70.52); H, 4.90 (5.07) %. IR (Nujol mull) 1200-1800 cm^{-1}: 1325w, 1435sh, 1563. (hexachlorobutadiene mull) 1200-1800 cm^{-1}: 1310w, 1326w, 1381, 1406w, 1435sh, 1480sh, 1565sb. ^1H NMR ($CDCl_3$) δ; 7.36-7.02 (m, 45H, $C_6\underline{H}_5$), 2.00 (s, 3H, $O_2CC\underline{H}_3$). ^{13}C NMR ($CDCl_3$) δ; 174.8 (O_2C-), 133.7 (d, 8.3 Hz, PPh_3), 133.2 (d, 10.1 Hz, PPh_3), 129.6 (PPh_3), 128.5 (d, 4.6 Hz, PPh_3), 22.2 ($-CH_3$). ^{31}P NMR (20°C, $CDCl_3$) δ; 5.79. ^{31}P NMR (-80°C, $CDCl_3/CH_2Cl_2$) δ; 7.4 (d, ~ 450 Hz), 4.9 (dd, 256 Hz).

The synthesis of silver pivalate - $AgO_2CC_4H_9$ (5)

Pivalic acid (5.0 g, 49 mmol) was suspended in 100 cm^3 of distilled water and stirred vigorously with gentle warming. The acid was solubilised with concentrated ammonia solution, then gently warmed to remove excess ammonia. The reaction mixture was filtered to remove unreacted acid and impurities found in the acid. Silver nitrate (8.5 g , 50 mmol) was dissolved in 25 cm^3 of distilled water and added to the solution resulting in an immediate thick white precipitate, which was filtered immediately in air. The precipitate was washed with distilled water followed by ethanol and diethyl ether and dried *in vacuo* for 3 hours. Yield 9.2 g, 88%.

Analysis : found (calculated for $C_5H_9O_2Ag$) C, 28.6 (28.7); H, 4.35 (4.3) %. IR (Nujol mull) 1200-1800 cm^{-1}: 1217wb, 1352sh, 1366sh, 1399sh, 1512sb, 1526w, 1564w. ^1H NMR (d^6-

DMSO) δ; 1.12 (s, C<u>Me</u>$_3$). ^{13}C NMR (d^6-DMSO) δ; 182.0 (O_2C-), 29.0 (-C<u>Me</u>$_3$). ^{109}Ag NMR (20°C, d^6-DMSO) δ; 303.

The synthesis of O,O'-pivalatobis(trimethylphosphine)silver(I) - $AgO_2CC_4H_9(PMe_3)_2$ (6)

Silver pivalate (5) (1.2 g, 5.5 mmol) was suspended in 15 cm^3 of toluene and stirred under a nitrogen atmosphere. To this was slowly added 3 equivalents of a 1 Molar solution of trimethylphosphine in toluene (17 cm^3, 17 mmol). The solid was solubilised on addition of approximately one equivalent of phosphine. The reactants were stirred in the absence of light for 24 hours. Solvent and excess ligand were removed *in vacuo* to give a brown crystalline solid. Yield 1.40 g, 70 %.

Analysis : found (calculated for $C_{11}H_{27}O_2AgP_2$) C, 34.8 (36.7); H, 7.82 (7.56) %. IR (Nujol mull) 1200-1800 cm^{-1}: 1219, 1283, 1304w, 1362s, 1401, 1422, 1557sb, 1653. ^{1}H NMR ($CDCl_3$) δ; 1.25 (s, 18H, P<u>Me</u>$_3$), 1.11 (s, 9H, -C<u>Me</u>$_3$). ^{13}C NMR ($CDCl_3$) δ; 184.7 (O_2C-), 39.4 (-<u>C</u>Me$_3$), 28.6 (-C<u>Me</u>$_3$), 15.3 (d, 8.3 Hz, P<u>Me</u>$_3$). ^{31}P NMR (20°C, $CDCl_3$) δ; -39.1. ^{31}P NMR (-80°C, $CDCl_3/CH_2Cl_2$) δ; -38.2 (br).

The synthesis of O,O'-pivalatobis(triphenylphosphine)silver(I) - $AgO_2CC_4H_9(PPh_3)_2$ (7)

Silver pivalate (5) (0.2 g, 1.0 mmol) and triphenylphosphine (1.0 g, 4.0 mmol) were suspended in 25 cm^3 of toluene. The whole was stirred in the absence of light for 24 hours. The reaction

mixture was filtered in air, washed with 2 cm^3 of toluene, sucked dry and further dried *in vacuo*. Yield 0.38 g, 52 %.

Analysis: found (calculated for $C_{41}H_{39}O_2AgP_2$) C, 66.9 (67.1); H, 5.31 (5.36) %. IR (Nujol mull) 1200-1800 cm^{-1}: 1225w, 1406w, 1435sh, 1477sh, 1543sh. IR (hexachlorobutadiene mull) 1200-1800 cm^{-1}: 1308, 1356, 1402, 1435sh, 1479sh, 1495w, 1562b. ^1H NMR ($CDCl_3$) δ; 7.45-7.22 (m, 30H, $C_6\underline{H}_5$), 1.23 (s, 9H, -CMe_3). ^{13}C NMR ($CDCl_3$) δ; 185.2 (O_2C-), 133.9 (d, 18.4 Hz, PPh_3), 132.5 (d, 27.6 Hz, PPh_3), 129.9 (PPh_3), 128.6 (d, 9.2 Hz, PPh_3), 39.4 (-$\underline{C}Me_3$), 28.7 (-$C\underline{Me}_3$). ^{31}P NMR (20°C, $CDCl_3$) δ; 8.51. ^{31}P NMR (-80°C, $CDCl_3/CH_2Cl_2$) δ; 7.75 (dd, 480 Hz). ^{109}Ag NMR (-80°C, $CDCl_3/CH_2Cl_2$) δ; 931 (t, 484 Hz).

The synthesis of silver mesitylate - $AgO_2CC_6H_2Me_3$ (8)

Mesitylenecarboxylic acid (3.3 g, 20 mmol) was suspended in 60 cm^3 of distilled water and stirred with gentle warming. The acid was solubilised by addition of a few drops of concentrated ammonia solution, until the solution was faintly ammoniacal. The solution was gently warmed to remove excess ammonia and filtered to remove unreacted acid. Silver nitrate (3.6 g, 21 mmol) in 10 cm^3 of distilled water was added resulting in an immediate white precipitate. The product was filtered in air , washed with distilled water, ethanol and diethyl ether and dried *in vacuo* for 3 hours. Yield 5.25 g, 96 %.

Analysis : found (calculated for $C_9H_{11}O_2Ag$) C, 44.0 (41.73); H, 4.11 (4.28) %. IR (Nujol mull) 1200-1800 cm^{-1}: 1393b, 1441b, 1557bs, 1613w. ^1H NMR (d^6-DMSO) δ; 6.76 (m, 2H,

O_2C-Ar-H), 2.23 (m, 6H, *o*-O_2C-Ar-Me), 2.20 (m, 3H, *m*-O_2C-Ar-Me). ^{13}C NMR (d^6-DMSO) δ; 174.3 (O_2C-), 139.0 (-$C_6H_2Me_3$), 135.1 (-$C_6H_2Me_3$), 132.4 (-$C_6H_2Me_3$), 127.5 (-$C_6H_2Me_3$), 20.7 (-$C_6H_2Me_3$), 20.1 (-$C_6H_2Me_3$). ^{109}Ag (20°C, d^6-DMSO) δ; 266.

The synthesis of O,O'-mesitylatobis(trimethylphosphine)silver(I) - $AgO_2CC_6H_2Me_3(PMe_3)_2$ (9)

Silver mesitylate (3.46 g, 13.4 mmol) was suspended in 20 cm^3 of toluene. The mixture was stirred under a dry nitrogen atmosphere. To this was slowly added a 1 Molar solution of trimethylphosphine in toluene (40 cm^3, 40 mmol, 3 equivalents). On addition, the mixture cleared to a solution, which was then stirred in the absence of light for 3 hours. The solvent was then removed *in vacuo* to give a light brown precipitate. Yield 5.32 g, 97 %.

Analysis : found (calculated for $C_{15}H_{29}O_2AgP_2$) C, 45.3 (43.8); H, 7.11 (7.11) %. The compound was successfully recrystallised from a heptane-dichloromethane solvent mixture, although analysis results were no closer. Analysis : found (calculated for $C_{15}H_{29}O_2AgP_2$) C, 45.4 (43.8); H, 7.21 (7.11) %. IR (Nujol mull) 1200-1800 cm^{-1}: 1287, 1304w, 1435, 1564. IR (hexachlorobutadiene mull) 1200-1800 cm^{-1}: 1286, 1387s, 1422, 1431. ^1H NMR ($CDCl_3$) δ; 6.66 (m, 2H, O_2C-Ar-H), 2.27 (m, 6H, *o*-O_2C-Ar-Me), 2.14 (m, 3H, *p*-O_2C-Ar-Me), 1.30 (s, 18H, PMe_3). ^{13}C NMR ($CDCl_3$) δ; 176.5 (O_2C-), 140.5 (-$C_6H_2Me_3$), 135.1 (-$C_6H_2Me_3$), 132.5 (-$C_6H_2Me_3$), 127.8 (-$C_6H_2Me_3$), 20.9 (-$C_6H_2Me_3$), 20.3 ($C_6H_2Me_3$), 16.1 (PMe_3). ^{31}P NMR (20°C, $CDCl_3$) δ; -39.6. ^{31}P NMR (-80°C, $CDCl_3/CH_2Cl_2$) δ; -38.0 (d, ~ 500+ Hz). ^{109}Ag NMR (-80°C, $CDCl_3/CH_2Cl_2$) δ; 834.

The synthesis of O,O'-mesitylatobis(triphenylphosphine)silver(I) - $AgO_2CC_6H_2Me_3(PPh_3)_2$ (10)

Silver mesitylate (1.87 g, 6.9 mmol) was suspended in 25 cm^3 of toluene and stirred. To this was added two equivalents of triphenylphosphine (3.62 g, 13.8 mmol) resulting in a thick cream precipitate. The reagents were stirred for 68 hours in the absence of light and filtered in air. The precipitate was sucked dry and further dried *in vacuo* for several hours. Yield 5.15 g, 6.5 mmol, 94 %.

Analysis : found (calculated for $C_{46}H_{42}O_2AgP_2$) C, 68.5 (69.35); H, 5.15 (5.31) %. The compound was satisfactorily recrystallised from a toluene-dichloromethane solvent mixture to give poor quality crystals approximating to the compound as a 1:1 dichloromethane solvate. Analysis : found (calculated for $C_{47}H_{44}O_2AgP_2Cl_2$) C, 64.0 (64.0); H, 4.69 (5.0) %. IR (Nujol mull) 1200-1800 cm^{-1}): 1304wb, 1435sh, 1479wsh, 1545sh, 1574wsh. IR (hexachloro butadiene mull) 1200-1800 cm^{-1}: 1312w, 1385sh, 1435ssh, 1482sh, 1545ssh. ^1H NMR ($CDCl_3$) δ; 7.35-7.15 (m, 30H, PPh_3), 6.65 (m, 2H, O_2CAr-H), 2.16 (m, 6H, *o*-O_2C-Ar-Me), 2.00 (m, 3H, *p*-O_2C-Ar-Me). ^{13}C NMR ($CDCl_3$) δ; 176.9 (O_2C-), 139.5 (-$C_6H_2Me_3$), 134.8 (-$C_6H_2Me_3$), 133.8 (d, 8.3 Hz, PPh_3), 133.1 (d, 9.2 Hz, PPh_3), 132.6 (-$C_6H_2Me_3$), 129.8 (PPh_3), 128.7 (d, 4.6 Hz, PPh_3), 127.2 (-$C_6H_2Me_3$), 20.9 (-$C_6H_2Me_3$), 19.4 (-$C_6H_2Me_3$). ^{31}P NMR (20°C, $CDCl_3$) δ; 5.56. ^{31}P NMR (-80°C, $CDCl_3/CH_2Cl_2$) δ; 7.98 (dd, 497 Hz). ^{109}Ag NMR (-80°C, $CDCl_3/CH_2Cl_2$) δ; 895 (t, 503 Hz).

CHAPTER THREE

SYNTHESIS, CHARACTERISATION AND CVD PROPERTIES OF SILVER(I) FLUOROCARBOXYLATES AND THEIR PHOSPHINE ADDUCTS

3.1 INTRODUCTION

Silver fluorocarboxylates have found similar applications to their non-fluorinated analogues, such as in organic synthesis. [104, 105] In addition, they have found applications as NMR shift reagents. [168, 169] Silver fluorocarboxylates were among the first silver carboxylates to be structurally characterised, the structures of the perfluorobutyrate and trifluoroacetate reported in 1955 and 1972, respectively. Recently silver fluorocarboxylates and various adducts have been prepared in connection with chemical vapour deposition studies. [170, 171]

Earlier studies, as outlined in Chapter 2, had identified the possibility of using silver(I) carboxylates as CVD precursors and attention was subsequently focused on the use of perfluorinated carboxylate ligands. The use of fluorine in ligands has long been known to have a beneficial effect on precursor volatility, due to the reduction in van der Waals interactions. Additionally, fluoroalkyl silver compounds are known to be considerably more stable than their alkyl counterparts and as these organosilver species are thought to be formed *in situ* via decarboxylation, it was reasoned that the increased stability of transient fluoroalkyl silver species might have a beneficial effect on film growth.

Silver fluorocarboxylates are also thought to decompose via decarboxylation [108] and this degradation has been implicated through mass spectrometry, [111, 113] thermal [109, 110, 170-172] and photochemical decomposition [109] studies. It has been suggested that this pathway may differ mechanistically from non-fluorinated carboxylates [110] as quantitative yields (80%) of coupling products are also produced in the reaction (Eqn 3-1).

$$2CF_3(CF_2)_nCO_2Ag \xrightarrow{\Delta} CF_3(CF_2)_n\text{-}(CF_2)_nCF_3 + 2CO_2 + 2Ag \qquad \textbf{(3-1)}$$

The decomposition of silver perfluorobutyrate has been studied in some detail. [110] Mechanisms which have been suggested involve formation of an anhydride and silver oxide as a primary step, with further degradation of the anhydride catalysed by silver oxide and reduction to the metal by reaction with CO (Eqn 3-2).

$$2C_3F_7CO_2Ag \longrightarrow (C_3F_7CO)_2O + Ag_2O \qquad \textbf{(3-2)}$$

$$(C_3F_7CO)_2O \longrightarrow n\text{-}C_6F_{14} + CO_2 + CO$$

$$Ag_2O + CO \longrightarrow CO_2 + 2Ag$$

In addition to the suggested mechanistic differences in decomposition routes, in this study silver fluorocarboxylates have been found to exhibit different physical characteristics as compared to unfluorinated silver carboxylates. They show increased volatility and solubility over their non-fluorinated analogues, as shown in mass spectrometry and film growth experiments. Indeed the addition of phosphines has been shown to have a detrimental effect on film growth rates, whereas it is essential in the case of non-fluorinated silver carboxylates. For these reasons silver fluorocarboxylates will be dealt with in this chapter as a separate topic. A number of sections of the preceding chapter will also apply here, specifically those concerning synthesis (2.1.1), general structural chemistry (2.1.2) and infra-red spectroscopy (2.2.2). This short

introduction will be limited to a brief summary, attention being largely directed at literature specifically relevant to silver fluorocarboxylates.

3.1.1 Synthetic Routes

Silver fluorocarboxylates are quite easy to prepare and are relatively stable to light, air and moisture at room temperature when in the solid phase. They are, however, known to be susceptible to photolysis by ultra-violet light at 25°C when in solution. [109] Stability may be greatly enhanced by the formation of adducts with Lewis bases, for example phosphines.

A number of silver(I) fluorocarboxylates are commercially available. Synthesis may be effected by a number of routes as outlined in 2.1.1. Where the fluorocarbon chain is short, the fluorocarboxylic acids are reactive enough to allow direct reaction with silver oxide (synthetic route II). As fluorinated chain length is increased, carboxylic acids become less soluble in aqueous solution and less acidic, thereby precluding direct reaction with silver oxide. In the case of longer chain fluorinated carboxylic acids, solubilisation with ammonia and precipitation of the silver salt with silver nitrate (synthetic route III) is a suitable alternative.

3.1.2 Structural Chemistry

Silver(I) fluorocarboxylates are also known to take up structures based upon the eight membered dimeric bis(silver)bis(carboxylato-*O,O'*) rings common in silver(I) carboxylate structures. Structures for silver carboxylates and the related betaines have been classified in the

literature as Types A-D, E_1 and E_2 (Figure 2-1). [114] Examples of silver fluorocarboxylates in the literature exist as Types A, B and a modified Type D. Silver fluorocarboxylates are notably more soluble and volatile in comparison to their non-fluorinated analogues and this suggests that inter-dimer bonds are weaker than the bonds within the eight membered rings. For example silver trifluoroacetate and silver perfluorobutyrate are reported to be soluble in benzene [142, 174] and this contrasts with non-fluorinated silver carboxylates prepared in this study which were insoluble except in very polar solvents (e.g. DMSO).

Silver(I) trifluoroacetate, as structurally determined in 1972, is reported as a Type A dimeric structure (Figure 3-1), with no mention of additional bridging silver-oxygen bonds. [173] Two slightly different dimers were found in the unit cell and this was confirmed by ^{19}F NMR of crystals of AgO_2CCF_3 at 40 K. Silver trifluoroacetate is known to be very soluble in a wide range of solvents including water which also indicates no more than very weak aggregation into a polymeric structure.

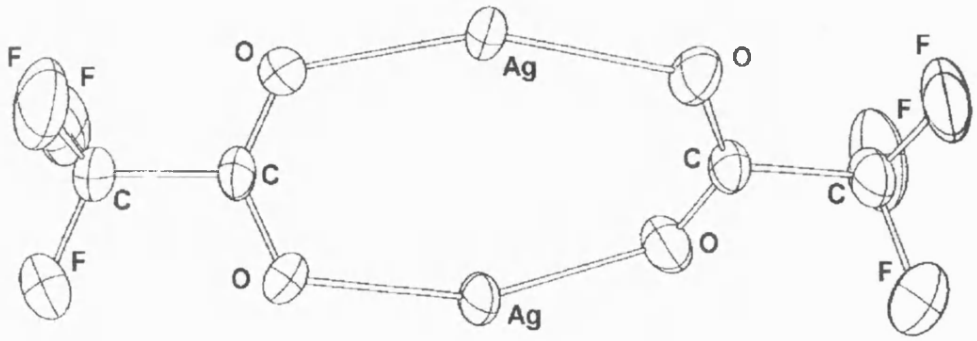

Figure 3-1 Crystal structure of silver (I) trifluoroacetate, [173] (Type A).

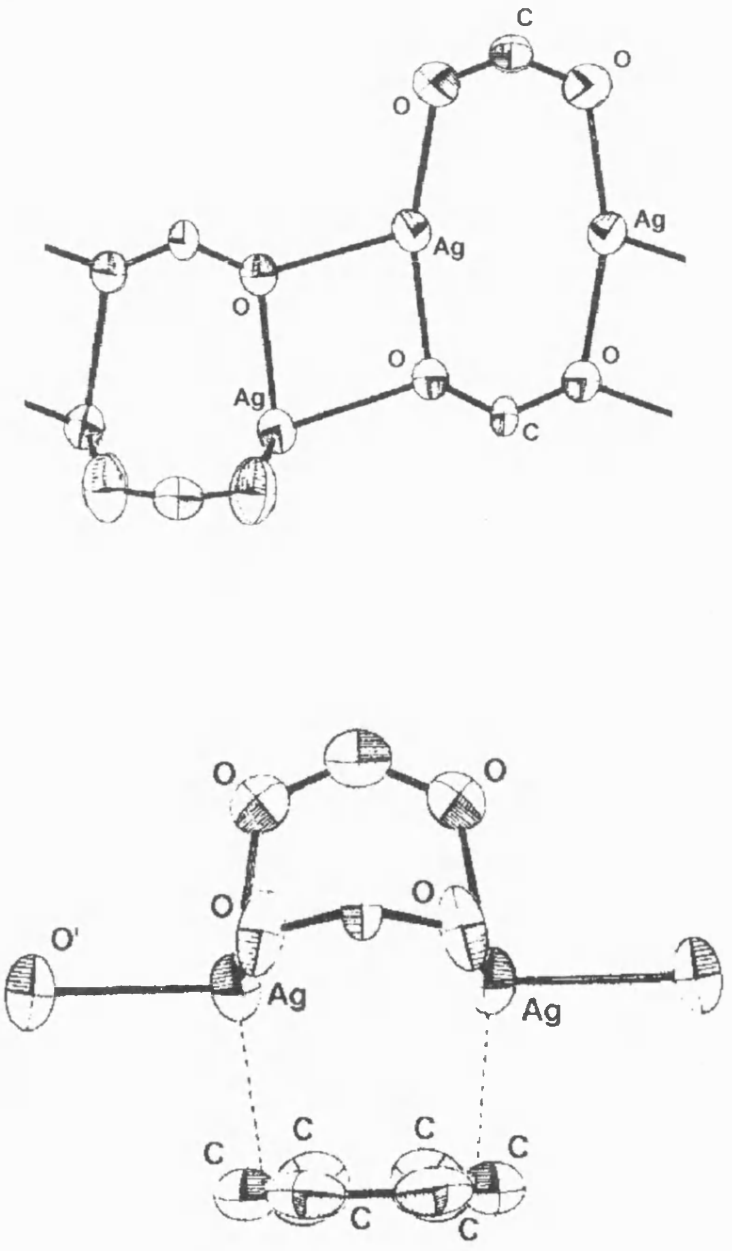

Figure 3-2 Crystal structure of silver trifluoroacetate benzene adduct, [142] (Type D), (a) silver carboxylate chain, (b) interaction with benzene.

Recrystallisation of silver trifluoroacetate from benzene results in a change from dimeric Type A to a polymeric Type D structure (Figure 3-2). Half of the silver atoms show additional bonding to a benzene via a π-interaction and other benzene molecules exist as independent molecules in the crystal lattice. [142] The formation of the silver trifluoroacetate chain in the adduct $(AgO_2CCF_3)_2.C_6H_6$ is presumably due to electronic considerations since sterically a less oligomeric adduct structure might be expected. The Ag-Ag distance in the benzene solvate is comparable to that in the unsolvated silver trifluoroacetate. However Ag-O bond lengths are on average slightly longer in the adduct where they additionally bridge across dimers. The $(AgO_2CCF_3)_2$ dimer is reported as essentially flat but the benzene adduct has a highly puckered chain that allows-π bonds to benzene molecules in a sterically less crowded underside.

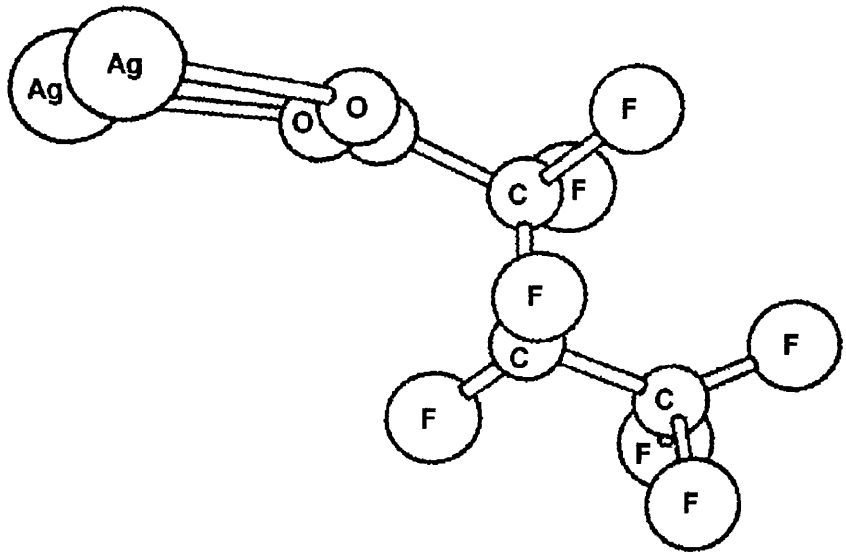

Figure 3-3 Partial crystal structure of silver(I) perfluorobutyrate, [174] (Type C).

Silver(I) perfluorobutyrate has also been described as dimeric (Figure 3-3), [172] although closer examination of the original publication [174] reveals that each silver atom additionally interacts with oxygens from two neighbouring dimers, resulting in a Type C structure. Bond lengths for these interactions are of the order of 2.6 Å, within the range of these bond lengths found in Type C silver carboxylate structures (2.5-2.7 Å). Due to the age of the publication, bond distances and angles are not as accurately determined as in later structures, however the bis(silver)bis(carboxylato-*O,O'*) ring appears essentially flat. This structure is also interesting in view of the fact that this compound is known to exist as dimers in benzene solution. [174]

The only remaining structurally characterised silver fluorocarboxylate adduct in the literature contains the donor ligand 2,2-dimethylbut-3-enyl methyl sulphide (V), which is potentially bidentate with bonding through the thioether sulphur and an alkene double bond. [175] The 1:1 adduct with silver trifluoroacetate results in the break up of the dimeric structure in favour of essentially monomeric units linked by bridging silver-sulphur bonds (Figure 3-4). The fluorocarboxylate ligand assumes a highly unsymmetrical chelating mode (Ag-O 2.29Å, 2.99Å) while the ligand (V) encloses the silver centre as part of a five-membered ring. Additionally, the sulphur bridges to a neighbouring silver (2.632Å versus 2.582Å in the ring) to form a polymeric geometry. Fluorine atoms in the trifluoroacetate are disordered over two sites. Solution studies of this compound suggest that the olefin group is labile on the NMR timescale.

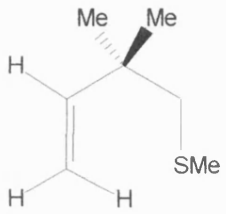

(V)

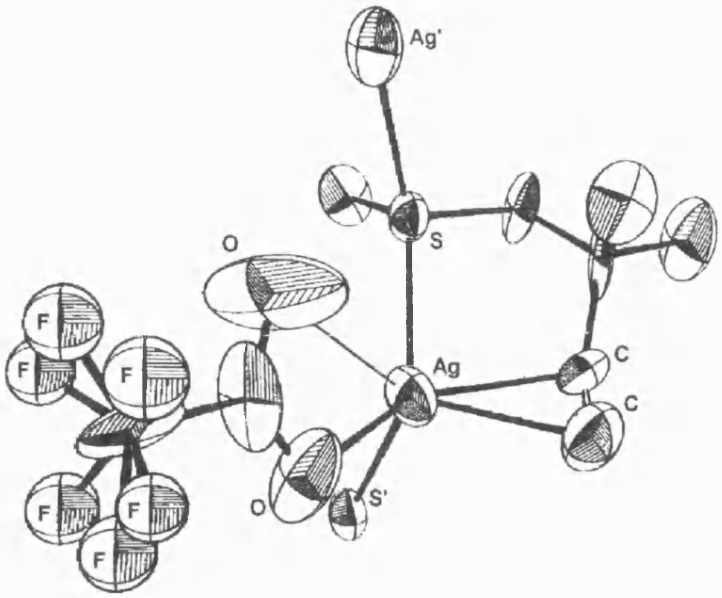

Figure 3-4 Crystal structure of (2,2-dimethylbut-3-enyl methyl sulphide) trifluoroacetatosilver(I). [175]

Silver fluorocarboxylates and their adducts have been studied by various techniques, including mass spectrometry, [111, 113] infra-red [172] and low frequency infra-red spectroscopy, [111] NMR [150] and thermal analysis. [110] Recent research interest in silver fluorocarboxylates and their adducts has led to preparation of representative compounds as potential CVD precursors by another research group. [170, 171] In these studies a range of silver fluorocarboxylates RCO_2Ag [R = $CF_3(CF_2)_2$, $CF_3(CF_2)_6$, $CF_3(CF_2)_8$, C_6F_5, $C_6F_5CH_2$] and their adducts $RCO_2Ag(PPh_3)$ (R = C_2F_5, C_3F_7, C_7F_{15}, C_9F_{19}, C_6F_5, $C_6F_5CH_2$) have been prepared and analysed. Additionally, the silver salt and 1:1 ($Ag:PPh_3$) adduct of $HO_2C\text{-}C_3F_6\text{-}CO_2H$ has also been isolated. These compounds have been characterised by IR, ^{13}C NMR and ^{19}F NMR and by thermal analysis under an oxygen atmosphere.

The present study has focused on silver fluorocarboxylates AgO_2CR with an increasing chain length (R = C_3F_7, C_6F_{13}, C_7F_{15}) and their bis-triphenylphosphine adducts. These compounds have been structurally characterised and their use as precursors for silver film formation explored.

3.2 RESULTS AND DISCUSSION

3.2.1 Synthesis

A series of silver fluorocarboxylates have been prepared in which the organic group of the carboxylate (R) has been varied as a function of chain length (R = C_3F_7, C_6F_{13} and C_7F_{15}) (Scheme 3-1). In contrast to the non-fluorinated carboxylates, these compounds exhibited an increased degree of volatility and solubility without addition of phosphines. Preparative yields were found within the range 53-77 %. Decomposition temperatures (as measured by TGA) showed similar thermal stabilities for non adduct silver fluorocarboxylates 250°C **(11)**, 250°C **(13)** and 275°C **(15)**.

Bis-triphenylphosphine adducts of each of these carboxylates were prepared (Scheme 3-1). Adducts could be prepared by stirring with either a stoicheometric amount or an excess of triphenylphosphine. In cases where in excess of three equivalents of triphenylphosphine was added to the silver salt **(12)** and in cases where two equivalents of triphenylphosphine were added **(14)**, **(16)** only the bis adducts were isolated. Recrystallisations resulted in isolation of the bis- adducts, no evidence was found for the presence of tris- or mono- phosphine adducts. Mono-triphenylphosphine adducts including 1:1 adducts of **(11)** and **(15)** have been prepared in

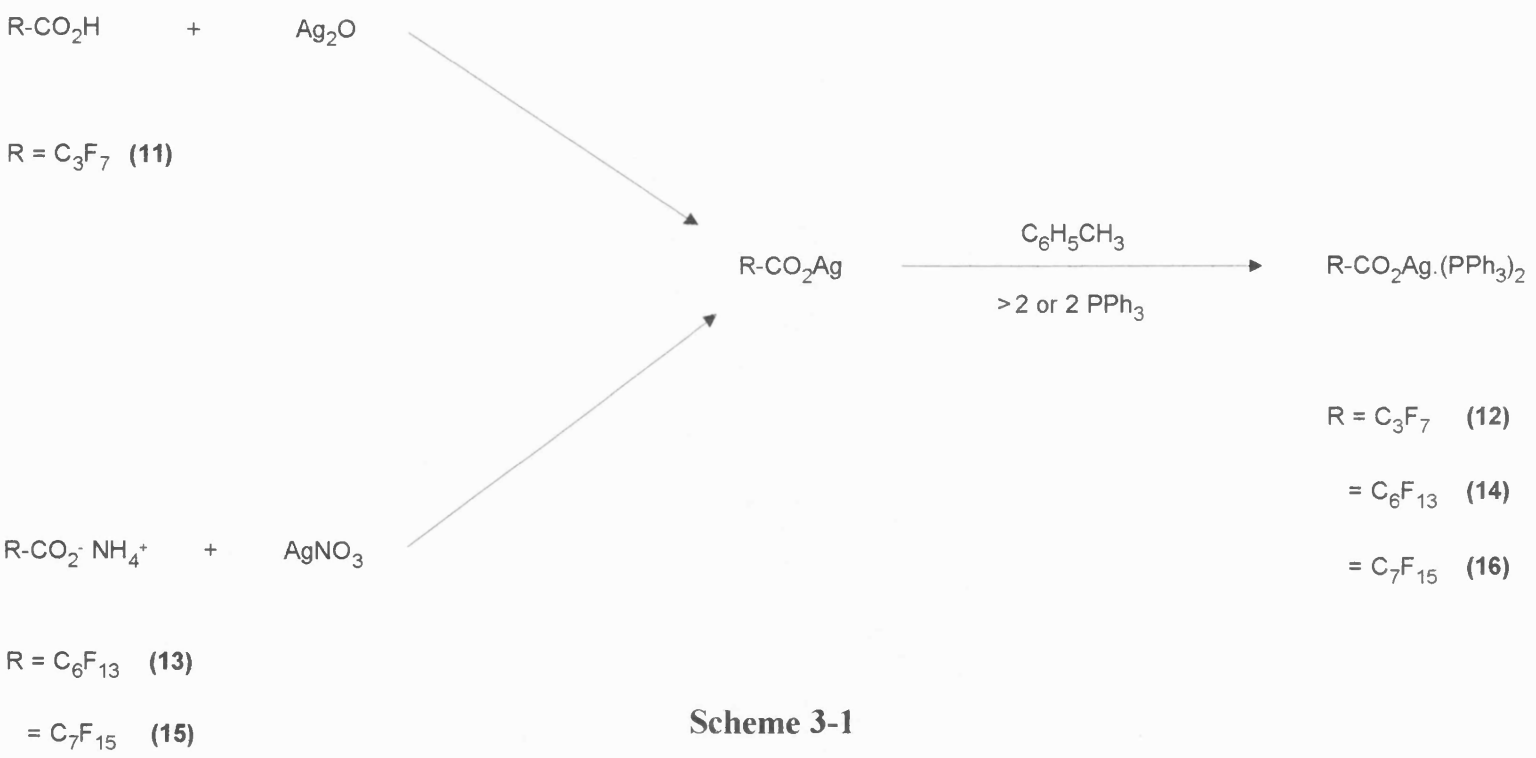
R-CO2H + Ag2O
R = C3F7 (11)
R-CO2Ag
C6H5CH3
>2 or 2 PPh3
R-CO2Ag.(PPh3)2
R = C3F7 (12)
= C6F13 (14)
= C7F15 (16)
R-CO2- NH4+ + AgNO3
R = C6F13 (13)
= C7F15 (15)

Scheme 3-1

other recent studies using stoicheometric quantities of phosphine. [171] Preparative yields for the bis-phosphine adducts in this study were found within the range 52-90%. Decomposition points were found lower than for the parent silver fluorocarboxylate at 211°C **(12)** and 210°C **(14)**. In the case of **(16)**, decomposition started at the lower temperature of 160°C although above 200°C the TGA trace appeared very similar to those obtained for other silver fluorocarboxylates.

3.2.2 Infra-red Spectroscopy

The arguments and limitations concerning the use of $\nu_a(CO_2^-)$ and $\nu_s(CO_2^-)$ for the structural assignment of silver carboxylates has been outlined in Chapter 2. On this basis, tentative assignments have been made for $\nu_a(CO_2^-)$ and $\nu_s(CO_2^-)$ (Table 3-1). Sharp strong peaks found in IR spectra of the triphenylphosphine adducts at 1435-7 cm^{-1} and at 1480 cm^{-1} are assigned to C-H vibrations from the triphenylphosphine and these compare well with those found in triphenylphosphine adducts of non-fluorinated carboxylates (Chapter 2). $\Delta\nu$ for the silver fluorocarboxylates is found to span a narrow range (183-193 cm^{-1}) implying a similar carboxylate bonding mode in compounds **(11)**, **(13)** and **(15)**. These results are not in accordance with recently published IR data on several of these compounds. Compounds **(11)** and **(15)** prepared from Ag_2CO_3 and the free acid are reported as exhibiting $\Delta\nu$ of 278 and 258 cm^{-1} respectively. [170] On this basis of high $\Delta\nu$, mono-dentate bonding of the carboxylates are proposed despite a literature report of a single crystal X-ray diffraction study of **(11)** which shows it to contain bridging carboxylates (Figure 3-3). [174]

The values of $\Delta\nu$ are increased on formation of adducts (265-266 cm^{-1}) for **(12)** and **(14)** and this is consistent with the formation of adducts for alkyl or aryl carboxylates described in Chapter 2. A single crystal X-ray diffraction study of compound **(12)** has shown that the perfluorobutyrate ligand takes up a symmetrical chelating mode. Compound **(14)** undergoes a similar change in $\Delta\nu$ on adduct formation implying an equivalent structural change. The infra red spectrum of compound **(16)** displays a strong, sharp band at 1692 cm^{-1} [assigned as $\nu_a(CO_2^-)$], this being considerably higher than for adducts **(12)** and **(14)**. The spectrum of **(16)** does not display a band due to $\nu_s(CO_2^-)$ in the expected region [$\nu_s(CO_2^-)$ = 1394 **(12)**, 1395 **(14)** cm^{-1}], the nearest assignable band being at 1360 cm^{-1}. If these assignments are correct then this suggests unidentate bonding for the carboxylate in **(16)** ($\Delta\nu$ = 332 cm^{-1}), although there is no obvious reason why the carboxylate groups in **(14)** ($C_6F_{13}CO_2^-$) and **(16)** ($C_7F_{15}CO_2^-$) should bond differently. Mono adducts of compounds **(11)** and **(13)** with triphenylphosphine are reported to increase $\Delta\nu$ further to 340 and 317 cm^{-1} respectively [171] and this has also been attributed to unidentate bonding.

3.2.3 ^{13}C and ^{19}F NMR Spectroscopy

Carbon-13 and fluorine-19 NMR of **(11)-(16)**, are shown in Tables 3-2 and 3-3 respectively. In the ^{13}C NMR spectra the carbonyl carbon in the carboxylate group (-$\underline{C}O_2Ag$) appears at a higher field in the fluorocarboxylates (135.6-159.8 ppm) as compared with non-fluorinated carboxylates (174.3-185.2 ppm). These ^{13}C carboxylate resonances were subject to ^2J coupling to nearby fluorine atoms to give a low intensity triplets with ^2J(F-C-C) coupling of 20-30 Hz. Carbon-13 resonances of CF_2 and CF_3 were often of low intensity caused by coupling to various fluorine atoms, the expected number of resonances was not observed although this may

Table 3-1 Selected IR data (cm^{-1}) for silver(I) fluorocarboxylates and their adducts. [a]

Compound		$\nu_a(CO_2^-)$	$\nu_s(CO_2^-)$	$\Delta\nu$ [b]
$AgO_2CC_3F_7$ [c]	**(11)**	1609	1426	183
$AgO_2CC_3F_7.(PPh_3)_2$	**(12)**	1660	1394	266
$AgO_2CC_6F_{13}$	**(13)**	1611	1424	187
$AgO_2CC_6F_{13}.(PPh_3)_2$	**(14)**	1660	1395	265
$AgO_2CC_7F_{15}$ [d]	**(15)**	1613	1420	193
$AgO_2CC_7F_{15}.(PPh_3)_2$	**(16)**	1692	1360	332

[a] IR spectra were recorded as nujol or hexachlorobutadiene mulls on KBr plates [b] $\Delta\nu = \nu_a(CO_2^-) - \nu_s(CO_2^-)$ [c] literature values $\nu_a(CO_2^-)$ 1678, $\nu_s(CO_2^-)$1400, $\Delta\nu$ 278 cm^{-1} see text [170] [d] literature value $\nu_a(CO_2^-)$ 1658, $\nu_s(CO_2^-)$ 1400, $\Delta\nu$ 258 cm^{-1} see text [170]

indicate merging of CF_2 signals. In the case of the adducts, triphenylphosphine ^{13}C resonances were readily identified whereas by comparison ^{13}C resonances from the fluorocarbon R group were unobserved. This was due both to the abundance of the phenyl carbon atoms and the reduction in intensity of the fluorocarbon ^{13}C resonances due to C-F coupling.

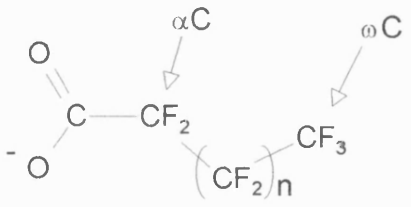

(VI)

Fluorine-19 NMR experiments gave the expected number of resonances and these were split by fluorine-fluorine coupling. Emsley [176] has reported that $^3J(F\text{-}F)$ is of the order of 1 Hz, whereas $^4J(F\text{-}F)$ is around ten times this value (9.9 Hz). On this basis, the first peak in each of the spectra (-80.7 to -81.7) can be assigned as the terminal CF_3 (ωC), and the nearby resonance (-115.0 to -119.2) as the CF_2 adjacent to the carboxylate (αC). Remaining CF_2's along the chain are split by an assortment of ^3J and ^4J fluorine-fluorine couplings which may appear as slightly broadened singlets. It should be noted while resonances due to the fluorocarbon chain are weak and often unobserved in the ^{13}C NMR spectra, they are however readily identified in the ^{19}F NMR spectra and this is attributable to the increased sensitivity of ^{19}F NMR.

Table 3-2 ^{13}C NMR data for silver(I) fluorocarboxylates and silver(I) fluorocarboxylate bis(triphenylphosphine) adducts.

Compound		CO_2 (ppm)	^2J(F-C-C) (Hz)	CF_n (multiplicity, Hz) [a]	PPh_3 (multiplicity, Hz) [a]
$AgO_2CC_3F_7$ [b]	**(11)**	135.6	30	89.9 (qt, 287, 30), 81.0 (m)	
$AgO_2CC_3F_7.(PPh_3)_2$ [c]	**(12)**	no [e]	no [e]	no [e]	133.8 (d, 18.4), 133.1 (d, 18.3), 129.8, 128.7 (d, 9.2)
$AgO_2CC_6F_{13}$ [d]	**(13)**	159.8	23.5	119.1 (m), 115.3 (m), 110.6 (m)	
$AgO_2CC_6F_{13}.(PPh_3)_2$ [c]	**(14)**	no [e]	no [e]	no [e]	133.8, 131.4 (d, 20), 130.4, 128.9
$AgO_2CC_7F_{15}$ [d]	**(15)**	159.0	23	118, 115, 112 (m), 108 (m)	
$AgO_2CC_7F_{15}.(PPh_3)_2$ [c]	**(16)**	no [e]	no [e]	no [e]	133.8 (d, 16.6), 131.9 (d, 27.6), 130.2, 128.8 (d, 9.2)

[a] d = doublet, qt = quartet of triplets, m = multiplet [b] NMR experiments on compound **(11)** were recorded as D_2O solutions [c] NMR experiments on compounds **(12)**, **(14)** and **(16)** were recorded as $CDCl_3$ solutions [d] NMR experiments on compounds **(13)** and **(15)** were recorded as d^6-DMSO solutions [e] no = not observed

Table 3-3 ^{19}F NMR data for silver(I) fluorocarboxylate and silver(I) fluorocarboxylate bis(triphenylphosphine) adducts.

Compound		^{19}F peaks (multiplicity, Hz) αCF_2 [d]	ωCF_3 [d]	other CF_2
$AgO_2CC_3F_7$ [a]	**(11)**	-119.2 (q, 8.1)	-81.7 (t, 8.1)	-128.3
$AgO_2CC_3F_7.(PPh_3)_2$ [b]	**(12)**	-117.3 (q, 9.3)	-81.2 (t, 9.2)	-127.3
$AgO_2CC_6F_{13}$ [c]	**(13)**	-115.0 (t, 12.1)	-80.7 (t, 9.9)	-121.8, -122.2, -123.0, -126.1
$AgO_2CC_6F_{13}.(PPh_3)_2$ [b]	**(14)**	-116.4 (t, 12.7)	-81.3 (t, 9.7)	-122.3, -122.9, -123.3, -126.6
$AgO_2CC_7F_{15}$ [c]	**(15)**	-115.1 (t, 11.2)	-80.9 (t, 8.7)	-121.8, -122.3, -122.4, -123.1, -126.4
$AgO_2CC_7F_{15}.(PPh_3)_2$ [b]	**(16)**	-116.4 (t, 12.7)	-81.3 (t, 9.8)	-122.1, -122.5, -122.8, -123.1, -126.6

[a] NMR experiments on compound **(11)** were recorded as D_2O solutions [b] NMR experiments on compounds **(12)**, **(14)** and **(16)** were recorded as $CDCl_3$ solutions [c] NMR experiments on compounds**(13)** and **(15)** were recorded as d^6-DMSO solutions [d] q = quartet, t = triplet

3.2.4 ^{31}P and ^{109}Ag Multinuclear NMR Spectroscopy

Adducts **(12)**, **(14)** and **(16)** were also investigated using ^{31}P NMR. At room temperature these spectra were observed as broad resonances consistent with rapid ligand exchange of phosphines in solution, as is noted in the literature for phosphine adducts of a variety of silver salts including AgO_2CCF_3 [150] and for non-fluorinated silver carboxylate-phosphine adducts (Chapter 2). Rapid dissociation also explains the absence of $^1J(Ag\text{-}^{31}P)$ coupling. The ^{31}P chemical shift differences between the complexes and the free phosphine are denoted $\Delta\delta$ and this parameter is largely independent of the carboxylate ligand. $\Delta\delta$ values range from 10.9 to 15.4 ppm. This is also consistent with results from similar bis-triphenylphosphine adducts in Chapter 2 ($\Delta\delta$ 10.8 to 13.8 ppm).

Silver-109 resonances were identified for five of the six compounds, the exception being **(16)**. The ^{109}Ag NMR spectra for the silver fluorocarboxylates **(11)**, **(13)**, **(15)** were recorded as d^6-DMSO solutions at room temperature. Although significantly more soluble in organic solvents than alkyl and aryl silver carboxylates, a strong donor solvent was necessary to achieve higher concentrations suitable for ^{109}Ag NMR. These three compounds gave signals in the narrow range 171 to 173 ppm. Observation of ^{109}Ag NMR spectra of the adducts was not possible at room temperature and cooling was required to slow ligand exchange and permit resolution of $^1J(^{31}P\text{-}^{109}Ag)$ coupling. At -80°C, adducts **(12)** (Figure 3-5) and **(14)** gave almost identical spectra, triplets observed at 823 ppm with $^1J(^{31}P\text{-}^{109}Ag)$ of 524 Hz. The ^{109}Ag resonances were shifted upfield by some 650 ppm on complexation by two triphenylphosphine ligands (compared with 630 ppm shifts observed with non-fluorinated silver carboxylates). Phosphorus - silver coupling values are consistent with literature values as determined in ^{31}P NMR studies. [177] For $[AgX(PR_3)_n]$ silver - phosphorus spin-spin coupling $^1J(Ag\text{-}P)$ has been shown

Table 3-4 ^{31}P and ^{109}Ag NMR data for silver(I) fluorocarboxylates and silver(I) fluorocarboxylate bis(triphenylphosphine) adducts.

Compound		δ ^{31}P [a] (ppm)	$\Delta\delta$ [b] (ppm)	δ ^{109}Ag (ppm)	$^{1}J(^{31}P\text{-}^{109}Ag)$ (Hz)
$AgO_2CC_3F_7$	**(11)**	---	---	173 [c]	---
$AgO_2CC_3F_7.(PPh_3)_2$	**(12)**	5.7	10.94	823 [d]	524
$AgO_2CC_6F_{13}$	**(13)**	---	---	171 [c]	---
$AgO_2CC_6F_{13}.(PPh_3)_2$	**(14)**	10.2	15.44	823 [d]	523
$AgO_2CC_7F_{15}$	**(15)**	---	---	173 [c]	---
$AgO_2CC_7F_{15}.(PPh_3)_2$	**(16)**	8.9	14.14	no [d, e]	---

[a] ^{31}P NMR experiments on compounds **(12)**, **(14)** and **(16)** were recorded as $CDCl_3$ solutions at 20°C [b] $\Delta\delta$ defined as the difference between chemical shift of the complexed phosphine compared to the free phosphine (for PPh_3 δ = -5.24 ppm) [c] ^{109}Ag NMR experiments on compounds **(11)**, **(13)** and **(15)** were recorded as d^6-DMSO solutions at 20°C [d] ^{109}Ag NMR experiments on compounds **(12)**, **(14)** and **(16)** were recorded as $CH_2Cl_2/CDCl_3$ solutions at -80°C [e] no = not observed.

to be highly dependent on n [X = O_2CCF_3, R = *p*-$C_6H_5CH_3$, $^1J(^{109}Ag\text{-}^{31}P)$ = 265 (n = 4), 357 (n = 3), 519 (n = 2)]. [177] The ^1J(Ag-P) coupling constant has also been correlated with percent s character in the Ag-P bond and the magnitude of the P-Ag-P angle. [177] A full summary of the ^{31}P and ^{109}Ag NMR results is given in Table 3-4.

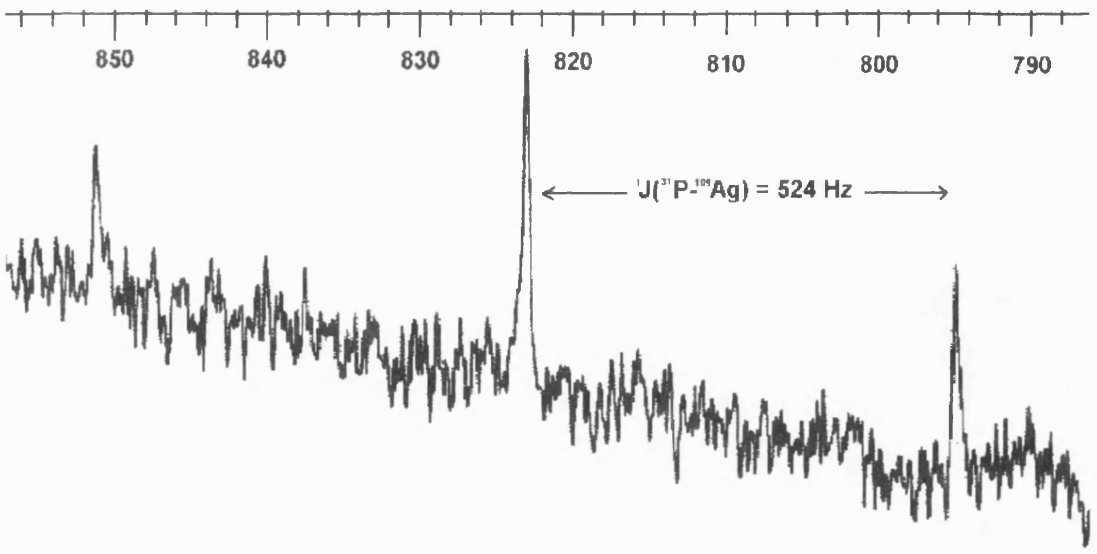

Figure 3-5 ^{109}Ag NMR spectrum for $Ag(O_2CC_3F_7)(PPh_3)_2$ **(12)**.

3.2.5 Mass Spectrometry

In order to determine the extent of oligomerisation and to provide preliminary data on possible decomposition routes, samples were submitted for FAB(LSIMS) mass spectrometry studies. Results from the fluorocarboxylates and their adducts are given in Tables 3-5 and 3-6 respectively. Of particular interest are silver-containing fragments identifiable as a result of observable patterns associated with isotopic abundances of silver-107 and silver-109 atoms

(Appendix 2). Mass spectrometry results in the literature are limited to silver fluoro-carboxylates containing smaller chains (R = CF_3, C_3F_7). [111, 113]

Mass spectrometry investigations on compound **(11)** have revealed several prominent features: I) The presence of Ag_2O_2CR and the lack of higher oligomers of this fragment concur with previous studies [111, 113] and suggest a dimeric based structure. The structure of this compound has been previously reported [174] and consists of $[Ag(O_2CC_3F_7)]_2$ dimeric rings linked by Ag-O bonds. This result therefore indicates that the Ag-O bonds within the dimeric fragment are significantly stronger than those linking the dimers. II) The presence of Ag_n (n = 2, 3) and $Ag_n(O_2CC_3F_7)$ (n = 3, 5, 7) fragments in the spectra indicate the formation of ions containing metal - metal bonds. Ag_n fragments have been identified in other studies of this compound but $Ag_n(O_2CC_3F_7)$ fragments have not (except where n = 2). [111, 113] A low intensity $Ag_3(O_2CC_3F_7)_2$ peak has also been previously observed. [113] A diagram showing the observed cluster at m/z 754 is shown in Figure 3-6 (i) along with the theoretical pattern imposed by the isotopic abundances of silver atoms in both $Ag_5(O_2CC_3F_7)$ (ii) and $Ag_3(O_2CC_3F_7)_2$ (iii). III) The presence of Ag_2F (the highest abundant silver containing peak) and Ag_3F_2 indicates that silver - fluorine species may be a final end product, if this is the case then fluorine incorporation into CVD grown films may be a problem.

Mass spectral investigations of compounds **(13)** and **(15)** gave spectra which were different to that obtained for **(11)**, with less silver-containing fragments observed. The spectrum of **(13)** revealed a number of fragments containing silver and fluorocarbon residues as organometallics or carboxylates, these fluorocarbon species however were shorter than the C_6F_{13} found in **(13)** being C_2F_5 and C_3F_7. The mass spectra of all three silver fluorocarboxylates contained a single high abundance organic fragment at m/z 285, this has been assigned to $C_5F_{11}O^+$. Species such

as this might be formed by the breakup of perfluorobutyric anhydride species that have been proposed as intermediates in the decomposition of silver fluorocarboxylates. [110]

Mass spectrometry studies on the triphenylphosphine adducts **(12)**, **(14)** and **(16)** gave results markedly different from those of the parent fluorocarboxylates. As observed in the case of triphenylphosphine adducts of alkyl or aryl carboxylates (Chapter 2), these spectra were dominated by AgL_n and $AgOL_n$ type fragments ($L = PPh_3$, $n = 1, 2$). Fragmentation of triphenylphosphine also occurred resulting in PPh_2 which was also identified in the spectra. This fragmentation of PPh_3 is as reported in the literature. [178] The few fragments containing fluorocarbon in the presence of silver were low in abundance. In contrast to the non-fluorinated adducts, fragments detected in the spectra of compounds **(12)**, **(14)** and **(16)** were found to contain C_3F_6 and C_3F_7 as the only non-phosphine fragments bound to silver. The lack of silver carboxylate species in these spectra may indicate that decarboxylation is more readily accomplished in the presence of phosphine ligands than when absent.

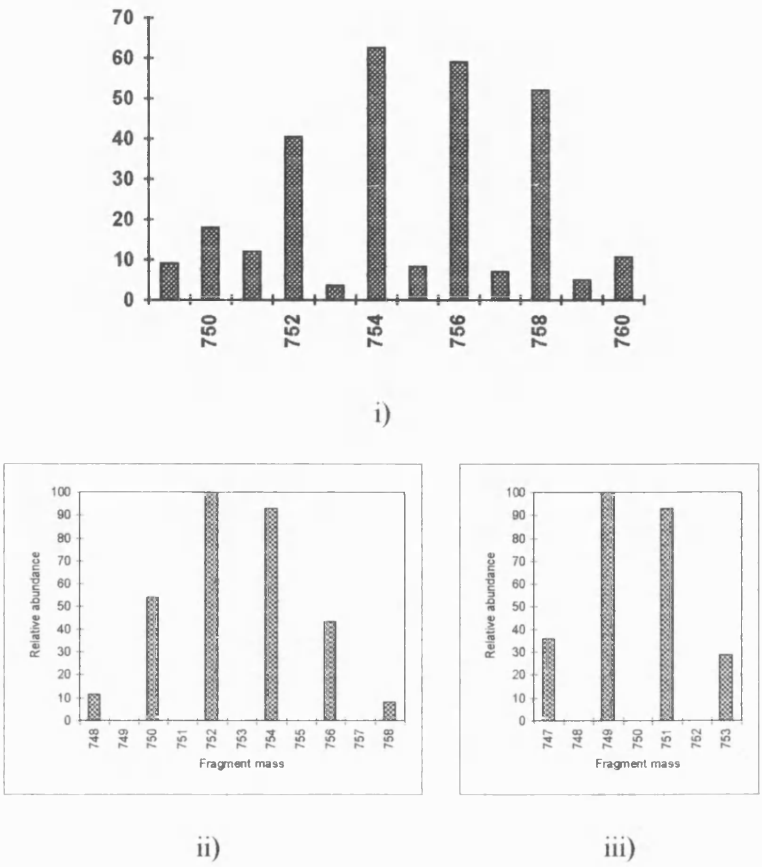

Figure 3-6 i) Selected area of the FAB mass spectrum of compound **(11)**, ii) calculated pattern for $Ag_5(O_2CC_3F_7)$, iii) calculated pattern for $Ag_3(O_2CC_3F_7)_2$.

Table 3-5 Selected mass spectrometric data for silver(I) fluorocarboxylates (AgO_2CR). [a]

	(11) [b]		(13) [c]		(15) [d]	
Fragment ions	**m/z**	**%**	**m/z**	**%**	**m/z**	**%**
$C_3F_7O(CF_2)_2$	285	49	285	100	285	100
Ag	107	2	107	24	107	18
AgC_2	—	—	131	15	—	—
$AgCF_2CF_3$	—	—	226	14	—	—
$Ag(O)O_2CC_3F_7$	—	—	336	5	—	—
Ag_2	214	5	—	—	—	—
Ag_2F	233	8	—	—	—	—
$Ag_2OCC_3F_7$	411	1	—	—	—	—
$Ag_2O_2CC_3F_7$	427	2	—	—	—	—
Ag_3	321	5	—	—	—	—
Ag_3F_2	359	<1	—	—	—	—
$Ag_3O_2CC_3F_7$	538 [e]	2	—	—	—	—
$Ag_5O_2CC_3F_7$	754 [e]	1	—	—	—	—
$Ag_7O_2CC_3F_7$	970 [e]	<0.5	—	—	970 [e]	3.5
Other fragments	—	—	629 [f]	10	679 [g]	5
	—	—	641 [f]	5	—	—

[a] based on ^{107}Ag, [b] R = C_3F_7, base peak m/z 109 (not containing Ag) [c] R = C_6F_{13} [d] R = C_7F_{15}

[e] peaks were found as a cluster, m/z is given as the major central signal of the cluster

[f] recognised by isotopic pattern as containing one silver atom [g] recognised by isotopic pattern as containing no silver atoms

Table 3-6 Selected mass spectrometric data for silver(I) fluorocarboxylate bis (triphenylphosphine) adducts $[AgO_2CR.(PPh_3)_2]$. [a]

	(12) [b]		(14) [c]		(16) [d]	
Fragment ions	**m/z**	**%**	**m/z**	**%**	**m/z**	**%**
PPh	---	---	108	27	108	14
PPh_2	183	44	183	82	183	45
PPh_3	262	43	262	92	262	29
$AgOC_3F_7$	292	2	292	8	---	---
$Ag(PPh_3)$	369	100	369	100	369	86
$AgO(PPh_3)$	385	6	385	18	385	4
$Ag(PPh_3)_2$	631	73	631	97	631	100
$AgO(PPh_3)_2$	647	5	647	27	647	8
$Ag(PPh_3)(PPh_2)_2$	---	---	---	---	739	<1
$AgO(PPh_3)(PPh_2)_2$	---	---	---	---	757	1
$Ag_2(PPh_3)_2OF$	---	---	773	17	773	1.6
$Ag(PPh_3)_3C_3F_6$	---	---	---	---	1043	0.5
$Ag_2(PPh_3)_3C_3F_6$	---	---	---	---	1151	1.8
Other fragments	---	---	917 [e]	4	---	---

[a] based on ^{107}Ag [b] $R = C_3F_7$ [c] $R = C_6F_{13}$ [d] $R = C_7F_{15}$ [e] recognised by isotopic pattern as containing two silver atoms

3.2.6 Thermal Analysis Studies

Compounds **(11)** - **(16)** were investigated using thermal gravimetric techniques under an inert (He) atmosphere (Table 3-7). The experiments were carried out to give an indication of the temperatures at which decomposition might be expected to start and to suggest the relative thermal stabilities of this range of compounds. The thermal gravimetric analysis (TGA) data presented here may be compared with recent TGA results published for silver fluoro-carboxylates [170] and their adducts [171] obtained in an oxygen containing atmosphere.

TGA of silver fluorocarboxylates **(11)**, **(13)** and **(15)** revealed a single thermal degradation stage, starting between 250-275°C and complete by 365-380°C, maximum rates of decompositions being in the region 350-370°C. The TGA of both **(11)** and **(15)** in air are reported to show a two step degradation with 10-15 % weight lost between 140-350°C followed by the remainder of the weight lost between 350-470°C. [170]

Bis(triphenylphosphine) adducts of silver fluorocarboxylates **(12)**, **(14)**, **(16)** start to decompose at a lower temperature (160-210°C), the decompositions being complete by 280°C. There is no evidence that decomposition occurs in discrete steps although **(14)** and **(16)** exhibited two maxima in the rate of weight loss. This may be indicative of a competing decomposition reaction having greater influence as the temperature is increased. These adducts were found to decompose at lower temperatures (maximum rates of decomposition 217-243°C) than the similar bis(triphenylphosphine) adducts of non-fluorinated silver carboxylates (maximum rates of decomposition 280-308°C) (Chapter 2). Decomposition temperature ranges were narrower in the case of silver fluorocarboxylate bis(triphenylphosphine) adducts

Table 3-7 Thermal analysis data for silver(I) fluorocarboxylates and silver(I) fluorocarboxylate bis(triphenylphosphine) adducts.

Compound		Decomposition temperature (°C)			Residue remaining (%)	
		start [a]	maxima [b]	end [c]	calc % Ag [d]	found
$AgO_2CC_3F_7$	**(11)**	250	367	380	33.6	24.5
$AgO_2CC_3F_7(PPh_3)_2$	**(12)**	211	243	270	12.8	15.1
$AgO_2CC_6F_{13}$	**(13)**	250	351	365	22.9	21.4
$AgO_2CC_6F_{13}(PPh_3)_2$	**(14)**	210	221, 238	267	10.8	7.0
$AgO_2CC_7F_{15}$	**(15)**	275	361	370	20.7	20.3
$AgO_2CC_7F_{15}(PPh_3)_2$	**(16)**	160	217, 243	280	10.3	12.1

[a] temperature corresponding to the onset of decomposition [b] temperature at which the rate of weight loss is at a maximum

[c] temperature at which decomposition is complete [d] calculated % mass of silver in undecomposed compounds

compared to non-fluorinated carboxylate bis(triphenylphosphine) adducts (Chapter 2) and mono(triphenylphosphine) adducts of **(11)** and **(15)** (decomposition range 165-400°C). [171]

The mass of residue remaining at the completion of the experiment was as expected for silver metal as the only final decomposition product. However in the case of **(11)** only 75% of the expected mass of residue was observed. This may be explained by partial sublimation of **(11)** during the TGA experiment.

3.3 SINGLE CRYSTAL X-RAY STRUCTURE DETERMINATION OF $AgO_2CC_3F_7(PPh_3)_2$ (12)

Crystallographic quality crystals of compound **(12)** were obtained by slow evaporation at room temperature of a toluene-ethanol solvent mixture. The crystals were found to be light, air and moisture stable.

Single crystal X-ray diffraction studies of compound **(12)** have revealed a monomeric structure with one molecule per asymmetric unit. The structure exhibits a chelating carboxylate group and two triphenylphosphine donors per silver centre (Figure 3-7) similar to that determined for compound **(3)** $[AgO_2CCH_3.(PPh_3)_2]$ (Figure 2-11). This appears to be the first report of a structure containing silver simultaneously bonded to a fluorocarboxylate group and phosphine ligands. However a number of publications discuss structures of silver complexes containing chelating carboxylates with additional phosphine ligands: i.e. $[AgO_2CH(PPh_3)_2]$, [154] $[AgO_2CH(PPh_3)_2].2HCO_2H$ [154] and $[AgO_2CCH_3.(dppm)]_2$ (where dppm = $Ph_2PCH_2PPh_2$). [156]

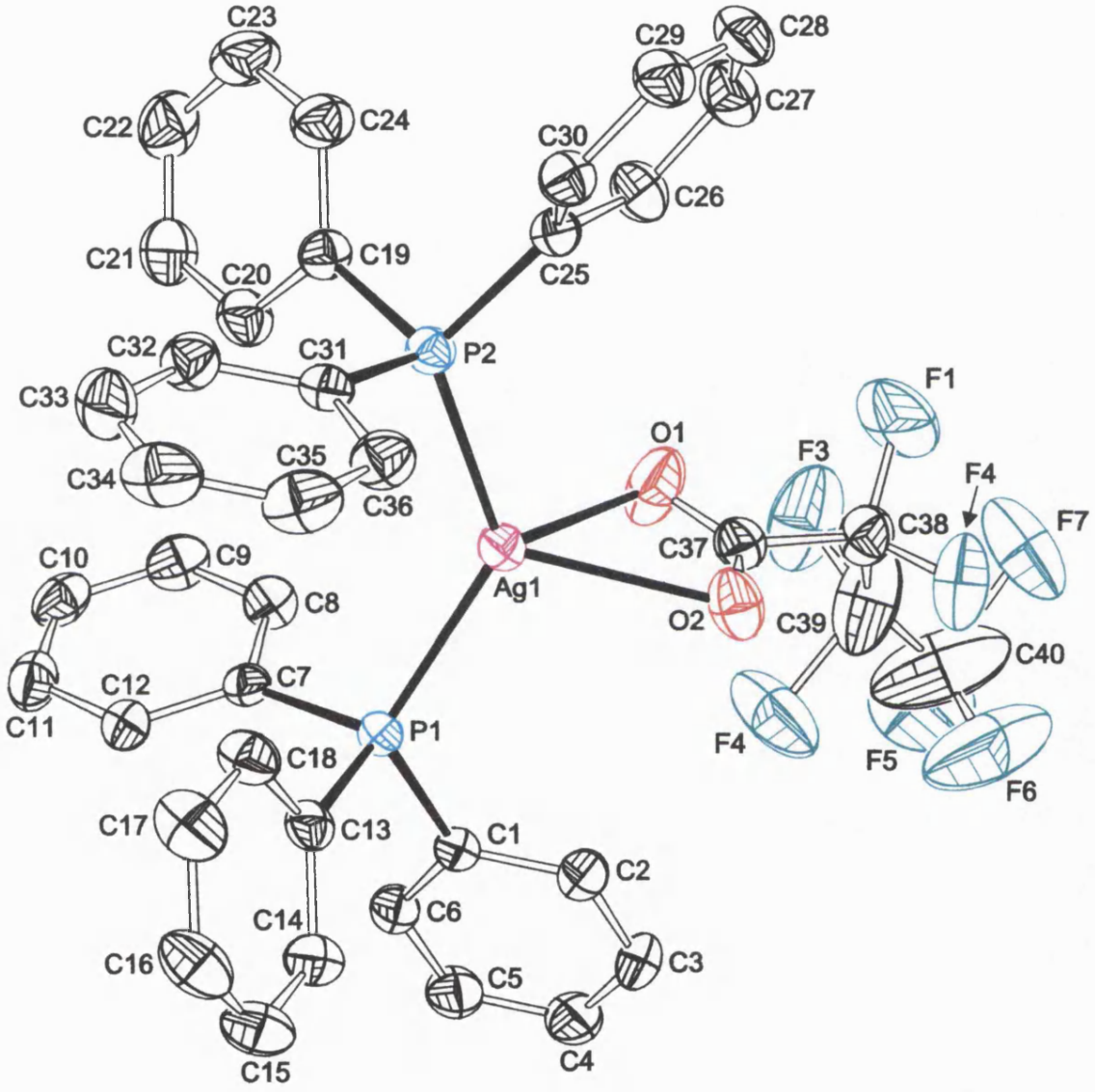

Figure 3-7 Structure of $AgO_2CC_3F_7.(PPh_3)_2$ **(12)**.

Other silver carboxylate-phosphine adducts have carboxylates in bridging [152, 153, 156, 157] or unidentate [156-158] bonding modes.

Ag-O bond lengths are noticeably longer in **(12)** (2.495 and 2.532 Å) when compared to a mean value of 2.44 Å in **(3)**. This is consistent with electron withdrawal from the oxygens by the electronegative C_3F_7 group. Lengthening of the Ag-O bond is also found where oxygen is hydrogen bonded to other species. [154, 156] The Ag-O bond lengths in **(12)** suggest a symmetrical chelating carboxylate, comparable to molecule 1 in **(3)** but more symmetrical than molecule 2 in **(3)**. The Ag-P bond lengths (2.43Å) are well within the expected range (2.352-2.521Å) for triphenylphosphine bound to silver although slightly shorter than found in compound **(3)**. The stronger Ag-P bonds in **(12)** are consistent with weaker Ag-O bonds.

Carbon-oxygen bond lengths are also found to be slightly shorter in **(12)**, 1.201 and 1.232 Å, as compared to a mean value of 1.24 Å for **(3)** and 1.21-1.28 Å for chelating AgO_2CR in general. This may be explained by the inductive effect of the C_3F_7 group withdrawing electron density from the Ag-O bonds. Longer Ag-O bonds in **(12)** compared to **(3)** have the effect of reducing the O-Ag-O angle from 53.1° in **(3)** to 51.3° in **(12)**, whereas P-Ag-P increases from 126.9° in **(3)** to 129.3° in **(12)**. Relevant bond distances and angles are summarised in Table 3-8, further data including atomic coordinates are provided in Appendix A4.2.

Table 3-8 Complex **(12)**, relevant bond lengths (Å) and angles (°).

Ag(1)-P(1)	2.436(2)	Ag(1)-P(2)	2.430(2)
Ag(1)-O(1)	2.495(5)	Ag(1)-O(2)	2.532(5)
C(37)-O(1)	1.232(8)	C(37)-O(2)	1.201(8)
P(1)-Ag(1)-P(2)	129.28(5)		
O(1)-Ag(1)-O(2)	51.3(2)		
O(1)-C(37)-O(2)	126.9(6)		

3.4 FILM GROWTH RESULTS

Compounds **(11)** - **(16)** were tested for potential use as CVD precursors. A full description of apparatus and film growth procedures is given in Appendix 6. This section includes a brief summary of results obtained from the characterisation of grown films. The results are collected in Tables 3-9 and 3-10.

Films were grown under fixed conditions of 300°C in a nitrogen atmosphere at 1 bar pressure. Precursors were delivered to the gas phase as an aerosol of the compound dissolved in THF and swept into the reactor using nitrogen as a carrier gas. Films were grown on glass substrates. Coating growth times were dependent on the volume of solvent used and diluent flow rates and were of the order of approximately 30 minutes. Typically 0.5-1.0 g of precursor was dissolved in 25 cm^3 of THF with nebuliser carrier flow rates were of the order of 1.0-1.2 $Lmin^{-1}$. The films were found to be soft and although well adhered to the substrate they could be scratched, or damaged by touch relatively easily. Films were examined using a number of techniques including visual inspection, scanning electron microscopy (SEM), conductivity and reflectance measurements. Additionally Energy Dispersive X-ray Spectrometry (EDXS) was used to confirm the elemental composition of the films and to estimate the film thickness.

By simple visual inspection, films grown from the adducts appeared more reflective and uniform than those grown from the corresponding fluorocarboxylates without phosphine ligands. This observation was supported by scanning electron microscopy, a number of examples of which are included (Plates 3-1 through 3-6). A number of photographs show crystalline material embedded into the film, $AgO_2CC_3F_7$ **(11)** being a good example (Plate 3-1). It should also be noted that the adducts had a significantly reduced growth rate [2.1-3.2 Å min^{-1}

Table 3-9 Appearance of silver films grown from silver(I) fluorocarboxylate and silver(I) fluorocarboxylate bis(triphenylphosphine) adduct precursors.

Compound		Visual appearance	SEM appearance	Detected impurities [a, b] (EDXS)	Plates
$AgO_2CC_3F_7$	**(11)**	thick white film	very rough surface includes crystalline material in film	C	3-1
$AgO_2CC_3F_7(PPh_3)_2$	**(12)**	silver film with brown tinge	very smooth surface	C, F (trace)	---
$AgO_2CC_6F_{13}$	**(13)**	heavy deposition but not reflective matt in places with white areas	quite rough surface	C, F	3-3, 3-5
$AgO_2CC_6F_{13}(PPh_3)_2$	**(14)**	silver film with slight brown tinge	smooth surface	C, F (trace)	3-4, 3-6
$AgO_2CC_7F_{15}$	**(15)**	silver film, whitish, slightly matt appearance	roughish surface	C, F (trace)	3-2
$AgO_2CC_7F_{15}(PPh_3)_2$	**(16)**	uniform silver film slightly matt	quite smooth surface	C, F (trace)	---

[a] the presence of oxygen in the films was masked by oxygen detected in the glass [b] trace quantities were at the limits of detection of this instrumentation

in **(12)**, **(14)** and **(16)**] compared to the fluorocarboxylates themselves [from 3.0-9.0 Å min^{-1} in **(11)**, **(13)** and **(15)**]. This may represent a correlation between slower growth rates and superior morphology (Section 1.2.2). The highest estimated growth rate was 9 Å min^{-1} for $AgO_2CC_6F_{13}$ **(13)**, the lowest 2.1 Å min^{-1} for $AgO_2CC_3F_7(PPh_3)_2$ **(12)**. This apparent order of growth rate is interesting in view of the fact that as shown by TGA results (Section 3.2.6), silver fluorocarboxylate adducts decompose at a lower temperature than the parent silver fluorocarboxylates.

EDXS could not provide accurate quantitative analysis of film composition or impurities. Carbon impurities were detected in all of the samples analysed, fluorine contaminants were identified in all of the films except that grown from **(11)**. Embedded crystalline deposits in the film grown from **(11)**, observed by SEM at x1000 magnification (Plate 3-1), could not be identified further, similar but less dramatic crystalline deposits could be seen with films **(14)**, **(15)**, and **(16)** (Plate 3-6) although only at higher magnifications (x10,000). Phosphorus could not be detected in any of the coatings. There remains some difficulty in confirming the presence of oxygen in the film. Due to the thin nature of films, the EDXS technique detected appreciable levels of Si and O (among others) from the glass substrate. The presence of oxygen in the films themselves has therefore not been either proved or disproved.

In terms of reflectance ability from the coating surface, the adducts gave films with superior qualities, this confirming the expected correlation against surface morphology. Each adduct gave an improvement over its parent fluorocarboxylate. For example $AgO_2CC_6F_{13}(PPh_3)_2$ **(14)** gave the most reflective film. This film was able to reflect 46 % of an incident beam of light (λ = 550 nm), whereas its parent fluorocarboxylate, $AgO_2CC_6F_{13}$ **(13)** gave a poorly reflecting film at 4.9 %. Of the six films, only three were thick enough to conduct electricity appreciably

Table 3-10 Properties of silver films grown from silver(I) fluorocarboxylate and silver(I) fluorocarboxylate bis(triphenylphosphine) adduct precursors.

Compound		Estimated film thickness (Å) [a]	Deposition time (minutes)	Estimated deposition rate (Å min^{-1})	% Reflectance [b] Coating	% Reflectance [b] Glass	Sheet Resistance [c] (Ω/□)
$AgO_2CC_3F_7$	**(11)**	90	30	3.0	0.5	42.5	4.2
$AgO_2CC_3F_7(PPh_3)_2$	**(12)**	65	31	2.1	6.8	8.1	∞
$AgO_2CC_6F_{13}$	**(13)**	260	29	9.0	4.9	29.8	14.5
$AgO_2CC_6F_{13}(PPh_3)_2$	**(14)**	90	33	2.7	45.9	34.9	∞
$AgO_2CC_7F_{15}$	**(15)**	220	46	4.8	18.1	36.5	2.7×10^6
$AgO_2CC_7F_{15}(PPh_3)_2$	**(16)**	95	30	3.2	20.4	19.8	∞

[a] film thickness was estimated using EDXS techniques (5 kV, 5×10^{-8} A), see Appendix 3 [b] λ = 550 nm corresponding to the peak in the eye response curve

[c] sheet resistance was measured over a 25 mm square

and hence give a resistance low enough to be measurable. Since films of approximately the same estimated thickness gave very different resistance measurements, [an example being the comparison of compounds **(11)** and **(14)**], it might assumed that in some cases the conductivity is also dependent on other factors, for example the film grown from **(11)** also contained appreciable levels of crystalline impurity embedded in the film.

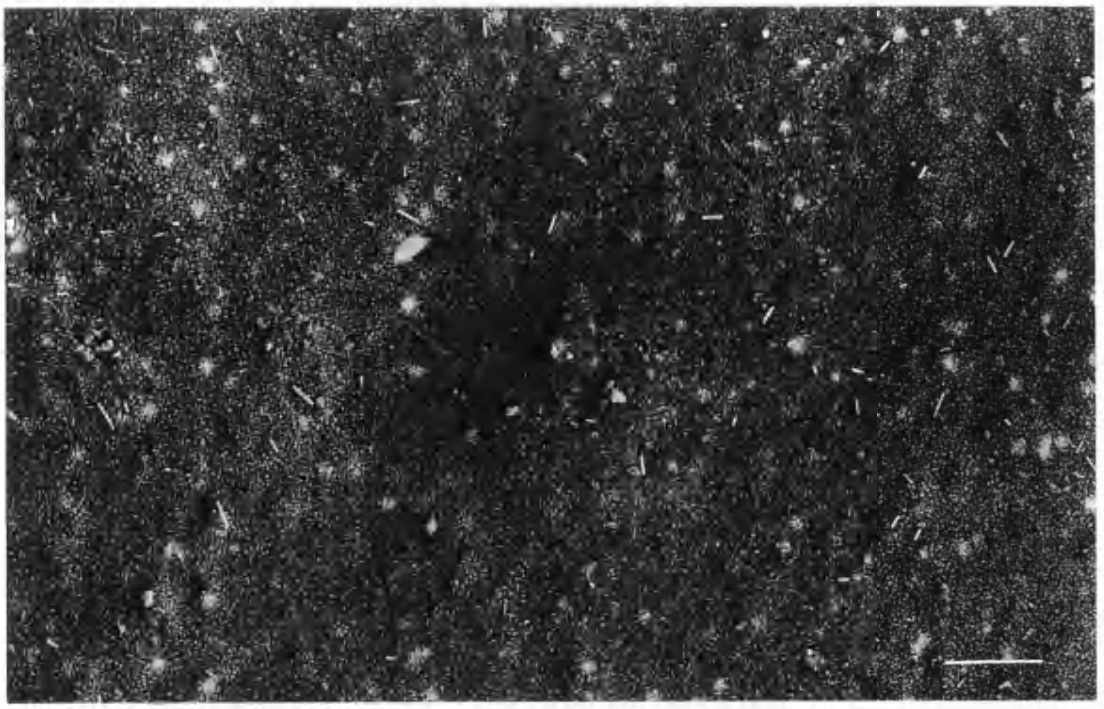

Plate 3-1 Scanning Electron Micrograph at 15 kV of a silver film obtained from the AACVD of $AgO_2CC_3F_7$ **(11)**, bar = 10 μm.

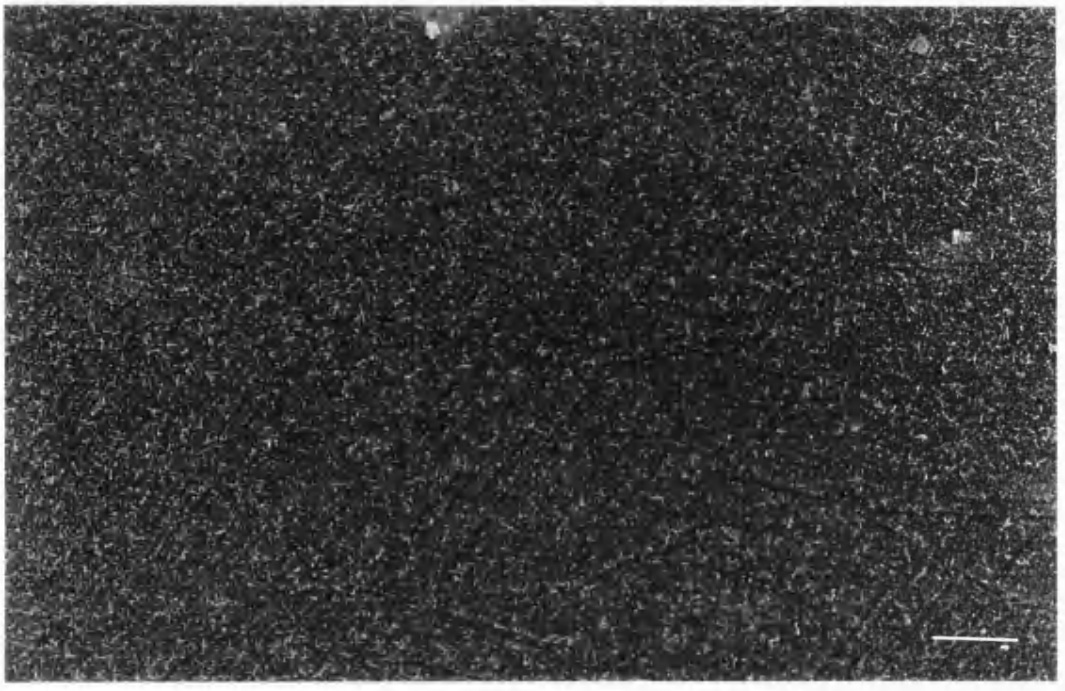

Plate 3-2 Scanning Electron Micrograph at 15 kV of a silver film obtained from the AACVD of $AgO_2CC_7F_{15}$ **(15)**, bar = 10 μm.

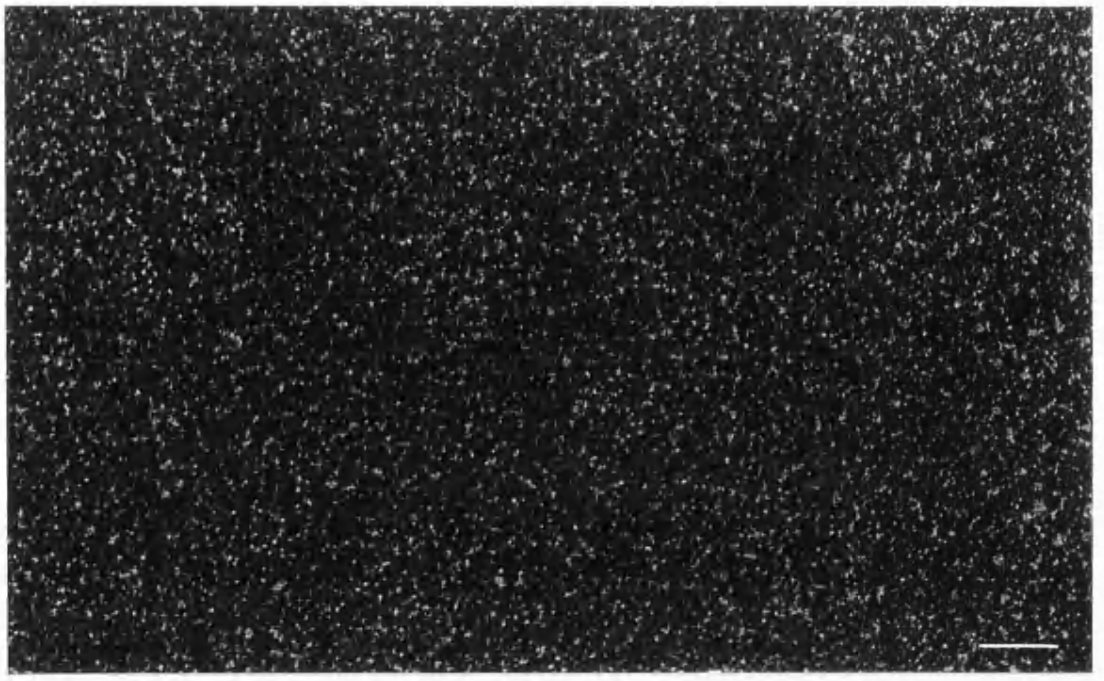

Plate 3-3 Scanning Electron Micrograph at 5 kV of a silver film obtained from the AACVD of $AgO_2CC_6F_{13}$ **(13)**, bar = 10 μm.

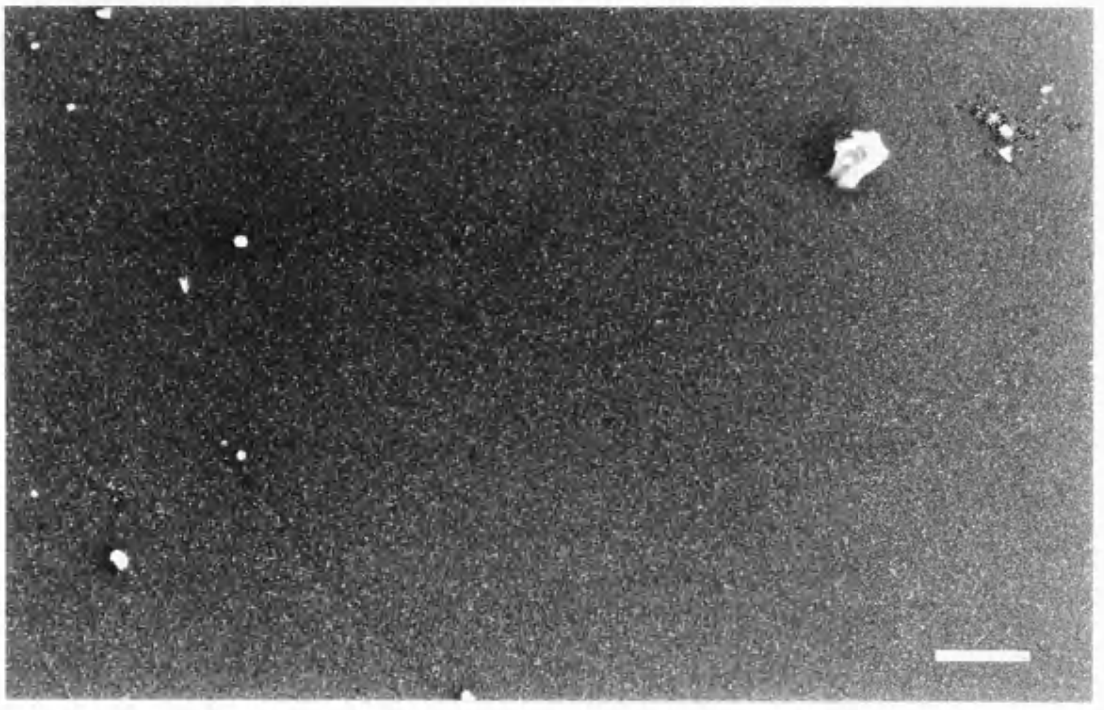

Plate 3-4 Scanning Electron Micrograph at 15 kV of a silver film obtained from the AACVD of $AgO_2CC_6F_{13}(PPh_3)_2$ **(14)**, bar = 10 μm.

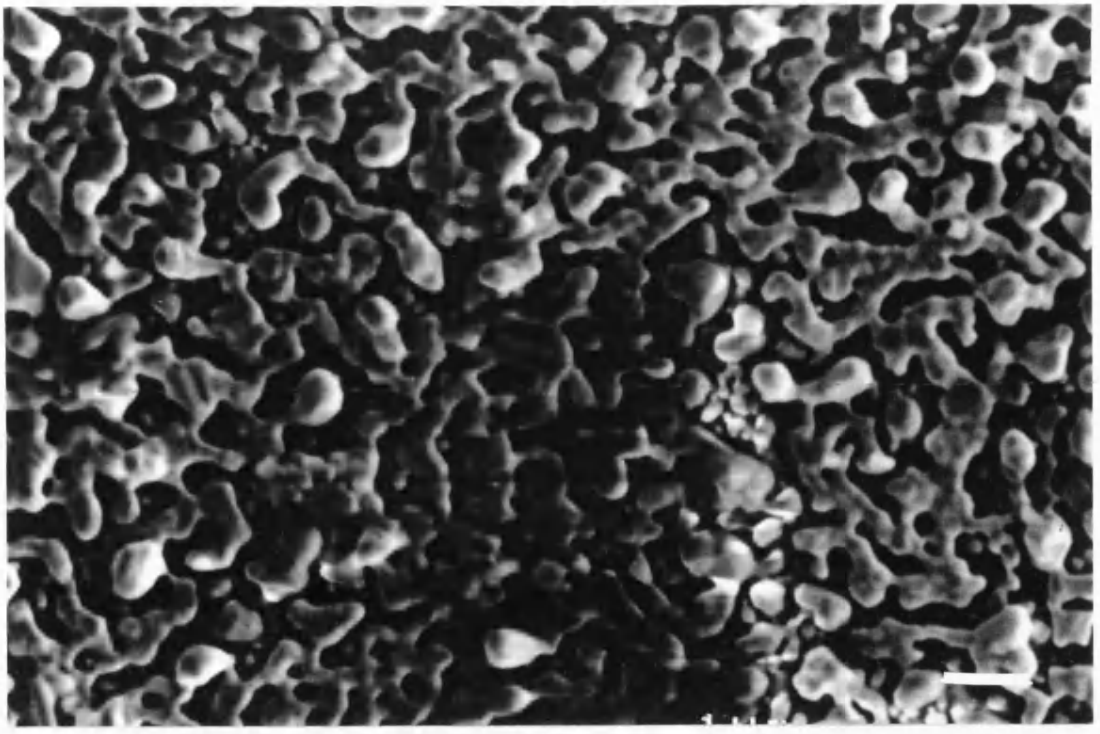

Plate 3-5 Scanning Electron Micrograph at 5 kV of a silver film obtained from the AACVD of $AgO_2CC_6F_{13}$ **(13)**, bar = 1 μm.

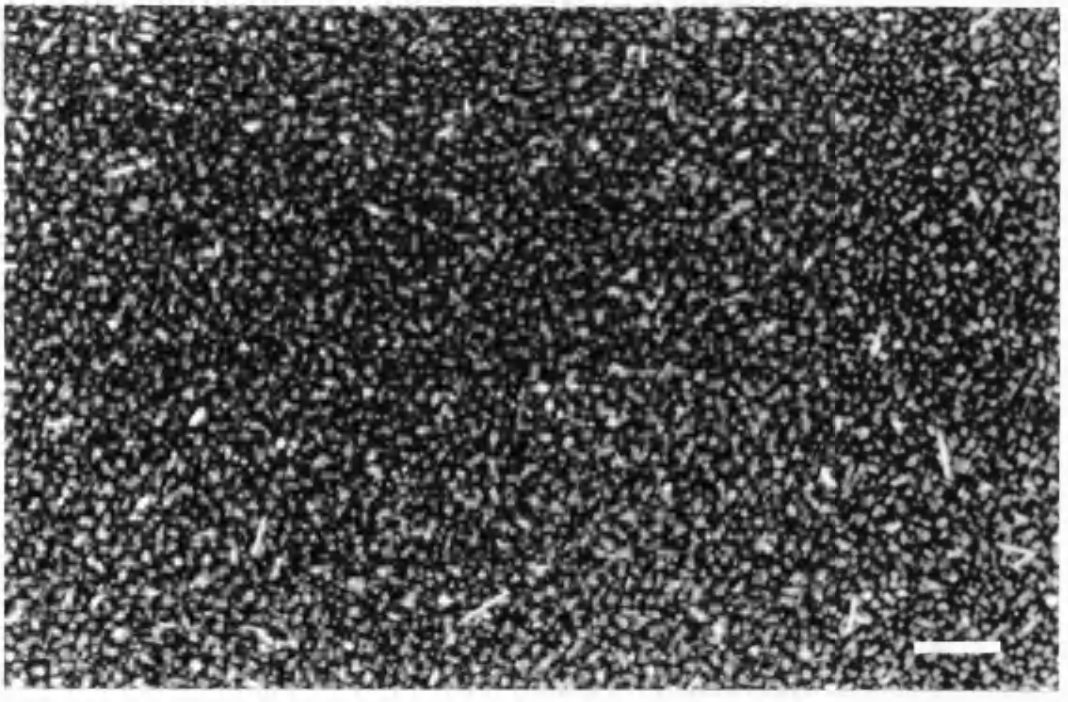

Plate 3-6 Scanning Electron Micrograph at 15 kV of a silver film obtained from the AACVD of $AgO_2CC_6F_{13}(PPh_3)_2$ **(14)**, bar = 1 μm.

3.5 EXPERIMENTAL

The synthesis of silver perfluorobutyrate - $AgO_2CC_3F_7$ (11)

Silver oxide (1.0 g, 4.3 mmol) was added to a stirred solution of perfluorobutyric acid (1.65 g, 7.7 mmol) in distilled water. After stirring for 30 minutes, the solution was filtered to remove unreacted silver oxide. Solvent and unreacted acid were removed *in vacuo* over four hours to leave a dry white solid. Yield 1.67 g, 68%.

Analysis: found (calculated for $C_4F_7O_2Ag$): C, 14.9 (14.9) %. Mp 298°C (by DSC). IR (Nujol mull) 1200-1800 cm^{-1} : 1225b, 1287, 1343shs, 1426shw, 1609s, 1669b. ^{13}C NMR (d^6-DMSO) δ; 135.6 (m, 30 Hz, CO_2), 89.9 (qt, 287, 30 Hz, CF_n), 81.0 (m, CF_n). ^{19}F NMR (d^6-DMSO) δ; -81.7 (t, 8.1 Hz, CF_3), -119.2 (q, 8.1 Hz, αCF_2), -128.3 (CF_2). ^{109}Ag NMR (20°C, d^6-DMSO) δ; 173.

The synthesis of O,O´-perfluorobutyratobis(triphenylphosphine)silver(I) - $AgO_2CC_3F_7(PPh_3)_2$ (12)

Silver perfluorobutyrate (11) (0.4 g, 1.3 mmol) was stirred in toluene (50 cm^3) with an excess of triphenylphosphine (2.0 g, 7.9 mmol). The mixture was stirred in the absence of light for 24 hours. The resulting cream precipitate was filtered in air, washed with 2 cm^3 of toluene, sucked dry and further dried *in vacuo*. Yield 0.55g, 52 %. The compound was recrystallised from a toluene-ethanol solvent mixture.

Analysis : found (calculated for $C_{40}H_{30}F_7O_2AgP_2$): C, 56.9 (56.8); 3.44 (3.58) %. Mp 186°C (by DSC). IR (Nujol mull) 1200-1800 cm^{-1}: 1208sh, 1229sh, 1267w, 1312w, 1343shw, 1437sh, 1659ssh. IR (hexachlorobutadiene mull) 1200-1800 cm^{-1}: 1208sh, 1229sh, 1265w, 1312w, 1343, 1395w, 1435sh, 1480sh, 1659sh. ^{13}C NMR ($CDCl_3$) δ; 133.8 (d, 18.4 Hz, PPh_3), 133.1 (d, 18.3 Hz, PPh_3), 129.8 (PPh_3), 128.7 (d, 9.2 Hz, PPh_3). ^{19}F NMR ($CDCl_3$) δ; -81.2 (t, 9.2 Hz, CF_3), -117.3 (q, 9.3 Hz, αCF_2), -127.3 (CF_2). ^{31}P NMR (20°C, $CDCl_3$) δ; 5.7 (br). ^{109}Ag NMR (-80°C, $CDCl_3/CH_2Cl_2$) δ; 823 (t, 524 Hz).

The synthesis of silver perfluoroheptanoate - $AgO_2CC_6F_{13}$ (13)

Perfluoroheptanoic acid (3.0 g, 8.3 mmol) was suspended in 30 cm^3 of distilled water and vigorously stirred. The acid was solubilised with a few drops of concentrated ammonia solution. The solution was stirred and gently warmed to remove excess ammonia. A solution of silver nitrate (1.4 g, 8.4 mmol) in 10 cm^3 of distilled water was added. This resulted in a fine white precipitate which was filtered in air and dried *in vacuo.* Yield 3.0 g, 77%.

Analysis : found (calculated for $C_7F_{13}O_2Ag$): C, 17.7 (17.8) %. Mp 282°C (by DSC). IR (Nujol mull) 1200-1800 cm^{-1} : 1233b, 1366, 1424, 1460, 1578, 1611s, 1660. ^{13}C NMR (d^6-DMSO) δ; 159.8 (m, 23.5 Hz, O_2C-), 119.1 (m, CF_n), 115.3 (m, CF_n), 110.6 (m, CF_n). ^{19}F NMR (d^6-DMSO) δ; -80.7 (t, 9.9 Hz, CF_3), -115.0 (t, 12.1 Hz, αCF_2), -121.8 (CF_2), -122.2 (CF_2), -123.0 (CF_2), -126.1 (CF_2). ^{109}Ag NMR (20°C, d^6-DMSO) δ; 171.

The synthesis of O,O'-perfluoroheptanoatobis(triphenylphosphine)silver(I) - $AgO_2CC_6F_{13}(PPh_3)_2$ (14)

Silver perfluoroheptanoate (0.5 g, 1.1 mmol) and two equivalents of triphenylphosphine (0.55 g, 2.1 mmol) were suspended in 50 cm^3 of toluene. The solution was stirred in the absence of light for eight hours. The solution was dried *in vacuo* to give a white precipitate. Yield 0.94 g, 90 %. The product was recrystallised from a toluene-ethanol solvent mixture and dried *in vacuo.*

Analysis : found (calculated for $C_{43}H_{30}F_{13}O_2AgP_2$): C, 51.8 (51.9); 2.94 (3.04) %. Mp 182°C (by DSC). IR (Nujol mull) 1200-1800 cm^{-1} : 1200s, 1237s, 1289w, 1310w, 1356sh, 1437ssh, 1480ssh, 1659ssh. IR (hexachlorobutadiene mull) 1200-1800 cm^{-1} : 1200, 1237, 1289w, 1312w, 1356sh, 1395sh, 1437sh, 1480sh, 1659sh. ^1H NMR ($CDCl_3$) δ; 7.43-7.36 (m, 20H, PPh_3), 7.34-7.28 (m, 10H, PPh_3). ^{13}C NMR ($CDCl_3$) δ; 133.8 (PPh_3), 131.4 (d, 20 Hz, PPh_3), 130.4 (PPh_3), 128.9 (PPh_3). ^{19}F NMR ($CDCl_3$) δ; -81.3 (t, 9.7 Hz, CF_3), -116.4 (t, 12.7 Hz, αCF_2), -122.3 (CF_2), -122.9 (CF_2), -123.3 (CF_2), -126.6 (CF_2). ^{31}P NMR (20°C, $CDCl_3$) δ; 10.2 (br). ^{109}Ag NMR (-80°C, $CDCl_3/CH_2Cl_2$) δ; 823 (t, 523 Hz).

The synthesis of silver perfluorooctanoate - $AgO_2CC_7F_{15}$ (15)

Perfluorooctanoic acid (1.0 g, 2.4 mmol) was suspended in distilled water (20 cm^3) and stirred. The acid was solubilised with concentrated ammonia solution, until the solution was faintly ammoniacal. The solution was gently warmed to remove excess ammonia, filtered to remove unreacted acid. To this was added a solution of silver nitrate (1.8 g, 10.6 mmol) in distilled

water (5 cm^3). This resulted in a fine white precipitate, which was filtered in air, washed with ethanol and diethyl ether and dried *in vacuo*. Yield 0.7 g, 53 %.

Analysis : found (calculated for $C_8F_{15}O_2Ag$): C, 18.2 (18.5) %. Mp 252-261°C (by DSC). IR (Nujol mull) 1200-1800 cm^{-1} : 1204, 1237, 1296w, 1323, 1366, 1420w, 1613. IR (hexachloro-butadiene mull) 1200-1800 cm^{-1} : 1204, 1237, 1296w, 1323, 1366, 1420, 1613. ^{13}C NMR (d^6-DMSO) δ; 159.0 (m, 23 Hz, O_2C-), 118 (CF_n), 115 (CF_n), 112 (CF_n), 108 (CF_n). ^{19}F NMR (d^6-DMSO) δ; -80.9 (t, 8.7 Hz, CF_3), -115.1 (t, 11.2 Hz, αCF_2), -121.8 (CF_2), -122.3 (CF_2), -122.4 (CF_2), -123.1 (CF_2), -126.4 (CF_2). ^{109}Ag NMR (20°C, d^6-DMSO) δ; 173.

The synthesis of O,O'-perfluorooctanoatobis(triphenylphosphine)silver(I) - $AgO_2CC_7F_{15}(PPh_3)_2$ (16)

Silver perfluorooctanoate (2.0 g, 3.8 mmol) was suspended in toluene (80 cm^3) with an excess of two equivalents of triphenylphosphine (2.25 g, 8.6 mmol). The solution was stirred in the absence of light for four hours. The solvent was removed *in vacuo* to give a pale cream precipitate. Yield 3.32 g, 83 %. The compound was recrystallised from an ethanol-toluene solvent mixture.

Analysis : found (calculated for $C_{44}H_{30}F_{15}O_2AgP_2$): C, 51.8 (50.6); H, 3.14 (2.89) %. Mp 133°C (by DSC). IR (Nujol mull) 1200-1800 cm^{-1}: 1206sb, 1242sb, 1310, 1437ssh, 1572wsh, 1586wsh, 1692. IR (hexachlorobutadiene mull) 1200-1800 cm^{-1} : 1208, 1240, 1310w, 1360b, 1435sh, 1480sh, 1692sh. ^1H NMR ($CDCl_3$) δ; 7.40-7.30 (m, 20H, PPh_3), 7.28-7.22 (m, 10H, PPh_3). ^{13}C NMR ($CDCl_3$) δ; 133.8 (d, 16.6 Hz, PPh_3), 131.9 (d, 27.6 Hz, PPh_3), 130.2 (PPh_3),

128.8 (d, 9.2 Hz, PPh_3). ^{19}F NMR ($CDCl_3$) δ; -81.3 (t, 9.8 Hz, CF_3), -116.4 (t, 12.7 Hz, αCF_2), -122.1 (CF_2), -122.5 (CF_2), -122.8 (CF_2), -123.1 (CF_2), -126.6 (CF_2). ^{31}P NMR (20°C, $CDCl_3$) δ; 8.9 (br).

CHAPTER FOUR

SYNTHESIS, CHARACTERISATION AND CVD PROPERTIES OF PHOSPHINE ADDUCTS OF SILVER β-DIKETONATE AND SILVER β-KETOIMINATE COMPLEXES

4.1 INTRODUCTION

Research interest concerning silver β-diketonates had remained largely academic until fairly recently, and apart from the use of fluorinated β-diketonates in lanthanide(III) - silver(I) binuclear NMR shift reagents [169, 179-182] these compounds have found few applications. Recent research in silver CVD however has revived interest in this area, as silver β-diketonates represent a large range of potentially volatile precursors. Metal β-diketonates are known to exhibit high vapour pressures and are widely employed as precursors for CVD, examples within metal CVD alone include Ru, [183] Co, [184] Rh, [185] Ir, [186] Pt, [187] Cu [188] and Au. [189] Increasingly more use is being made of silver β-diketonates for silver CVD, particularly adducts of silver hexafluoroacetylacetonate (hfac). A brief review of silver β-diketonate CVD precursor literature is included in Chapter 1.

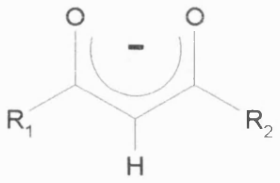

(VII)

The volatile nature of metal acetylacetonates was recognised as early as 1914, [190] this property being due primarily to the ability of the ligand (VI) to effectively crowd a metal centre. The effect of shielding the coordinating centre with ligand atoms from the substituents R_1 and R_2 reduces intermolecular attractions, charge, dipole, Van der Waals interactions and hydrogen bonds. These compounds are also known to exhibit relatively high thermal stability in the vapour phase and this has been attributed to the strong coordination nature of the metal-chelate core.

Comparative studies of the volatility of metal β-diketonates have shown general trends in properties, dependent largely on the nature of substituent R groups. Substitution of hydrogen by fluorine in the organo groups R_1 and R_2 will increase volatility due to a reduction in van der Waals forces, and perhaps a reduction in hydrogen bonding. [191] Where R_1 or R_2 are straight chain alkanes, volatility is lowered as the length of chain is increased, [192] and similarly substitution with an aryl group is reported to have a detrimental effect on volatility. [191] Adduct formation in some cases is said to reduce volatility slightly but increases the thermal stability range of the compound. [192]

The thermal decomposition of metal β-diketonates can take a number of potential routes;

- loss of complete ligand
- elimination of metal with one or two oxygen atoms
- elimination of metal with carbon and oxygen
- elimination of metal with R group
- elimination of metal with H^- or F^-

Mass spectrometry and thermal analysis investigations [193, 194] have revealed that the particular decomposition reaction observed depends on a large number of factors: the metal involved, the nature of the ligand, temperature, pressure, the type of atmosphere (whether inert, oxidising or reducing) and the presence of surface catalysis.

4.1.1 Synthetic Routes

Silver acetylacetonate was first prepared in 1893, by the mixing of equimolar quantities of sodium acetylacetonate and silver nitrate (Eqn 4-1), the creamy white complex precipitating immediately. [195] The complex was found to be relatively unstable, but could be stored for several days when pure with only slight decomposition (observed as a darkening of the precipitate).

$$Na(acac) + AgNO_3 \xrightarrow{H_2O} NaNO_3 + Ag(acac) \qquad \textbf{(4-1)}$$

$$AgNO_3 + H(acac) + NEt_3 \xrightarrow{MeOH/MeCN} Ag(acac) + Et_3NH^+NO_3^- \qquad \textbf{(4-2)}$$

Silver β-diketonates have recently been prepared from reactions of silver nitrate and β-diketones in the presence of triethylamine in a variety of organic solvents (Eqn 4-2). [196] In a methanol-acetonitrile solvent mixture at (1-3°C) high purity compounds have been precipitated in high yield. When pure, silver β-diketonates may be stored with little decomposition at low temperatures, degradation occurring at a faster rate if exposed to UV light, oxygen, water, solvents or higher temperatures. Lewis base adducts are notably more stable, particularly in the solid state and a wide variety have been synthesised, various routes to these adducts having been proposed in the literature.

I) These compounds may be synthesised by the reaction of thallium β-diketonates with adducts of silver chloride. In benzene this reaction is driven by the insolubility of thallium(I) chloride

(Eqn. 4-3). This method has been used to prepare mono- and bis- triphenylphosphine adducts of various β-diketonates [hexafluoroacetylacetonate (hfac), trifluoroacetylacetonate (tfac), acetylacetonate (acac), benzoylacetonate (bzac)]. [197, 198]

$$Tl(acac) + AgCl(PPh_3)_n \xrightarrow{C_6H_6} TlCl + Ag(acac)(PPh_3)_n \qquad \textbf{(4-3)}$$

II) A large number of olefin adducts of Ag(hfac) have been prepared in aqueous solution [199, 200] (Eqn 4-4). The olefin adducts once isolated and dried may be further reacted in organic solvents with stronger donors such as PR_3 to displace the olefin in favour of the phosphine [98, 201] (Eqn 4-5).

$$AgNO_3(olefin) + Na(hfac) \xrightarrow{H_2O} Ag(hfac)(olefin) + NaNO_3 \qquad \textbf{(4-4)}$$

$$Ag(hfac)(olefin) \xrightarrow[\text{hydrocarbon solvent}]{PR_3} Ag(hfac)PR_3 + olefin \qquad \textbf{(4-5)}$$

III) Finally, silver oxide may be reacted directly with a β-diketone (Eqn 4-6) and this reaction followed by addition of a Lewis base (Eqn 4-7). This synthetic route requires the β-diketone to exhibit a relatively high level of acidity (hfac > tfac > acac) for a quantitative reaction although

freshly prepared silver oxide may be used to increase reactivity. Alternatively, the preparation may be achieved as a one-pot reaction with the Lewis base present in solution. This method has been reported in a number of recent publications [97, 101, 202-206] where THF and diethyl ether are preferred solvents for use as these can be removed quickly *in vacuo.* Temperatures lower than room temperature have been used in some cases, as this may increase yields due to the thermally unstable nature of the silver β-diketonates, which are particularly vulnerable to decomposition in solution. This was the chosen synthetic route for compounds prepared in this study.

$$Ag_2O + 2H(hfac) \xrightarrow[-20^{o}C]{Et_2O} [\{Ag(hfac)\}_2(H_2O)] \qquad \textbf{(4-6)}$$

$$[\{Ag(hfac)\}_2(H_2O)] \xrightarrow{2\ L\ (donor\ ligand)} 2Ag(hfac)L + H_2O \qquad \textbf{(4-7)}$$

4.1.2 Structural Chemistry

The variety of bonding modes associated with β-diketonates relates to the ability of the free β-diketone ligand to exist as a number of different tautomers. Hydrogen atoms bonded to C_3 are known to be acidic due to the activation by two adjacent COR groups. Loss of a proton from C_3 in the 'keto' form results in a conjugate system arising from a prototropic shift to the 'enol' form (Eqn 4-8). This tautomerism gives rise to a number of potential bonding configurations for metals.

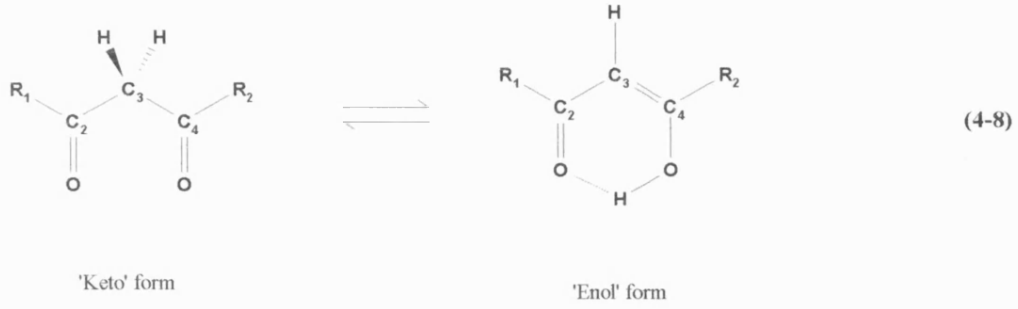

'Keto' form

'Enol' form

(4-8)

Metal β-diketonates can be classified according to the mode of bonding encountered (Figure 4-1). These include the β-diketonate bonded through one oxygen as a unidentate ligand (VIII), bonded through two oxygens as a bidentate chelating ligand (IX), bonded through two oxygens as a neutral donor ligand ('keto' form) (X), bonded through C_3 as a unidentate ligand (XI) or bonded with a double bond from an 'enol' tautomer (XII). While structurally determined examples for silver are generally of type IX, a number of examples of silver - carbon interactions are known which may be described as type XI.

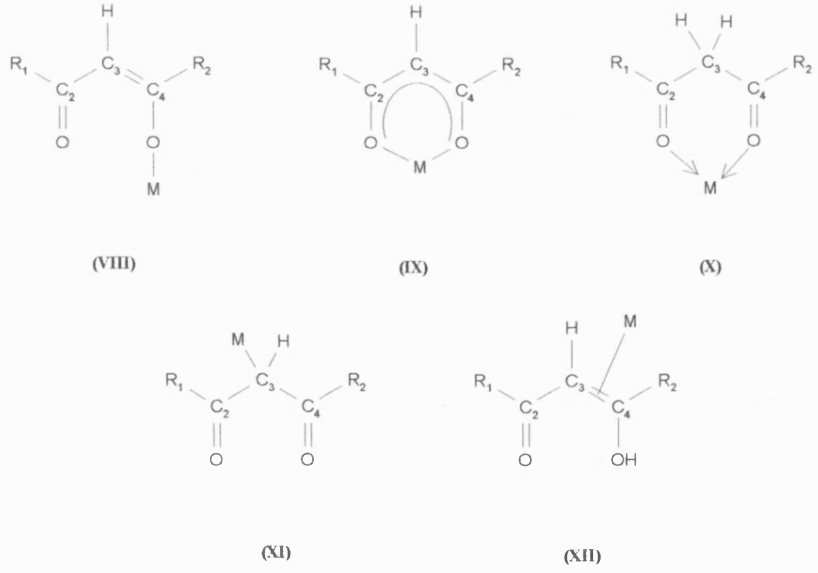

(VIII) (IX) (X)

(XI) (XII)

Figure 4-1 Principal bonding conformations of β-diketone ligands with metals

Table 4-1 Structural data for silver (I) β-diketonates.

	Lewis base [a]	Structural Description	Coordination sphere around Ag	β-diketonate bonding mode		Ref
				Ag-O	Ag-C	
Ag(hfac)	C≡NMe	monomeric	distorted trigonal (O_2C)	y	n	101
Ag(hfac)	PMe_3	monomeric	distorted trigonal (O_2P)	y	n	97-99
Ag(hfac)	SEt_2	monomeric	distorted trigonal (O_2S)	y	n	203
Ag(hfac)	2(1,4-oxathiane)	monomeric	distorted tetrahedral (O_2S_2)	y	n	202
Ag(hfac)	2(PMe_3)	monomeric	distorted tetrahedral (O_2P_2)	y	n	97
Ag(hfac)	1,5-cod	dimeric	distorted sq. pyramidal ($O_3C{=}C_2$)	y	n	204
Ag(hfac)	dmcod	dimeric	distorted octahedral ($O_4C{=}C_2$)	y	n	206
Ag(hfac)	½(H_2O)	H-bonded and Ag-C	(A) distorted sq. pyramidal (O_4C)	y	y	202
		bonded dimers	(B) tetragonal (O_3C)	y	y	
Ag(hfac)	½(nbd)	tetramer	(A) distorted tetrahedral (O_4)	y	n	202
			(B) tetragonal ($O_3C{=}C$)	y	n	
Ag(hfac)	¼(SEt_2)	bridged tetramers	(A) distorted tetrahedral (O_3S)	y	n	203
			(B) distorted tetrahedral (O_4)	y	n	
$AgNi(acac)_3.2AgNO_3.H_2O$		polymeric	various ($O_{1\text{-}2}C_{0\text{-}1}(NO_3)_{0\text{-}2}$)	y	y	207
$[Pd_2Ag(C_6F_5)_4(acac)_2](NBu_4)$		trinuclear cluster	linear (C_2)	n	y	208

[a] 1,5-cod = 1,5-cyclooctadiene, dmcod = 1,5-dimethyl-1,5-cyclooctadiene, nbd = norbornadiene

Structure determination of silver β-diketonates, usually in conjunction with CVD studies, reported in the literature are listed in Table 4-1. Adducts of silver hexafluoroacetylacetonate are found as small oligomers (monomers, [97-101, 202] dimers, [204, 206] tetramers, [202]) or occasionally as polymeric structures *via* Ag-C bonds. [202] Additionally a number of structures exist where silver has been found to interact with acetylacetonate in the presence of other metals. [207, 208]

Structures containing the hexafluoroacetylacetonate ligand (hfac) show the ligand's ability to bind silver in a bidentate fashion (Type VIII). An example of this mode of bonding is shown in the structure of the methyl isocyanide adduct of silver hexafluoroacetylacetonate. [101] The hfac ligand bonds unsymmetrically through both oxygens and a distorted trigonal configuration is completed by C≡NMe (Figure 4-2). The distortion is towards a linear O-Ag-L (L = CNMe) with the remaining oxygen more weakly coordinated (Ag-O: 2.250 and 2.309Å, respectively). The cause of this distortion is unexplained, although a weak intermolecular hydrogen bond has been identified between a fluorine from a CF_3 and a hydrogen from the methyl isocyanide (2.235 Å). Similar distortions are observed in the structure of the related mono-trimethylphosphine adduct, although these have been attributed to packing effects. [97-99]

The 1:1 adduct of Ag(hfac) with 1,5-cyclooctadiene (1,5-cod) is reported to be a dimer (Figure 4-3). [204] Unlike monomeric Cu(hfac)(1,5-cod) [209] this compound has two distinct hfac ligands, one chelates and bridges two silver atoms in a μ^4,η^2-fashion, the other bridges the two silver atoms in a μ^2-fashion. The latter β-diketonate ligand is markedly asymmetric (Ag-O: 2.46 and 2.72Å) as compared to the μ^4,η^2- β-diketonate (AgO: 2.51-2.58Å). The coordination spheres of the silver centres are completed by π-donor bonds from the 1,5-cod molecules.

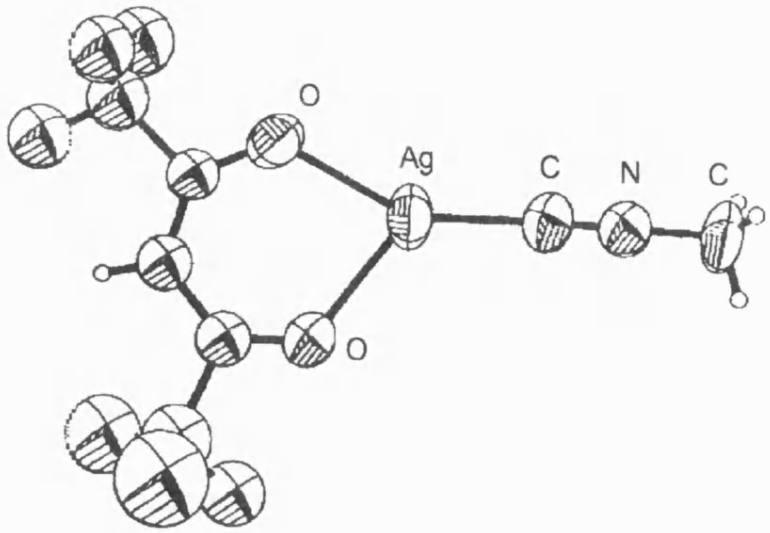

Figure 4-2 Structure of Ag(hfac)(CNMe). [101]

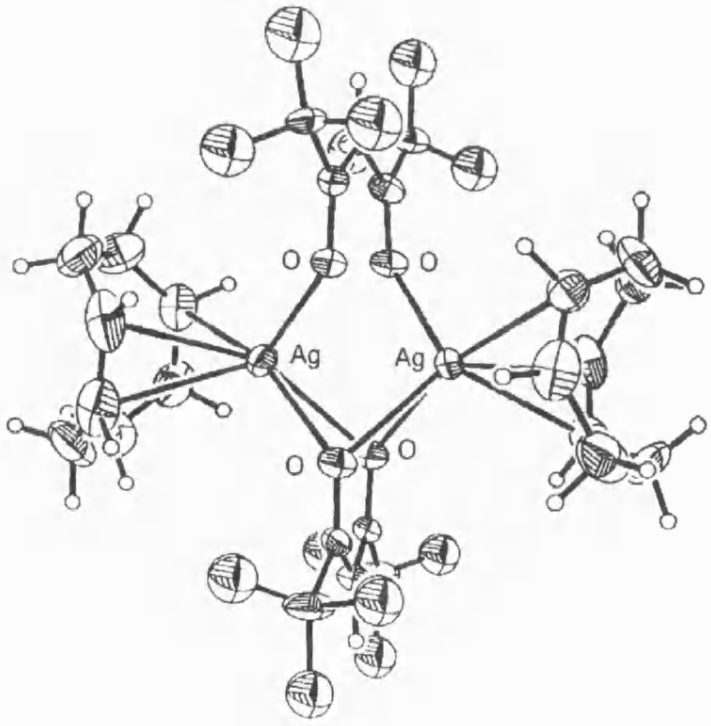

Figure 4-3 Structure of [Ag(hfac)(1,5-cod)]$_2$ [204]

Dimeric $Ag_2(hfac)_2L_2$ units are also to be found in the recently reported 1,5-dimethyl-1,5-cyclo octadiene adduct (L = dmcod). [206] In this case the hfac ligands again display marked asymmetry with respect to bonding to silver {AgO: 2.35-2.39Å (short), 2.64-2.78Å (long)}, however both hfac ligands chelate each silver and bridge between them (μ^4,η^2). Interestingly, the four methyl groups from the olefin are oriented towards the molecule with silver - carbon (methyl) distances of 3.2-3.6Å, forming a methylated hydrophobic cage around the two silver atoms.

The reaction of silver oxide with hexafluoroacetylacetone in THF has yielded a complex that has been tentatively described as $[\{Ag(hfac)\}_2(THF)]$. [99] The reaction in diethyl ether produces a complex with water present as a donor ligand $[\{Ag(hfac)\}_2(H_2O)]$, [202] the structure of which has been determined. The compound takes up a dimeric form with two inequivalent silver atoms present, one chelated by the two hfac ligands, the other bridging two oxygens from different β-diketonates with an additional water molecule completing its coordination sphere (Figure 4-4). Additionally, silver atoms are subject to intermolecular silver-carbon interactions (Ag-C: 2.391, 2.492Å), the two silver atoms thus achieving a coordination sphere of tetrahedral and square-pyramidal geometry, respectively.

An example of silver bonded to β-diketonates solely by silver - carbon bonds is $[Pd_2Ag(C_6F_5)_4(acac)_2](NBu_4)$, where silver atoms bridge $Pd(acac)(C_6F_5)_2$ anionic fragments (Figure 4-5). [208] The silver coordination is linear, with silver bonded only to the central carbon (C_3) with a bond length of 2.237 Å. As a result of the Ag-C bond, the C_3 atom uses sp^3 orbitals for bonding and the Pd(acac) ring loses its planarity to adopt a boat conformation. Conductivity experiments suggest that Ag-C bond cleavage occurs readily and reversibly in solution.

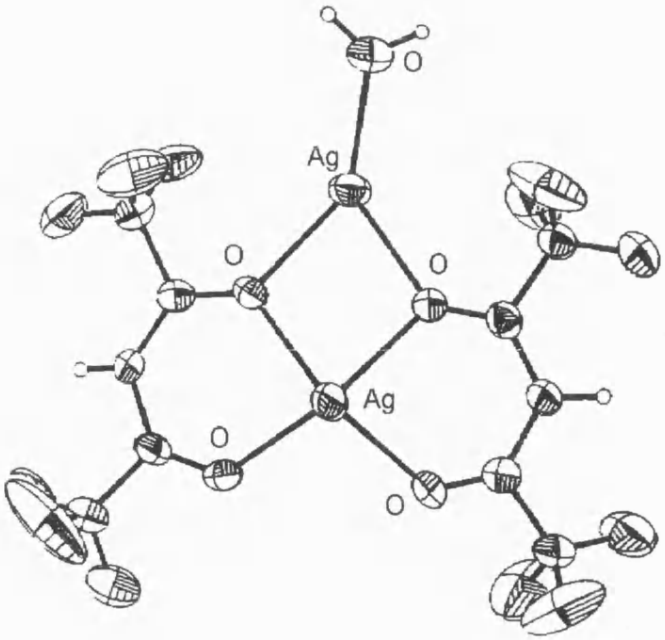

Figure 4-4 Structure of $[\{Ag(hfac)\}_2(H_2O)]$. [202]

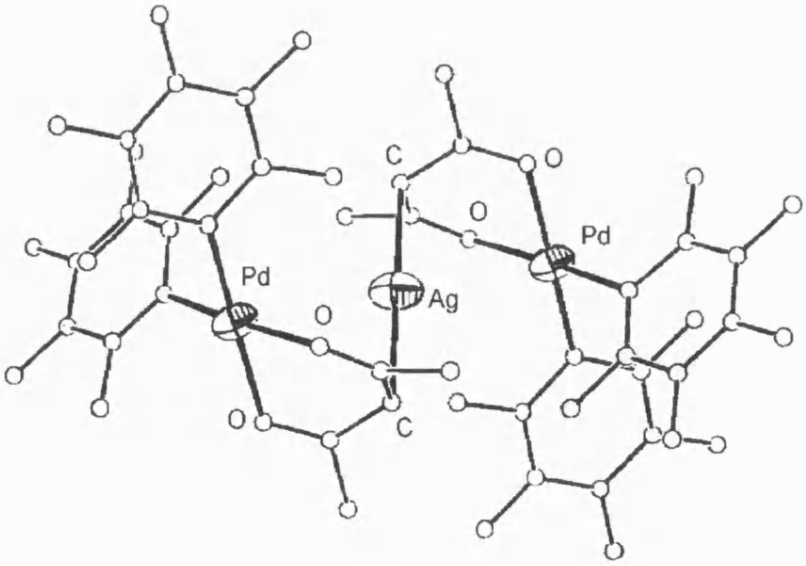

Figure 4-5 Structure of $[Pd_2Ag(C_6F_5)_4(acac)_2](NBu_4)$. [208]

In addition to X-ray crystallographic studies, a number of silver β-diketonate adducts have been prepared and characterised by infra-red and proton NMR spectroscopy. Olefin adducts of silver hexafluoroacetylacetonate (hfac) prepared include those containing cyclooctatetraene, cycloheptene, cyclohexene, [199] bicyclo [2.2.1]-2-heptene, [205] 1,5-cyclooctadiene and cyclooctene. [199, 205] Additionally, the 1,5-cyclooctadiene and cyclooctatetraene adducts of silver trifluoroacetylacetonate have also been prepared. [199] Osmometrically determined molecular weight experiments indicate that these compounds exist as monomers in halogenated solvents, [201] although a structure determination of Ag(hfac)(1,5-cod) has since shown it to be dimeric in the solid state. [204] Infra-red studies have suggested that the β-diketonate ligand bonds via oxygen atoms. [199]

Triphenylphosphine adducts, Ag(β-diketonate)$(PPh_3)_n$, have been isolated (β-diketonate = hfac, bzac, n = 2; β-diketonate = acac, tfac, n = 1), and characterised by infra-red and proton NMR spectroscopy. [197, 198] The β-diketonate ligands were proposed to be oxygen bonded although the possibility of silver-carbon bonds was considered in the case of fluorinated β-diketonates. Finally, heats of reaction of triphenylphosphine with various Ag(hfac)olefin adducts have been determined, along with relative silver - Lewis base dissociation energies. [201]

4.1.3 Derivatives of metal β-diketonates

The reactive nature of the carbonyl functionalities in β-diketones allow synthetic modifications of the ligand where an oxygen may be substituted for a sulphur (thio-β-diketonates) or NR (β-keto-iminates). These modifications are fairly straightforward and provide an additional synthetic tool in the modification of structure and physical properties of these compounds.

Thio-β-diketones are readily synthesised by the addition of H_2S to β-diketones in alcoholic solution saturated with hydrogen chloride [210] (Eqn 4-9). The hydrogen chloride appears to shift the tautomeric equilibrium in the reaction toward the diketo form, which reacts with the hydrogen sulphide. In cases where $R_1 \neq R_2$ the attack of the hydrogen sulphide is observed to be at the carbonyl adjacent to the less electronegative R group and thus only one isomer is formed. [211]

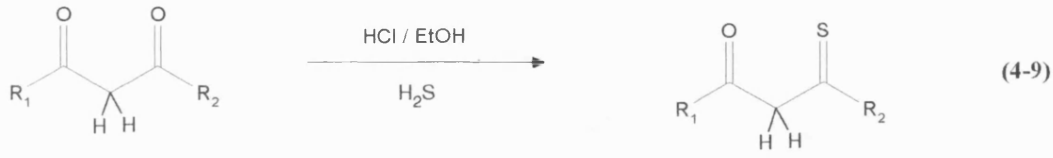

(4-9)

Relevant reports involving thio-β-diketones include that of silver thiodibenzoylmethanate which, on the basis of IR work, is believed to bond through the sulphur only. [212] Additionally the silver salt of 1,1,1-trifluoro-4-(2-thienyl)-4-mercapto-3-buten-2-one has been synthesised and is reported as sublimable with some decomposition (2×10^{-2} Torr, 86-112°C). [213] As silver is known to be thiophilic these compounds may be potentially interesting as β-diketonate ligand analogues.

β-Ketoimines are readily synthesised by condensation of a β-diketone with a primary amine NH_2R. In many cases the condensation may be achieved with the removal of water as an azeotropic mixture using the Dean and Stark procedure (Eqn 4-10). [214] Where the β-diketone is a stronger acid (notably the fluorinated analogues), acid-base chemistry predominates and this synthetic approach is no longer valid (Eqn 4-11). To circumvent this reaction, the sodium salt may be reacted with R_3SiCl to give the silyl enol ether which can be further reacted with the primary amine (Eqn. 4-12). [214, 216]

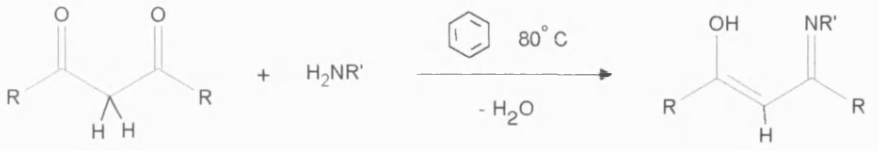

(4-10)

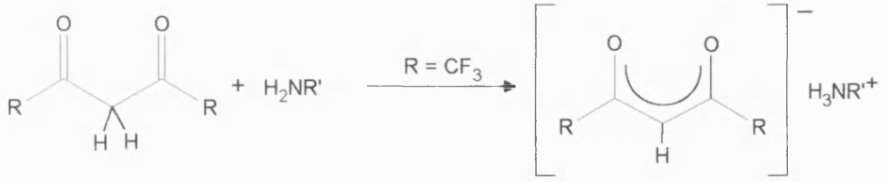

(4-11)

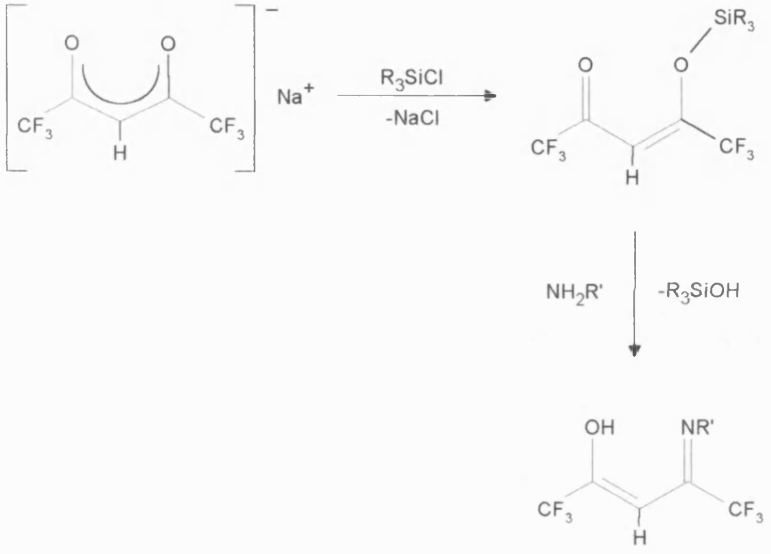

(4-12)

The preparation of β-ketoiminato complexes is a useful approach to preparing volatile compounds and has been used successfully in Cu and Ba CVD precursor chemistry. Variation of the R group attached to nitrogen allows for further steric crowding of the metal centre as shown in the CVD precursor copper (I)4-(isopropyl)imino-1,1,1,5,5,5-hexafluoropentan-2-onate (Figure 4-6). [216] Additionally, the R group chosen may incorporate additional coordination sites, as for example in a range of barium β-ketoiminates containing appended ether 'lariats' (Figure 4-7). In cases such as this the oxygen containing R' group wraps around the metal centre to further coordinatively saturate the metal via intra-molecular bonds. [214, 215] There are no reports of silver β-ketoiminates in the literature.

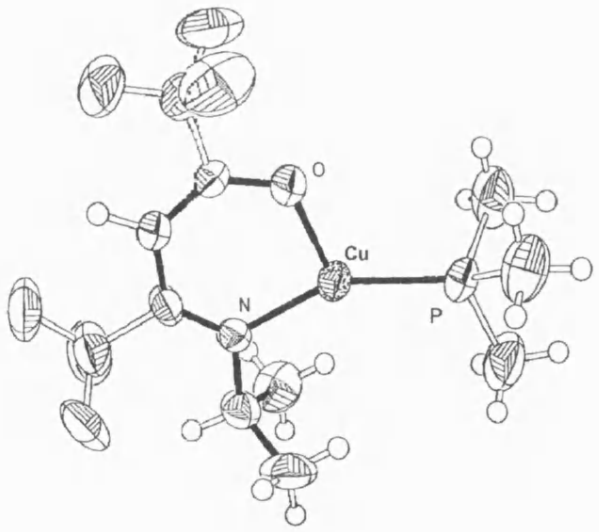

Figure 4-6 Structure of [4-(isopropyl)imino-1,1,1,5,5,5-hexafluoropentan-2-onato]copper(I) [216]

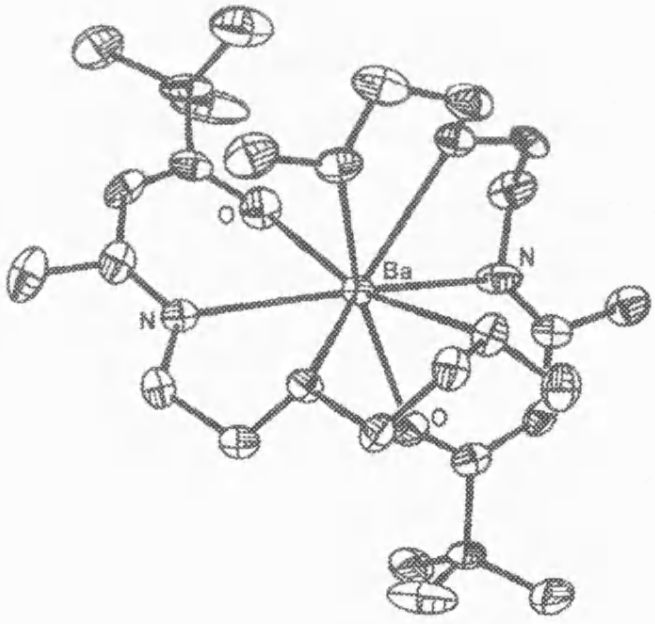

Figure 4-7 Structure of bis[2,2-dimethyl-5-N-(2-(2-methoxy)ethoxy-ethylimino)-3-hexanonato]barium(II) [214]

4.2 RESULTS AND DISCUSSION

The vast majority of silver β-diketonate work published in the context of silver CVD has been concerned with the preparation of various adducts of Ag(hfac) and more recently Ag(fod). [96-103] The emphasis of this present work is in understanding the effect of variation of the β-diketonate itself in terms of molecular structure, thermal stability and film growth properties. To this end, mono adducts of various silver β-diketonates and β-ketoiminates have been synthesised with the Lewis base donor (triphenylphosphine) remaining constant.

4.2.1 Synthesis

A series of triphenylphosphine adducts of silver β-diketonates have been prepared where the two R groups have been varied (CH_3, ^tBu, CF_3, C_3F_7) (Scheme 4-1). A slight excess of the β-diketone was used in all the preparations, except for **(17)** where a larger excess was used to ensure higher consumption of the β-diketone ligand. The addition of one molar equivalent of triphenylphosphine to a silver β-diketonate, prepared *in situ*, produced in all cases 1:1 ($Ag:PPh_3$) adducts except for **(19)**. Preparative yields were found to be within the range of 71-86 % with the exception of **(19)**. The reaction of silver oxide, Hfod and triphenylphosphine resulted in the isolation of a complex **(19)** with unexpected stoicheometry, $[Ag(fod)]_3(PPh_3)_5$, in a lower yield (28%).

The compounds **(17-21)** could be stored at room temperature in the absence of light for extended periods with only moderate decomposition (observed as darkening of the precipitate). The observed stability for the complexes at room temperature is in the order; hfac > tfac ~ fod > dpm > acac.

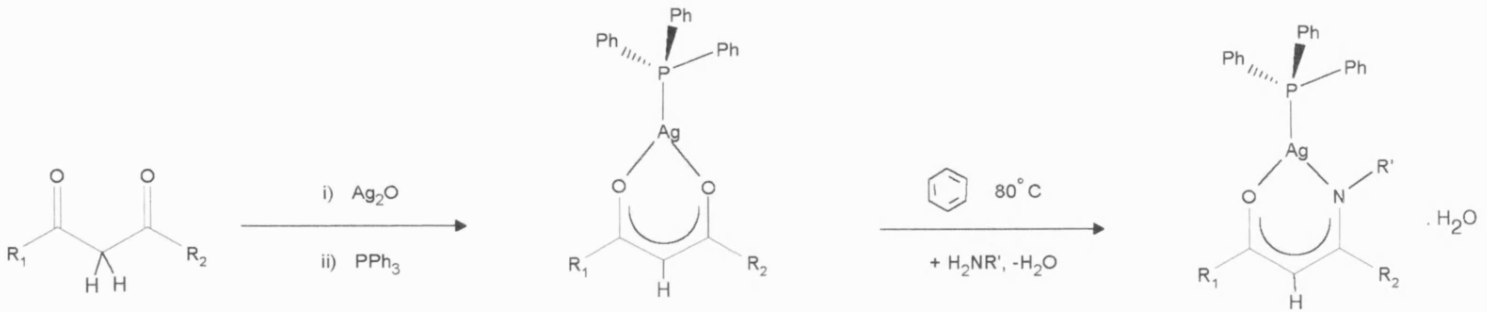

$R_1 = CH_3$ $R_2 = CH_3$ (acac) **(17)**

$R_1 = {}^tBu$ $R_2 = {}^tBu$ (dpm) **(18)**

$R_1 = {}^tBu$ $R_2 = C_3F_7$ (fod) **(19)**

$R_1 = CH_3$ $R_2 = CF_3$ (tfac) **(20)**

$R_1 = CF_3$ $R_2 = CF_3$ (hfac) **(21)**

$R_1 = CF_3$ $R_2 = CF_3$ R' = hexyl (hfacNhex) **(22)**

$R_1 = CF_3$ $R_2 = CF_3$ R' = cyclohexyl (hfacNchex) **(23)**

all complexes were found to exhibit a 1:1 (Ag:PPh_3) stoicheometry, except **(19)** which was formed as a 3:5 complex.

Scheme 4-1

Initial decomposition points for the non-fluorinated silver β-diketonate adducts were considerably lower [**(17)** 150°C, **(18)** 140°C] than for the fluorinated compounds, [**(19)** 210°C, **(20)** 200°C, **(21)** 250°C].

Two triphenylphosphine adducts of silver β-ketoiminates have been synthesised by the condensation reaction of [Ag(hfac)PPh_3] **(21)** with H_2NR' (R′ = hexyl, cyclohexyl) (Scheme 4-1). Complex **(21)** was chosen for this reaction due to its observed higher thermal stability compared to the other β-diketonate adducts. The reaction was carried out using the Dean and Stark procedure in boiling benzene (80°C). Attempts at this reaction with toluene met with higher rates of decomposition due to the higher boiling point of the solvent (111°C). Direct reaction of primary amines with β-diketones normally results in the formation of acid-base salts (Eqn 4-10). [216] However the β-diketonate ligand is a much weaker acid and it appears that the metal may act as a template for the reagents. The 1:1 adducts were isolated as hydrates, as evidenced by microanalysis and infra-red spectra, despite the observed removal of water during the reaction over some two hours. Preparative yields were high (81-89%). Attempts at the recrystallisation of **(22)** in air resulted in hydrolysis and reversion to the β-diketonate adduct. Decomposition temperatures for the β-ketoiminato complexes [**(22)** 100°C and **(23)** 115°C] were lower than for the parent β-diketonate [250°C for Ag(hfac)PPh_3 **(21)**].

4.2.2 Infra-red Spectroscopy

As in the case of carboxylates, bonding modes of the β-diketonate ligand may be distinguished using IR spectroscopy, through the ν(CO), ν(CC) and ν(MO) stretching modes. On complexation

with a metal, ν(OH) due to the presence of the 'enol' tautomer of the free ligand is replaced by metal-oxygen stretching frequencies at low frequencies (300-500 cm^{-1}). [217] There has been some confusion as to the relative positions of ν(CO) and ν(CC) but this issue has been somewhat resolved with isotopic labelling studies. [218] It is now widely accepted that the vibration with the highest ν(CO) character is found at a higher frequency than that with the most ν(CC) character but it must be recognised that significant mixing of ν(CO) and ν(CC) occurs in both cases. The higher frequency ν(CO) is more readily identified over the weaker ν(CC) vibration.

The position of the ν(CO) and ν(CC) stretching modes are found to be highly dependent on R_1 and R_2. Replacement of CH_3 with CF_3 is said to shift bands to higher wavenumber. [219] Tentative assignments of ν(CO) for compounds **(17)-(21)** (Table 4-2) confirm this; ν(CO) bands for non-fluorinated β-diketonates **(17-18)** were observed at 1582-1615 cm^{-1}, whereas ν(CO) bands for β-diketonates containing CF_3 **(19-21)** were found at 1661-1669 cm^{-1}.

The observed vibrational frequency of 1669 cm^{-1} in Ag(hfac)PPh_3 **(21)**, is assigned as ν(CO) and compares favourably with ν(CO) found in similar compounds such as Ag(hfac)L and Cu(hfac)L (structurally determined as monomers), and a wide variety of Ag(β-diketonate)olefins (1660-1678 cm^{-1}). [199] This would suggest that in **(21)** the β-diketonate also bonds to silver via the oxygens and this has been confirmed crystallographically (discussed further in 4.3).

Compound **(19)** may be compared with the related Ag(fod)PEt_3 which has been studied closely using RAIRS (reflection absorption infra red spectroscopy) techniques and its IR spectrum assigned between 3000 and 930 cm^{-1}. [100] The main ν(CO) vibration in **(19)** was observed at 1628 cm^{-1} with a shoulder at higher wavenumbers (1661 cm^{-1}). A similar ν(CO) is found in Ag(fod)PEt_3

Table 4-2 Tentative assignments of ν(CO) (cm^{-1}) for silver(I) β-diketonate adducts. [a]

Compound		This study ν(CO)	Related data Compound	ν(CO)	Ref
$Ag(acac)(PPh_3)$	**(17)**	1615	$Ag(acac)PPh_3$	1614s	198
			$Cu(acac)PMe_3$	1587s	188
$Ag(dpm)(PPh_3)$	**(18)**	1582	$Cu(dpm)PMe_3$		188
$[Ag(fod)]_3(PPh_3)_5$	**(19)**	1628ssh, 1661sh	$Ag(fod)PEt_3$	1631s	100
$Ag(tfac)(PPh_3)$	**(20)**	1667sb	$Ag(tfac)PPh_3$	1658	198
			$Cu(tfac)PMe_3$	1623s	188
$Ag(hfac)(PPh_3)$	**(21)**	1669b	$Ag(hfac)PMe_3$	1671	98
			$Ag(hfac)PEt_3$	1674	98
			Ag(hfac)CNMe	1670	101
			$Cu(hfac)PMe_3$	1672s	188
$Ag(hfacNhex)(PPh_3)$	**(22)**	1661sh			
$Ag(hfacNchex)(PPh_3)$	**(23)**	1661sb			

[a] IR spectra were recorded as nujol and hexachlorobutadiene mulls on KBr plates

at 1631 cm^{-1}, and this also exhibits a medium intensity shoulder at slightly higher wavenumbers (the frequency was not reported). The assignments of ν(CC) is at 1580 cm^{-1} in Ag(fod)PEt_3 and an analogous band is found at 1586 cm^{-1} in **(19)**. Such results suggest that despite a different stoicheometry, **(19)** exhibits a not dissimilar β-diketonate bonding mode to that found in Ag(fod)PEt_3.

The infra red spectra of the silver β-ketoiminate adducts **(22)** and **(23)** can be compared with their parent silver β-diketonate adduct **(21)**. A change in the frequency of the ν(CO) vibration would be expected if an oxygen is replaced by nitrogen and such a change is observed using nujol mulls of **(22)** and **(23)**, both displaying a shift to 1661 cm^{-1} and this is reproducible when the compound is many months old (Figure 4-8). Curiously, this shift in ν(CO) is not observed in hexachloro-butadiene mulls where the vibration is detected at 1671 and 1669 cm^{-1} for **(22)** and **(23)**, respectively, close to the value observed in **(21)** (1669 cm^{-1}). The β-ketoiminate compounds are however slightly soluble in hexachlorobutadiene and this may suggests that in solution the β-ketoiminate complex reverts to the β-diketonate plus free amine. Water molecules could be provided for this reaction either from the compound [both **(22)** and **(23)** were observed to be hydrates] or from 'wet' mulling agent. Both **(22)** and **(23)** also exhibit sharp, weak vibrations at 3060-3275 cm^{-1} in nujol within the range expected for water of crystallisation (3100-3600 cm^{-1}) [220] rather than amine ν(NH) (3300-3400 cm^{-1}). [221]

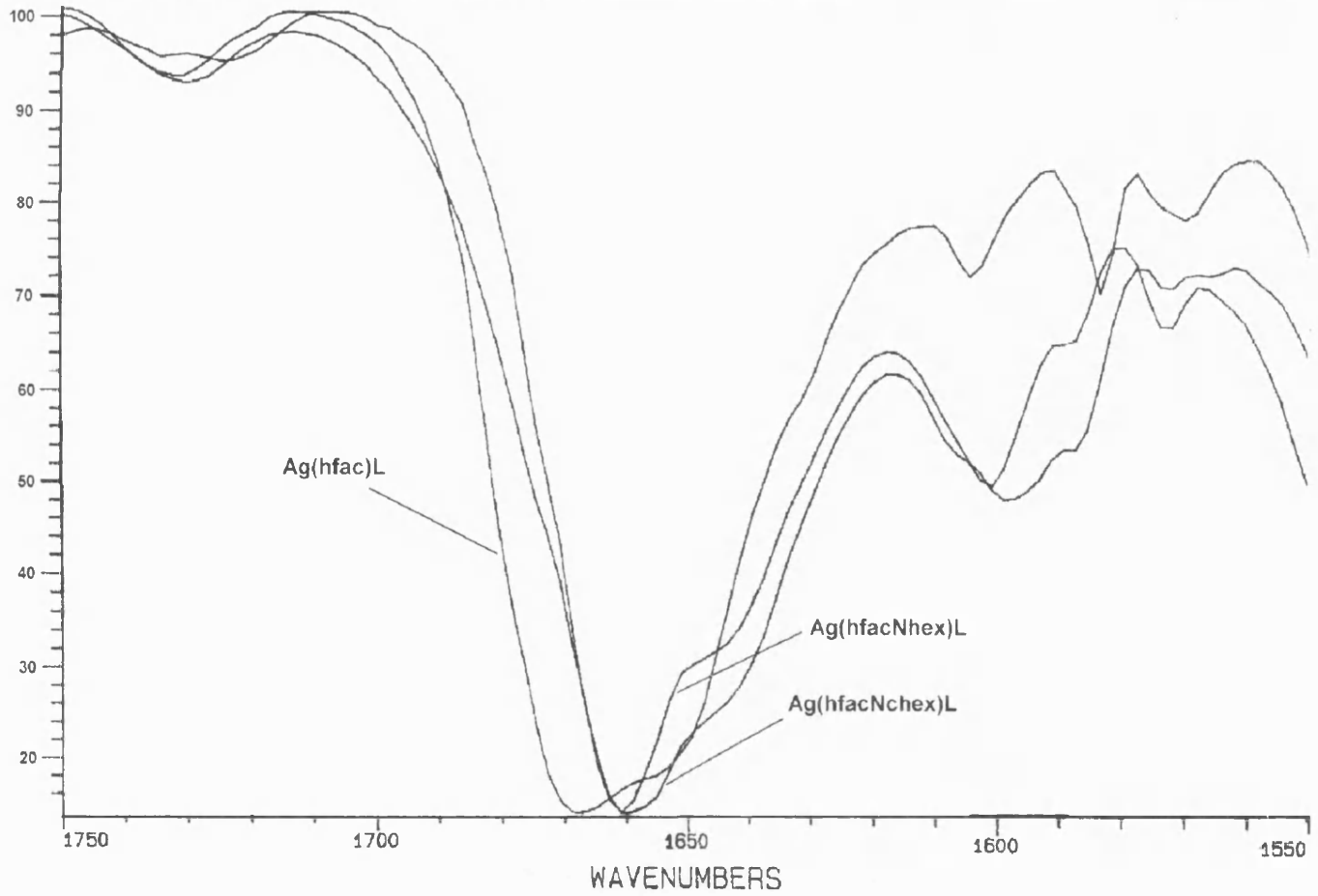

Figure 4-8 Comparison of IR traces (Nujol mulls, 1750-1550 cm^{-1}) of compounds **(21)-(23)**, (L = PPh_3).

4.2.3 ^{1}H, ^{13}C, and ^{19}F NMR Spectroscopy

^{1}H, ^{13}C and ^{19}F NMR measurements of silver(I) β-diketonate adducts gave no unexpected results. The presence of fluorinated R groups deshield the proton of the CH unit, as the C<u>H</u> is observed at a lower field in the ^{1}H NMR. Consequent to this there is a increase in electron density on the carbon of the <u>C</u>H which is seen at a higher field where fluorinated R groups are incorporated.

Carbonyl resonances in the ^{13}C NMR were relatively easily assigned except for cases of unsymmetric β-diketonates [**(19)**, **(20)**] where two different ^{13}<u>C</u>-O resonances were observed. In cases such as these the carbon-13 resonance adjacent to the fluorinated group was coupled to fluorine atoms and consequently weaker. In the case of **(19)**, although ^{1}H NMR integrals confirmed the unusual three to five ($Ag:PPh_3$) stoicheometry of the complex, only one type of β-diketonate ligand was observed at room temperature in the ^{1}H, ^{13}C and ^{19}F spectra.

In the case of β-ketoiminate adducts **(22)** and **(23)**, ^{1}H, ^{13}C and ^{19}F NMR observations were perturbed from expected positions for compound **(21)**, the β-diketonate analogue. However, the expected resonances for <u>C</u>=NR could not be identified and only one resonance could be identified due to the CF_3 in both the ^{13}C and ^{19}F spectra despite the fact that the carbons of the NR groups were identified in all spectra. Such spectroscopic data suggest that the β-ketoiminate may have reverted to the β-diketonate and free amine in solution, as was also suggested by IR results (4.2.2).

Table 4-3 Selected ^{1}H and ^{13}C NMR data for silver(I) β-diketonate and β-ketoiminate adducts. [a]

Compound		^{1}H NMR		^{13}C NMR					
		C<u>H</u> (ppm)	C<u>H</u>$_3$ (ppm)	<u>C</u>H (ppm)	<u>C</u>X [b] (ppm)	^{2}J (C-C-F) (Hz)	<u>C</u>H$_3$ (ppm)	CO<u>C</u>F$_3$ (ppm)	^{1}J (C-F) (Hz)
Ag(acac)(PPh$_3$)	**(17)**	5.26	1.95	98.5	191.0	-	28.8	-	-
Ag(dpm)(PPh$_3$)	**(18)**	5.73	1.18	90.7	201.5	-	27.4	-	-
[Ag(fod)]$_3$(PPh$_3$)$_5$	**(19)**	5.71	1.12	90.6	205.8	-	27.9	-	-
					171	no [c]	-	-	-
Ag(tfac)(PPh$_3$)	**(20)**	5.50	1.99	92.8	197.0	-	30.2	119.2	289
					170.1	29.4	-	-	-
Ag(hfac)(PPh$_3$)	**(21)**	6.05		87.9	177.5	33.0	-	117.7	289
Ag(hfacNhex)(PPh$_3$) [d]	**(22)**	5.61		86.2	175.7	31.3		118.0	291
Ag(hfacNchex)(PPh$_3$) [d]	**(23)**	5.69		86.0	175.4	31.9		118.0	291

[a] NMR experiments were recorded as $CDCl_3$ solutions [b] X = O, NR [c] no = not observed [d] ^{1}H and ^{13}C resonances for the NR group were identified and are listed fully in experimental

4.2.4 ^{31}P and ^{109}Ag Multinuclear NMR

Phosphorus-31 resonances of compounds **(17)-(23)** were observed as broadened singlets at room temperature, between 9-26 ppm. The absence of $^{1}J(Ag\text{-}^{31}P)$ coupling indicates a significant dynamic equilibrium due to lability of the ligands, and this is as found in the case of phosphine adducts of silver carboxylates (Sections 2.2.4 and 3.2.4) and in the literature. [82, 98, 99, 222] The ^{31}P NMR of recrystallised **(21)** however showed a sharp doublet of doublets at room temperature indicating that this behaviour is somewhat dependent on purity, i.e. dynamic equilibrium may be reduced if traces of free phosphine are absent. $^{1}J(^{109}Ag\text{-}^{31}P)$ coupling of 822 Hz in this case was comparable to that found in the ^{109}Ag NMR spectrum at -80°C (831 Hz) and to reported values of $^{1}J(^{107}Ag\text{-}^{31}P)$ observed for Ag(β-diketonate)PR_3 (where β-diketonate = hfac, fod, R = Me, Et) at low temperature [99] [$^{1}J(^{107}Ag\text{-}^{31}P)$ = 702-760 Hz, $^{1}J(^{109}Ag\text{-}^{31}P) / {}^{1}J(^{107}Ag\text{-}^{31}P) \approx 1.15$ [177]].

Silver-109 resonances observed at low temperature were invariably doublets [with the exception of **(19)**] and were found in the range 513-641 ppm with ^{1}J coupling of 720-830 Hz (Table 4-4). There are no reports of ^{109}Ag NMR chemical shift values in the literature for silver(I) β-diketonates although the observed chemical shifts for these adducts are midway between AgO_2CR and $AgO_2CR(PPh_3)_2$ (Table 4-5). ^{109}Ag resonances for the Ag(β-diketonate)PPh_3 compounds move to higher field with increasing fluorination of the β-diketonate. The coupling parameters in all cases, except **(19)**, are consistent with a single phosphine ligand bound to silver and compare well to those found in the literature; for $AgX(PR_3)$ (R = 2,4,6-trimethoxyphenyl, X = Cl, Br, I) $^{1}J(^{109}Ag\text{-}^{31}P)$ = 745-821 Hz. [82]

Table 4-4 ^{31}P and ^{109}Ag NMR data for silver(I) β-diketonate and β-ketoiminate adducts.

Compound		^{31}P NMR [a] δ [c] (ppm)	Low Temp ^{109}Ag NMR [b] δ [d] (ppm)	$^{1}J(^{31}P-^{109}Ag)$ [d] (Hz)
$Ag(acac)(PPh_3)$	**(17)**	15.1	613, d	772
$Ag(dpm)(PPh_3)$	**(18)**	9.1	no	no
$[Ag(fod)]_3(PPh_3)_5$	**(19)**	12.3, b	943, t	496
			823, t	523
			564, d	800
$Ag(tfac)(PPh_3)$	**(20)**	10.7	560, d	809
$Ag(hfac)(PPh_3)$	**(21)**	26.0 [e]	513, d	831
$Ag(hfacNhex)(PPh_3)$	**(22)**	13.2		
$Ag(hfacNchex)(PPh_3)$	**(23)**	12.7	641, d	726

[a] NMR experiments were recorded as $CDCl_3$ solutions at room temperature [b] NMR experiments were recorded as $CH_2Cl_2/CDCl_3$ solutions at -80°C [c] b = broad resonance [d] d = doublet, t = triplet, no = not observed [e] ^{31}P NMR of recrystallised compound allowed observation of $^{1}J(Ag-^{31}P)$ at room temperature as a doublet of doublets at 23.1 ppm, $^{1}J(^{107}Ag-^{31}P) = 717$ Hz, $^{1}J(^{109}Ag-^{31}P) = 822$ Hz

Table 4-5 Comparison of ^{109}Ag chemical shifts of silver(I) compounds $AgX(PPh_3)_n$.

X	n = 0	n = 1	n = 2
O_2C^tBu [a]	303 **(5)**		931 **(7)**
$O_2C\text{-}C_6H_2Me_3$ [a]	266 **(8)**		895 **(10)**
$O_2CC_3F_7$ [b]	173 **(11)**		823 **(12)**
$O_2CC_6F_{13}$ [b]	171 **(13)**		823 **(14)**
acac		613 **(17)**	
fod [c]		564 **(19)**	823, 943 **(19)**
tfac		560 **(20)**	
hfac		513 **(21)**	

[a] Chapter 2 [b] Chapter 3 [c] this compound was found to exhibit a 3:5 ($Ag:PPh_3$) stoicheometry, i.e. $[Ag(fod)](PPh_3)_5$

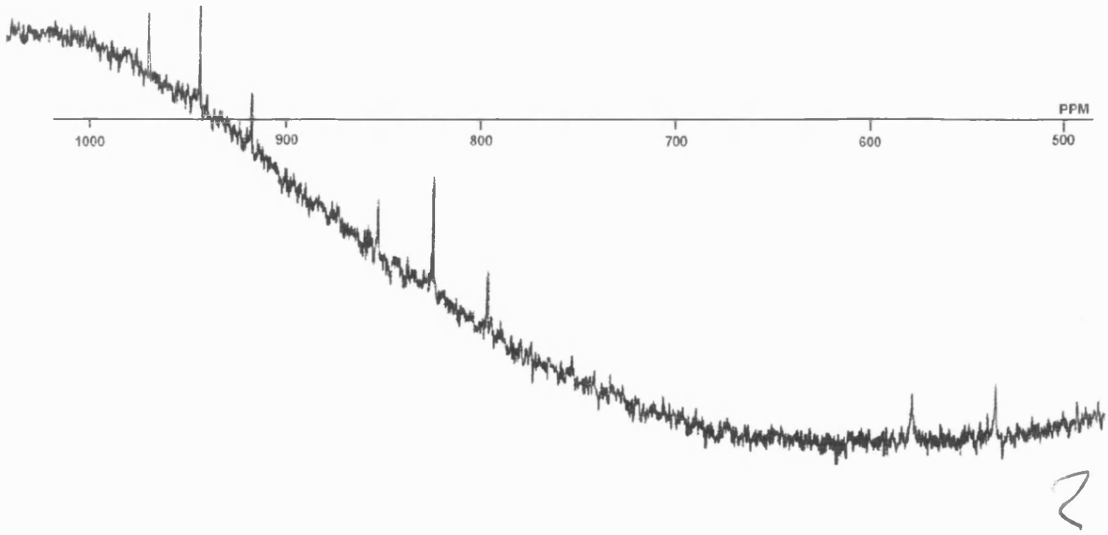

Figure 4-9 ^{109}Ag NMR spectrum for **(19)**, $[Ag(fod)]_3(PPh_3)_5$.

The case for **(19)** is more complicated in that three resonances were identified in the ^{109}Ag NMR indicating the presence of at least three different silver environments in solution (Figure 4-9). The doublet at 564 ppm [$^1J(^{31}P\text{-}^{109}Ag)$ = 800 Hz] is very similar to that observed for other Ag(β-diketonate)(PPh_3) complexes (Table 4-4). The remaining resonances are observed as triplets at 943 and 823 ppm indicating two phosphine ligands bound to each silver. Coupling constants for these resonances, 496 and 523 Hz respectively, concur with this conclusion and compare favourably with reported $^1J(^{107}Ag\text{-}^{31}P)$ for Ag(hfac)(PEt_3)$_2$ (468 Hz) [99] and bis(triphenylphosphine)silver carboxylates previously discussed in Chapters 2 and 3 (484-524 Hz). Since two triplets represent two silver atoms each bound to two phosphines, the difference in chemical shift must arise from bonding differences with respect to the β-diketonate. It is difficult to envisage a single molecular species that would give rise to this type of spectrum, although silver β-diketonate structures have been reported containing two, but not three, distinct silver environments (for example as shown in Figure 4-4). Proposals for potential molecular species consistent with this spectrum are complicated by the fact that in both the ^{1}H and ^{13}C NMR spectra only one type of β-diketonate

ligand is observed, although it may be the case that these nuclei are so remote as to remain equivalent. There also remains the possibility that in solution **(19)** dissociates into a number of smaller oligomers, for instance a dimer (containing inequivalent silver atoms) and a monomer. This structural conundrum awaits crystallographic resolution.

The NMR spectrum of Ag(hfacNchex)(PPh_3) shows an expected doublet at lower field than other monomeric silver(I) β-diketonate adducts (641 ppm), the $^1J(^{31}P\text{-}^{109}Ag)$ coupling again being comparable with mono-phosphine adducts although it is the lowest observed in this group of compounds (726 Hz).

4.2.5 Mass Spectrometry

The FAB mass spectra of silver β-diketonate adducts **(17)-(21)** were found to be dominated by silver-triphenylphosphine fragments (Table 4-6). Fragments such as AgL_n where n = 1, 2, 3 (L = PPh_3) were identified in high abundance and (AgL_3-1) was observed as a low abundance cluster at m/z 892 in all cases. Examples of (Ag_2L_n-1) (n = 1, 2) were observed in all spectra except **(18)** and $AgOL_n$ (n = 1, 2) fragments were readily identified in all cases.

Low abundance β-diketonate containing fragments were identified in all compounds except **(18)**, for example [Ag(β-diketonate)L_2-1] in **(19)**, Ag_2(β-diketonate)L in **(17)** and Ag_2(β-diketonate)L_2 in **(17)**, **(19)**, **(20)** and **(21)**. The dinuclear fragments are not necessarily indicative of dimeric species in the solid state as **(21)** has been crystallographically determined as monomeric despite showing dinuclear fragments in the vapour state.

Table 4-6 Selected mass spectrometric data for Ag(β-diketonate)L_n adducts. [a]

	(17) [b]		(18) [c]		(19) [d]		(20) [e]		(21) [f]	
Fragment ions	**m/z**	**%**	**m/z**	**%**	**m/z**	**%**	**m/z**	**%**	**m/z**	**%**
PPh_2	183	**17**	183	21	183	24	183	73	183	99
PPh_3	262	15	262	24	262	10	262	42	262	48
Ag	---	---	---	---	107	5	---	---	---	---
AgL	369	100	369	73	369	100	369	100	369	100
AgOL	385	3.3	385	3.0	385	3	385	5.5	385	41
AgL_2	631	65	631	100	631	84	631	13	631	13
$AgOL_2$	647	2.5	647	5	647	4.2	647	1.3	---	---
(AgL_3-1) [g]	892	5	893	0.4	892	1.1	894	0.6	892	0.5
[Ag(β-diketonate)L_2-1]	---	---	---	---	925	0.2	---	---	---	---

Table 4-6 Continued

(Ag_2L-1)	475	1.3	---	---	---	---	475	1.5	475	0.7
(Ag_2OL-1)	491	1.3	---	---	---	---	---	---	---	---
Ag_2(β-diketonate)L	575	1.0	---	---	---	---	---	---	---	---
(Ag_2L_2-1)	737	0.6	---	---	737	0.2	---	---	737	0.3
Ag_2(β-diketonate)L_2	837	0.2	---	---	1033	1.1	891	0.4	945	0.2
Other fragments	661 [i]	0.5	---	---	687 [h]	0.4	---	---	---	---
	773 [i]	<0.1	773 [i]	5	773 [i]	1.3	773 [i]	0.5	---	---
	753 [k]	0.5	---	---	755 [k]	1.1	---	---	---	---

[a] based on ^{107}Ag, L = PPh_3 [b] β-diketonate = acac, n = 1 [c] β-diketonate = dpm, n = 1 [d] β-diketonate = fod, n = 1.66 [e] β-diketonate = tfac, n = 1 [f] β-diketonate = hfac, n = 1 [g] peak was observed as a cluster, m/z is given as the major central signal of the cluster [h] recognised by isotopic pattern as containing a single silver atom [i] recognised by isotopic pattern as containing two silver atoms [k] recognised by isotopic pattern as containing three silver atoms

Table 4-7 Selected mass spectrometric data for $Ag(hfac)PPh_3$ **(21)** and derived β-ketoiminate adducts **(22)**, **(23)**. [a]

	(21) [b]		(22) [c]		(23) [d]	
Fragment ions	**m/z**	**%**	**m/z**	**%**	**m/z**	**%**
PPh_2	183	99	183	37	183	43
PPh_3	262	48	262	20	262	23
AgL	369	100	369	100	369	100
AgOL	385	41	385	3	385	3
$AgL(H_2NR)$			470	10	468	12
AgL_2	631	13	631	36	631	56
$AgOL_2$			647	2	647	3
$(AgL_3\text{-}1)$ [e]	892	0.5				
$(Ag_2L\text{-}1)$	475	0.7				
$(Ag_2L_2\text{-}1)$	737	0.3				
$Ag_2(\beta\text{-diketonate})L_2$	945	0.2				

[a] based on ^{107}Ag, L = PPh_3 [b] compound **(21)** $Ag(hfac)PPh_3$ [c] compound **(22)** Ag(hfacNhex)PPh_3 [d] compound **(23)** Ag(hfacNchex)PPh_3 [e] peak was observed as a cluster, m/z is given as the major central peak of the cluster

The dominance of AgL fragments over Ag(β-diketonate)L fragments in these spectra is in agreement with mass spectrometric results for $Ag(hfac)PMe_3$ and $Ag(hfac)PEt_3$ reported previously. [98, 99] The relatively high abundance of AgL fragments over β-diketonate containing fragments is indicative that the Ag-P bonds may be significantly more stable. Fragmentation of the Ag(β-diketonate) to yield [Ag(β-diketonate)-R] is not observed in these spectra, unlike mass spectra reported for other similar β-diketonate adducts such as $Ag(fod)PMe_3$, [98,99] $Ag(fod)PEt_3$, [98,99] Ag(hfac)CNMe [101] and $Cu(hfac)PPh_3$. [223]

Mass spectra of silver β-ketoiminates were also dominated by mono-nuclear silver-phosphine fragments, to the extent that no β-diketonate or β-ketoiminate containing fragments were observed. In both **(22)** and **(23)** $AgL(H_2NR)$ fragments confirmed the presence of free amine coordinating to silver. As the FAB/LSIMS mass spectrometry technique used is solution based (Appendix 2), this provides further evidence for reversion of β-ketoiminates to free amine and β-diketonate in solution. Selected mass spectrometry data for compounds **(21)-(23)** are collected in Table 4-7.

4.2.6 Thermal Analysis Studies

Compounds **(17)** to **(23)** were investigated using thermogravimetric analysis under air-purged or helium-purged conditions. As expected, an increase in fluorine content of the β-diketonate had a beneficial effect on the thermal stability. Thermal degradation of the β-diketonate adducts proceeded in a single step in all cases except **(17)**, starting between 140-250°C and being complete by 320-350°C. Maximum rates of decomposition were in the region 269-315°C. Decomposition of **(17)**, $Ag(acac)PPh_3$, was observed to occur in several stages with maximum rates of decomposition occurring at 191 and 287°C. Differential scanning calorimetry work carried out with **(19)** revealed

Table 4-8 Thermal analysis data for silver(I) β-diketonate and β-ketoiminate adducts. [a]

Compound		Decomposition temperature (°C)			Residue remaining (%)	
		start [b]	maxima [c]	end [d]	calc % Ag [e]	found
$Ag(acac)PPh_3$	**(17)**	150	191, 287	330	23.0	24.1
$Ag(dpm)PPh_3$	**(18)**	140	297	320	19.5	18.4
$[Ag(fod)]_3(PPh_3)_5$	**(19)**	220	310	320	12.8	11.0
$Ag(tfac)PPh_3$	**(20)**	200	269	330	20.6	20.9
$Ag(hfac)PPh_3$	**(21)**	250	315	350	18.7	17.7
$Ag(hfacNhex)PPh_3$	**(22)**	100	198, 314	340	15.9	17.4
$Ag(hfacNchex)PPh_3$	**(23)**	115	206, 304	320	16.0	15.8

[a] TGA experiments were run under an air purged atmosphere except for **(23)** which was carried out under a He purge [b] temperature corresponding to the onset of decomposition [c] temperature(s) at which the rate of weight loss is at a maximum [d] temperature at which decomposition is complete [e] calculated % mass of silver in undecomposed compounds

a sharp melt-like endotherm at 101°C followed by further endotherm at 142°C, both taking place before initial weight loss.

Thermal degradations of silver β-ketoiminate adducts **(22)** and **(23)** were observed to proceed in two steps, these not being completely distinct from each other. The first step commenced at 100-115°C, rising to a maximum at 198-206°C. After this temperature the rate of weight loss declined with increasing temperatures to about 250°C. This first stage of decomposition in both cases resulted in a weight loss of about 25%, somewhat larger than can be accounted for by H_2NR alone (about 15% in both cases). At about 250°C the second stage of decomposition rapidly completes the degradation, which is over by 320-340°C. It should be noted that TGA experiments for **(22)** and **(23)** were carried out under air and helium respectively and this appears to have not drastically altered their decomposition profiles. Differential scanning calorimetry work undertaken on **(23)** has shown two sharp melt-like endotherms at 84 and 100°C occurring prior to initial weight loss.

4.3 SINGLE CRYSTAL X-RAY STRUCTURE DETERMINATION OF Ag(hfac)PPh_3 (21)

X-ray diffraction quality crystals of Ag(hfac)PPh_3 were obtained at room temperature in air by slow evaporation of a saturated solution of **(21)** in acetone. The crystals were found to be very stable to light, heat and moisture.

The results have revealed that the solid state structure of **(21)** consists of independent monomeric molecules, the silver centre bound by chelating (*O,O'*-hexafluoroacetylacetonato) and

triphenylphosphine in a distorted trigonal arrangement (Figure 4-10). The β-diketonate ligand is somewhat unsymmetrically bound resulting in the structure tending towards a linear P-Ag-O1 configuration (∠P-Ag-O1: 158.7°, ∠P-Ag-O2: 119.2°) with significantly different Ag-O bond lengths (2.218, 2.341 Å).

This distortion is similar to that found in other monomeric silver β-diketonate adducts, although in this case the difference in P-Ag-O angles is exaggerated; **(21)** (39.5°), Ag(hfac)PMe_3 (3.1, 8.2, 16.2°), [99] Ag(hfac)CNMe (24°). [101] Perturbations from the expected trigonal geometry in the literature examples have been attributed to packing effects and possible intermolecular H-F interactions (2.235Å) respectively. In the case of **(21)**, the nearest H-F interactions of 2.561 Å (intramolecular) and 2.485 Å (intermolecular) and nearest H-O interactions of 2.463 Å (intermolecular) suggest that weak hydrogen bonds are unlikely to cause such distortions in this case. O-Ag-O 'bite' angles are very similar in these three structures (80.0-81.8°).

Mean Ag-O bond lengths for **(21)** (2.28 Å) are comparable with those found in monomeric Ag(hfac)PMe_3 (2.29 Å) [99] and Ag(hfac)CNMe (2.28 Å) [101] and significantly shorter than Ag-O in silver β-diketonates where Ag is greater than three-coordinate (typically 2.35-2.64). [97, 202, 204, 222] Average C-O bond lengths of 1.247 Å in **(21)** are comparable to those in similar Ag(hfac)L_n complexes (1.213-1.255Å). [97, 99, 101, 202, 204, 222] The Ag-P distance (2.346 Å) is slightly longer than that found for the trimethylphosphine adduct Ag(hfac)PMe_3, (2.32 Å). [99]

Relevant bond angles and distances are summarised in Table 4-9 while further data including atomic coordinates are listed in Appendix A4.3.

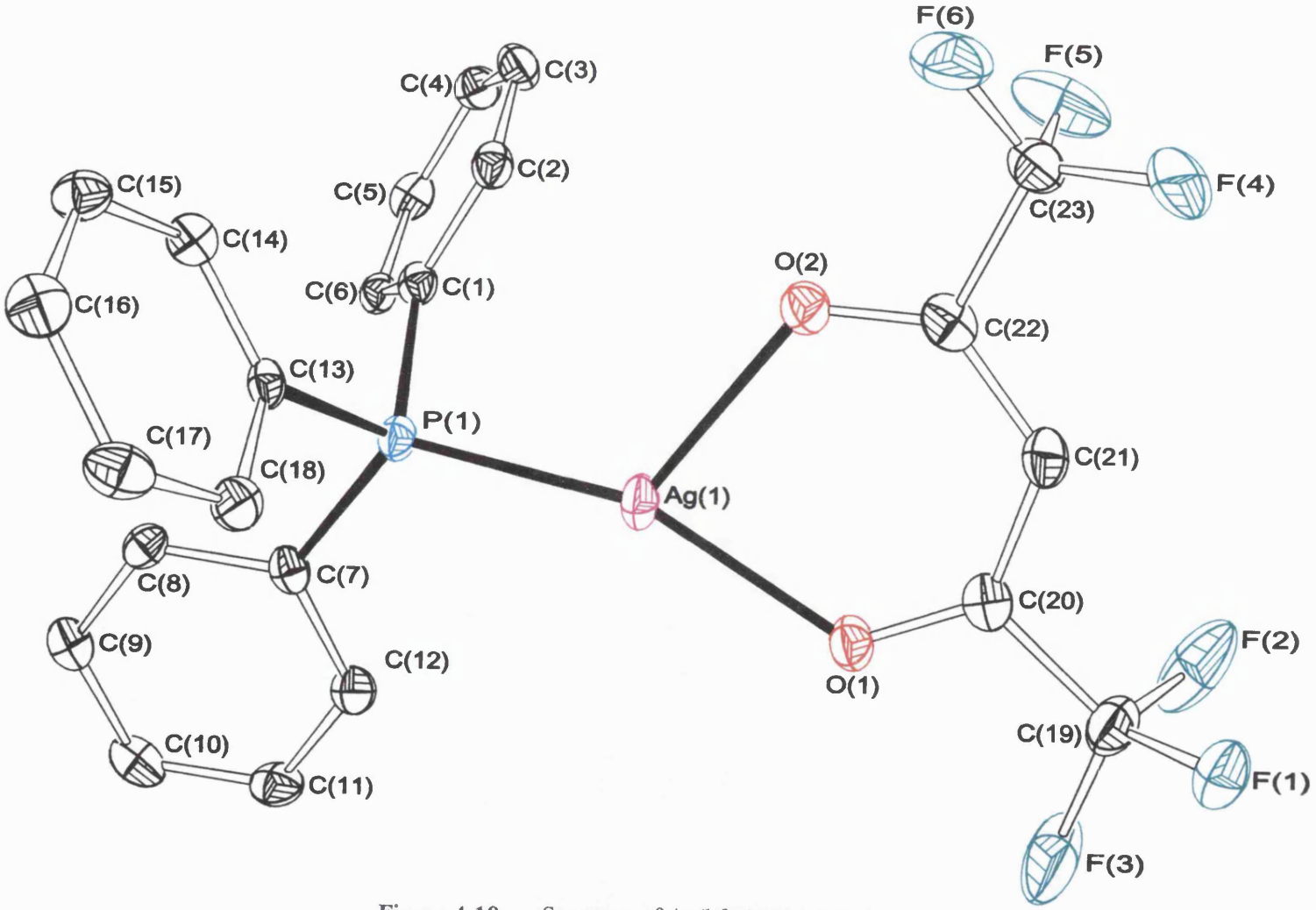

Figure 4-10 Structure of $Ag(hfac)PPh_3$ **(21)**.

Table 4-9 Selected bond lengths (Å) and angles (°) for **(21)**.

Ag(1)-P(1)	2.346(3)	P(1)-Ag(1)-O(1)	158.7(1)
Ag(1)-O(1)	2.218(5)	P(1)-Ag(1)-O(2)	119.2(2)
Ag(1)-O(2)	2.341(5)	O(1)-Ag(1)-O(2)	81.8(2)
O(1)-C(20)	1.253(6)	Ag(1)-O(1)-C(20)	128.9(4)
O(2)-C(22)	1.240(7)	Ag(1)-O(2)-C(22)	125.8(4)

4.4 FILM GROWTH RESULTS

Compounds **(17)**-**(23)** were screened as potential precursors for silver CVD. The results are collected in Table 4-10, Table 4-11 and 4-12.

The films were grown under fixed conditions of 310°C and 1 bar pressure in a nitrogen atmosphere. Precursors were dissolved in THF, the solution nebulised and swept into the reactor deposition chamber using a nitrogen carrier gas. Films were grown on glass substrates. Coating growth times were largely dependent on the volume of solvent used and carrier gas flow rates, in all cases they were of the order of 15-30 minutes. Typically 0.5-0.8 g of precursor was dissolved in 40 cm^3 of THF, nebuliser flow rates were of the order of 0.8 $Lmin^{-1}$. The films were observed to be soft and although adhered well to the substrate, they could be damaged by scratching or wiping very easily. Films were examined by visual inspection and scanning electron microscopy. Film thickness was estimated using quantitative electron probe microanalysis (EDXS) and contaminants were also identified using this technique, additionally coatings grown from **(20)** and **(22)** were further characterised by Auger techniques and High Resolution Scanning Electron Microscopy (HRSEM). All films were characterised with respect to reflectivity and conductivity.

Compounds **(17)** and **(18)** (non-fluorinated silver β-diketonate adducts) were very ineffective at silver film growth under these conditions. Despite a number of attempts, only faint transparent films could be visually identified and these were of insufficient quality to characterise fully. The remainder of compounds tested **(19)**-**(23)** (fluorinated silver β-diketonate and silver β-ketoiminate adducts) were all capable of growing silver-containing films. In terms of growth rates, compound **(19)** was the least effective of the fluorinated precursors (7.6 $Åmin^{-1}$) although it was still possible to grow a reflective silver film with this compound. In contrast, of the silver β-diketonates, **(20)**

grew at the fastest rate (16+ Åmin^{-1}). Growth rates of silver β-ketoiminate adducts **(22)** and **(23)** exceeded those measured for their parent silver β-diketonate adduct **(21)** and the coatings appeared more reflective. Growth rates of compound **(23)** were estimated to exceed 19 Åmin^{-1}, the highest observed during this study.

Deposition rates appear to have no obvious relationship with decomposition points, and all of these precursors should have high rates of decomposition at the substrate temperature used (310°C). β-Ketoiminates were observed to display decomposition at much lower temperatures than fluorinated β-diketonates in TGA experiments and yet displayed film growth rates of the same order of magnitude.

Films grown from compounds **(19)** to **(23)** were conducting enough to allow inspection by SEM (up to 10,000x). The surface of **(19)** were found to be uneven with a high concentration of protrusions from the bulk surface (Plates 4-1, 4-2). The surface of **(21)** was observed to resemble a thick mat of long, thin crystals (Plates 4-5, 4-6), very similar to that observed for $AgO_2CR(PMe_3)_2$ (Chapter 2, Plates 2-1 to 2-4). Films grown from **(20)**, **(22)** and **(23)** appeared as fairly uniform, smooth films at this magnification (Plates 4-3, 4-4 and 4-7 to 4-10). High Resolution SEM work, at higher magnification (50,000x), on coatings grown from **(20)** and **(22)** has revealed that these two films are in fact made up from several layers of loosely packed spheres of silver (Plates 4-11 to 4-18), the size of the spheres being approximately 500-1000Å. These HRSEM results also suggest that the quoted thickness estimates may have been underestimated although more investigation is required to confirm this.

Carbon was the only consistent contaminant in all the films, as detected by EDXS. This impurity appears independent of the precursor utilised and of the film thickness. The heights of carbon and

Table 4-10 Appearance of silver films grown from silver β-diketonate and silver β-ketoiminate adducts.

Compound		visual appearance	SEM appearance	Detected impurities [a, b] (EDXS)	Plates
$Ag(acac)PPh_3$	**(17)**	very faint yellow transparent marks	thin, discontinuous or non conducting film	---	---
$Ag(dpm)PPh_3$	**(18)**	faint transparent yellow film	thin, discontinuous or non conducting film	C	---
$[Ag(fod)]_3(PPh_3)_5$	**(19)**	silver reflective film	uneven film with high concentration of surface protrusions	C	4-1, 4-2
$Ag(tfac)PPh_3$	**(20)**	heavy deposition, highly reflective in places, dark grey matt area at downstream side	fairly smooth, regular surface	C	4-3, 4-4
$Ag(hfac)PPh_3$	**(21)**	thick grey matt film, not particularly reflective	even surface comprised of a thick mat of long, thin crystals	C, P(trace)	4-5, 4-6
$Ag(hfacNhex)PPh_3$	**(22)**	silver reflective film, slightly matt white in areas of heaviest deposition	fairly smooth, even surface	C	4-7, 4-8
$Ag(hfacNchex)PPh_3$	**(23)**	silver reflective film on entire substrate, whitish matt in areas of heaviest deposition	fairly smooth although undulating	C	4-9, 4-10

[a] the presence of oxygen in the films was masked by oxygen detected in the glass [b] trace quantities were at the limits of detection of this instrumentation

silver peaks in the EDXS spectrum were observed to be very approximately in a similar ratio in all the spectra. Levels of carbon are certainly in excess of trace amounts, probably in the region of 5-10%+. Accurate results for %C cannot be obtained using this experimental procedure without modification. The presence of oxygen contaminants in the film was neither proved or disproved by EDXS due to the masking effect of the glass substrate (largely SiO_2), however in the case of very thick films, the x-rays characteristic of oxygen were considerably reduced and the intensity ratio of silicon to oxygen peaks appears fairly constant. This may indicate that generally oxygen contamination is at least smaller than carbon contamination. Trace phosphorus contamination was detected only in the film grown from **(21)**, no fluorine was detected in any of the films.

Subsequent Auger depth profiling analysis of the films grown from **(20)** and **(22)** has confirmed that these films are predominantly silver (91.3-91.5 atom%) with carbon (6.4-7.5 atom%) and trace oxygen (1.2-2.0 atom%). Fluorine and phosphorus contaminants were not detected and this concurs with the EDXS studies. Such film analysis results compare favourably with reports of thermal CVD of Ag(β-diketonate)L (β-diketonate = hfac, fod, L = PMe_3, PEt_3) in the literature where, in the absence of hydrogen, contamination was of the order of 5-35% carbon, 5% oxygen with trace fluorine and phosphorus. [99] Auger electron surface analysis spectra for **(20)** and **(22)** are presented in Figures 4-11 and 4-12 respectively, elemental concentrations are listed in Table 4-11.

Reflectance measurements on films grown from precursors **(17)-(23)** included measurements from both the coated surface and from the film-glass interface (i.e. through the glass). Metallic films on glass generally exhibit lower reflectance from the coating surface as compared to the

Table 4-11 Elemental concentrations of films grown from **(20)** and **(22)** as determined by Auger depth profiling analysis.

		Atom	Concentration (Atom%)
$Ag(tfac)PPh_3$	**(20)**	Ag	91.3
		C	7.5
		O	1.2
$Ag(hfacNhex)PPh_3$	**(22)**	Ag	91.5
		C	6.4
		O	2.0

Table 4-12 Properties of silver films grown from silver β-diketonate and silver β-ketoiminate adducts.

Compound		Estimated film thickness (Å)	Deposition time (minutes)	Estimated deposition rate ($Åmin^{-1}$)	% Reflectance [b] coating	% Reflectance [b] glass	Sheet Resistance ($\Omega/\square$) [c]
$Ag(acac)PPh_3$	**(17)**	---	19	---	12.9	10.9	∞
$Ag(dpm)PPh_3$	**(18)**	---	20	---	12.2	10.5	∞
$[Ag(fod)]_3(PPh_3)_5$	**(19)**	167	22	7.6	19.4	19.8	∞
$Ag(tfac)PPh_3$	**(20)**	320 [a]	20	16 +	62.5	70.3	2.2
$Ag(hfac)PPh_3$	**(21)**	306	29	10.6	0.3	18.0	186
$Ag(hfacNhex)PPh_3$	**(22)**	295	18	16.4	64.7	85.3	1.1
$Ag(hfacNchex)PPh_3$	**(23)**	248	13	19.1	51.4	30.0	167

[a] due to the thickness of this film, counts of X-rays from the film were approximately equal to those obtained from the pure Ag bulk sample, the film thickness for this sample may be in excess of this estimate [b] $\lambda = 550$ nm corresponding to the peak in the eye response curve [c] sheet resistance was measured over a 25 mm square

coating-glass interface, this being primarily a function of surface roughness and its ability to scatter light.

Films grown from precursors **(17)** - **(18)** gave poor reflectance results. Films deposited from **(19)** appeared considerably more reflective by visual inspection although reflectivity at 550 nm was less than 20%. The sheet resistance of films grown from **(17)** - **(19)** was not quantifiable.

Films deposited with precursors **(20)**, **(22)** and **(23)** gave highly reflective films with reflectance from the coating surface of 50-65% and reflectivity from the glass-coating interface of up to 85%. Surprisingly, coatings grown using **(21)** as the precursor gave thick matt films which had poor reflectivity from both surfaces. Precursors similar to **(21)** have been widely studied in the literature. All films grown from **(20)**-**(23)** (estimated thickness 250-320Å) had a measurable sheet resistance, sheet resistances of 1.1 Ω/□ **(22)** and 2.2 Ω/□ **(20)** were the lowest observed during the course of these studies. From the data displayed in Table 4-12, there appears to be an approximate correlation between reflectance and sheet resistance and not between reflectance and deposition rate as may have been expected. This may suggest that reflectance is affected largely by impurities in these cases, rather than by surface morphology as influenced by growth rates.

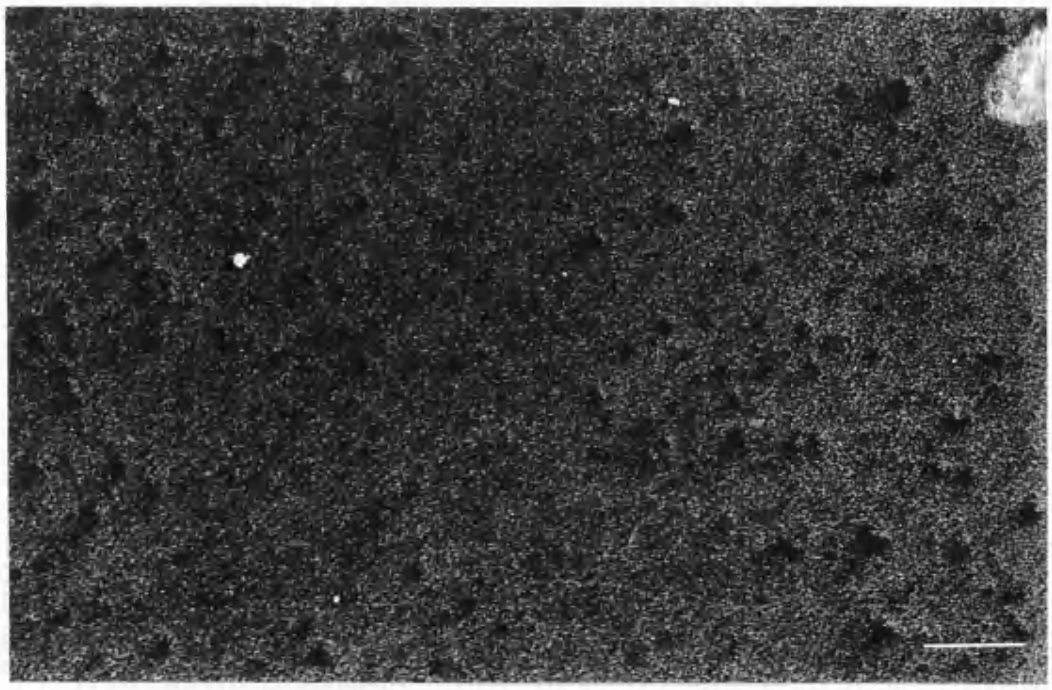

Plate 4-1 Scanning Electron Micrograph at 10 kV of a silver film obtained from the AACVD of $[Ag(fod)]_3(PPh_3)_5$ **(19)**, bar = 10 μm.

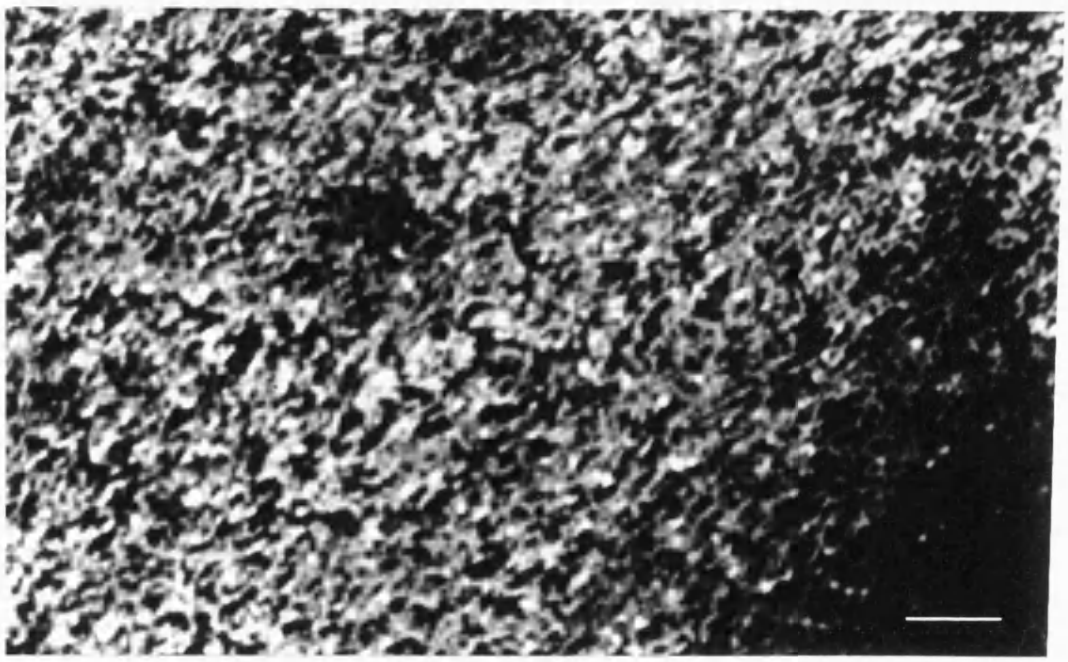

Plate 4-2 Scanning Electron Micrograph at 10 kV of a silver film obtained from the AACVD of $[Ag(fod)]_3(PPh_3)_5$ **(19)**, bar = 1 μm.

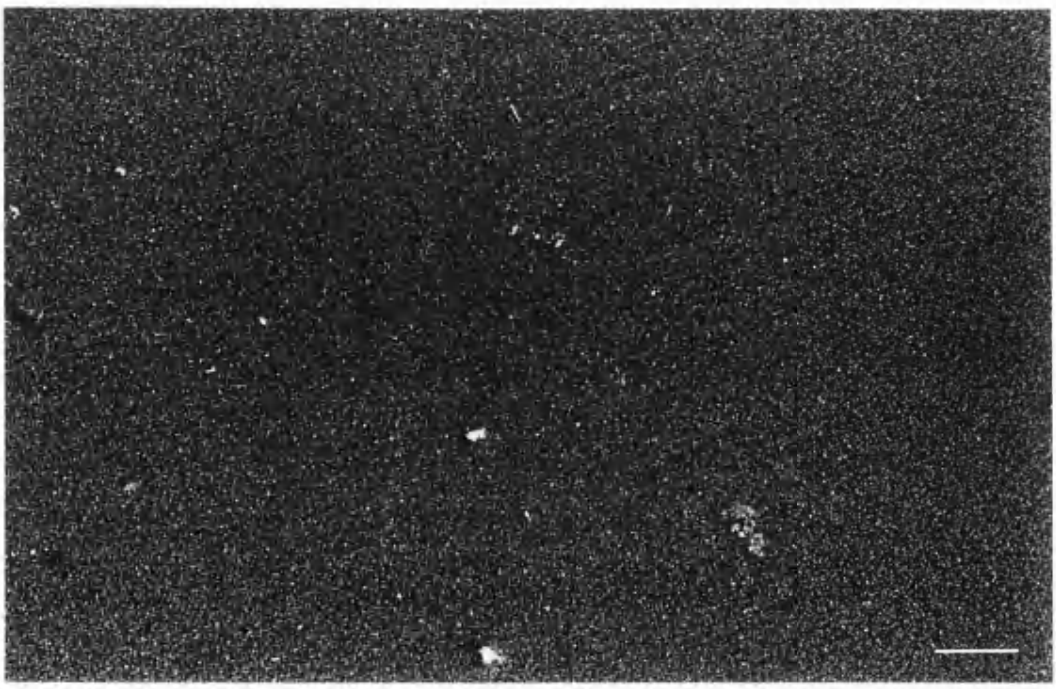

Plate 4-3 Scanning Electron Micrograph at 10 kV of a silver film obtained from the AACVD of Ag(tfac)PPh_3 **(20)**, bar = 10 μm.

Plate 4-4 Scanning Electron Micrograph at 10 kV of a silver film obtained from the AACVD of Ag(tfac)PPh_3 **(20)**, bar = 1 μm.

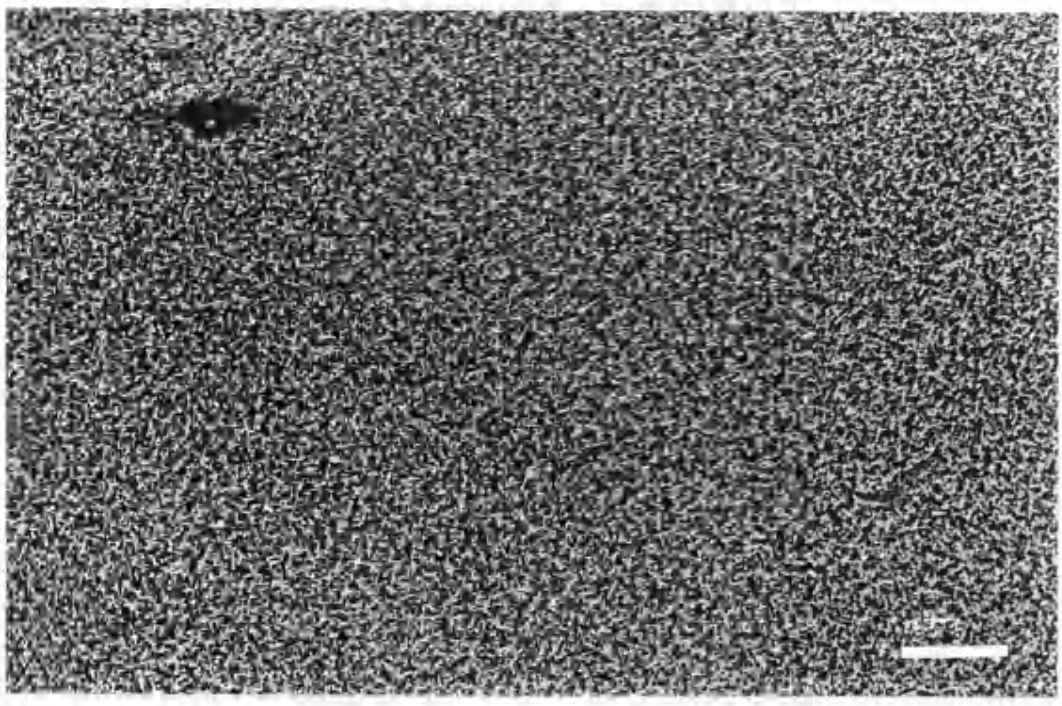

Plate 4-5 Scanning Electron Micrograph at 10 kV of a silver film obtained from the AACVD of $Ag(hfac)PPh_3$ **(21)**, bar = 10 μm.

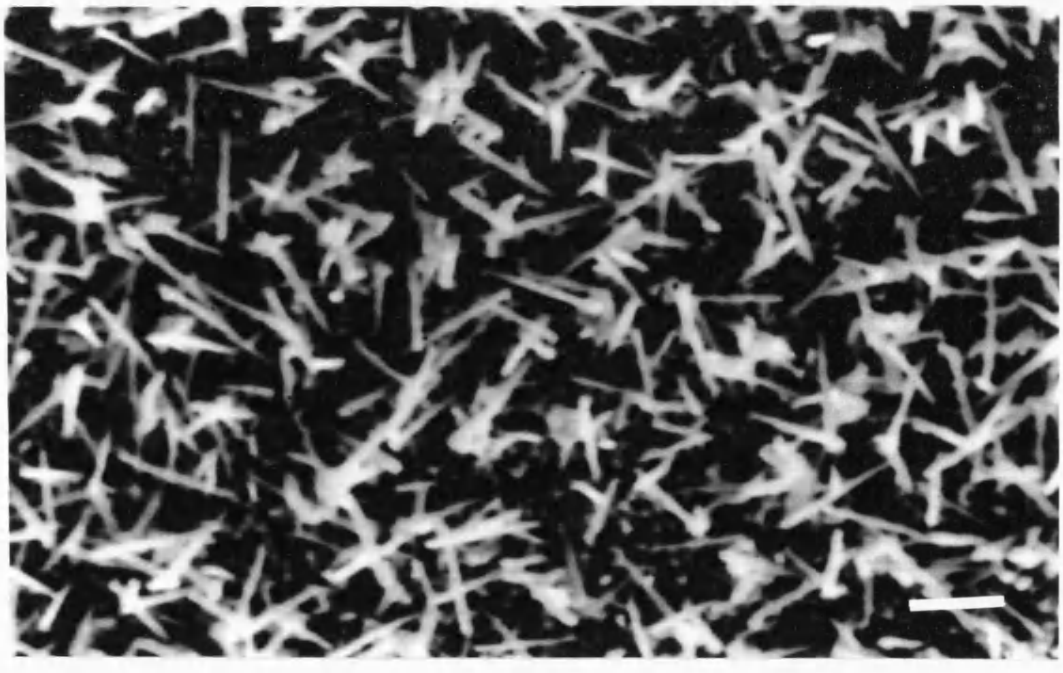

Plate 4-6 Scanning Electron Micrograph at 10 kV of a silver film obtained from the AACVD of $Ag(hfac)PPh_3$ **(21)**, bar = 1 μm.

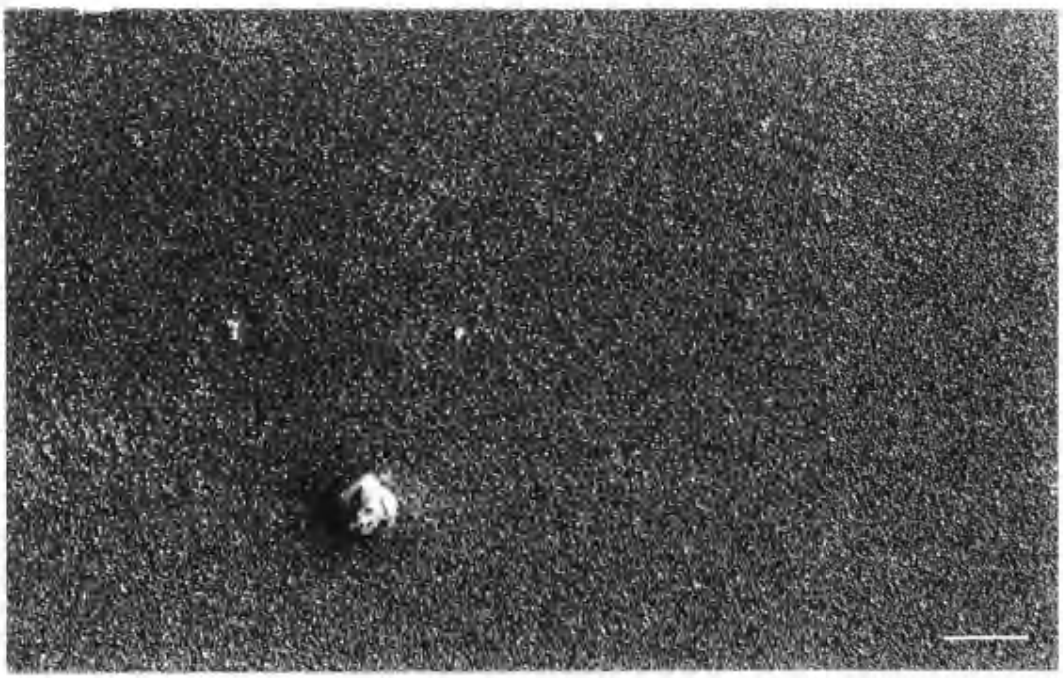

Plate 4-7 Scanning Electron Micrograph at 10 kV of a silver film obtained from the AACVD of Ag(hfacNhex)PPh_3 **(22)**, bar = 10 μm.

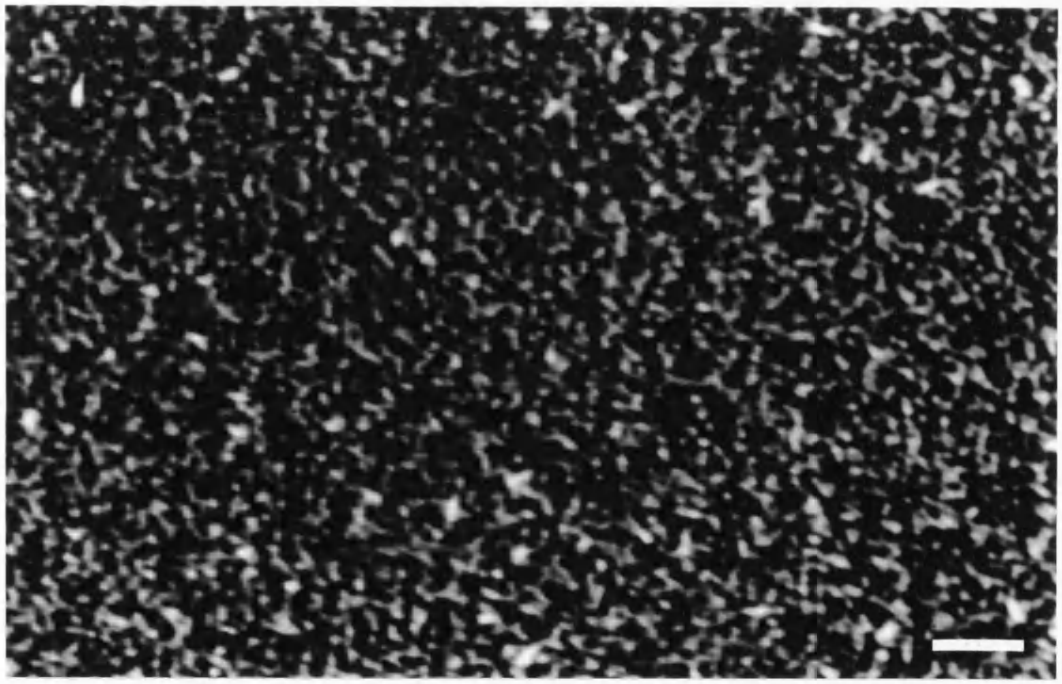

Plate 4-8 Scanning Electron Micrograph at 10 kV of a silver film obtained from the AACVD of Ag(hfacNhex)PPh_3 **(22)**, bar = 1 μm.

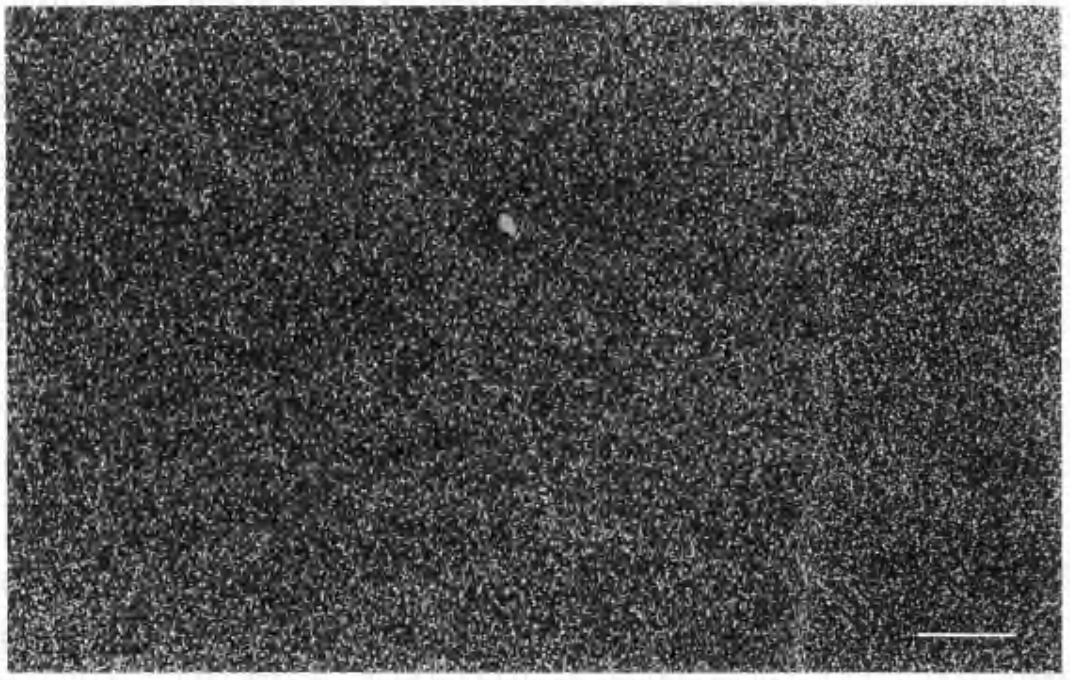

Plate 4-9 Scanning Electron Micrograph at 10 kV of a silver film obtained from the AACVD of Ag(hfacNchex)PPh_3 **(23)**, bar = 10 μm.

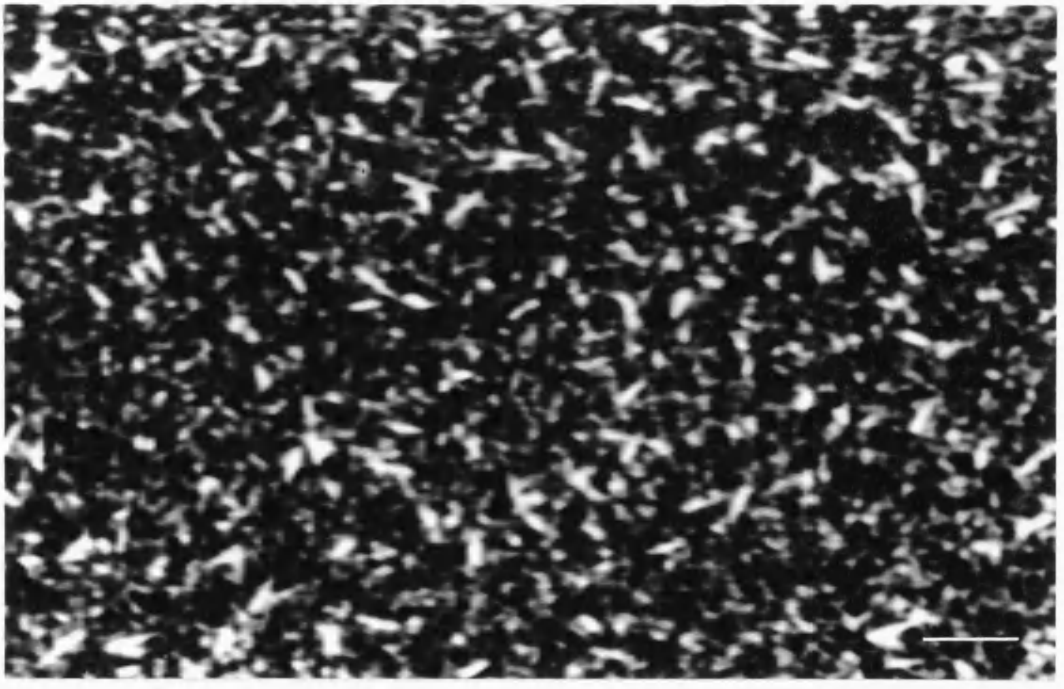

Plate 4-10 Scanning Electron Micrograph at 10 kV of a silver film obtained from the AACVD of Ag(hfacNchex)PPh_3 **(23)**, bar = 1 μm.

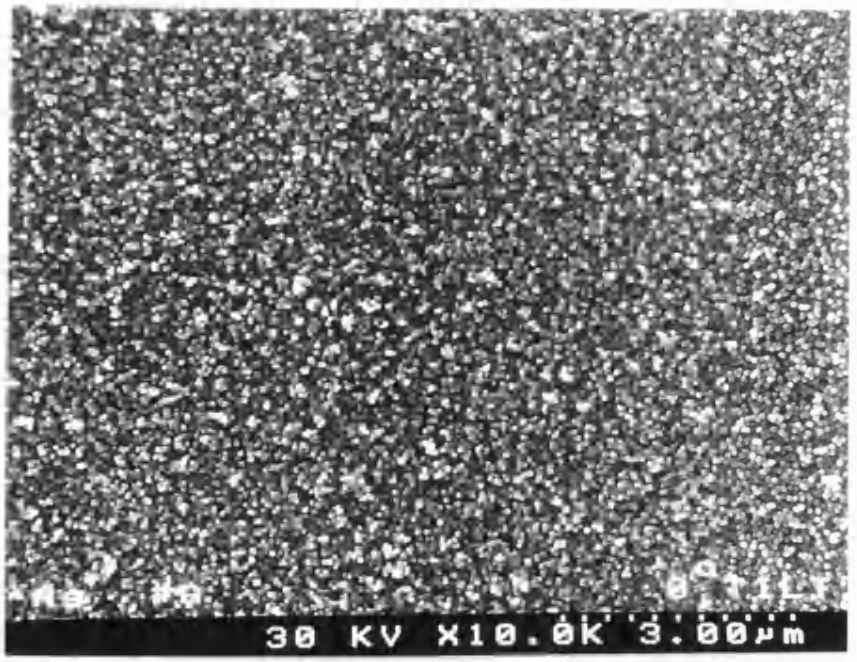

Plate 4-11 High Resolution Scanning Electron Micrograph at 30 kV of a silver film obtained from the AACVD of $Ag(tfac)PPh_3$ **(20)**.

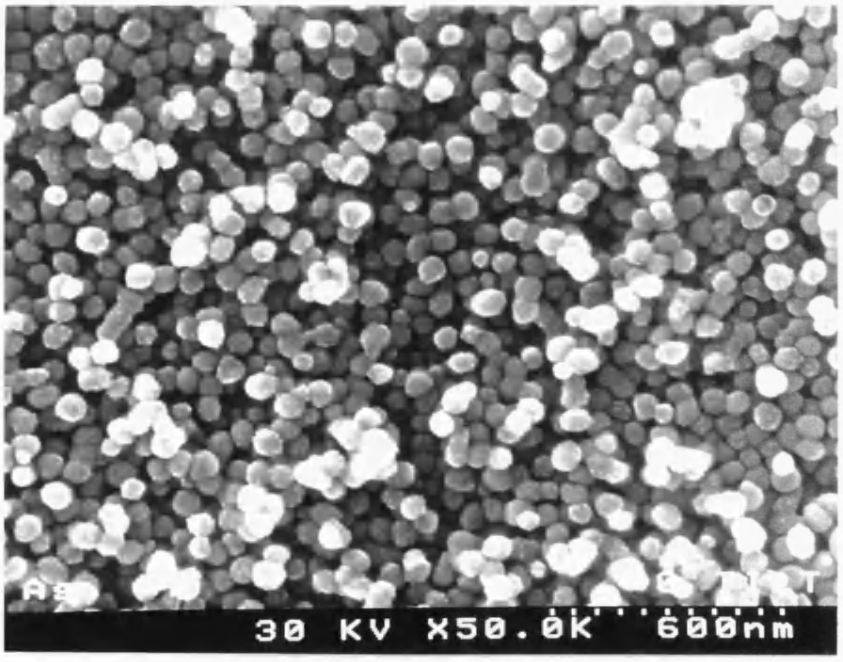

Plate 4-12 High Resolution Scanning Electron Micrograph at 30 kV of a silver film obtained from the AACVD of $Ag(tfac)PPh_3$ **(20)**.

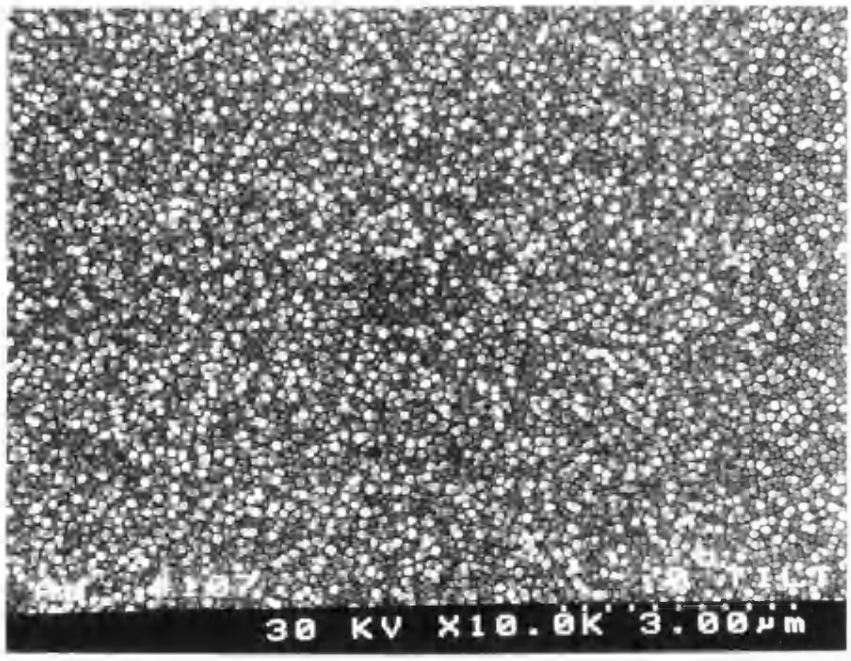

Plate 4-13 High Resolution Scanning Electron Micrograph at 30 kV of a silver film obtained from the AACVD of Ag(hfacNhex)PPh_3 **(22)**.

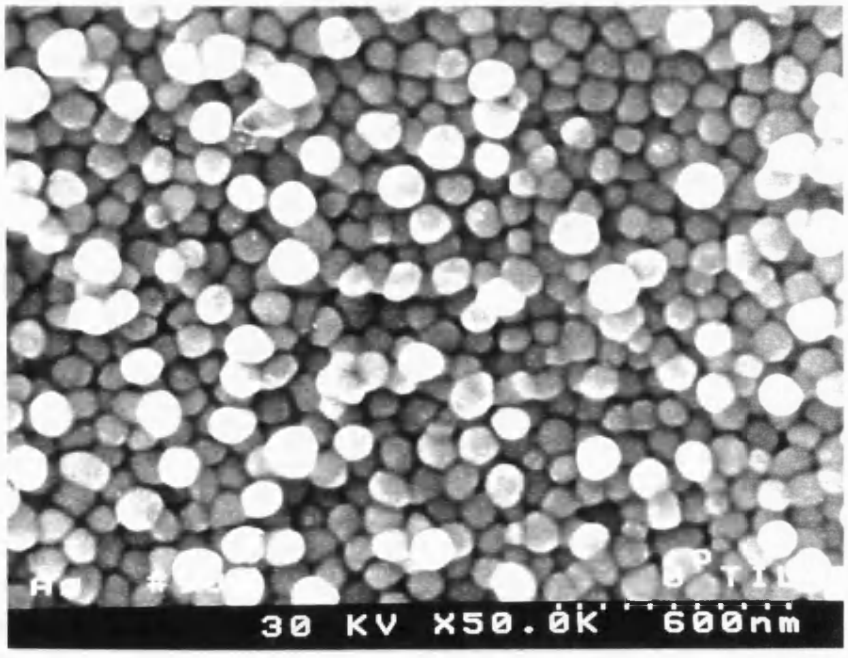

Plate 4-14 High Resolution Scanning Electron Micrograph at 30 kV of a silver film obtained from the AACVD of Ag(hfacNhex)PPh_3 **(22)**.

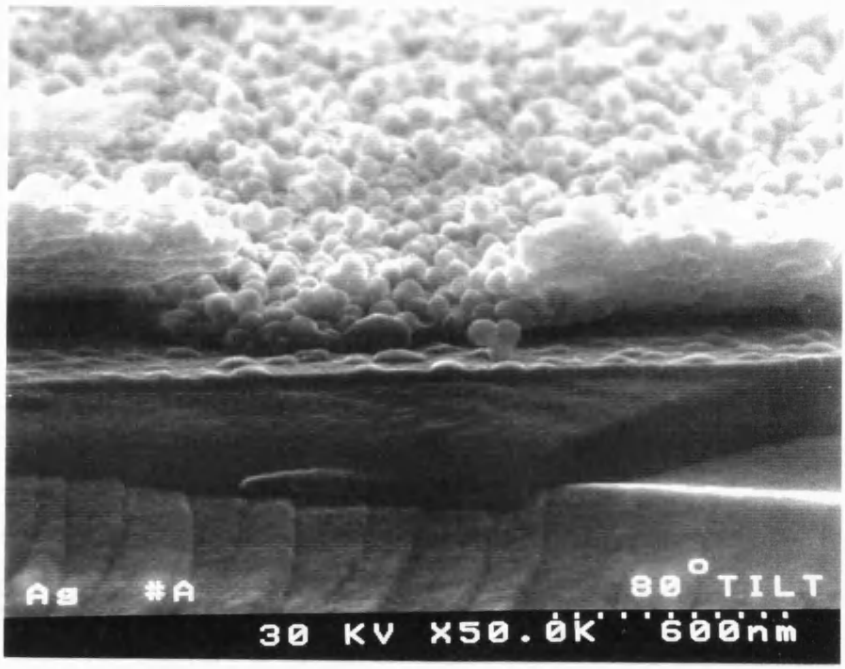

Plate 4-15 High Resolution Scanning Electron Micrograph at 30 kV of a silver film obtained from the AACVD of Ag(tfac)PPh_3 **(20)**, 80° tilt.

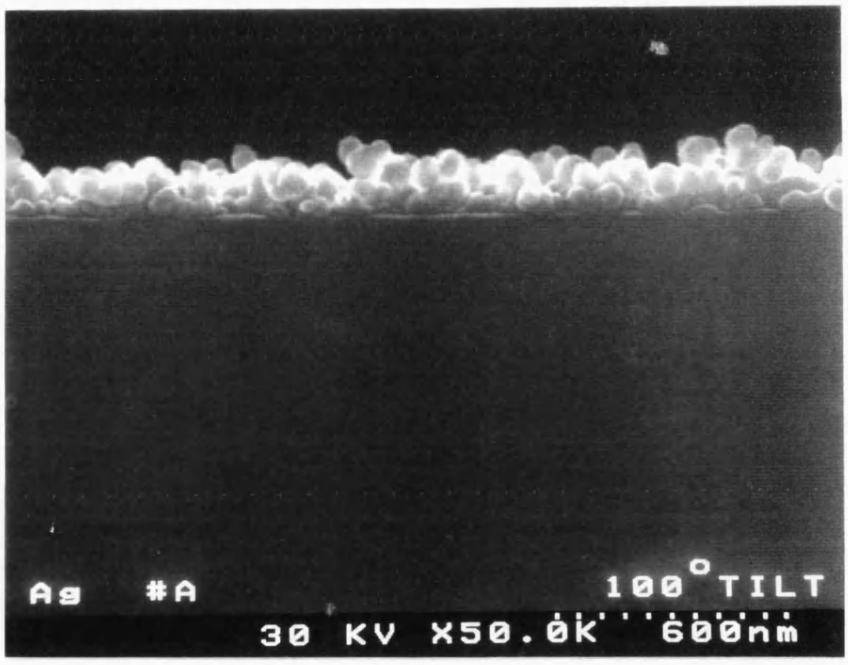

Plate 4-16 High Resolution Scanning Electron Micrograph at 30 kV of a silver film obtained from the AACVD of Ag(tfac)PPh_3 **(20)**, 100° tilt.

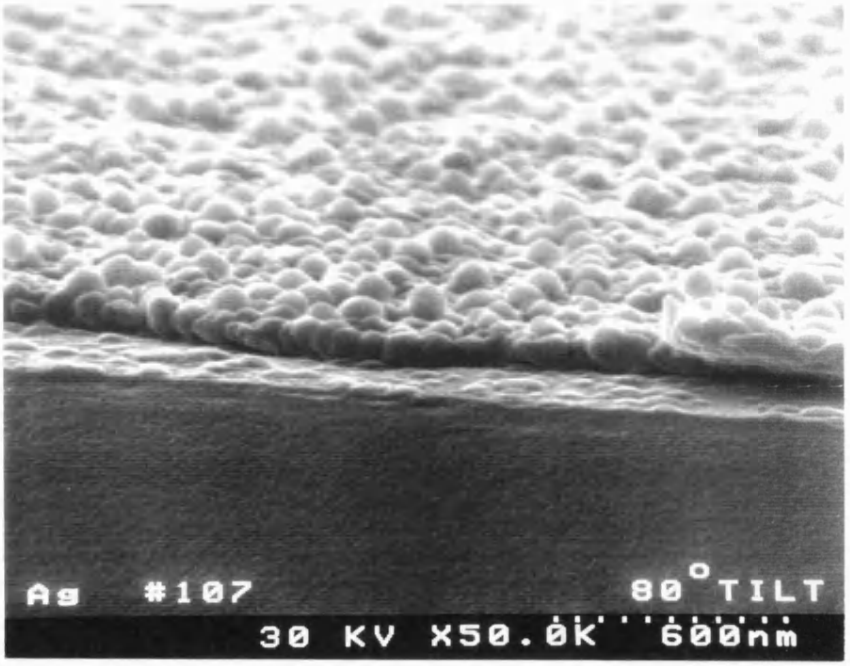

Plate 4-17 High Resolution Scanning Electron Micrograph at 30 kV of a silver film obtained from the AACVD of Ag(hfacNhex)PPh_3 **(22)**, 80° tilt.

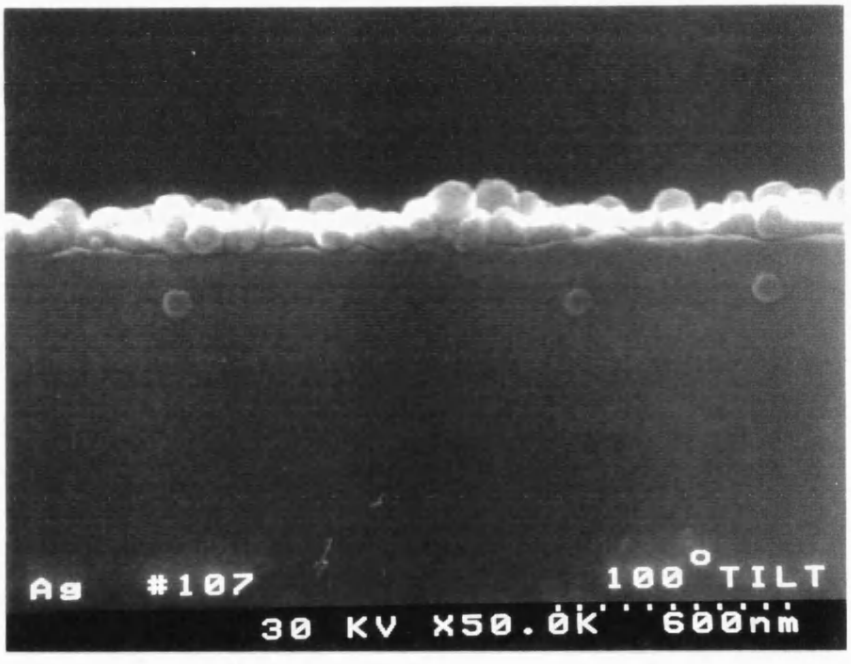

Plate 4-18 High Resolution Scanning Electron Micrograph at 30 kV of a silver film obtained from the AACVD of Ag(hfacNhex)PPh_3 **(22)**, 100° tilt.

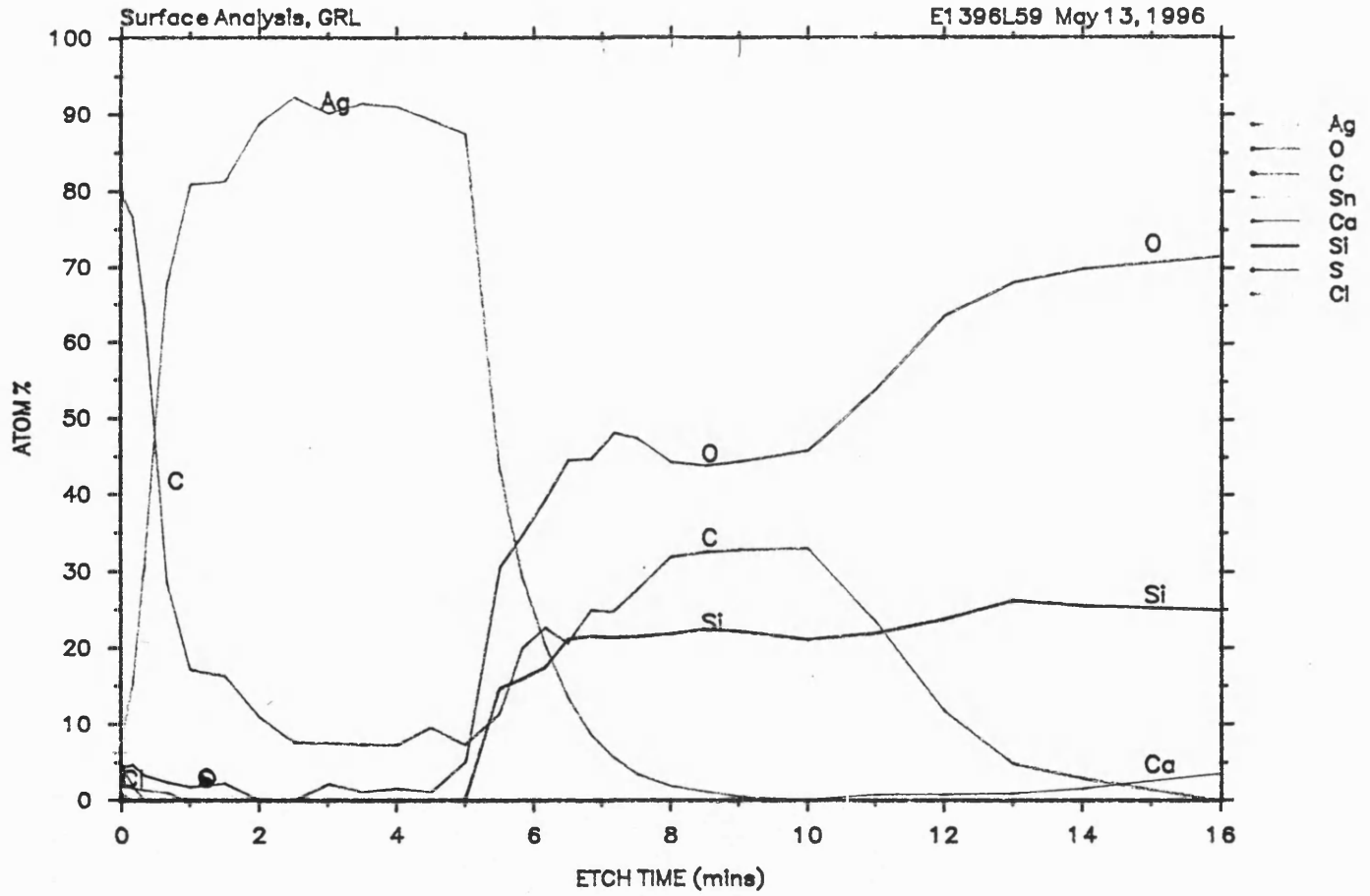

Figure 4-11 Auger depth profile analysis of a silver film obtained from the AACVD of $Ag(tfac)PPh_3$ **(20)**.

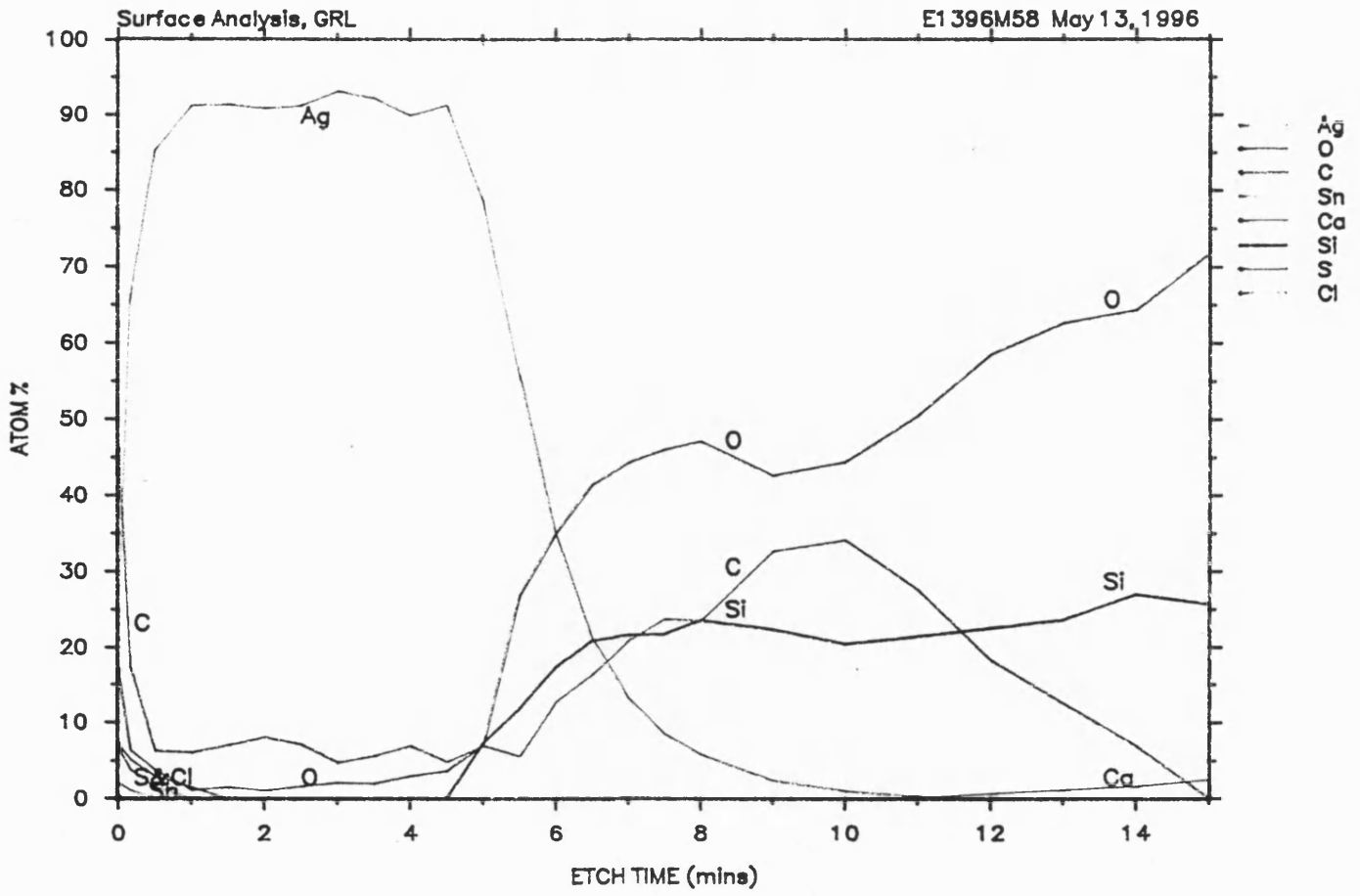

Figure 4-12 Auger depth profile analysis of a silver film obtained from the AACVD of Ag(hfacNhex)PPh_3 **(22)**.

4.5 EXPERIMENTAL

The synthesis of pentane-2,4-dionato(triphenylphosphine)silver(I), [Ag(acac)PPh_3] ***(17)***

Silver oxide (1.50 g, 6.5 mmol) was suspended in diethyl ether (15 cm^3). To this was slowly added pentane-2,4-dione (1.85 ml, 1.9 g, 19 mmol). The mixture was stirred for 5 minutes, resulting in a grey precipitate. To this was added triphenylphosphine (3.39 g, 12.9 mmol), the mixture was stirred for one hour, filtered in air, and pumped dry *in vacuo.* The precipitate could be satisfactorily recrystallised from diethyl ether.

Analysis : found (calculated for $C_{23}H_{22}O_2AgP$) C, 59.0 (58.9); H, 4.71 (4.73) %. Thermal decomposition initiated at 150°C (by TGA/air). IR (Nujol mull) 1200-1800 cm^{-1}: 1225w, 1507w, 1615. IR (hexachlorobutadiene mull) 1200-1800 cm^{-1}: 1225w, 1308w, 1331w, 1347w, 1433b, 1466b, 1508. ^1H NMR ($CDCl_3$) δ; 7.49-7.30 (m, 15H, PPh_3), 5.26 (s, COC<u>H</u>CO), 1.95 (s, CH_3). ^{13}C NMR ($CDCl_3$) δ; 191.0 (CO), 133.8 (d, 16.5 Hz, PPh_3), 131.5 (d, 34.2 Hz, PPh_3), 130.3 (PPh_3), 128.7 (d, 10 Hz, PPh_3), 98.5 (CO<u>C</u>HCO), 28.8 (CH_3). ^{31}P NMR ($CDCl_3$) δ; 15.1.

The synthesis of dipivaloylmethanato(triphenylphosphine)silver(I), [Ag(dpm)PPh_3] ***(18)***

Silver oxide (1.5 g, 6.5 mmol) and 2,2,6,6-tetramethyl-3,5-heptanedione (2.45 g, 13.3 mmol) were suspended in diethyl ether(15 cm^3), and stirred for 5 minutes. This resulted in a cloudy grey precipitate in a black mixture. To this was added triphenylphosphine (3.4 g, 13.0 mmol) in diethyl ether (5 cm^3). The mixture was stirred for 18 hours in a closed flask in the absence of light to give

a light grey precipitate. This was filtered in air, washed with diethyl ether, and dried *in vacuo*. Yield 6.1g, 85 %.

Analysis : found (calculated for $C_{29}H_{34}O_2AgP$) C, 62.6 (62.9); H, 5.90 (6.19) %. Thermal decomposition initiated at 140°C (by TGA/air). IR (Nujol mull) 1200-1800 cm^{-1}: 1229, 1321w, 1354sh, 1381, 1406, 1435, 1501, 1530, 1564, 1582. IR (hexachlorobutadiene mull) 1200-1800 cm^{-1}: 1229, 1354, 1385, 1406, 1435, 1449, 1480, 1501, 1530. ^1H NMR ($CDCl_3$) δ; 7.40-7.33 (m, 9H, PPh_3), 7.33-7.24 (m, 6H, PPh_3), 5.73 (s, CO<u>CH</u>CO), 1.18 (s, -C<u>Me</u>$_3$). ^{13}C NMR ($CDCl_3$) δ; 201.5 (CO), 134.0 (d, 16.5 Hz, PPh_3), 132.1 (d, 11.1 Hz, PPh_3), 130.2 (PPh_3), 128.8 (d, 11Hz, PPh_3), 90.7 (CH), 39.4 (-<u>C</u>Me$_3$), 27.4 (-C<u>Me</u>$_3$).

The synthesis of tris(2,2-dimethyl-6,6,7,7,8,8,8-heptafluoro-3,5-octadionato)tetrakis (triphenylphosphine)trisilver(I), $[Ag(fod)]_3(PPh_3)_5$ ***(19)***

Silver oxide (1.04 g, 4.5 mmol) was suspended in diethyl ether (40 cm^3) and stirred. To this was added 2,2-dimethyl-6,6,7,7,8,8,8-heptafluoro-3,5-octadione (2.50 g, 8.5 mmol) and a further 10 cm^3 of diethyl ether, with no immediate result. The whole mixture was stirred for one hour to give a dark brown, hazy solution, which was then filtered into a Schlenk tube containing triphenylphosphine (2.21 g, 8.4 mmol). After stirring for a further 10 minutes, the solution gradually cleared and was filtered using fine filter paper. The solvent was removed and the resulting solid dried *in vacuo*. Recrystallisation was satisfactorily accomplished by allowing a hexane-acetone solvent mixture to evaporate at room temperature. Yield 1.4 g, 28 %.

Analysis : found (calculated for $C_{120}H_{105}O_6Ag_3P_5F_{21}$) C, 57.0 (57.2); H, 3.62 (4.20) %. Mp 101°C (by DSC/He). Thermal decomposition initiated at 220°C (by TGA/He). IR (Nujol mull) 1200-1800 cm^{-1}: 1202s, 1225s, 1273, 1312w, 1345sh, 1366, 1435sh, 1468bs, 1505sh, 1528w, 1570w, 1586w, 1628ssh. IR (hexachlorobutadiene mull) 1200-1800 cm^{-1}: 1204, 1227s, 1273wb, 1312w, 1343sh, 1362w, 1393w, 1435sh, 1480s, 1505, 1524w, 1628ssh, 1661sh. ^1H NMR ($CDCl_3$) δ; 7.50-7.31(m, 25H, PPh_3), 5.71 (s, 1H, COCHCO), 1.12 (s, 9H, -CMe_3). ^{13}C NMR ($CDCl_3$) δ; 205.8 (CO), 172.0 (m, CO), 134.0 (d, 16.6 Hz, PPh_3), 131.7 (d, 33.1Hz, PPh_3), 130.5 (PPh_3), 128.9 (d, 11Hz, PPh_3), 119 (m, CF_n), 117 (m, CF_n), 110.8 (m, CF_n), 90.6 (COCHCO), 27.9 (-CMe_3). ^{19}F NMR ($CDCl_3$) δ; -81.0 (t, 9.2 Hz, CF_n), -119.7 (s, CF_n), -127.1 (s, CF_n).

The synthesis of 1,1,1-trifluoro-2,4-pentanedionato(triphenylphosphine)silver(I), [Ag(tfac)PPh₃] ***(20)***

Silver oxide (1.5 g, 6.5 mmol) was suspended in diethyl ether (5 cm^3). To this was slowly added 1,1,1-trifluoro-2,4-pentanedione (1.8 cm^3, 2.29 g, 14.8 mmol) resulting in the mixture solidifying to give a sand coloured precipitate. To this was added triphenylphosphine (3.4 g, 13 mmol) in diethyl ether (60 cm^3), and the mixture was stirred for 20 minutes in the absence of light. The volume was reduced by one quarter, and the contents were filtered in air to give a sand brown precipitate. The crude product was washed twice with diethyl ether and dried *in vacuo*. Yield 4.84 g, 71 %.

Analysis : found (calculated for $C_{23}H_{19}F_3O_2AgP$) C, 52.8 (52.6); H, 3.76 (3.66) %. Thermal decomposition initiated at 200°C (by TGA/air). IR (Nujol mull) 1200-1800 cm^{-1}: 1254s, 1312,

1333w, 1435ssh, 1520b, 1667bs. IR (hexachlorobutadiene mull) 1200-1800 cm^{-1}: 1254, 1312, 1331w, 1435 ssh, 1524, 1541, 1667b. ^{1}H NMR ($CDCl_3$) δ; 7.50-7.40 (m, 9H, PPh_3), 7.37-7.31 (m, 6H, PPh_3), 5.50 (s, CO<u>CH</u>CO), 1.99 (s, -<u>CH_3</u>). ^{13}C NMR ($CDCl_3$) δ; 197.0 (<u>CO</u>CH_3), 170.1 (q, 29.4 Hz, <u>CO</u>CF_3), 133.9 (d, 16.5 Hz, PPh_3), 132.0 (d, 31.3 Hz, PPh_3), 130.2 (PPh_3), 128.8 (d, 9.2 Hz, PPh_3), 119.2 (q, 289 Hz, <u>CF_3</u>), 92.8 (CH), 30.2 (<u>CH_3</u>). ^{19}F NMR ($CDCl_3$) δ; -76.1 (CF_3).

The synthesis of 1,1,1,5,5,5-hexafluoro-2,4-pentanedionato(triphenylphosphine)silver(I), [Ag(hfac)PPh_3] (21)

Silver oxide (5.0 g, 21.6 mmol) was suspended in THF (30 cm^3). To this was added 1,1,1,5,5,5-hexafluoro-2,4-pentanedione (6.0 cm^3, 8.8 g, 42.2 mmol). The mixture was stirred for five minutes, then filtered on to triphenylphosphine (11.1 g, 42.4 mmol). The resulting brown hazy mixture was stirred for five minutes, then filtered in air using a fine filter paper. The solvent was removed *in vacuo* to give a sand coloured crystalline solid. Recrystallisation from acetone gave the title compound. Yield 21.0 g, 86 %.

Analysis : found (calculated for $C_{23}H_{16}F_6O_2AgP$) C, 48.0 (47.9), H, 2.81 (2.79) %. Thermal decomposition initiated at 250°C (by TGA/air). IR (Nujol mull) 1200-1800 cm^{-1}: 1254, 1312w, 1331w, 1435ssh, 1518b, 1669b. IR (hexachlorobutadiene mull) 1200-1800 cm^{-1}: 1254s, 1312, 1331w, 1435ssh, 1480sh, 1522sb, 1541ssh, 1669bs. ^{1}H NMR ($CDCl_3$) δ; 7.54-7.28 (m, 17H, PPh_3 + $CDCl_3$), 6.05 (s, 1H, CO<u>CH</u>CO). ^{13}C NMR ($CDCl_3$) δ; 177.5 (q, 33 Hz, CO), 133.9 (d, 14.7 Hz, PPh_3), 131.2 (PPh_3), 130.0 (d, 40.5 Hz, PPh_3), 129.3 (d, 11.1 Hz, PPh_3), 117.7 (q, 289 Hz, CF_3), 87.9 (CO<u>C</u>HCO). ^{19}F NMR ($CDCl_3$) δ; -77.0 (CF_3).

The synthesis of 1,1,1,5,5,5-hexafluoro 4-(hexylimino)-2-pentanonato (triphenylphosphine)silver(I) monohydrate, [Ag(hfacNhex)PPh_3].H_2O ***(22)***

1,1,1,5,5,5-Hexafluoro-2,4-pentanedionato(triphenylphosphine)silver(I) **(21)** (5.4 g, 9.4 mmol) was suspended in benzene (150 cm^3). To this was added hexylamine (1.2 cm^3, 0.9 g, 9.4 mmol). The mixture was refluxed gently in a Dean and Stark apparatus for 2½ hours with minimal decomposition. The mixture was filtered in air to give a deep orange solution. The solvent was removed *in vacuo* to give a brown precipitate. Yield 5.7 g, 89 %.

Analysis : found (calculated for $C_{29}H_{29}F_6ONAgP.H_2O$) C, 51.4 (51.3); H, 4.39 (4.61); N, 1.98 (2.06) %. Thermal decomposition initiated at 100°C (by TGA/air). IR (Nujol mull) 1200-1800 cm^{-1}: 1254, 1310w, 1439sh, 1507w, 1522, 1601, 1661sh. IR (hexachlorobutadiene mull) 1200-1800 cm^{-1}: 1254sh, 1310w, 1435sh, 1482, 1532s, 1563, 1611w, 1671. ^1H NMR ($CDCl_3$) δ; 7.38-7.27 (m, PPh_3), 5.61 (s, COCHCO), 2.38 (b, 2H, CH_2), 1.43 (m, 2H, CH_2), 1.16 (m, 6H, CH_2), 0.76 (t, 6.9 Hz, 3H, CH_3). ^{13}C NMR ($CDCl_3$) δ; 175.7 (q, 31.3 Hz, CO), 133.8 (d, 16.5 Hz, PPh_3), 131.3 (d, 34.9 Hz, PPh_3), 130.6 (PPh_3), 129.0 (d, 11 Hz, PPh_3), 118.0 (q, 291 Hz, CF_3), 86.2 (CO<u>CH</u>CO), 43.5 (CH_2), 33.3 (CH_2), 31.5 (CH_2), 26.2 (CH_2), 22.5 (CH_2), 13.9 (CH_3). ^{19}F NMR ($CDCl_3$) δ; -77.2 (CF_3).

The synthesis of 1,1,1,5,5,5-hexafluoro 4-(cylclohexylimino)-2-pentanonato(triphenylphosphine)silver(I) monohydrate, [Ag(hfacNchex)PPh_3].H_2O ***(23)***

1,1,1,5,5,5-Hexafluoropentane-2,4-dionato(triphenylphosphine)silver(I) **(21)** (4.1 g, 7.0 mmol) was suspended in benzene (150 cm^3). To this was added cyclohexylamine (0.7 g, 7.0 mmol). The

mixture was gently refluxed in a Dean and Stark apparatus for two hours, to give a yellow-orange mixture, with minimal signs of decomposition. Solvent was removed *in vacuo* to give a sticky oil. The oil was dissolved in diethyl ether, filtered in air and dried *in vacuo* to give a brown solid. Yield 3.83 g, 81 %.

Analysis: found (calculated for $C_{29}H_{27}NOF_6PAg.H_2O$); C, 51.3 (51.5); H, 4.38 (4.32); N, 1.96 (2.07) %. Mp 84°C (by DSC/He). Thermal decomposition initiated at 115°C (by TGA/He). IR (Nujol mull) 1200-1800 cm^{-1}: 1250s, 1314w, 1325w, 1437ssh, 1526sb, 1599b, 1661sb. IR (hexachlorobutadiene mull) 1200-1800 cm^{-1}: 1252s, 1310w, 1325w, 1373w, 1387w, 1437ssh, 1451, 1482sh, 1532bs, 1559bs, 1669s. ^1H NMR ($CDCl_3$) δ; 7.43-7.38 (m, 15H, PPh_3), 5.69 (s, 1H, CO<u>CH</u>CO), 2.85-2.65, 2.0-1.8, 1.8-1.65, 1.65-1.55, 1.3-1.15, 1.15-0.95 (-C_6<u>H_{11}</u>). ^{13}C NMR ($CDCl_3$) δ; 175.4 (q, 31.9 Hz, CO), 133.8 (d, 16.5 Hz, PPh_3), 131.5 (d, 34.2 Hz, PPh_3), 130.6 (s, PPh_3), 128.9 (d, 9.9, PPh_3), 118.0 (q, 291 Hz, CF_3), 86.0 (s, CO<u>CH</u>CO), 36.2 (CH_2), 25.1 (CH_2), 24.8 (CH_2). ^{19}F NMR ($CDCl_3$) δ; -77.2 (CF_3).

CHAPTER FIVE

SYNTHESIS, CHARACTERISATION, REACTIVITY AND CVD PROPERTIES OF ORGANOMETALLIC SILVER COMPLEXES

5.1 INTRODUCTION

In contrast to the coordination chemistry of silver, which bears little or no resemblance to copper chemistry, the organometallic chemistries of copper and silver are closely linked. [224] Organocopper chemistry research has in the past been focused by applications in organic synthesis, and similar applications are now being developed for organosilver complexes [225-229] which often behave in a complementary way to organocopper reagents. [230]

Some interest in organometallic silver compounds has been initiated by the search for suitable silver CVD precursors, notably $[CF_3CF=C(CF_3)Ag]_4$ [21] and $(C_5H_5)AgPR_3$, [231] although this area remains largely unexploited. In contrast, organometallic precursors have been utilised for both copper CVD [for example $(C_5H_5)CuPR_3$ [232, 233]] and more notably gold CVD, where organogold precursors [$R_2Au(\beta$-diketonate), [234-237] $RAuPMe_3$, [238, 239] R_3AuPMe_3 [239-241] and others [238, 242]] have played a pivotal role. Additionally, in the CVD of other metals, organometallic precursors have been used for Zr, [243] Cr, [244] Co, [245] Pt [187] and Al deposition. [246]

In comparison with organocopper chemistry, organosilver chemistry is less well developed, no doubt as a result of the relative instability of silver-carbon σ-bonds. Alkyl silver compounds are particularly unstable (typically decomposing above -50°C) and although alkenyl and aryl silver compounds are significantly more stable, they are still susceptible to photolysis, hydrolysis and oxidation. [224] Silver alkynyl compounds are the most stable class and are reportedly stable up to 100°C. [224] Stabilities of Ag-C bonds have been increased in cases where steric hindrance, [247, 248] intra-molecular donors [249, 250] or the use of fluorinated ligands has been utilised. [21, 251] Thermal stabilities are also reported to be increased where the organometallic species forms complexes with inorganic salts such as LiBr [226] and $AgNO_3$, [252] although this

may reduce compound volatility. Further, stability is also known to be increased where the carbanion is more nucleophilic, as in silver methanides, [253] ylides [254-257] and carbenes. [258]

5.1.1 Synthetic routes

I) The majority of organosilver (particularly alkyl and aryl) compounds have been prepared from the reaction of silver salts (generally halides) with organometallic reagents containing a metal more electropositive than silver. [224] Attempts to prepare ethylsilver from silver chloride and diethyl zinc were made as early as 1859 by Buckton [259] and in 1861 by Wanklyn and Carius. [260] These synthetic attempts were unsuccessful because of the low thermal stability of alkyl silvers, and it was not until 1941 that alkyl silvers were first isolated. Aryl silvers were found to be more amenable to study and these were first prepared in 1919 by Kraus and Schmitz. [261]

Organosilver compounds (AgR) are readily prepared at low temperatures from the reaction of silver nitrate and tetraorganotin (where R = aryl) or tetraorganolead compounds (where R = alkyl, aryl) in alcoholic solvents (Eqn 5-1). The compounds precipitate on formation as yellow to red-brown precipitates and depending on stability may decompose on warming. In the case of alkyl silver compounds, alkyllithium and alkylmagnesium reagents have also been used in combination with silver halides and their phosphine adducts (Eqn 5-2). For the preparation of aryl silver compounds, aryl lithium (with silver bromide) and aryl zinc (with silver nitrate) (Eqn 5-3) have been found to be more convenient in the transmetallation reaction.

$$AgNO_3 + R_4Pb \longrightarrow AgR + R_3PbNO_3 \quad \textbf{(5-1)}$$

R = alkyl, aryl

$$AgI(PBu_3) + LiR \longrightarrow AgR(PBu_3) + LiI \quad \textbf{(5-2)}$$

R = alkyl

$$AgNO_3 + ZnR_2 \longrightarrow AgR + RZnNO_3 \quad \textbf{(5-3)}$$

R = aryl

The preparation of arylsilver compounds from aryllithium reagents and silver halides is further complicated by the formation of argentate complexes of the form $[Ag_xLi_yR_{x+y}]$, [263] analogous to complexes found in copper [262] and gold chemistry. [264, 265] These compounds may be synthesised quantitatively by the reaction of silver halide with two equivalents of aryllithium, or alternatively via a 1:1 reaction of aryl silver and aryl lithium compounds (Eqn 5-4). A number of argentates have been isolated and characterised as tetramers in solution, isostructural with the aurate analogue in the solid state. [265]

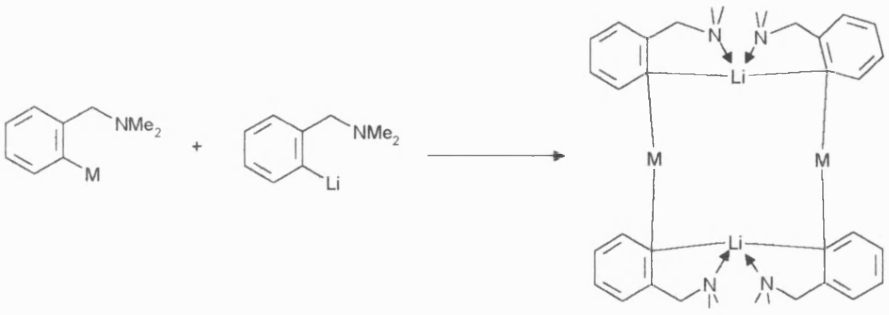

(5-4)

M = Cu, [262] Ag, [263] Au [264, 265]

II) Silver fluoride is known to add across double or triple bonds of perfluoroalkenes and perfluoroalkynes, respectively, to give perflouroalkyl and perfluoroalkenyl groups bound to silver. Reaction of AgF with perfluoropropene proceeds in acetonitrile at room temperature to give a solvated silver alkyl species (Eqn 5-5) [266] and a similar reaction can be found with addition of AgF to CF_3-C≡C-CF_3 (Eqn 5-6). [21, 267] These reactions require low temperatures to condense the alkene or alkyne reagent, but once in a sealed vessel the reaction proceeds at room temperature over several days. A number of silver perfluoroalkyls have been prepared in a similar reaction with independent sources of silver and fluoride (Eqn 5-7), although the products were not isolated. [268]

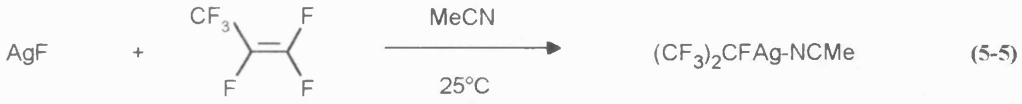

(5-5)

(5-6)

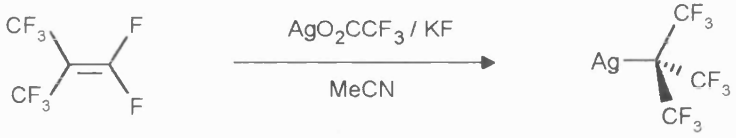

(5-7)

III) Silver-carbon bonds are also formed by a number of other routes. Alkynes of the type R-C≡C-H react directly with silver salts in the presence of ammonia to give insoluble coordination polymers via a direct metallation reaction. [269] These compounds are however soluble in strongly coordinating solvents (amines, pyridines) and in the presence of phosphines. Donor ligands successfully compete with coordinated alkyne groups, resulting in a partial breakdown of the coordination polymer. A number of η^1-cyclopentadienylsilver derivatives have been isolated from the reaction between cyclopentadienyl-boronic acids and silver nitrate in the presence of ammonia, although this reaction has not been widely used. [270] Silver carbon bonds are also readily formed with the reaction of silver halides with various triorganomethylenephosphoranes to give a variety of silver ylides. [254, 255]

5.1.2 Structure and stability of organosilver compounds

Although silver alkyls are readily prepared at low temperature, decomposition usually takes place on warming. For simple alkyl silver compounds, stability decreases with increasing chain length, [224] and is also dramatically influenced by the presence of impurities. Methyl silver is reported as decomposing between -80°C and -50°C [269] and n-propylsilver at -60°C. [271] Where the alkyl chain incorporates an additional donor the organosilver is somewhat stabilised, thus $Ag(CH_2)_3NMe_2$ is stable up to 15°C. [272]

A small number of silver alkyl and perfluoroalkyl complexes have been structurally determined since 1984, as both neutral AgR and anionic $[AgR_2]^-$. All these complexes are highly substituted at C_α and no β-hydrogens are present (β-hydrogen elimination is postulated as a major first step in the decomposition pathway for alkyl silvers). As a result of this substitution,

all of the complexes show increased steric bulk around the Ag-C bond. Of note, and in contrast to aryl silver complexes, these compounds do not exhibit electron deficient three centre-two electron bonding.

A structure determination of the alkyl silver $[\{(2\text{-}Me_3Si)_2C(Ag)C_5H_4N\}_2]$, prepared from the alkyl lithium and silver tetrafluoroborate, shows it to be a dimer in the solid state. Each silver is bonded to a sterically crowded sp^3-hybridised carbon with further stabilisation of each silver provided by the pyridine nitrogen (Figure 5-1). Despite increased stability and the fact that the crystal structure determination was carried out at 295 K, the complex was found to decompose at 303 K. [273, 274] The geometry around silver is approximately linear with C-Ag-N of 174.5° and the short Ag-Ag distance of 2.654 Å may be indicative of a metal-metal interaction.

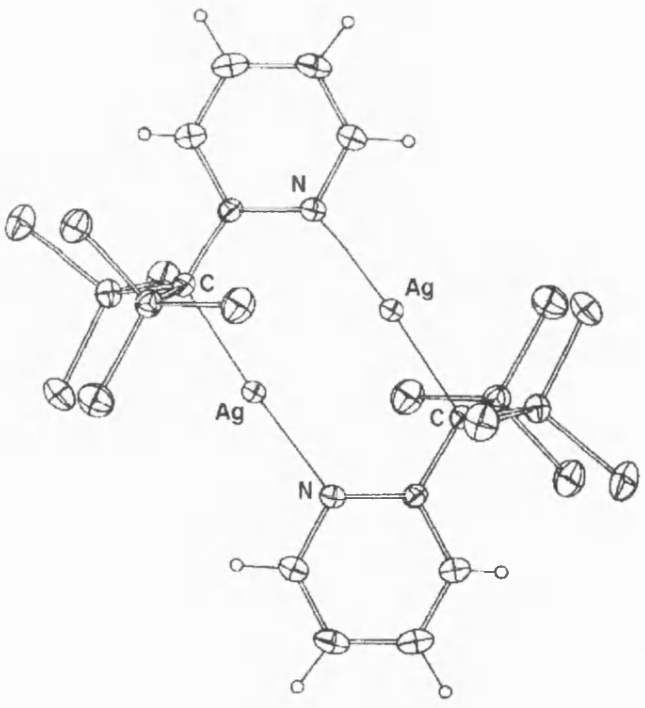

Figure 5-1 The structure of $[\{(2\text{-}Me_3Si)_2C(Ag)C_5H_4N\}_2]$. [273]

The related $[Ag\{C(SiMe_3)_3\}_2]^-$ anion in $[Li(THF)_4][Ag\{C(SiMe_3)_3\}_2]$ was also prepared by the addition of alkyl lithium and silver halide. The anion exhibits a similar linear geometry around silver with two highly crowded ligands (Figure 5-2) and the compound is observed to be slightly more stable (decomposes at 65°C). [275] The ionic structures are suggested as persisting in solution and this is confirmed by a single ^{109}Ag resonance at 700 ppm in d_8-toluene.

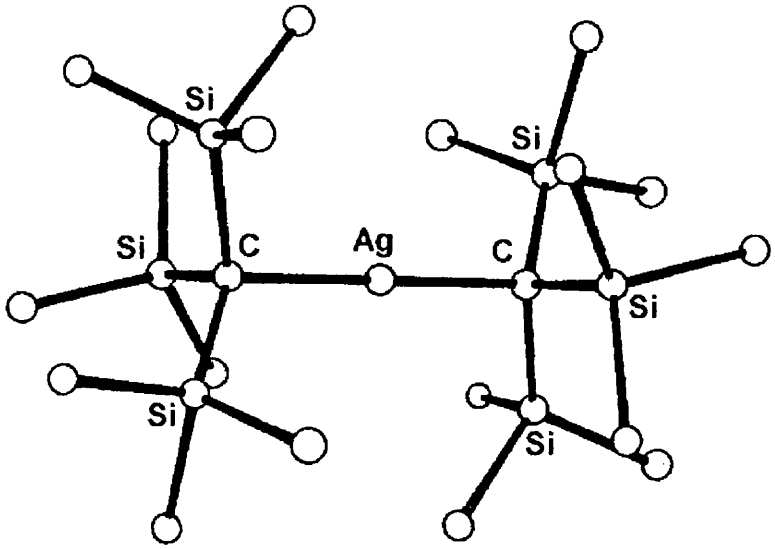

Figure 5-2 Structure of one of the anions of $[Li(THF)_4][Ag\{C(SiMe_3)_3\}_2]$. [275]

A similar bis(alkyl)silver anion, bis(perfluoroisopropyl)silver, has also been structurally determined as found in $[AgR_2][Rh(dppe)_2]$ [where R = $(CF_3)_2CF$]. [266] Both this anion and the neutral complex $(CF_3)_2C(F)Ag(MeCN)$ (Figure 5-3) repeat the linear two coordinate silver geometry common to silver alkyl structures. The neutral complex further reflects the possibility of ligand stabilised perfluoroalkyl complexes. The perfluoroisopropyl ligand has been shown to be kinetically labile [unlike $-C(SiMe_3)_3$] and may be regarded as a 'pseudohalogen'.

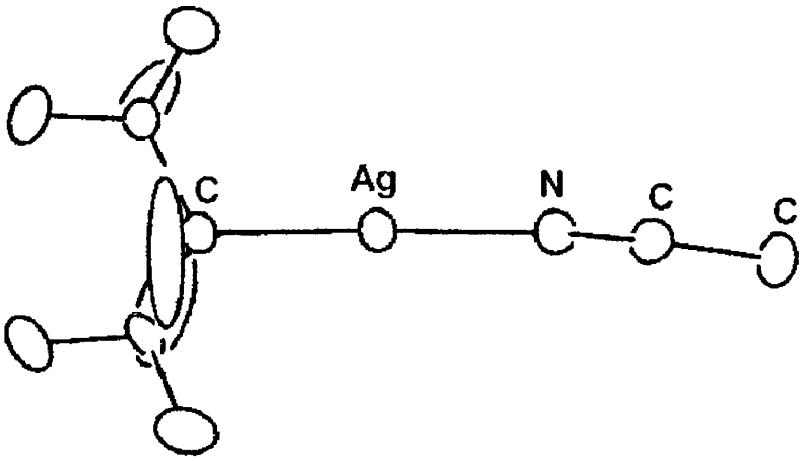

Figure 5-3 Structure of $(CF_3)_2C(F)Ag(MeCN)$. [266]

Silver alkenyls are significantly more stable than silver alkyl compounds. Styrenylsilver Ag(CH=CHPh) is stable up to 80°C [276] and complete decomposition requires several days at room temperature or several hours in boiling ethanol. Perfluorinated alkenyls are even more stable, perfluoroisopropenylsilver [$AgC(CF_3)=CF_2$] can be sublimed in vacuo at 160°C. [277]

Structural studies of compounds where silver is bound to an sp^2-hybridised carbon (i.e. alkenyls and aryls) reveal that two electron-three centre bonding is common. The crystal structure of perfluoro-1-methyl-1-propenyl silver is reported as a tetramer with a central square plane of silver atoms to which each edge is bound a perfluoro-1-methyl-1-propenyl ligand (Figure 5-4). [21] Each silver atom is in a nearly linear geometry [$\angle$CAgC : 166.7°] and the Ag-Ag distances (2.761Å) are lower than found in the metal (2.89Å) indicating a possible Ag-Ag interaction.

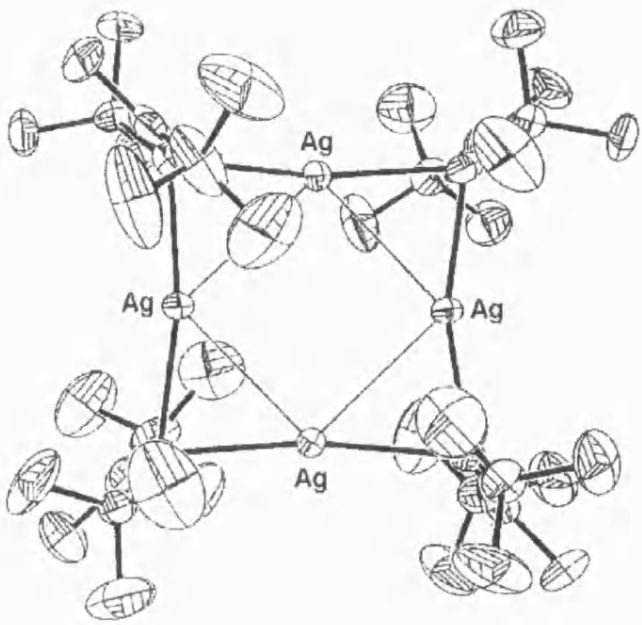

Figure 5-4 Structure of $[CF_3CF=C(CF_3)Ag]_4$. [21]

Aryl silver compounds are of a similar stability to silver alkenyls. Phenylsilver has an observed decomposition at 74°C as determined by TGA, [278] perfluorophenylsilver possesses increased stability and decomposes only slowly at 150°C [251] and adducts of this perfluorophenylsilver display decomposition temperatures in the range 155-190°C. [279] The structure of a number of aryl silver compounds have also been determined, such as tetrameric 2-silver(dimethyl aminomethyl)-ferrocene (Figure 5-5) [280] and mesitylsilver (Figure 5-6). [247, 248] Each structure contains a single silver environment and in both cases the geometry approaches linearity with the C-Ag-C angle of 170.7° and 169.0°, respectively. Silver-silver distances are slightly lower than found in the alkenyl complex (Ag-Ag: 2.74 Å and 2.73 Å, respectively). Successful attempts to prepare organosilvers with very bulky ligands (e.g. 2,4,6-triphenylphenyl) have been reported and crystal structures determined, [281] however these results have since been shown to be ambiguous as reported Ag-C distances are significantly lower than expected and very close to C-Br in the reagent. [282]

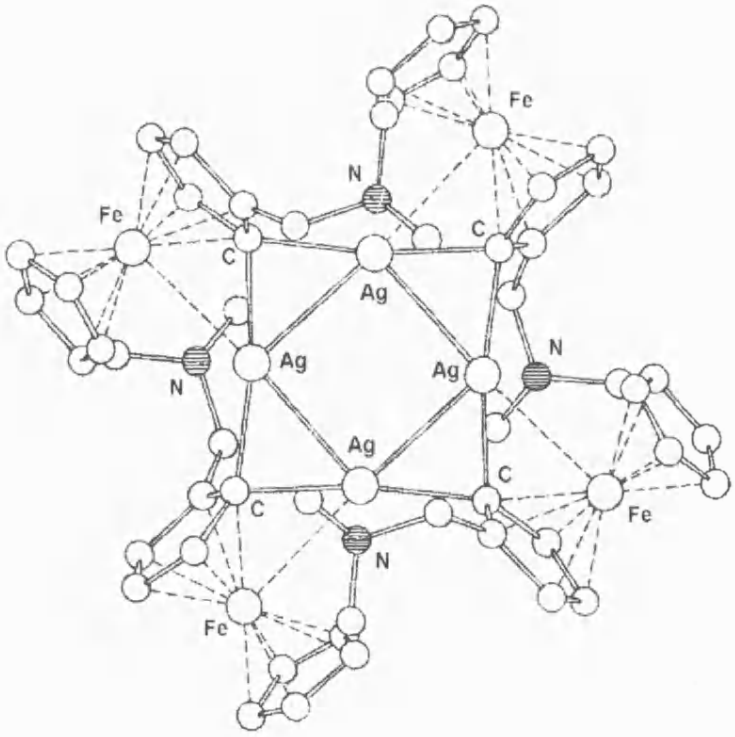

Figure 5-5 Structure of 2-silver(dimethylaminomethyl)ferrocene. [280]

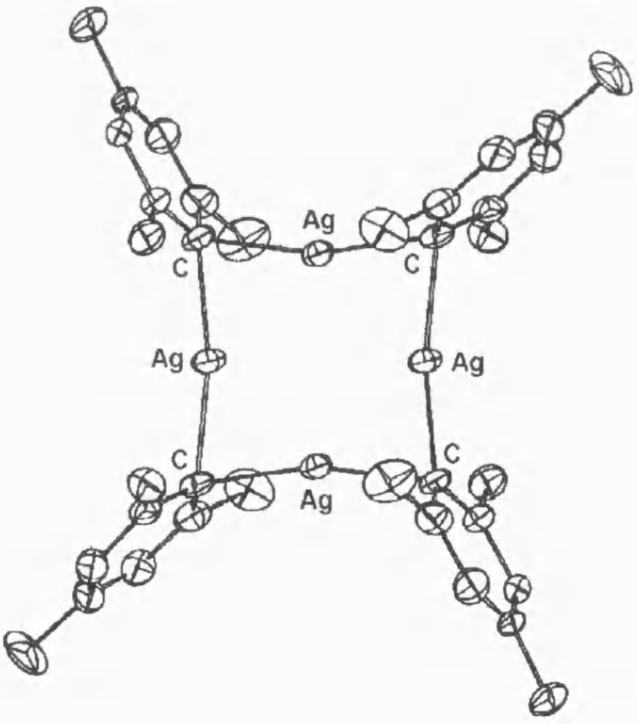

Figure 5-6 Structure of mesitylsilver. [247, 248]

Two arylsilver compounds reveal structures where the organosilver compounds do not aggregate to form clusters, though in these cases the silver centre is further coordinated by other ligands. In the pentafluorophenyl(ylide)silver(I) complex $[Ag(C_6F_5)(CH_2PPh_3)]$ the silver centre is coordinated by both a pentafluorophenyl and a methylene of an ylide (Figure 5-7) resulting in a linear geometry [∠C-Ag-C: 175.4-178.2°] [256] Attempts to increase the coordination number of this complex by addition of pyridine or 2,2'-bipyridyl have failed, with no apparent reaction. A final example of a η^1-bonded arylsilver can be found in the crystal structure of $[(\eta^5\text{-}C_5H_4SiMe_3)_2Ti(C{\equiv}CSiMe_3)_2]Ag(\eta^1\text{-}2,4,6\text{-}Me_3C_6H_2)$ where silver is bound to a single mesityl group and two alkyne groups from a bis(alkynyl)titanocene molecule. [283]

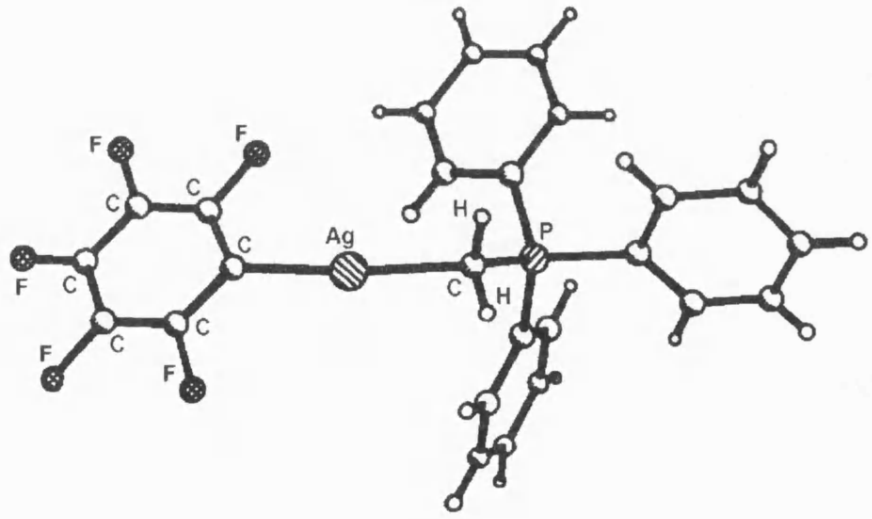

Figure 5-7 Structure of $[Ag(C_6F_5)(CH_2PPh_3)]$. [256]

The structures of a number of phosphine adducts of silver alkynyls have been crystallographically determined and range from the polymeric $[Me_3PAgC{\equiv}CPh]_\infty$ [284] and $[Me_3PAgC{\equiv}CSiMe_3]_\infty$ [285] to the tetrameric $[Ph_3PAgC{\equiv}CPh]_4.(THF)_{3.5}$. [285] Crystallographic

studies of these compounds reveal that they are all constructed from $Ag(C{\equiv}CR)_2^-$ and $Ag(PR_3)_2^+$ groups with the size of the phosphine apparently determining the extent of oligomerisation. The tetranuclear complex $[Ph_3PAgC{\equiv}CPh]_4.(THF)_{3.5}$, where Ag is bound to sp-hybridised carbon, exhibits electron deficient three centre-two electron bonds in a similar fashion to that often observed when silver is bound to sp^2-hybridised carbons. However, in the former case the Ag_4 core is arranged in a 'flat-butterfly' arrangement (Figure 5-8), as compared to the square planar Ag_4 arrangement with Ag-C(sp^2). The silver alkynyl cluster $[Ph_3PAgC{\equiv}CPh]_4.(THF)_{3.5}$ can be described as two nearly linear (174.6°) $Ag(C{\equiv}CPh)_2^-$ units bridged by $Ag(PPh_3)_2^+$ moieties. Apart from the distance between $Ag(PPh_3)_2^+$ units, Ag-Ag distances within the core are fairly constant (2.9-3.1Å) although higher than found in Ag-C(sp^2) tetramers.

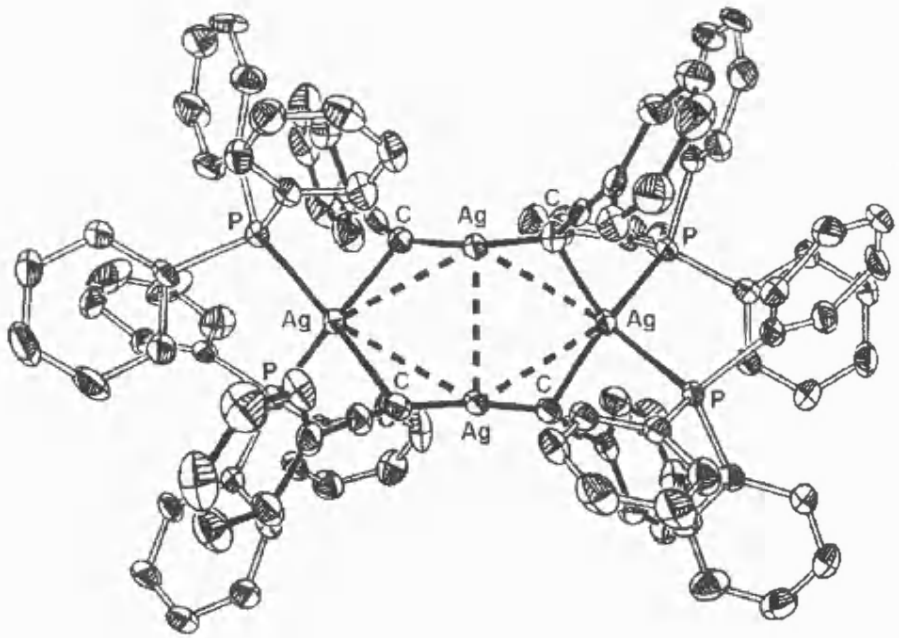

Figure 5-8 Structure of $[Ph_3PAgC{\equiv}CPh]_4.(THF)_{3.5}$.[285]

As the use of organometallic precursors for the CVD of silver has remained largely unexploited, there was considerable interest in developing a number of such precursors within the scope of this project. This study has focused on arylsilvers for CVD applications as they are known to have thermal stabilities of a similar order to those found for alkenylsilvers. Specifically this study has been interested in the use of steric hindrance and intra-molecular coordination of silver (from pendant donor groups on the aryl ring) to coordinatively saturate the metal centre. Additionally the formation of phosphine adducts of such complexes have been explored. These strategies have been invoked in the present work to prevent oligomerisation, to increase chemical and thermal stability, and to promote greater volatility.

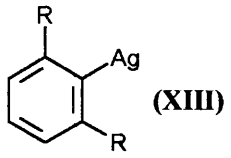

(XIII)

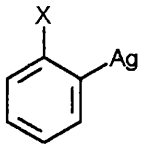

(XIV)

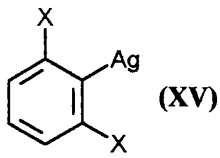

(XV)

R = Me [247, 248, 283]

= H [287]

X = NMe_2 [249]

= CH_2NMe_2 [249]

X = OMe [249]

The use of steric hindrance (XIII) and/or additional coordination sites (XIV and XV) ortho to the metal has been shown to have a stabilising influence on the chemistry of arylsilver compounds. Examples of this include methyl, [247, 248, 283] dimethylamino, [249] (dimethylamino)-methyl [249] and methoxy [249, 288] groups in the ortho position relative to silver. The use of intra-molecular coordination in these and similar ligands has been successfully utilised for the isolation of a number of other organometallic (Li, [289] Ni, [290-292] Pd, [290, 292, 293] Pt, [290, 292, 293] Rh, [290] Ir, [290] Cu, [294] Ga, [295-298] Al, [298] In [298] and Sn [299]) and aryloxide compounds (Ga [300] and In [300]). A general discussion of these compounds is available. [294]

5.2 RESULTS AND DISCUSSION

5.2.1 Synthesis and characterisation of {2-(dimethylaminomethyl)phenyl}silver(I) **(24)**

{2-(dimethylaminomethyl)phenyl}silver(I) **(24)** has been prepared, structurally characterised, and tested as a potential CVD precursor. Reports of organosilver CVD precursors in the literature are limited to those concerning (perfluoro-1-methyl-1-propenyl)silver(I) as a precursor for LPCVD [21] and PECVD. [95] A number of patents also cite the use of $Ag(\eta^5\text{-}C_5H_5)\ PR_3$ for the growth of thin silver films although no experimental data has been given. [231, 286]

The compound of interest, {2-(dimethylaminomethyl)phenyl}silver(I), has previously been prepared by van Koten et al.. [249] The compound was reported to be isolated as a colourless or pink coloured solid in 61% yield, with a much improved thermal stability [mp 160-180°C (dec)] over phenylsilver [mp 74°C (dec)]. [278] Van Koten et al. have however noted that melting points and molecular weight results were variable between experiments [melting points 106-195°C (dec), molecular weights 835-1215]. Proton NMR data suggested a number of species in solution differing in their degree of association although no specific molecular species were proposed. Apart from microanalysis and a listing of a number of IR absorptions, this compound was not characterised further.

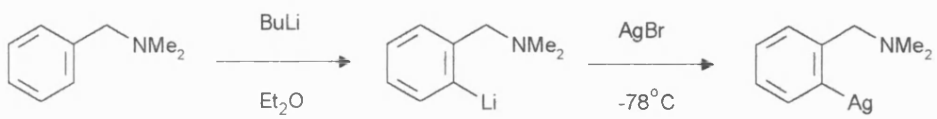

(5-8)

The compound {2-(dimethylaminomethyl)phenyl}silver(I) **(24)** was prepared in low yield (14%) by the same synthetic route as van Koten, via the reaction of silver bromide with 2-(dimethylaminomethyl)phenyllithium at -78°C (Eqn 5-8). The red compound isolated in this study was fairly stable to light, oxygen and moisture for short periods and no obvious signs of decomposition were observed after storage at -5°C for six months. The infra-red spectrum of crude **(24)** gave a number of characteristic bands at 841 cm^{-1} and 752, 744 cm^{-1} which compare favourably with the reported infra-red spectrum of {2-(dimethylaminomethyl)phenyl} silver(I) [846s (group vibration), 745vs (*ortho*-substituted benzene)]. [249]

The crude **(24)** was however found to have slightly low carbon and nitrogen microanalysis results [found (calculated for $C_9H_{12}NAg$) C, 43.0 (44.7); H, 5.40 (5.00); N, 4.70 (5.79) %] and its decomposition point is significantly lower [mp (uncorrected) 91-120°C (dec)] than previously reported [literature mp 160-180°C (dec)]. [249] These anomalies may be explained by the presence of {2-(dimethylaminomethyl)phenyl}silver(I).silver(I)bromide as an impurity which has been found to have a lower melting point [mp 108°C (dec)]. [249] This explanation also accounts for the appearance of crude **(24)** as{2-(dimethylaminomethyl)phenyl}silver.silver bromide has been isolated as a rust-brown complex from the reaction of {2-(dimethylamino methyl)phenyl}silver with silver bromide. [249] Recrystallisation of crude **(24)** proved impractical due to its vulnerability with respect to decomposition while in solution for extended periods.

Compound **(24)** was slightly soluble in $CDCl_3$ which allowed its solution characterisation by NMR techniques. ^1H and ^{13}C NMR gave expected results and no spin-spin coupling was observed from silver to the aromatic protons of the ligand. A resonance from the carbon bound to silver was not observed in the ^{13}C NMR although this resonance would be expected to be weak even before coupling to both ^{107}Ag and ^{109}Ag nuclei. As a result of ^1H NMR evidence van

Table 5-1 Selected mass spectrometric data, compound **(24)**. [a]

Fragment ions [b]	m/z [c]	% [d]
R	134	42 (134)
[AgR (-NMe_2)]	197	8 (197)
[AgR (-1)]	240	41 (240)
Ag_2R	348	11 (350)
Ag_3	321	10 (325)
[Ag_3R (-1)]	454	2.9 (458)
Ag_3R_2	589	3.1 (593)
[Ag_4 (+1)]	429	4.5 (433)
Ag_4R	562	2.8 (564)
[Ag_4R_2 (-1)]	695	1.1 (701)
Ag_4R_3	830	14 (834)
Ag_5	535	4.9 (539)
Ag_5R_2	803	2.8 (807)
[Ag_5R_4 (-1)]	1070	5.9 (1076)
[Ag_6 (+2)]	644	1.7 (648)
Ag_6R_3	1044	2.9 (1048)
[Ag_7 (+1)]	750	2.1 (756)
[Ag_7R_4 (+1)]	1286	5.3 (1294)

[a] highest abundance peak (100%) R(-2) at m/z 132 [b] R = 2-(dimethylaminomethyl) phenyl [c] based on ^{107}Ag [d] based on highest abundant peak for the fragment (highest abundant mass fragment)

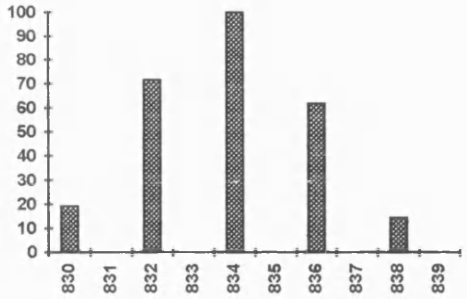

a) calculated pattern for Ag_4R_3

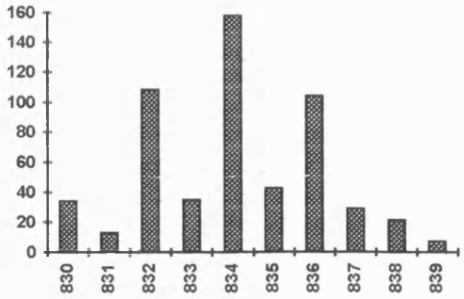

b) observed fragment abundances

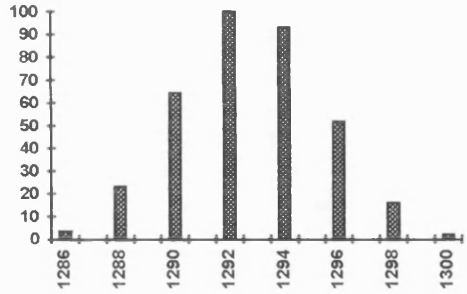

c) calculated pattern for Ag_7R_4+1

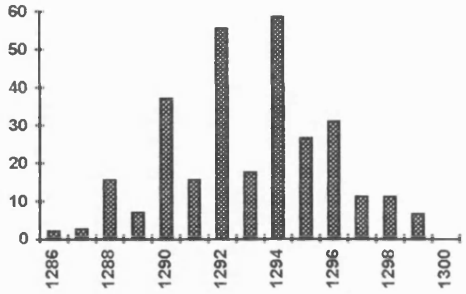

d) observed fragment abundances

Figure 5-9 Comparison of some calculated and observed fragments from the FAB(LSIMS) mass spectrum of **(24)**.

Koten et al. reported two species in solution [249] but this observation was not made during this work. Attempts to observe ^{109}Ag resonances of **(24)** in solution were unsuccessful even at low temperature (-80°C). The absence of observable ^{109}Ag resonances may be a function of the solubility of the compound or its dynamic behaviour in solution.

Mass spectrometry studies of **(24)** (Table 5-1) using Fast Atom Bombardment (Liquid SIMS) techniques (see Appendix 2) have revealed a large number of Ag_n and Ag_nR_m type fragments. High abundance peaks were observed for [AgR(-1)] (41%) and R (42%), while [AgR(-NMe_2)] was also observed, presumably a decomposition product of [AgR(-1)]. Surprisingly, the expected tetrameric fragment Ag_4R_4 was not observed (see below for crystallographic details), although Ag_4R_m (m = 1, 2, 3) fragments were identifiable. Finally, a number of Ag_5, Ag_6 and Ag_7 based ions were observed suggesting that higher oligomers may be present in solution. Van Koten et al. have observed molecular weights in solution of 880, 940 and 1215 (tetramer molecular weight 964-968) also indicative of higher oligomers. [249] Graphs displaying observed fragment clusters and their theoretical abundance patterns for Ag_4R_3 and [Ag_7R_4(+1)] are shown in Figure 5-9.

5.2.2 Reactivity of {2-(dimethylaminomethyl)phenyl}silver(I) **(24)** *and characterisation of the novel decomposition by-product* $[Ag(PPh_3)]_4(Me_2(O)SiOSi(O)Me_2)_2$ **(25)**

When in solution, **(24)** was vulnerable to decomposition, particularly at elevated temperatures (60-70°C). An attempt to crystallise **(24)** in the presence of triphenylphosphine at -5°C has been found to result in cleavage of the Ag-C bond, apparently by reaction with trace quantities of dimethylsiloxane polymer present in the apparatus as high vacuum silicone grease (Eqn 5-9).

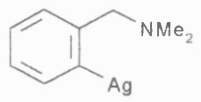

$$\xrightarrow[[Me_2SiO]_n]{2\ PPh_3} [Ag(PPh_3)]_4[Me_2(O)SiOSi(O)Me_2]_2 \qquad \textbf{(5-9)}$$

(24) **(25)**

The decomposition of **(24)** in solution was very specific and adducts of **(24)** were not isolated from the recrystallisation attempt. Crystals of a novel silver siloxide triphenylphosphine cluster **(25)** $[Ag(PPh_3)]_4[Me_2(O)SiOSi(O)Me_2]_2$ were the only isolable product. The ligand (XVI) can formally be identified as a doubly deprotonated dimethylsilane diol species. Although a fairly slow reaction at this temperature (crystals started to appear after a number of weeks), the siloxide cluster was isolated in significant quantities to allow further spectroscopic investigation. This unique silver siloxide complex has also been structurally characterised by single crystal X-ray diffraction and its molecular structure is discussed in 5.4.

There has been only one report of isolated compounds containing the Ag-O-Si linkage, this paper reporting the synthesis and characterisation (^{1}H NMR and molecular weight measurements) of $[(Me_3P)_nAg\text{-}O\text{-}SiMe_3]$ where n = 1, 2, 3. [301] These compounds remain the only spectroscopically characterised examples of silver siloxides to date. There have been no reports of crystallographically characterised silver siloxide compounds in the literature.

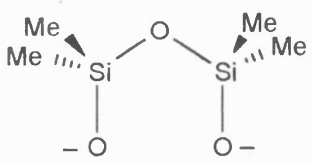

(XVI)

Infra-red spectroscopic analysis revealed little useful data, largely due to the lack of comparable compounds. The strong sharp absorption at 1435 cm^{-1} is characteristic of triphenylphosphine C-H vibrations. Silver-oxygen vibrations in silver siloxide complexes have

been reported at around 380 cm^{-1} [301] although this was beyond the range of instrumentation used in this study. However sharp ν(Si-O-Si) are reported at 1110-1120 cm^{-1} when $Ph_2(O)SiOSi(O)Ph_2$ chelates a metal centre. [302] In the IR spectrum of **(25)** an absorption band was observed near this frequency (1096 cm^{-1}, sharp).

Three methyl resonances from the siloxide ligand were observed in both the ^{1}H and ^{13}C NMR at room temperature, indicating non-equivalent methyl groups in the solution structure. Integrals determined from ^{1}H NMR suggest methyl groups in approximately a 1:1:~2 ratio.

Silicon-29 variable temperature NMR experiments revealed two distinct silicon environments at -80, -40 and 20°C and this is in accordance with the determined solid state structure (see below). At room temperature these resonances are observed at -8.1 and -18.9 ppm and are comparable with those observed when this ligand is bound to tin (-17.0 to -19.9 ppm). [302] A number of minor resonances were also detected at room temperature possibly representative of solution decomposition products.

Room temperature ^{31}P NMR revealed a slightly broadened singlet which was resolved on cooling to -80°C into a pair of doublets suggesting a single phosphorus environment with the phosphorus directly bound to a silver atom. From consideration of the solid state structure, the phosphorus NMR might have been expected to display two phosphorus resonances. This however is not the case which might indicate that the two phosphorus environments may be sufficiently close as to be unresolvable, indeed the spectrum appeared slightly broader than expected. Spin-spin coupling values [$^{1}J(^{109}Ag\text{-}^{31}P)$ = 694 Hz, $^{1}J(^{107}Ag\text{-}^{31}P)$ = 602 Hz] were slightly lower than those reported for $[(AgX)PR_3]_4$ in the literature [where R = 2,4,6-trimethoxy phenyl, X = Cl, Br, I, $^{1}J(^{109}Ag\text{-}^{31}P)$ = 745-821 Hz]. [82]

Attempts to record silver NMR spectra for this compound failed to yield any observable resonances. At room temperature this is as expected due to the lability of PPh_3 (as demonstrated by the ^{31}P NMR). However despite extended run times, no resonances were observed even at low temperature (PPh_3 lability has been shown to be dramatically slowed at -80°C [150]). The lack of ^{109}Ag resonances may be explained by a) a number of different species and/or environments in solution, b) spin-spin coupling by both ^{31}P and ^{29}Si or, c) limited solubility. One or more of these reasons might reduce ^{109}Ag resonances (normally weak and difficult to observe) to a point where observation is impractical.

Mass spectrometry (FAB/LSIMS) experiments on compound **(25)** allowed observation of a large number of silver containing fragments. Nineteen fragments were identified containing $Ag_{1-4}(silox)_{0-4}L_{0-4}$ [where silox = $Me_2(O)SiOSi(O)Me_2$, L = PPh_3]. The lack of fragments containing more than four silver atoms, $[Ag_5O_3(silox)(+2)]$ being the only species observed, indicates that solution species are predominantly of tetranuclear (Ag_4) size or smaller.

The most abundant species observed were $Ag(O)_{0-1}L_n$ (n = 1, 2) and such species are as observed in the mass spectra of numerous other (triphenylphosphine)silver adducts (Chapters 2-4). A number of other low intensity silver-phosphine fragments were also identified, e.g. $[Ag_2L_2(-1)]$, $[Ag_2O_3L_2(+3)]$, Ag_3OL_3. In fragments containing more than one silver atom and no siloxide ligands, the silver to phosphine ratio is 1:1. In cases where both siloxide and phosphine are present the silver to phosphine ratio is always 1:1 or greater. The lack of fragments displaying silver to phosphine ratios of less than one indicates that silver appears to be coordinatively saturated, thus suggesting a lack of $Ag(PPh_3)_2$ units within solution species.

Table 5-2 Selected mass spectrometric data, compound **(25)**.

Fragment ions [a]	m/z [b]	% [c]
AgL	369	100 (369)
AgOL	385	7 (385)
AgL_2	631	70 (631)
$AgOL_2$	647	6 (647)
$[Ag_2(silox)_3$ (+3)]	715	2.7 (717)
$[Ag_2L_2$ (-1)]	737	1.3 (739)
$[Ag_2O_3L_2$ (+3)]	789	2.9 (791)
$[Ag_2(silox)L_2$ (-1)]	903	1.2 (905)
$[Ag_2(silox)_3L$ (+3)]	977	1.0 (979)
$[Ag_3(silox)_3$ (+2)]	821	1.0 (825)
$Ag_3(silox)L_2$	1011	0.7 (1013)
$[Ag_3(silox)_3L$ (+2)]	1083	5.1 (1087)
Ag_3OL_3	1123	0.6 (1125)
$[Ag_3O_3(silox)_2L_2$ (+2)]	1227	1.3 (1229)
$Ag_3(silox)L_3$	1273	< 0.5 (1275)
$[Ag_3O_3(silox)_2L_3$ (+2)]	1489	< 0.5 (1491)
$[Ag_4(silox)_2$ (+2)]	762	3.6 (766)
$Ag_4O_2(silox)L$	888	3.0 (892)
$[Ag_4O_4(silox)_4$ (+1)]	1157	1.7 (1161)
$[Ag_5O_3(silox)$ (+2)]	751	2.1 (757)

[a] L = PPh_3, silox = $Me_2(O)SiOSi(O)Me_2$ [b] based on ^{107}Ag [c] based on highest abundant peak for the fragment (highest abundant mass fragment)

Numerous fragments were identified containing the siloxide ligand although only in combination with Ag_2-Ag_3. A significant number are seen to contain a higher siloxide to silver ratio than predicted by the crystal structure (expect 2:4). The expected ion for the tetramer adduct $[Ag_4(silox)_2L_4]$ was not observed although $[Ag_4(silox)_2$ (+2)] was, paralleling the known Ag-L bond lability in solution at room temperature. [150]

The reactivity of the Ag-C bond of organosilver compounds has been noted in a number of reactions where interesting silver containing products have been isolated. Cyclopentadienyl silver compounds have been utilised *in situ* to prepare a range of silver acetylide adducts (Eqn 5-10). [285] The preparation of such compounds demonstrates the synthetic utility of nucleophilic substitution at silver where, in this instance, cyclopentadienyl acts as an anionic leaving group.

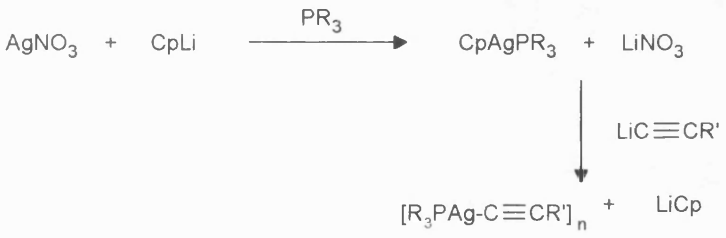

(5-10)

More closely related to the attempt to crystallise **(24)** in the presence of PPh_3, is the literature report of attempts to recrystallise Ag_4Mes_4 (Figure 5-6) in the presence of donor ligands (PPh_3, 2,2′-bipy, THT). [247, 248] Such attempts have also been unsuccessful, and reaction with dppm has cleaved the Ag-C bond to give a novel $Ag_3(Ph_2PCHPPh_2)_3$ complex (Eqn 5-11).

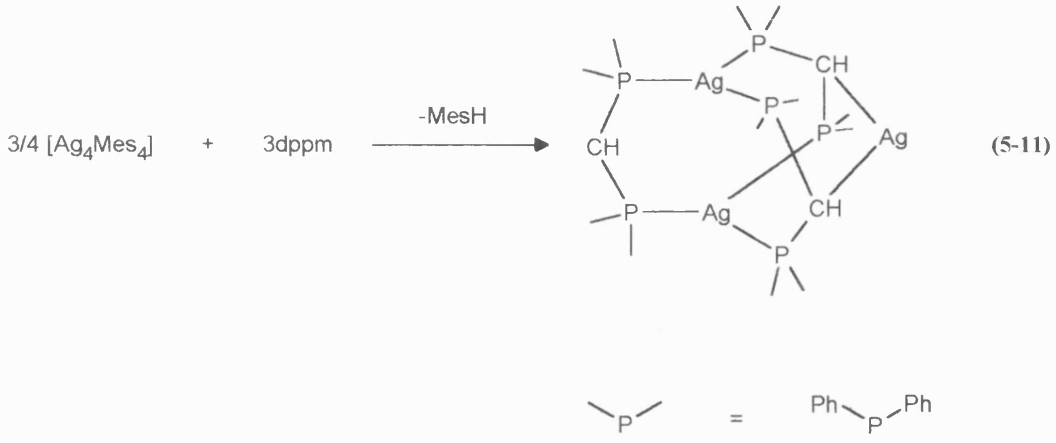

The reactivity of silicone grease towards metal centres has been highlighted by a number of cases where silanone and siloxane fragments have been identified in crystallographically determined coordination compounds. Silicone grease is reported to consist primarily of polydimethylsiloxane (>80%), dimethylcyclosiloxane (<1%, ring size unknown) and hydroxy terminated dimethylsiloxane (5-10%). [303] Recrystallisation of $K[InH(CH_2CMe_3)_3]$ in the serendipitous presence of silicone grease has been reported to yield a pseudo-crown ether type complex $[K^+]_3[K(Me_2SiO)_7^+][InH(CH_2CMe_3)_3^-]$ where one quarter of the potassium atoms are enclosed by a planar cyclo-$(Me_2SiO)_7$ ligand. The crystallisation is reported as taking less than 24 hours although the silicone grease was in high concentration. [303] Silicone grease is also thought to be responsible for unprecedented insertion of a dimethylsilanone moiety into a Yb-N bond. In this case recrystallisation of $[Yb(C_3N_2HMe_2\text{-}3,5)_2(C_5H_4Me)]$ in the presence of trace silicone grease over several months resulted in the complex $[\{Yb(\eta^2\text{-}C_3N_2HMe_2\text{-}3,5)(\mu\text{-}\eta^1\text{: }\eta^2\text{-}OSiMe_2C_3N_2HMe_2\text{-}3,5)(\eta\text{-}C_5H_4Me)\}_2]$. [304]

5.3 SINGLE CRYSTAL X-RAY STRUCTURE DETERMINATION OF {2-(dimethylaminomethyl)phenyl}silver(I) (24)

X-Ray diffraction quality crystals were isolated by refrigeration of the toluene extract of crude **(24)** obtained during its preparation. The crystals appeared fairly stable to light and moisture at room temperature, although in solution and at higher temperatures decomposition was a problem. X-ray diffraction was carried out at low temperature (-100°C), to minimise crystal degradation.

The crystal structure of **(24)** is comprised of an Ag_4 planar core where adjacent pairs of silver atoms are bridged by aryl groups. Pendant $-CH_2NMe_2$ groups bound to each of the aryl ligands additionally coordinate to only two of the silver atoms, resulting in two distinct silver environments, a two coordinate distorted linear array (AgC_2, Ag1 and Ag3) and a distorted four-coordinate geometry (AgC_2N_2, Ag2 and Ag4). The crystal structure is shown in plan and side view in figures 5-10 and 5-11 respectively.

The Ag_4 core is essentially flat, deviations from the plane are only 0.01Å for the silver atoms. The core however is not a perfect square but distorted significantly into a parallelogram arrangement. The Ag-Ag-Ag angles are smaller where two coordinate silver (Ag1, Ag3) occupies the apex of the angle [∠Ag-Ag-Ag : 82.21, 82.76°]. The angles around the four coordinate silvers (Ag2, Ag4) are appreciably larger [∠Ag-Ag-Ag : 97.41, 97.59°]. This parallelogram arrangement results in the four coordinate silver atoms occupying positions further into the core than might otherwise be expected. Distances within the core between adjacent silver atoms are fairly constant [Ag-Ag: 2.729-2.748Å] despite the core distortion away from a perfect square. The mean Ag-Ag distance of 2.738Å is slightly shorter than

observed in the metal (2.89Å) and this might indicate some weak metal-metal bonding interactions.

The aryl rings lie approximately perpendicular to the plane of the Ag_4 core. The bridging carbons do not lie in this plane but are displaced some 0.82-0.97 Å (27.0-32.7 °) from it. Two of these carbons lie above and two below the plane, arranged around the ring in an alternate up-down pattern (Figure 5-11). The aryl groups bridging silver atoms are bound closer to the two coordinate silvers (Ag-C: 2.140-2.172Å) than to the four coordinate silver atoms (Ag-C : 2.351-2.416Å). This is brought about by the perpendicular planes containing the aryl rings being twisted with respect to the Ag_4 parallelogram.

Pendant $-CH_2NMe_2$ groups on the aryl rings bind only to Ag2 and Ag4. Each of these silver atoms are coordinated by nitrogen from both above and below the Ag_4 plane. Where the bridging carbon in an aryl group is displaced above the plane, its pendant amine coordinates from below it, and vice-versa. The silver-nitrogen distances in **(24)** are significantly longer (Ag-N : 2.49-2.56Å) than typical Ag-N distances found in donor adducts of silver iodide with morpholine (2.39Å), [305] piperazine (2.32Å) [306] and piperidine (2.329Å). [307] Longer Ag-N distances are observed in a related structure 2-silver(dimethylaminomethyl)ferrocene tetramer (Figure 5-5) (2.94Å) where silver is essentially digonal with no significant Ag-N interactions.[280] However Ag-N distances in the structure of **(24)** are significant and are of the order of those found in AgN_3 (2.561Å). [305]

The structure of **(24)** is related to those of other complexes e.g. perfluoro-1-methyl-1-propenyl silver(I) $[CF_3CF=C(CF_3)Ag]_4$ (Figure 5-4), [21] mesitylsilver(I) $[AgMes]_4$ (Figure 5-6) [247, 248] 2-silver(dimethylaminomethyl)ferrocene (Figure 5-5), [280] and is similar to a number of copper

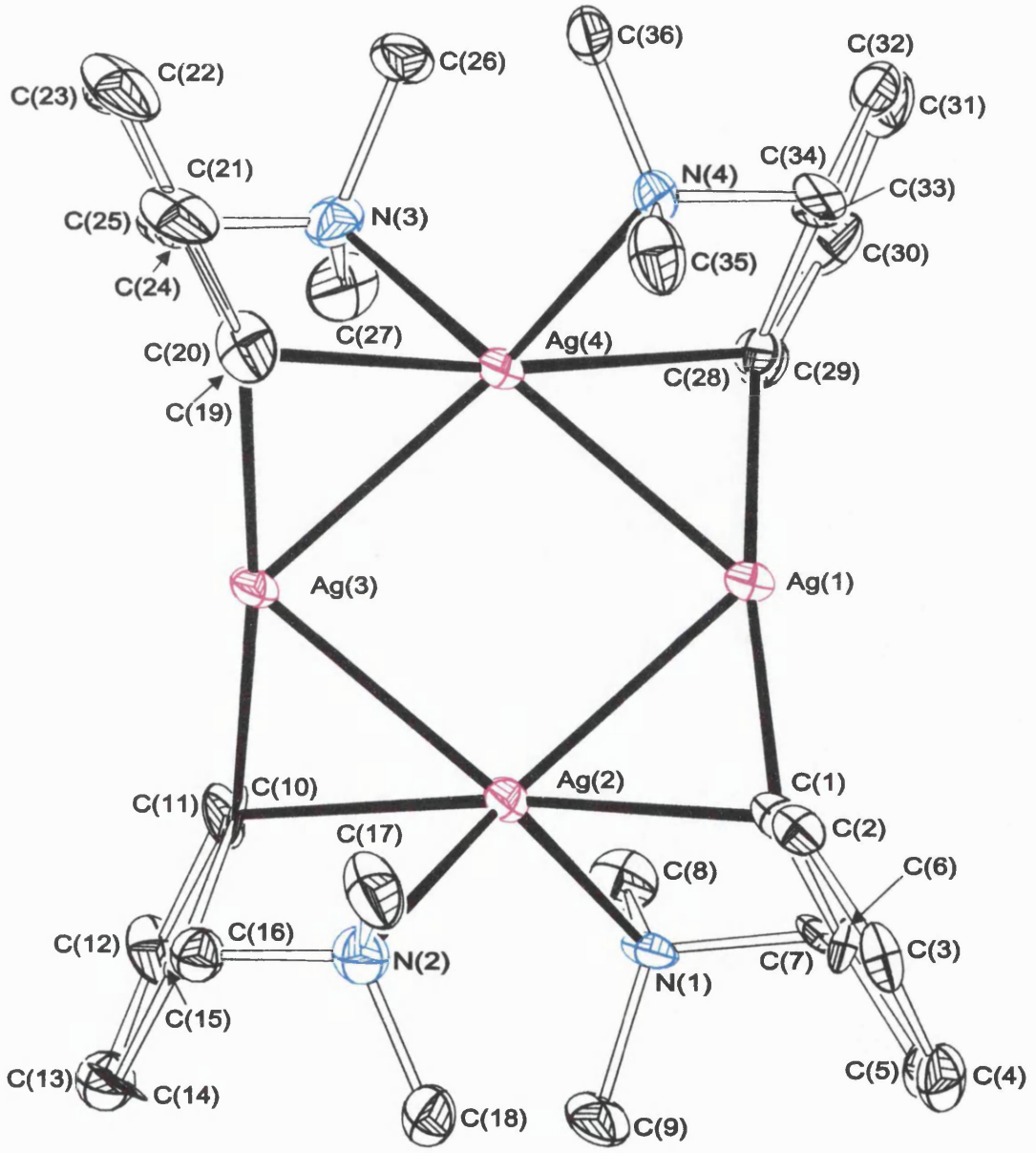

Figure 5-10 Structure of {2-(dimethylaminomethyl)phenyl}silver(I) **(24)**, viewed from above the plane of silver atoms.

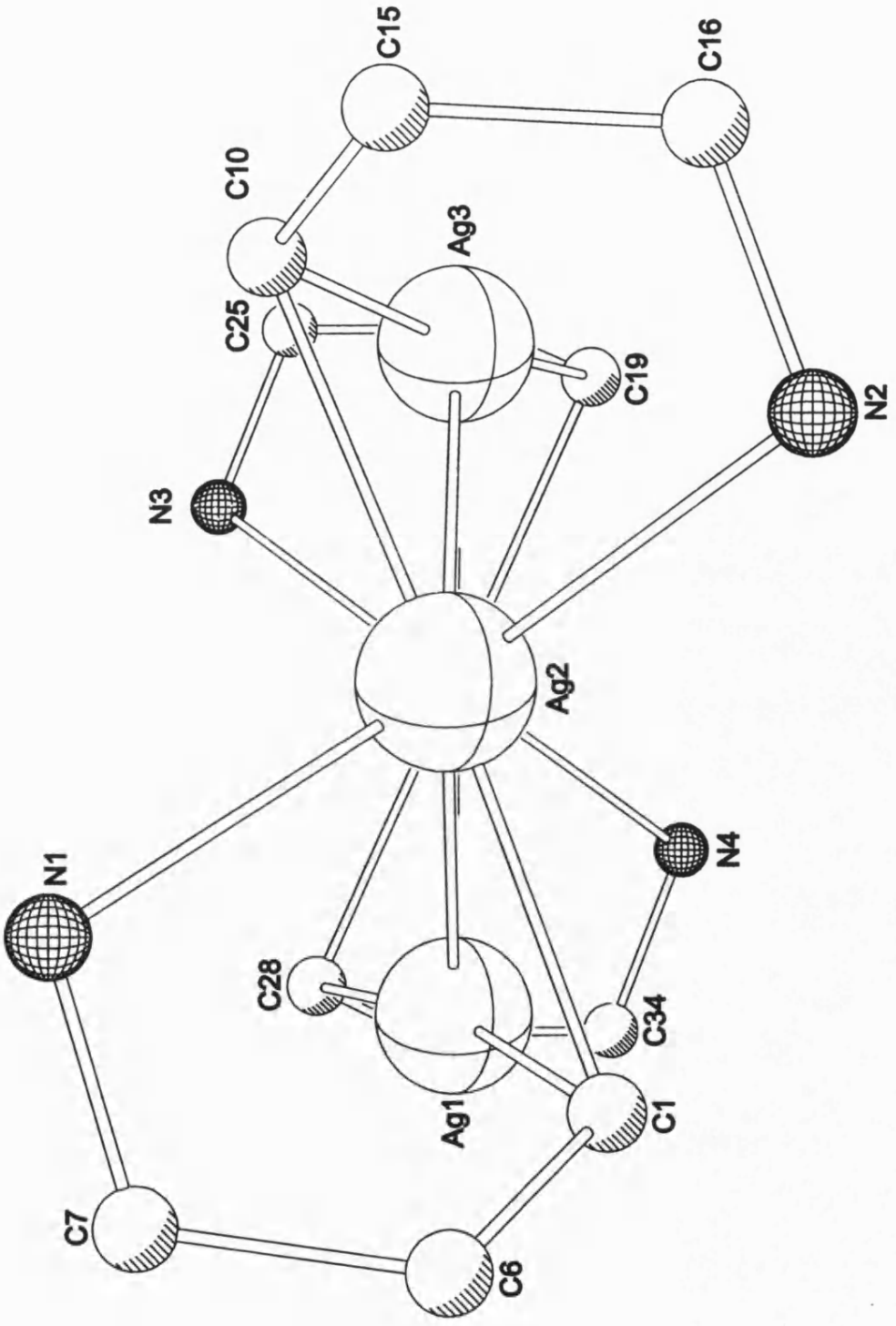

Figure 5-11 Structure of {2-(dimethylaminomethyl)phenyl}silver(I) **(24)**, viewed in the plane of silver atoms.

tetramers. [308] In all the silver derivatives, silver is bound to a sp^2-hybridised carbons. Whereas each of the reported silver structures is essentially symmetrical, the structure of **(24)** is unique in that it contains two distinct silver environments.

Mean silver-silver distances (2.738Å) are shorter in **(24)** than in the related perfluoroalkenyl (2.761Å) and mesitylsilver (2.744Å) complexes although comparable to the 2-silver(dimethyl aminomethyl)methyl ferrocene tetramer (2.740Å). Silver-carbon bonds in these related compounds are in the range 2.17-2.20Å, slightly longer than the shorter Ag-C observed in **(24)**.

The structure of **(24)** may be visualised as two distorted linear $[R\text{-}Ag\text{-}R]^-$ anions (∠C-Ag-C : 171-173 °) bridged by two base-stabilised Ag^+ cations, $[R_2Ag]^-$ anions being a common feature of organosilver chemistry (see for example Figure 5-2). This visualisation has been used recently to describe the structure of the silver acetylide adduct $[Ph_3PAgC{\equiv}CPh]_4$. [285] In this case a central Ag_4 core is grossly distorted into a 'flat-butterfly' configuration and the $[AgR_2]^-$ and $[Ag(PPh_3)_2]^+$ units are easier to identify.

The tetramer arrangement found in **(24)** is also strikingly similar to that found in the aurate complex $[Au_2Li_2(C_6H_4CH_2NMe_2\text{-}2)_4]$ (Figure 5-12) where $[R_2Au]^-$ anionic fragments are bridged by the lithium cations each bonded to two $-CH_2NMe_2$ groups. [265] Solution NMR studies on the analogous argentate complex suggest that it displays a similar arrangement in solution. [263] It has been postulated that the asymmetry of the aryl bridge in these bimetallic clusters increases down the series Cu, Ag, Au, but until now no evidence of this asymmetry was apparent in $[AgR]_4$ tetramers.

Relevant bond lengths and bond angles are summarised in Table 5-3, while further data including atomic coordinates are listed in Appendix A4.4.

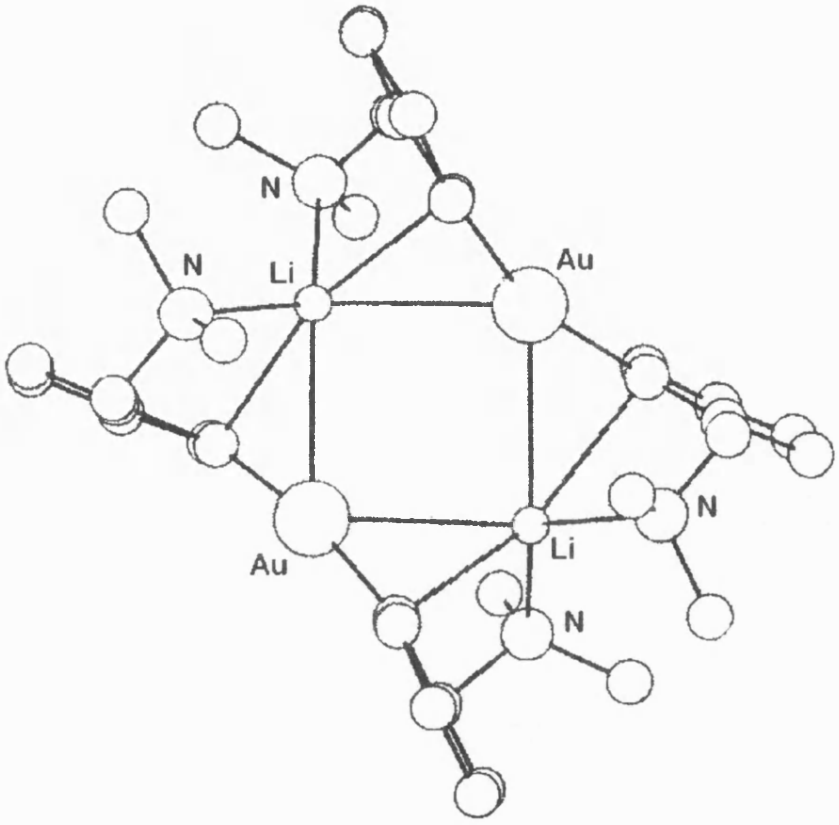

Figure 5-12 Structure of the aurate complex $[Au_2Li_2(C_6H_4CH_2NMe_2\text{-}2)_4]$. [263]

Table 5-3 Relevant bond lengths (Å) and angles (°), complex **(24)**.

Ag-Ag		**Ag-$C_{(short)}$**		**Ag-$C_{(long)}$**		**Ag-N**	
Ag1-Ag2	2.732(2)	Ag1-C1	2.162(14)	Ag2-C1	2.403(14)	Ag2-N1	2.539(10)
Ag2-Ag3	2.748(2)	Ag1-C28	2.167(12)	Ag2-C10	2.416(12)	Ag2-N2	2.493(11)
Ag3-Ag4	2.743(2)	Ag3-C10	2.140(13)	Ag4-C19	2.362(12)	Ag4-N3	2.544(11)
Ag4-Ag1	2.729(2)	Ag3-C19	2.172(12)	Ag4-C28	2.351(12)	Ag4-N4	2.563(10)
Ag-Ag-Ag		**C-Ag-C**		**Ag-C-Ag**		**N-Ag-N**	
Ag1-Ag2-Ag3	97.41(6)	C1-Ag1-C28	171.0(5)	Ag1-C1-Ag2	73.3(4)	N1-Ag2-N2	119.1(3)
Ag2-Ag3-Ag4	82.21(5)	C1-Ag2-C10	173.0(4)	Ag2-C10-Ag3	73.9(4)	N3-Ag4-N4	117.0(3)
Ag3-Ag4-Ag1	97.59(5)	C10-Ag3-C19	173.4(4)	Ag3-C19-Ag4	74.3(4)		
Ag4-Ag1-Ag2	82.76(5)	C19-Ag4-C28	173.1(4)	Ag4-C28-Ag1	74.2(4)		

5.4 SINGLE CRYSTAL X-RAY STRUCTURE DETERMINATION OF $[Ag(PPh_3)]_4(Me_2(O)SiOSi(O)Me_2)_2$ (25)

X-ray diffraction quality crystals of **(25)** were isolated from toluene after an attempt to recrystallise **(24)** in the presence of triphenylphosphine. The crystals rapidly lost solvent and data collection was carried out at low temperature (-100°C).

The structure of **(25)** consists of an Ag_4O_4 core arranged in a step conformation where oxygen atoms within the core are part of two equivalent bridging siloxide ligands. Additionally each silver is bonded to a single triphenylphosphine molecule resulting in two distinct silver environments; namely, distorted trigonal (AgO_2P, Ag1) and distorted tetrahedral (AgO_3P, Ag2). The molecular structure is made up of two asymmetric units with an inversion centre at the centre of the cluster. The full structure of **(25)** is shown in Figure 5-13. A number of atoms are omitted in Figure 5-14 to allow a clear view of the central core.

Silver-silver distances within the core are too large to indicate any metal-metal interactions (Ag-Ag: 3.090, 3.336Å). The angle between adjacent Ag_2O_2 rings as typified by Ag1-O1-Ag2 is 99° and is presumably dictated by the bite angle of the siloxide ligand. Silver-oxygen bond lengths in the core are in the range 2.321-2.368Å except for Ag1-O1′ which is considerably shorter (Ag1-O1: 2.010Å) thus indicating that the structure is slightly tapered at both ends. Each siloxide ligand provides two distinct oxygen atoms to the core. At the corner (O1) the oxygen bonded to Si1 is bridging two silver atoms while in the centre (O2) the oxygen bonded to Si2 bridges three silver atoms. Silver-oxygen bond distances are not consistently different between these two types.

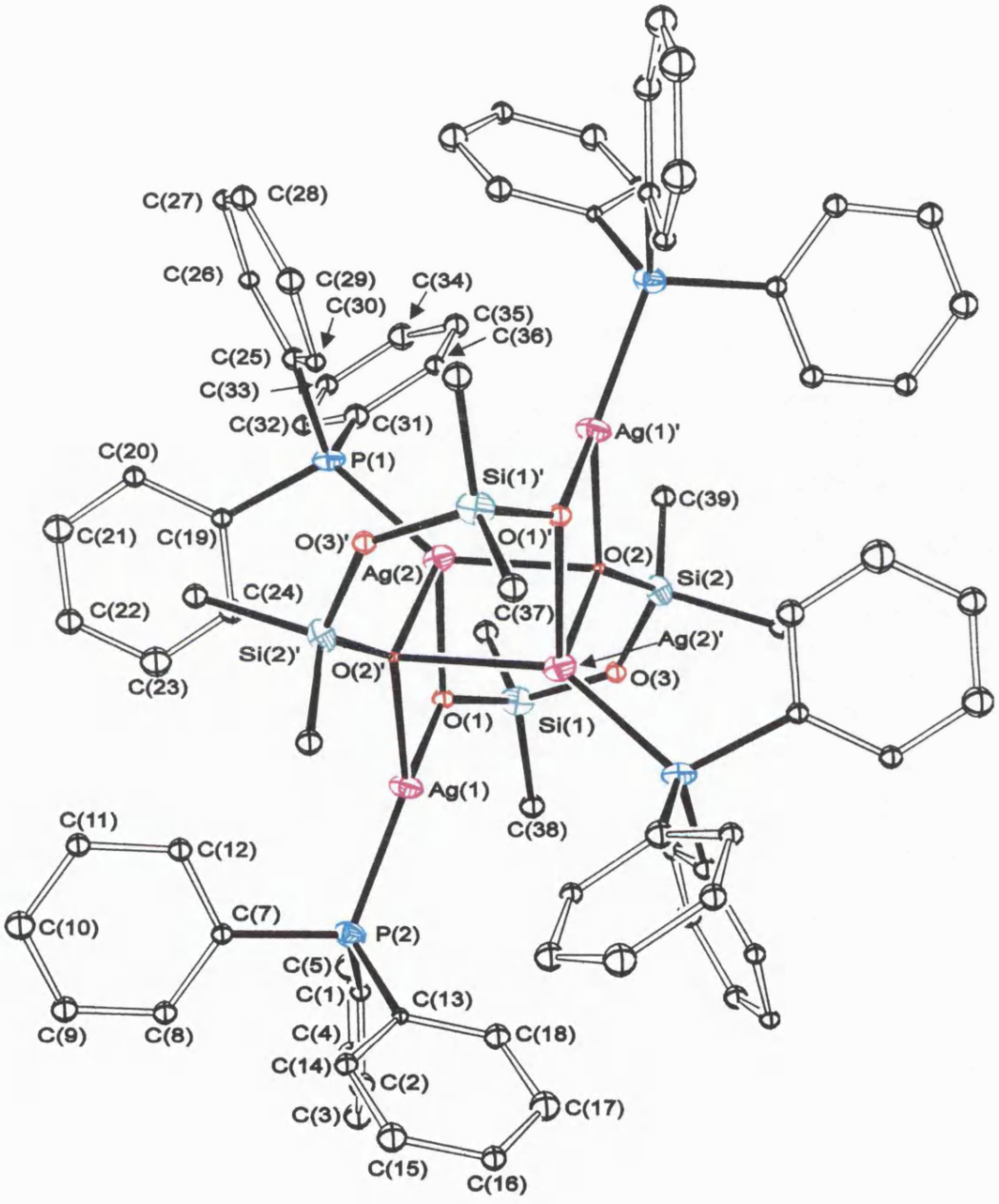

Figure 5-12 Structure of $[Ag(PPh_3)]_4(Me_2(O)SiOSi(O)Me_2)_2$ **(25)**.

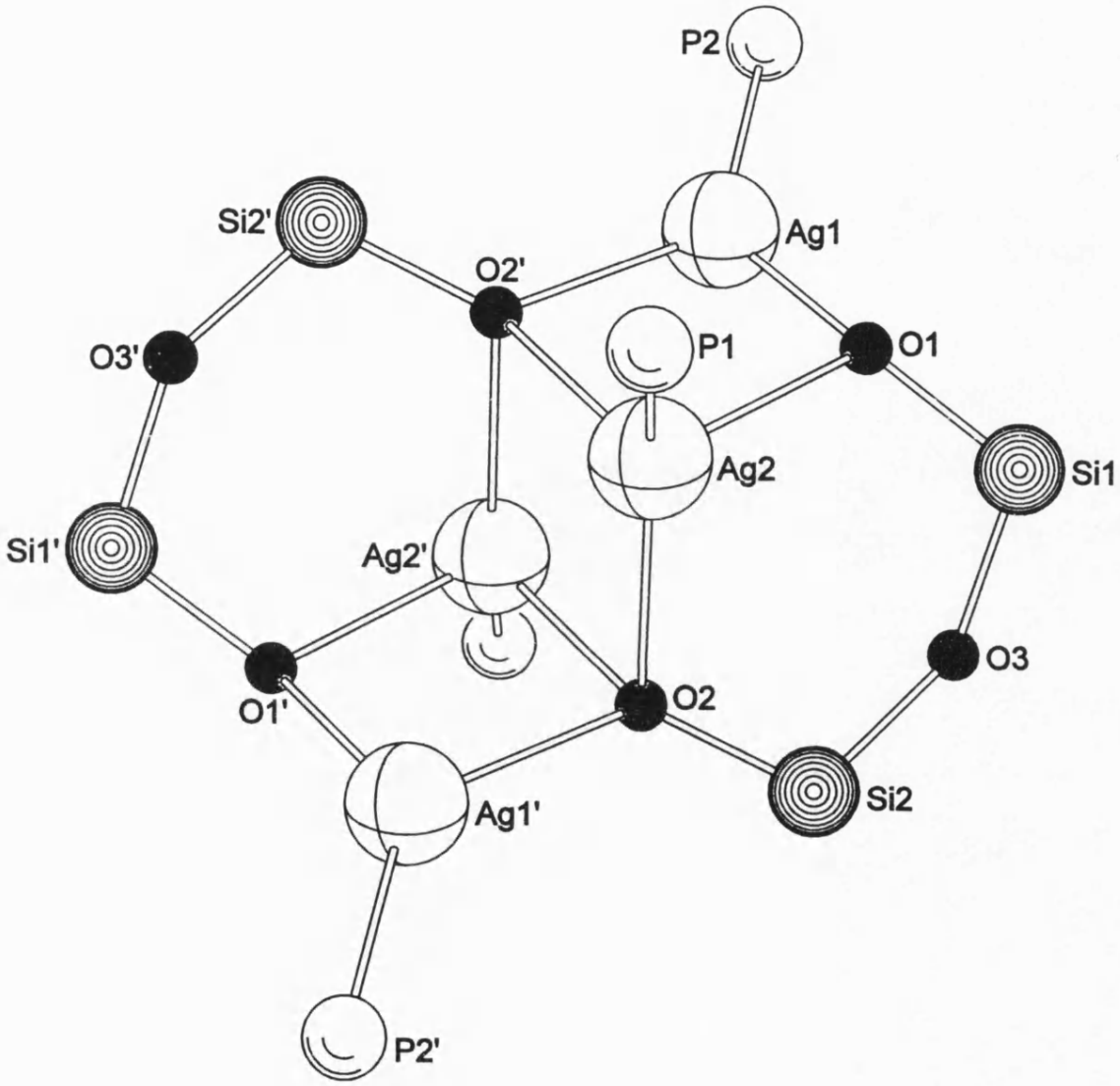

Figure 5-13 Core structure of $[Ag(PPh_3)]_4(Me_2(O)SiOSi(O)Me_2)_2$ **(25)**, incidental atoms are omitted for clarity.

A phosphorus bonded to each silver completes their coordination sphere. The Ag-P bonds are shorter than expected (Ag-P: 2.246-2.262Å), other bond lengths for triphenylphosphine adducts of silver halides such as $[AgX(PPh_3)]_4$ (X = Cl, I) being considerably longer at 2.372-2.466Å. Similarly silicon-oxygen bonds where oxygen is part of the Ag_4O_4 unit are considerably shorter (Si-O: 1.568-1.578Å) than the silicon-oxygen bond lengths in the ligand (Si-O3: 1.647-1.649Å).

The three-coordinate silver displays a distorted trigonal geometry and similarly the four-coordinate silver is highly distorted from a tetrahedral arrangement. In general the phosphorus-silver-oxygen angles in both cases are larger than the corresponding oxygen-silver-oxygen angles (∠PAgO: 134.2, 114.9, 142.1°; ∠OAgO: 91.7°). Relevant angles and bond lengths are summarised in Tables 5-4 and 5-5 respectively, further structural data (including atomic coordinates) are provided in Appendix A4.5.

Silver siloxide and alkoxide compounds are rare and poorly characterised due to their instability as silver(I) is known to prefer 'softer' ligands over the 'harder' oxygen containing ligands. The compound **(25)** is the first example of a structurally characterised molecule containing an Ag-O-Si linkage.

The overall structure of **(25)** is similar to that determined for the 'step' type silver iodide-triphenylphosphine adducts $[AgI(PPh_3)]_4$, [87] where the core is made up of an Ag_4I_4 unit and each silver is further coordinated by a triphenylphosphine to give three and four coordinate silver atoms (Figure 1-11), analogous to **(25)**. Unfortunately only incomplete structural data have been reported for this tetramer. The $(AgO)_2$ rings in the structure of **(25)** are somewhat similar to those found for linked silver carboxylate dimers (Figure 2-4) and in cases such as

this, Ag-O distances are of the order of 2.2-2.9Å. A number of copper(II) siloxide structures have been determined e.g. $[Cu(OSiPh_2OSiPh_2O)_2 - \mu - \{Li(py)_2\}_2]$ [309] and $[Cu\{OSi(OCMe_3)_3\}_2py_2]$, [310] these structures containing chelating and terminal siloxide ligands with respect to copper, rather than bridging ligands as in **(25)**.

Table 5-4 Relevant bond angles (°), compound **(25)**.

P2-Ag1-Ag2	167.0(2)	O1-Ag1-Ag2	44.5(4)
O1-Ag1-P2	134.2(4)	P1-Ag2-Ag1	124.2(3)
O1-Ag2-Ag1	36.5(5)	O1-Ag2-P1	114.9(5)
O2-Ag2-Ag1	93.3(4)	O2-Ag2-P1	142.1(4)
O2-Ag2-O1	91.7(6)	Ag2-O1-Ag1	99.0(7)
Si1-O1-Ag1	133.7(9)	Si1-O1-Ag2	113.3(11)
Si2-O2-Ag2	116.0(7)	Si2-O3-Si1	137.1(11)

Table 5-5 Relevant bond lengths (Å), compound **(25)**.

Ag-Ag		**Ag-O**		**Ag-P**		**O-Si**	
Ag(1)-Ag(2)	3.336(6)	Ag(1)-O(1)	2.010(21)	Ag(1)-P(2)	2.246(9)	O(1)-Si(1)	1.578(25)
Ag(2)-Ag(2a)	3.090(6)	Ag(2)-O(1)	2.368(16)	Ag(2)-P(1)	2.262(8)	O(3)-Si(1)	1.647(21)
		Ag(2)-O(2)	2.321(18)			O(2)-Si(2)	1.568(20)
						O(3)-Si(2)	1.649(17)

5.5 FILM GROWTH RESULTS

Crude compound **(24)** was tested as a potential precursor for the growth of thin silver films by AACVD. Chemical vapour deposition studies were carried out at 310°C under a nitrogen atmosphere at 1 bar pressure. Samples were dissolved in THF, nebulised and swept into the reaction chamber using a nitrogen carrier gas. Films were grown on glass substrates (substrate preparation procedures are outlined in Appendix 6).

Two experiments were undertaken a) with compound **(24)** and b) with compound **(24)** in the presence of a stoicheometric quantity of triphenylphosphine. Some 0.5-0.6g of precursor dissolved in 40 cm^3 of THF was utilised in each case. With flow rates of 0.8-0.9 $Lmin^{-1}$ the solution was passed into the reactor in 17 minutes. In the case of a), a faint yellow mark on the upstream end of the substrate was the only evidence of deposition having occurred. Additionally, solubility in the nebulised solvent was observed to be less than ideal. In an attempt to increase solubility, compound **(24)** was dissolved in THF in the presence of one molar equivalent of triphenylphosphine. However, the solution decomposed within the nebuliser within a few minutes and no signs of deposition were observed.

5.6 EXPERIMENTAL

Preparation of [2-(dimethylaminomethyl)phenyl]silver(I) ***(24)***

A solution of butyllithium (51.2 mmol) in diethyl ether (15 cm^3) was added dropwise to a solution of N,N-dimethylbenzylamine (7.0g, 51.8 mmol) in diethyl ether (50 cm^3). The reactant mixture was stirred for 72 hours under nitrogen resulting in a thick lemon precipitate. The mixture was cooled to -77°C using a dry ice-acetone bath. Silver bromide (9.7g, 51.7 mmol) was added slowly to the constantly stirred reaction mixture. The reagents were stirred at this temperature for several hours and allowed to warm to room temperature overnight. While cold the mixture appeared grey in colour, although on warming a brown precipitate was evident.

The precipitate was allowed to settle and the supernatant liquid removed using a cannula. The precipitate was washed successively with diethyl ether (40 cm^3) and pentane (20 cm^3). The product was extracted with toluene (300 cm^3 in three aliquots). Toluene was immediately removed from the combined extracts to yield a red solid. A small amount of the toluene extract was refrigerated to yield crystals that were subsequently analysed by X-ray diffraction. Yield 1.8 g, 14 %.

Analysis of recrystallised material: found (calculated for $C_9H_{12}NAg$) C, 44.6 (44.7); H, 5.02 (5.00); N, 5.72 (5.79) %. IR (Nujol mull) 400-1800 cm^{-1}: 745sh, 752sh, 804w, 841sh, 1009sh, 1038w, 1098w, 1154w, 1169w, 1260w, 1306w, 1352w, 1401w, 1568w. ^1H NMR ($CDCl_3$) δ: 7.34-7.29 (m, 4H, $C_6\underline{H}_4CH_2NMe_2$), 3.42 (s, 2H, $-CH_2-$), 2.24 (s, 6H, $-NMe_2$). ^{13}C NMR ($CDCl_3$) δ: 129.1 ($\underline{C}_6H_4CH_2NMe_2$), 128.2 ($\underline{C}_6H_4CH_2NMe_2$), 127.0 ($\underline{C}_6H_4CH_2NMe_2$), 65.8 ($-CH_2$), 45.4 ($-NMe_2$).

Hydrolysis of [2-(dimethylamino)methyl]phenylsilver(I) ***(24)*** *and the formation of* $[Ag(PPh_3)]_2\{Me_2(O)SiOSi(O)Me_2\}$ ***(25)***

[2-(dimethylamino)methyl]phenylsilver(I) **(24)** (0.10g, 0.4 mmol) and triphenylphosphine (0.22g, 0.8 mmol) were dissolved in $30cm^3$ of freshly distilled toluene. The glass joint of the flask was lightly greased with high vacuum dimethylsilicone grease. The stoppered flask was wrapped in foil and stored at -10°C for several weeks, at which point small clear crystals began to form.

Analysis: found (calculated for $C_{40}H_{42}O_3P_2Si_2Ag_2$) C, 53.1 (53.1); H, 4.59 (4.68) %. IR (Nujol mull) 400-1800 cm^{-1}: 411w, 505wsh, 519wsh, 693sh, 745, 774, 843wb, 943, 988b, 1028w, 1096wsh, 1240wsh, 1435ssh. ^1H NMR ($CDCl_3$) δ: 7.50-7.14 (m, 45H, PPh_3 + $C_6\underline{H}_5CH_3$), 2.35 (s, 12H, $C_6H_5C\underline{H}_3$), 0.17 (s, ~3H, O-Si$\underline{Me}_2$), 0.14 (s, ~3H, O-Si$\underline{Me}_2$), 0.11-0.10 (m, ~6H, O-Si$\underline{Me}_2$). ^{13}C NMR ($CDCl_3$) δ: 137.8 (s, $\underline{C}_6H_5CH_3$), 134.1 (d, 16.5Hz, PPh_3), 132.1 (d, 28.6Hz, PPh_3), 130.1 (s, PPh_3), 129.0 (s, $\underline{C}_6H_5CH_3$), 128.7 (d, 10Hz, PPh_3), 128.2 (s, $\underline{C}_6H_5CH_3$), 125.3 (s, $\underline{C}_6H_5CH_3$), 21.4 (s, $C_6H_5\underline{C}H_3$), 0.92 (s, OSi$\underline{Me}_2$), 0.87 (s, OSi$\underline{Me}_2$), 0.71 (s, OSi$\underline{Me}_2$). ^{31}P NMR ($CDCl_3/CH_2Cl_2$) (22°C) δ: 8.7 (s). (-40°C) δ: 7.2 [d-unresolved, $^1J(^{109}Ag\text{-}^{31}P)$~470Hz]. (-80°C) δ: 6.3 (dd, $^1J(^{107}Ag\text{-}^{31}P)$ = 602 Hz, $^1J(^{109}Ag\text{-}^{31}P)$ = 694 Hz). ^{29}Si NMR ($CDCl_3/CH_2Cl_2$/ $Cr(acac)_3$) (21°C) δ: -8.1 (s), -18.9 (s). (-40°C) δ: -8.0 (s), -18.2 (s). (-80°C) δ: -7.1 (s), -17.1 (s).

CONCLUSIONS

Four classes of potential precursors for the CVD of silver have been investigated. Compounds synthesised have been fully charaterised and screened in a limited number of CVD experiments. This short conclusion aims to compare and contrast the compounds prepared in Chapters Two to Five and assess their suitability as precursors for the AACVD of silver. Selected film growth results are shown in Table 6-1.

In terms of the ease of preparation, silver carboxylates and their phosphine adducts are extremely easy to prepare and are reasonably stable in air at room temperature for extended periods. Trimethylphosphine adducts were noticed to slowly lose trimethylphosphine at room temperature, although it is not known how significant the rate of loss is. Fluorinated carboxylate precursors and their phosphine adducts are also simple to synthesise and are stable at room temperature in air. The silver β-diketonate and β-ketoiminate adducts are fairly simple to prepare, provided that a few precautions are taken during the synthesis. These compounds have a variable stability at room temperature dependent on the nature of the β-diketonate or β-ketoiminate itself, compounds containing fluorinated β-diketonates being the most stable. The organosilver compounds are the most synthetically challenging precursors looked at during the course of this project. The compound synthesised being stable in air at room temperature for short periods, stability reduced at higher temperature or in solution.

Of the range of silver carboxylates and their phosphine adducts prepared, only the adducts have displayed significant film growth properties. Triphenylphosphine adducts have been shown to achieve only limited growth rates, but in cases where films could be grown, they were of

reasonable reflectivity. Trimethylphosphine adducts showed substantially increased growth rates although in some cases this was detrimental to surface quality and reflectivity. Carbon was the only consistent contaminant in these films, although trace phosphorus was detected in cases where trimethylphosphine adducts were used.

In contrast to the unfluorinated carboxylates, the fluorinated carboxylates achieved sufficient solubility and volatility to grow films without the need for additional phosphines. These films grew at moderately high rates but were of limited quality. Bis(phosphine) adducts of these carboxylates were shown to grow higher quality films but at reduced growth rates (in contrast to the unfluorinated carboxylates where addition of phosphines increased growth rates). Carbon was a consistent contaminant in these films with fluorine (generally trace amount only) detected in all but one film.

Silver β-diketonate adducts displayed a variety of film growth properties dependant on the nature of the β-diketonate ligand. Fluroinated β-diketonates displayed superior film growth properties over unfluorinated β-diketonates. Of note is the fact that in these screening tests the compound containing the tfac ligand proved to be superior (in both growth rates and film quality) than to the compound containing the hfac ligand (upon which most current literature work has been based). β-Ketoiminates also grew high quality films at high growth rates. Carbon was the only consistent contaminant in films grown from these precursors.

Only one organosilver compound was tested during these studies and as such these results should not necessarily be regarded as representative. The compound proved ineffective at film growth under these conditions in the presence or absence of solubilising triphenylphosphine.

Table 6-1 Selected data for the comparison of films grown from precursors form Chapters 2-4.

	Estimated Growth Rates (Åmin^{-1})	% Reflectivity [a] (coating side)	Sheet Resistance [b] Ω/□	Detected Impurities EDXS	Surface Morphology
$AgO_2CMe(PPh_3)_3$	—	49.7	∞	too thin for analysis	too thin for analysis
$AgO_2CtBu(PMe_3)_2$	13.7	0.7	168	C, P (trace)	level surface comprised of a thick mat of crystals
$AgO_2CtBu(PPh_3)_2$	5.7	22.2	∞	C	smooth film
$AgO_2CMes(PMe_3)_2$	4.1	46.6	∞	C	rough undulating surface
$AgO_2CC_3F_7$	3.0	0.5	4.2	C	very rough surface containing crystalline material
$AgO_2CC_6F_{13}$	9.0	4.9	14.5	C, F	quite rough surface
$AgO_2CC_6F_{13}(PPh_3)_2$	2.7	45.9	∞	C, F (trace)	smooth surface
$AgO_2CC_7F_{15}$	4.8	18.1	2.7×10^6	C, F (trace)	roughish surface
$Ag(tfac)PPh_3$	16+	62.5	2.2	C	fairly smooth regular surface
$Ag(hfac)PPh_3$	10.6	0.3	186	C, P (trace)	even surface comprised of a thick mat of crystals
$Ag(hfacNhex)PPh_3$	16.4	64.7	1.1	C	fairly smooth even surface
$Ag(hfacNchex)PPh_3$	19.1	51.4	167	C	fairly smooth but undulating surface

[a] $\lambda = 550$ nm, corresponding to the peak in the eye response curve [b] resistance was measured over a 25 mm square

APPENDICES

APPENDIX ONE *^{109}Ag Nuclear Magnetic Resonance Spectroscopy*

At first glance there appears no obvious reason why silver NMR is not a more commonly used tool in chemistry. The high abundance of two I = ½ nuclei appear to make this area of chemistry amenable to multinuclear NMR studies. However in addition to the problem of low resonant frequencies (normally requiring a low frequency probe), there are two major difficulties; receptivity and relaxation times.

Naturally occurring silver contains approximately equal amounts of the two isotopes 107 and 109 (Table 6-2). Due to the larger magnetogyric ratio, the less abundant 109 nucleus is more receptive to NMR observation, but only by a factor of 1.4, having a relative receptivity about 28% that of carbon 13. [311]

Table 6-2 Nuclear Properties of Silver. [311]

Isotope	Spin	Natural abundance N / %	Nuclear Magnetic moment m	Magnetogyric ratio g, /10^7radT^{-1}s^{-1}	NMR frequency, MHz [a]	Relative receptivity [b]
107	-½	51.83	-0.1135	-1.08	4.05	0.195
109	-½	48.17	-0.1305	-1.24	4.65	0.276

[a] (^{1}H = 100 MHz, 2.3488T) [b] in comparison with ^{13}C NMR

The other major difficulty lies in the fact that the relaxation times for these nuclei are so long (for ^{109}Ag in $AgNO_3/D_2O$, T_1 is 1115 seconds). [312] This has been attributed to the lack of quadrapolar nuclei (quadrapolar relaxation mechanism) and because silver does not normally exist in proximity to protons (dipolar relaxation mechanism). [313] The relaxation times may be reduced by the addition of paramagnetic materials, but this may also induce shifts and/or line broadening. Additionally the improvement of spectra from nuclear Overhauser enhancement (NOE) experiments is not possible due to the negative gyromagnetic ratios of both nuclei. Polarisation transfer experiments (INEPT) have been shown to increase the quality of spectra (ie. the signal to noise ratio) by up to 20 fold, [314] although to reach this level of enhancement, the silver atom has to be directly bonded to a more sensitive nucleus (^1H or ^{31}P).

Initial detection of the nuclear magnetic resonance of silver dates from the 1950's with reports of silver resonances found in strong aqueous solutions of silver nitrate, [315, 316] and in AgF crystals. [317] Aside from studies of the metal, silver NMR did not progress to any large extent until the advent of Fourier transform methods. Early work reported 'Quadriga' pulse techniques to detect very weak Ag NMR signals, [318] and studies of silver ions in aqueous solutions. [319] Subsequent work investigated inorganic and organic silver complexes by dissolving silver salts in various solvents; acetonitrile, propionitrile, pyridine, ethylamine, aqueous sodium thiosulphate, [320] and water - ethylamine mixtures. [312]

These studies are complemented by work examining the concentration dependence of Ag(I) salts in solutions of water, acetonitrile and water/acetonitrile, [321] and in non-aqueous solvents, acetone, methanol, THF, pyridine. [322] Silver nitrate - thiourea reactions in DMSO have been observed using a combination of ^{13}C and ^{109}Ag NMR data. [323] Similar work subsequently observed complexation with various nitrogen and nitrogen-sulphur ligands. [324]

Spin-spin coupling with silver has been observed with ^{1}H, ^{7}Li, ^{13}C, ^{19}F, ^{31}P and ^{195}Pt (Table 6-3). The majority of coupling constants for silver have been reported via ^{31}P NMR, silver coupling to phosphine ligands is readily observed although cooling may be required to reduce the lability of complexes. [325]

Table 6-3 Spin-spin coupling constants for ^{109}Ag.

J	Complex type	Range (Hz)	Ref
$^{n}J(^{109}Ag\text{-}^{1}H)$	Organometallic or N-donors	0.3-14	327
$^{1}J(^{109}Ag\text{-}^{7}Li)$	$[Ag_2Li_2(C_6H_4CH_2NMe_2\text{-}2)_4]$	3.9	265
$^{1}J(^{109}Ag\text{-}^{13}C)$	Organometallic	96-164	283, 328-330
$^{1}J(^{109}Ag\text{-}^{13}C)$	Carbonyl	190-284	331
$^{n}J(^{109}Ag\text{-}^{19}F)$	Fluoroalkyl	8-37	268
$^{1}J(^{109}Ag\text{-}^{31}P)$	PR_3, $P(OR)_3$	253-1217	325, 326
$^{2}J(^{109}Ag\text{-}^{31}P)$	$[Ag(CHRPPh_3)X]$	9-10	329, 330
$^{1}J(^{107,109}Ag\text{-}^{107,109}Ag)$	Ag_2Ru_4 clusters	30-49	332, 333
$^{1}J(^{195}Pt\text{-}^{109}Ag)$	$[L_3PtN\sim\sim\sim NAgBr]$	~170	334

A number of publications report the application of doping agents to decrease relaxation times, using metal ions; (Mn^{2+}), [315, 316] (Ni^{2+}), [321, 322] or organic ligands. [335-337] This technique is not in

widespread use due to shifting or broadening of resonance signals, however the use of organic species has been found to have a less drastic effect. Addition of 0.02M TANOL (2,2,6,6-tetramethyl-4-hydroxypiperidine-1-oxyl) as a doping agent to aqueous solutions of various silver salts has reduced the need for long experimental run times. These spectra are found to remain sharp although the chemical shift was also found to be dependant on the concentration of TANOL (chemical shifts were corrected by 10ppm for 0.02M TANOL).

Enhancement techniques have been developed for cases where spin-spin coupling is observed in ^{1}H or ^{31}P NMR. [338, 339] The INEPT technique (Insensetive Nuclei Enhancement by Polarization Transfer) depends on a transfer of polarization from a more sensitive nucleus S (^{1}H or ^{31}P) to a less sensitive nucleus I (^{109}Ag). The gain in signal-to-noise ratio using the INEPT sequence can lead under optimal conditions to a factor of up to 20. The attainment of such improvements in the S/N ratio however is difficult, in general the metal centre is not always directly bonded to the S nucleus, and thus the effect of a remote S nucleus reduces the theoretical enhancement to a few percent. However the pulsing rate of the INEPT sequence is no longer governed by the silver T_1 but rather by the S nucleus T_1, the intrinsic experimental time saving derived from the absence of long relaxation delays is appreciable and is about a factor of 400 for ^{109}Ag.

INEPT sequence studies of silver(I) with neutral multidentate donor ligands have progressed to the point of a valuable technique, but only when $^{3}J(H\text{-}Ag)$ is found in the proton spectra. [340-342] Subsequent ^{31}P-Ag INEPT studies have used the ^{31}P nuclei as the sensitive nucleus S, [343] where many values for $^{1}J(Ag\text{-}^{31}P)$ are known. The technique has also provided evidence for direct Ag-Pt bonding [334] and observation of one bond silver-silver coupling. [332, 333] A number of reviews of silver NMR have been published by Goodfellow (1978), [344] Henrichs (1983), [313] Goodfellow (1987) [345] and Mann (1991). [346]

APPENDIX TWO *FAB mass spectrometry*

Fast atom bombardment - mass spectrometry (FAB/MS) is a soft ionisation technique that is readily applied to those compounds for which conventional Electron Ionisation (EI) or Chemical Ionisation (CI) mass spectrometry methods are problematic. The term Fast Atom Bombardment and its acronym (FAB) were first coined in 1981 [347] and resulted from work derived from the established Secondary Ion Mass Spectrometry (SIMS) methodology, the techniques sharing many features. The methods utilise beams of neutral or charged atoms to dislodge (sputter) charged species from the sample into the vapour phase for mass spectrometric analysis.

Distinctions between FAB/MS and SIMS are not clearly defined and there remains some debate as to exact definitions. [348] FAB/MS usually takes place with the sample dissolved in a liquid matrix and SIMS is typically carried out with sputtering from solid samples. However, SIMS techniques may also be used on samples in the form of a liquid matrix and this methodology is distinguished as Liquid-SIMS (LSIMS). SIMS has further developed into a powerful surface analysis tool [349-351] and more recently through Imaging-SIMS to scanning ion microscopy (SIM). [352, 353] FAB/MS experiments carried out in connection with this present study are best described as LSIMS.

In this technique a fast atom beam (Ar, Xe, Cs^+ of 2-25 keV) is aimed at a liquid sample suspended on a probe tip. Liquid samples may be used neat although most compounds are dissolved in a non-volatile liquid matrix, sometimes with the aid of a co-solvent. The liquid droplet form allows for a continually renewed surface area from which the species are sputtered. Glycerol remains the most popular matrix liquid but other possible candidates

include 3-nitrobenzyl alcohol, thioglycerol, DMSO, di-*tert*-amylphenol and various crown ethers. [354] The liquid droplet is suspended on a direct insertion probe tip, typically made of copper or stainless steel. Copper (from the probe) has occasionally been found to incorporate into clusters with the sample or matrix. [355] The beam and sample probe are arranged in such a way that the sputtered species are directed toward the mass spectrum analyser (Figure 6-1).

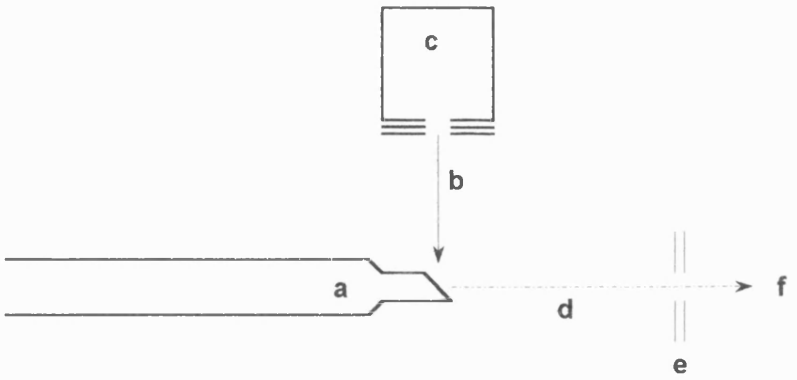

Figure 6-1 Schematic diagram of a simplified FAB or LSIMS source.

(a - probe, b - fast atom beam, c - atom gun, d - sputtered secondary ion beam, e - source ion optics, f - to mass analyser)

'Soft' ionisation techniques have the advantage of producing high mass cluster ions from normally involatile compounds where hard ionisation methods (EI/CI) cannot. FAB/MS spectrometry is reported as being able to detect fragments as large as 15,000 daltons, [354] although a 250-3000 dalton mass-fragment range is more common. Additionally these spectra can be obtained at room temperature which allows analysis of thermally unstable compounds.

Both positive and negative ions may be produced by alterations in the acid-base equilibrium inside the liquid matrix and observation of both cations and anions by fast atom methods are common in the literature. Most FAB spectra resemble CI spectra in comprising even-electron cations and anions, often including the molecular ion. Fragmentation pathways are normally identified by removal of a neutral molecule and hydrogen transfer is also often involved. [348]

Mass-spectral fragments of most interest to this study are those containing silver atoms. These fragments are readily identified by the pattern resulting from the isotopic abundances of the two naturally occuring isotopes 107 and 109. These isotopes occur in almost equal proportions (51.83% ^{107}Ag, 48.17% ^{109}Ag) at two mass units apart. Distinct patterns are identifiable for fragments containing 1-3 silver atoms and fragments containing more silver atoms than this also exhibit characteristic features. Where the number of silver atoms is larger (>3) there is some difficulty in identifying the exact number of silver atoms involved because the low intensity peaks are lost to the background noise level. Figure 6-2 shows the expected patterns for Ag, Ag_2, Ag_3 and Ag_4 containing species.

There have been a number of reports of silver compounds being examined using FAB/MS and related 'soft' ionisation techniques in the literature. [356-361]

APPENDIX THREE *Energy Dispersive X-Ray Spectrometry*

The action of high energy electrons allows the generation of element specific X-rays for both qualitative and quantitative elemental analysis. The detection and measurement of these X-rays is the basis for a number of techniques of which Energy Dispersive X-ray Spectrometry

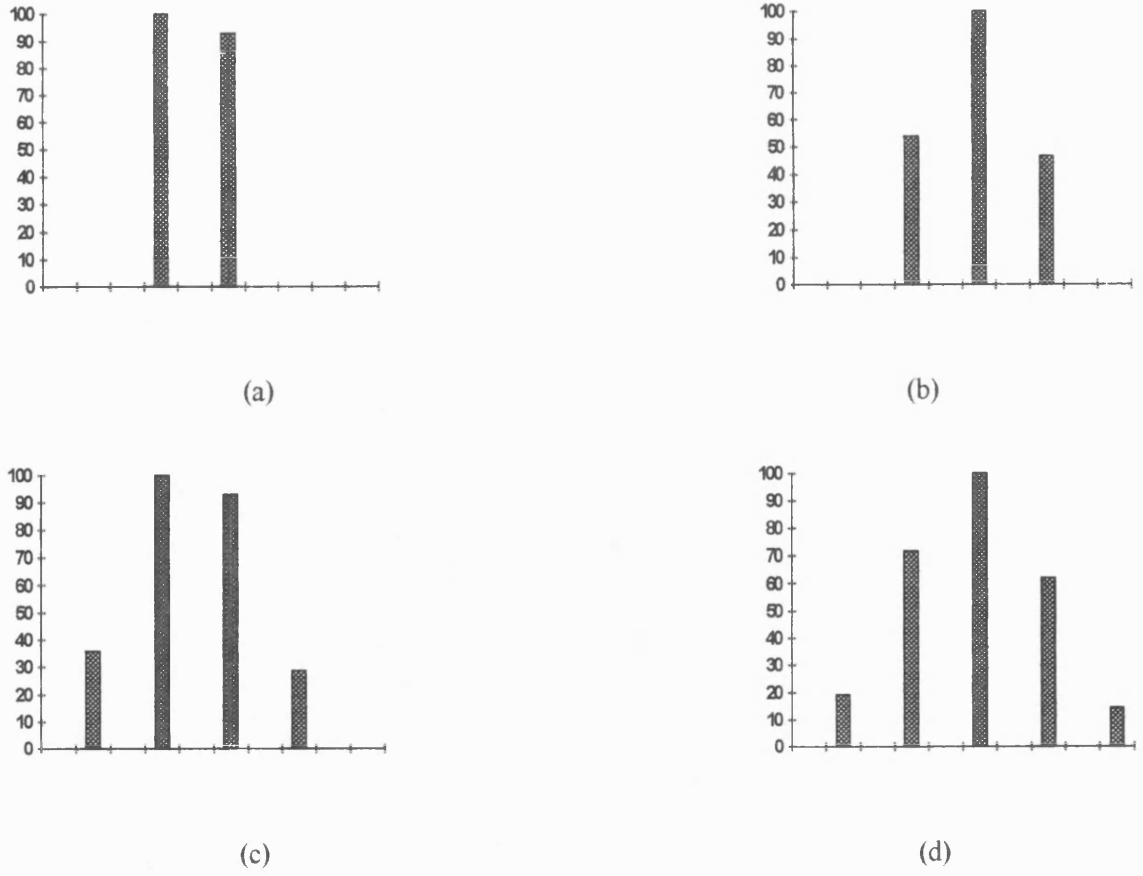

Figure 6-2 Expected mass-spectral patterns for (a) Ag, (b) Ag_2, (c) Ag_3 and (d) Ag_4 containing clusters.

(EDXS or ED) is one. [362] Films grown using the AACVD of silver in this study were analysed using these techniques under electron microscope conditions.

Accelerated electrons within the electron microscope cause ionisation of atoms within the sample where electrons can be ejected from any shell. The probability of ionisation of a particular atom (defined as its ionisation cross-section) varies in complex ways with the energy of the electron beam, atomic number and numerable other parameters. The energy of the electron beam must be in excess of the binding energy of the electron to cause ionisation, this energy may vary from several hundred electron volts (eV) (for light elements) to up to a hundred thousand electron volts (keV) (inner shells for heavy elements). Elemental characteristic X-rays are then emitted when electrons in outer shells move to fill the vacant orbitals and this is the basis for energy dispersive X-ray spectroscopy.

These X-rays are also responsible for the ejection of high energy electrons from outer shells, and these are known as 'Auger' electrons. The energies of these electrons are also element and shell characteristic, their detection and measurement forming the basis of Auger Electron Spectroscopy (AES).

The shells of electrons around the atom are defined K, L, M, N etc. with K being the innermost shell. An X-ray emitted from a particular shell carries the designation of that shell. For instance, if an electron is removed from the K shell and the vacancy refilled from the L shell, this gives rise to X-rays of a characteristic wavelength denoted K_{α}. If the vacancy is filled from the M shell, this gives rise to X-rays of a different wavelength denoted K_{β}. In more complex situations further numbers are used to designate which orbitals within a shell are involved in transitions.

In Energy Dispersive X-ray Analysis, the energy range of observable X-rays is divided into channels and the number of X-rays detected within a channel's range is counted. These results are plotted in graph form with energy (in eV) on the x-axis and X-ray count numbers on the y-axis. A typical example of a sample examined by ED in this study is shown (Figure 6-3). A number of points are worthy of note.

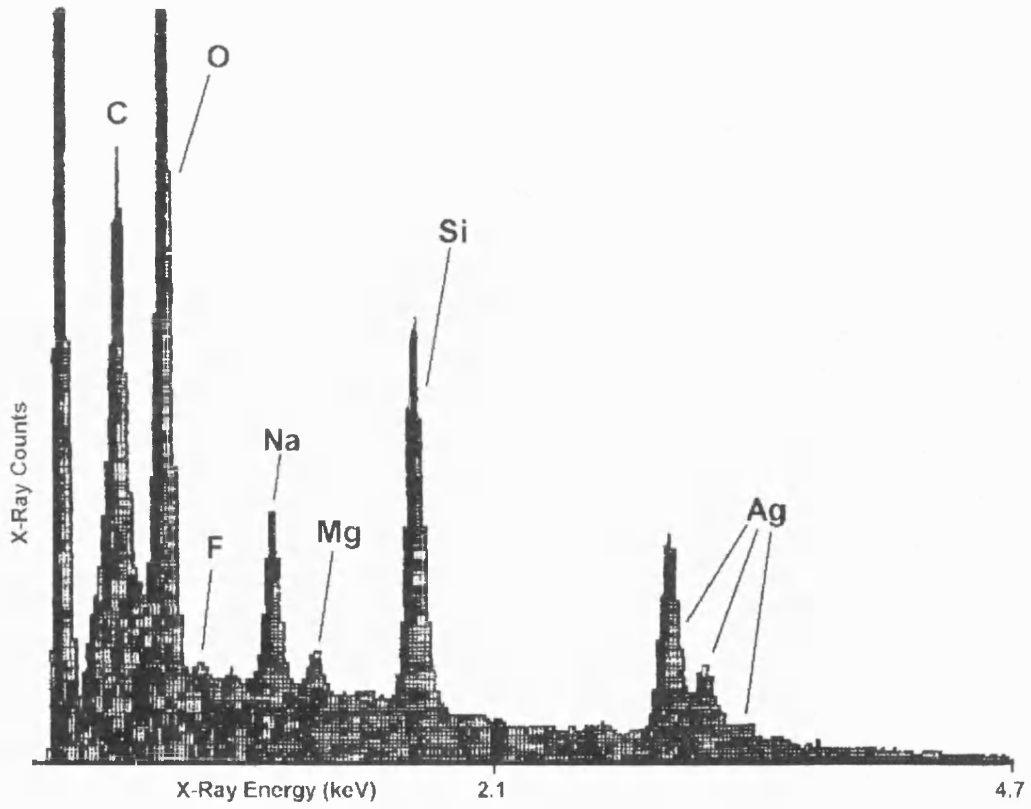

Figure 6-3 Example of an energy dispersive X-ray spectrum of a thin silver film on a glass substrate.

- The X-ray detector is capable of detecting a wide energy range of X-rays emitted from the sample. For a given experiment X-rays detected will be between zero and the energy of the incident electrons. As protection, a beryllium window (typically 8μm thickness foil) is fitted over the detector to prevent gas leaking into the detector vacuum chamber. The window is transparent to X-rays of 3 keV or higher but below this transmission of X-rays fall off rapidly to cut-off at around 1 keV. Measurement of X-rays at this lower energy (ie. from the lighter elements C, O, F etc.) requires a high vacuum in the SEM chamber to allow for removal of the window, thus detection of the lighter elements is more difficult and time consuming.

- Examination of a suitable sample by ED or SEM requires a conducting surface with a conducting route to ground. If the surface of the sample is not conducting enough, ie. if the film is too thin, discontinuous or resistive due to the presence of impurities, an electric charge will build up on the surface of the sample where electrons cannot escape to ground. The build up of an electric field, known as 'charging', will also decelerate the incoming electron beam, lower the kinetic energy of the electrons and artificially reduce the maximum energy of X-rays detected. Figure 6-3 is an example of a sample examined by ED with the beryllium window removed, there is no evidence of 'charging' as the energy of detected X-rays tends to zero close to the kinetic energy of the incident electrons (5 keV).

- The large peak at the low energy end of the spectrum is a feature of the technique and is not indicative of elemental characteristic X-rays. The lighter elements give higher numbers of X-rays and therefore this technique is more sensitive to impurities of lighter elements. If a peak from a light element is resolved in the ED spectra then the element's concentration is likely to be upwards of 0.5%wt. [363] The electron accelerating voltage influences the

intensity of X-rays produced by the sample. In order to obtain a reasonable intensity of X-rays it is desirable to use an electron accelerating voltage substantially higher than the peaks of interest.

- The electron accelerating voltage also influences the penetration of electrons into the sample, higher energy electrons will have a higher penetration and will result in X-rays from elements deeper inside the sample. This is shown in Figure 6-3 as the presence of silicon, oxygen, sodium and magnesium from the glass substrate are detected as well as silver. By reducing the accelerating voltage of the electrons, the surface region is found to have a greater influence on the X-rays detected (Figure 6-4). ED measurements on the samples in this study were carried out with an accelerating voltage of 5 keV.

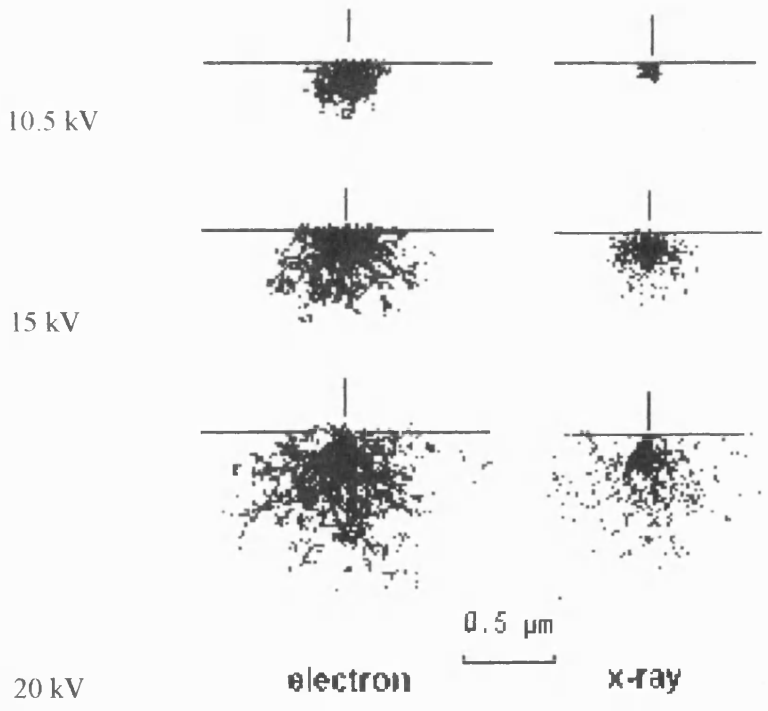

Figure 6-4 Computer prediction plots of electron trajectories and X-ray generation in copper at varying accelerating voltages.

In addition to qualitative analysis, ED may be used as a quantitative analytical method for the estimation of the thickness of thin films and this method is fairly well developed. [362, 363] The film thickness can be estimated by the correlation of the number of X-rays detected as compared to a bulk sample of a silver standard under identical conditions. In this manner the thickness of thin films of silver on glass were estimated by comparing the number of X-rays detected in the peak channel of silver $L_{\alpha 1}$ in both the sample and standard after background levels are subtracted. The combination of statistical, instrumental and measurement errors are estimated to be not more than ± 20 % for thickness measurements, but due to a number of factors the thinner films are likely, if anything, to be underestimated. It should also be noted that each sample analysed was subject to relatively few measurements, and since we cannot be certain of the variation in thickness across a substrate, there is a possibility that these coating thickness estimates may not be representative of the film. Discussions of error assessment for this technique can be found in the literature. [362, 363]

APPENDIX FOUR *X-Ray Crystallographic Data*

A4.1 Structural data for compound (3), $AgO_2CCH_3(PPh_3)_2$

A crystal of approximate dimensions 0.3 x 0.3 x 0.4 mm was used for data collection.

Crystal data: $C_{38}H_{33}O_2P_2Ag$, $M = 691.5$ triclinic, $a = 10.092(2)$, $b = 13.783(3)$, $c = 24.179(5)$Å, $\alpha = 92.04(2)$, $\beta = 90.60(2)$, $\gamma = 100.19(2)$, $U = 3307.8$ Å^3, space group P-1 (No. 2), Z = 4, $D_c = 1.39$ gcm^{-3}, μ(Mo-K$_\alpha$) = 7.30 cm^{-1}, $F(000) = 1416$. Data were measured at room temperature on a CAD4 automatic four-circle diffractometer in the range $2 \geq \theta \geq 22^\circ$. 8339 reflections were collected of which 5491 were unique with $I \geq 2\sigma(I)$. Data were corrected for Lorentz and polarization but not for absorption. The structure was solved by Patterson methods and refined using the SHELX [364, 365] suite of programs. Benzene rings were refined as rigid hexagons. One phenyl group, attached to P4, exhibited 39% disorder. The minor occupancy atoms (C64' - C68') were refined isotropically although all other atoms in the structure were treated anisotropically. The asymmetric unit was seen to consist of 2 independant molecules which were refined in separate blocks during the latter stages of convergence. Hydrogen atoms were included at calculated positions except in the case of the disordered phenyl group with minor occupancy (C64' - C68'). Final residuals after 10 cycles of least squares were R = 0.0395, $R_w = 0.0385$, for a weighting scheme of $w = 2.4850/[\sigma^2(F) + 0.000355(F)^2]$. Max. final shift/esd was 0.002. The max. and min. residual densities were 0.26 and -0.21 eÅ^{-3} respectively. Final fractional atomic coordinates, isotropic thermal parameters, bond distances and angles are presented in full in the following tables. The asymmetric unit is shown in Figure 6-5, along with the labelling scheme used.

Table 6-4 Complex **(3)**, fractional atomic co-ordinates ($x10^4$) and equivalent isotropic temperature factors ($Å^2 x10^3$).

	x	y	z	U
Ag(1)	1699	1934	1274	49
P(1)	2162(1)	261(1)	1372(1)	44(1)
P(2)	2797(1)	3248(1)	702(1)	47(1)
O(1)	-534(4)	2161(3)	1564(2)	69(2)
O(2)	1088(4)	2478(3)	2182(2)	74(2)
C(2)	701(5)	-1554(3)	1703(2)	90(3)
C(3)	-226(5)	-2123(3)	2037(2)	127(4)
C(4)	-827(5)	-1674(3)	2470(2)	116(5)
C(5)	-502(5)	-656(3)	2569(2)	102(4)
C(6)	425(5)	-87(3)	2234(2)	70(3)
C(1)	1026(5)	-535(3)	1801(2)	50(2)
C(8)	870(3)	-724(3)	444(2)	66(3)
C(9)	787(3)	-1212(3)	-74(2)	79(3)
C(10)	1949(3)	-1429(3)	-321(2)	78(3)
C(11)	3193(3)	-1158(3)	-50(2)	85(3)
C(12)	3276(3)	-670(3)	468(2)	64(3)
C(7)	2115(3)	-453(3)	715(2)	50(2)
C(14)	4137(4)	-505(2)	1971(2)	65(3)
C(15)	5464(4)	-524(2)	2131(2)	86(3)
C(16)	6500(4)	215(2)	1968(2)	81(3)
C(17)	6210(4)	973(2)	1646(2)	69(2)
C(18)	4883(4)	992(2)	1486(2)	56(2)
C(13)	3846(4)	253(2)	1649(2)	48(2)
C(20)	4749(4)	3877(3)	1496(2)	82(3)
C(21)	6052(4)	4062(3)	1721(2)	97(4)
C(22)	7142(4)	3952(3)	1389(2)	87(4)
C(23)	6929(4)	3657(3)	832(2)	78(3)
C(24)	5626(4)	3473(3)	608(2)	62(2)
C(19)	4536(4)	3582(3)	940(2)	49(2)
C(26)	3065(3)	5328(3)	710(2)	68(3)
C(27)	2543(3)	6200(3)	710(2)	87(3)

C(28)	1155(3)	6166(3)	731(2)	87(4)
C(29)	289(3)	5260(3)	752(2)	108(5)
C(30)	811(3)	4388(3)	753(2)	87(3)
C(25)	2199(3)	4422(3)	731(2)	52(2)
C(32)	2928(4)	1932(3)	-172(2)	65(3)
C(33)	3046(4)	1636(3)	-724(2)	82(3)
C(34)	3152(4)	2328(3)	-1135(2)	85(3)
C(35)	3139(4)	3317(3)	-995(2)	75(3)
C(36)	3022(4)	3613(3)	-442(2)	66(3)
C(31)	2916(4)	2921(3)	-31(2)	50(2)
C(37)	-125(6)	2392(4)	2041(3)	54(2)
C(38)	-1113(6)	2538(5)	2486(3)	75(3)
Ag(2)	3411	3298	-3697	56
P(3)	2033(2)	1943(1)	-4221(1)	50(1)
P(4)	3114(2)	5031(1)	-3732(1)	50(1)
O(3)	5475(5)	3219(4)	-3232(2)	84(2)
O(4)	3779(5)	3118(5)	-2676(2)	114(3)
C(40)	-267(4)	2396(2)	-3745(2)	56(2)
C(41)	-1587(4)	2206(2)	-3558(2)	79(3)
C(42)	-2314(4)	1245(2)	-3584(2)	88(3)
C(43)	-1720(4)	474(2)	-3797(2)	94(4)
C(44)	-400(4)	664(2)	-3984(2)	74(3)
C(39)	327(4)	1625(2)	-3958(2)	53(2)
C(46)	2690(5)	172(3)	-4669(2)	87(3)
C(47)	3309(5)	-654(3)	-4641(2)	110(4)
C(48)	3969(5)	-831(3)	-4156(2)	106(4)
C(49)	4010(5)	-183(3)	-3697(2)	102(4)
C(50)	3391(5)	643(3)	-3724(2)	79(3)
C(45)	2731(5)	820(3)	-4210(2)	55(2)
C(52)	2914(3)	2359(3)	-5276(2)	74(3)
C(53)	2782(3)	2470(3)	-5844(2)	85(3)
C(54)	1506(3)	2322(3)	-6093(2)	85(3)
C(55)	362(3)	2063(3)	-5775(2)	82(3)
C(56)	494(3)	1952(3)	-5207(2)	68(3)
C(51)	1770(3)	2100(3)	-4957(2)	55(2)
C(58)	3875(3)	6910(2)	-3206(2)	47(2)
C(59)	4761(3)	7628(2)	-2900(2)	51(2)

C(60)	6005(3)	7433(2)	-2725(2)	52(2)
C(61)	6364(3)	6521(2)	-2855(2)	50(2)
C(62)	5478(3)	5803(2)	-3161(2)	45(2)
C(57)	4233(3)	5998(2)	-3337(2)	40(2)
C(64)	3468(11)	4916(6)	-4855(3)	124(9)
C(65)	3597(11)	5244(6)	-5394(3)	159(11)
C(66)	3315(11)	6169(6)	-5515(3)	93(7)
C(67)	2905(11)	6767(6)	-5096(3)	117(10)
C(68)	2776(11)	6439(6)	-4556(3)	98(7)
C(63)	3057(11)	5513(6)	-4436(3)	65(3)
C(70)	1368(5)	4722(3)	-2878(2)	87(3)
C(71)	142(5)	4665(3)	-2609(2)	126(4)
C(72)	-954(5)	4943(3)	-2878(2)	139(6)
C(73)	-825(5)	5278(3)	-3416(2)	137(6)
C(74)	401(5)	5335(3)	-3685(2)	100(4)
C(69)	1498(5)	5057(3)	-3416(2)	63(3)
C(75)	5001(8)	3179(5)	-2758(3)	69(3)
C(76)	5956(7)	3268(6)	-2267(3)	93(4)

Table 6-5 Complex **(3)**, anisotropic temperature factors (Å x10^3).

	U_{11}	U_{22}	U_{33}	U_{23}	U_{13}	U_{12}
Ag(1)	41	44	61	5	10	9
P(1)	42(1)	41(1)	51(1)	5(1)	3(1)	8(1)
P(2)	39(1)	42(1)	62(1)	8(1)	9(1)	8(1)
O(1)	45(2)	99(3)	62(3)	-12(3)	0(2)	16(2)
O(2)	36(3)	104(4)	81(3)	-32(3)	-8(2)	11(2)
C(2)	120(6)	65(5)	74(5)	14(4)	0(5)	-15(4)
C(3)	146(9)	98(7)	109(8)	40(6)	-25(6)	-60(6)
C(4)	66(5)	151(9)	117(8)	82(7)	-17(5)	-32(6)
C(5)	65(5)	162(9)	87(6)	68(6)	25(4)	31(5)

C(6)	59(4)	81(5)	77(5)	26(4)	8(4)	23(4)
C(1)	43(3)	50(4)	56(4)	12(3)	-1(3)	4(3)
C(8)	61(4)	77(4)	62(4)	-7(4)	-11(3)	19(3)
C(9)	76(5)	82(5)	75(5)	-4(4)	-22(4)	8(4)
C(10)	97(6)	69(5)	65(5)	-6(4)	-7(4)	13(4)
C(11)	78(5)	96(6)	81(6)	-21(4)	13(4)	15(4)
C(12)	61(4)	70(4)	61(4)	-15(3)	1(3)	15(3)
C(7)	51(4)	36(3)	65(4)	6(3)	-4(3)	10(3)
C(14)	63(4)	58(4)	76(5)	0(4)	-16(4)	15(3)
C(15)	86(6)	69(5)	105(6)	-2(4)	-32(5)	24(4)
C(16)	60(5)	90(5)	95(6)	-35(5)	-30(4)	31(4)
C(17)	49(4)	79(5)	75(5)	-18(4)	-3(3)	6(3)
C(18)	45(4)	63(4)	57(4)	-3(3)	1(3)	3(3)
C(13)	56(4)	42(3)	47(4)	-1(3)	-2(3)	13(3)
C(20)	55(5)	130(7)	61(5)	15(4)	8(4)	15(4)
C(21)	72(5)	156(8)	61(5)	22(5)	-9(4)	9(5)
C(22)	57(5)	98(6)	103(6)	40(5)	-18(5)	3(4)
C(23)	50(4)	78(5)	107(6)	6(4)	3(4)	12(3)
C(24)	37(4)	60(4)	87(5)	-2(3)	6(3)	6(3)
C(19)	47(4)	40(3)	61(4)	15(3)	4(3)	3(3)
C(26)	62(4)	50(4)	94(5)	7(4)	11(4)	10(3)
C(27)	101(6)	41(4)	116(6)	2(4)	14(5)	7(4)
C(28)	102(6)	60(5)	108(6)	7(4)	14(5)	41(4)
C(29)	67(5)	66(5)	197(10)	3(5)	12(5)	29(4)
C(30)	45(4)	53(4)	167(8)	12(4)	8(4)	13(3)
C(25)	45(4)	42(3)	72(4)	6(3)	8(3)	10(3)
C(32)	68(4)	54(4)	74(5)	2(3)	14(4)	13(3)
C(33)	73(5)	80(5)	92(6)	-21(5)	6(4)	13(4)
C(34)	86(5)	109(6)	58(5)	-13(5)	5(4)	20(5)
C(35)	86(5)	89(5)	49(5)	8(4)	2(4)	13(4)
C(36)	61(4)	67(4)	71(5)	14(4)	-1(3)	14(3)
C(31)	35(3)	53(4)	63(4)	6(3)	-1(3)	11(3)
C(37)	48(4)	47(4)	62(4)	-12(3)	3(3)	1(3)
C(38)	57(4)	87(5)	78(5)	-24(4)	12(4)	12(4)
Ag(2)	51	42	74	-6	-5	10
P(3)	54(1)	38(1)	58(1)	-1(1)	0(1)	7(1)
P(4)	43(1)	37(1)	68(1)	-6(1)	-9(1)	8(1)

O(3)	71(3)	107(4)	82(4)	6(3)	-6(3)	41(3)
O(4)	60(4)	159(6)	114(5)	43(4)	7(3)	-13(3)
C(40)	54(4)	54(4)	62(4)	4(3)	7(3)	13(3)
C(41)	72(5)	77(5)	89(5)	-3(4)	9(4)	21(4)
C(42)	58(5)	112(6)	89(6)	-1(5)	16(4)	3(5)
C(43)	75(5)	78(5)	118(7)	-12(5)	4(5)	-13(4)
C(44)	69(5)	56(4)	93(5)	-8(4)	11(4)	-2(3)
C(39)	50(4)	48(4)	58(4)	0(3)	3(3)	2(3)
C(46)	116(6)	57(4)	95(6)	-22(4)	-14(5)	39(4)
C(47)	134(8)	73(6)	131(8)	-18(5)	7(6)	46(5)
C(48)	105(7)	54(5)	168(9)	-3(6)	0(6)	37(4)
C(49)	112(7)	69(5)	132(8)	13(5)	-19(6)	37(5)
C(50)	103(6)	49(4)	88(6)	5(4)	-5(5)	23(4)
C(45)	52(4)	42(3)	69(4)	7(3)	4(3)	5(3)
C(52)	69(5)	85(5)	64(5)	12(4)	3(4)	4(4)
C(53)	84(6)	89(5)	80(6)	17(4)	15(4)	4(4)
C(54)	112(7)	70(5)	72(5)	13(4)	7(5)	11(4)
C(55)	79(5)	87(5)	78(6)	13(4)	-14(4)	14(4)
C(56)	64(5)	74(5)	65(5)	12(4)	-3(4)	10(3)
C(51)	59(4)	39(3)	64(4)	1(3)	4(3)	4(3)
C(58)	48(3)	40(3)	57(4)	-4(3)	5(3)	15(3)
C(59)	62(4)	42(3)	49(4)	-5(3)	2(3)	10(3)
C(60)	53(4)	51(4)	49(4)	-6(3)	-2(3)	-2(3)
C(61)	42(3)	55(4)	51(4)	-1(3)	0(3)	3(3)
C(62)	39(3)	44(3)	53(4)	-2(3)	-4(3)	10(3)
C(57)	38(3)	40(3)	41(3)	-1(2)	1(3)	8(2)
C(64)	238(21)	129(12)	37(8)	-6(7)	-21(9)	122(13)
C(65)	256(25)	185(17)	82(12)	-5(11)	1(12)	164(18)
C(66)	104(13)	120(14)	50(9)	17(9)	-13(9)	8(11)
C(67)	220(23)	54(8)	78(11)	-13(8)	-22(12)	31(11)
C(68)	183(18)	50(7)	67(9)	-13(6)	-16(10)	43(9)
C(63)	71(4)	49(4)	74(5)	-19(3)	-32(4)	19(3)
C(70)	64(5)	69(5)	130(7)	-1(5)	24(5)	19(4)
C(71)	114(7)	82(6)	193(10)	33(6)	79(7)	33(5)
C(72)	71(6)	58(5)	292(15)	30(7)	69(8)	14(4)
C(73)	47(5)	103(7)	270(14)	46(8)	17(7)	25(5)
C(74)	53(5)	77(5)	176(9)	20(5)	-10(5)	23(4)

C(69)	40(4)	32(3)	113(6)	-9(3)	-9(4)	4(3)
C(75)	63(5)	54(4)	90(6)	25(4)	-1(5)	0(3)
C(76)	80(5)	96(6)	94(6)	19(5)	-15(5)	-12(4)

The temperature factor exponent takes the form:

$-2\ (U\ .h\ .a^* + \ ...\ +2U\ .h.k.a^*.b^*)$

Table 6-6 Complex **(3)**, hydrogen fractional atomic co-ordinates ($x10^4$) and isotropic temperature factors ($Å^2\ x10^3$).

	x	y	z	U
C(64')	2122(22)	4802(15)	-4745(9)	88(7)
C(65')	2026(23)	5030(16)	-5306(9)	95(7)
C(66')	2691(26)	5886(19)	-5489(11)	86(8)
C(67')	3525(23)	6566(18)	-5147(10)	70(7)
C(68')	3589(15)	6339(13)	-4575(7)	46(5)
H(21)	1114(5)	-1863(3)	1405(2)	121(5)
H(31)	-450(5)	-2824(3)	1970(2)	121(5)
H(41)	-1465(5)	-2066(3)	2701(2)	121(5)
H(51)	-915(5)	-347(3)	2867(2)	121(5)
H(61)	649(5)	614(3)	2302(2)	121(5)
H(81)	71(3)	-575(3)	614(2)	121(5)
H(91)	-70(3)	-1398(3)	-260(2)	121(5)
H(101)	1891(3)	-1764(3)	-677(2)	121(5)
H(111)	3992(3)	-1307(3)	-220(2)	121(5)
H(121)	4133(3)	-483(3)	655(2)	121(5)
H(141)	3423(4)	-1014(2)	2083(2)	121(5)
H(151)	5663(4)	-1046(2)	2352(2)	121(5)
H(161)	7413(4)	201(2)	2079(2)	121(5)
H(171)	6923(4)	1481(2)	1535(2)	121(5)
H(181)	4683(4)	1514(2)	1265(2)	121(5)
H(201)	3999(4)	3953(3)	1725(2)	121(5)

H(211)	6199(4)	4265(3)	2104(2)	121(5)
H(221)	8039(4)	4079(3)	1543(2)	121(5)
H(231)	7679(4)	3582(3)	604(2)	121(5)
H(241)	5479(4)	3270(3)	225(2)	121(5)
H(261)	4021(3)	5351(3)	695(2)	121(5)
H(271)	3140(3)	6824(3)	695(2)	121(5)
H(281)	796(3)	6766(3)	731(2)	121(5)
H(291)	-667(3)	5237(3)	767(2)	121(5)
H(301)	214(3)	3764(3)	767(2)	121(5)
H(321)	2855(4)	1456(3)	112(2)	121(5)
H(331)	3054(4)	955(3)	-821(2)	121(5)
H(341)	3233(4)	2124(3)	-1515(2)	121(5)
H(351)	3212(4)	3793(3)	-1278(2)	121(5)
H(361)	3013(4)	4294(3)	-346(2)	121(5)
H(381)	-2002(6)	2451(5)	2326(3)	121(5)
H(382)	-876(6)	3191(5)	2650(3)	121(5)
H(383)	-1091(6)	2063(5)	2766(3)	121(5)
H(401)	233(4)	3058(2)	-3727(2)	121(5)
H(411)	-1996(4)	2736(2)	-3411(2)	121(5)
H(421)	-3222(4)	1114(2)	-3455(2)	121(5)
H(431)	-2220(4)	-188(2)	-3815(2)	121(5)
H(441)	9(4)	134(2)	-4131(2)	121(5)
H(461)	2235(5)	294(3)	-5003(2)	121(5)
H(471)	3280(5)	-1100(3)	-4957(2)	121(5)
H(481)	4395(5)	-1400(3)	-4137(2)	121(5)
H(491)	4465(5)	-305(3)	-3362(2)	121(5)
H(501)	3420(5)	1089(3)	-3408(2)	121(5)
H(521)	3792(3)	2460(3)	-5104(2)	121(5)
H(531)	3570(3)	2648(3)	-6063(2)	121(5)
H(541)	1416(3)	2398(3)	-6484(2)	121(5)
H(551)	-516(3)	1962(3)	-5947(2)	121(5)
H(561)	-294(3)	1774(3)	-4988(2)	121(5)
H(581)	3018(3)	7044(2)	-3327(2)	121(5)
H(591)	4514(3)	8255(2)	-2811(2)	121(5)
H(601)	6615(3)	7927(2)	-2514(2)	121(5)
H(611)	7220(3)	6387(2)	-2734(2)	121(5)
H(621)	5724(3)	5175(2)	-3251(2)	121(5)

H(641)	3662(11)	4279(6)	-4772(3)	121(5)
H(651)	3879(11)	4833(6)	-5683(3)	121(5)
H(661)	3404(11)	6395(6)	-5886(3)	121(5)
H(671)	2711(11)	7404(6)	-5178(3)	121(5)
H(681)	2493(11)	6850(6)	-4268(3)	121(5)
H(701)	2122(5)	4530(3)	-2693(2)	121(5)
H(711)	53(5)	4434(3)	-2239(2)	121(5)
H(721)	-1798(5)	4904(3)	-2693(2)	121(5)
H(731)	-1579(5)	5469(3)	-3601(2)	121(5)
H(741)	490(5)	5565(3)	-4055(2)	121(5)
H(761)	6860(7)	3308(6)	-2396(3)	121(5)
H(762)	5728(7)	2699(6)	-2045(3)	121(5)
H(763)	5891(7)	3851(6)	-2048(3)	121(5)

Table 6-7 Complex **(3)**, bond lengths (Å).

P(1)-Ag(1)	2.452(4)	P(2)-Ag(1)	2.433(3)
O(1)-Ag(1)	2.437(6)	O(2)-Ag(1)	2.416(6)
C(37)-Ag(1)	2.762(10)	C(1)-P(1)	1.805(7)
C(7)-P(1)	1.833(6)	C(13)-P(1)	1.822(6)
C(19)-P(2)	1.816(6)	C(25)-P(2)	1.824(6)
C(31)-P(2)	1.822(7)	C(37)-O(1)	1.233(9)
C(37)-O(2)	1.251(8)	C(3)-C(2)	1.395(7)
C(1)-C(2)	1.395(7)	C(4)-C(3)	1.395(8)
C(5)-C(4)	1.395(7)	C(6)-C(5)	1.395(7)
C(1)-C(6)	1.395(8)	C(9)-C(8)	1.395(7)
C(7)-C(8)	1.395(6)	C(10)-C(9)	1.395(6)
C(11)-C(10)	1.395(6)	C(12)-C(11)	1.395(7)
C(7)-C(12)	1.395(6)	C(15)-C(14)	1.395(7)
C(13)-C(14)	1.395(6)	C(16)-C(15)	1.395(6)
C(17)-C(16)	1.395(6)	C(18)-C(17)	1.395(7)
C(13)-C(18)	1.395(6)	C(21)-C(20)	1.395(7)

C(19)-C(20)	1.395(6)	C(22)-C(21)	1.395(7)
C(23)-C(22)	1.395(6)	C(24)-C(23)	1.395(7)
C(19)-C(24)	1.395(7)	C(27)-C(26)	1.395(6)
C(25)-C(26)	1.395(6)	C(28)-C(27)	1.395(5)
C(29)-C(28)	1.395(6)	C(30)-C(29)	1.395(6)
C(25)-C(30)	1.395(5)	C(33)-C(32)	1.395(7)
C(31)-C(32)	1.395(6)	C(34)-C(33)	1.395(7)
C(35)-C(34)	1.395(6)	C(36)-C(35)	1.395(7)
C(31)-C(36)	1.395(7)	C(38)-C(37)	1.507(11)
P(3)-Ag(2)	2.429(3)	P(4)-Ag(2)	2.464(4)
O(3)-Ag(2)	2.378(7)	O(4)-Ag(2)	2.518(9)
C(75)-Ag(2)	2.792(11)	C(39)-P(3)	1.826(6)
C(45)-P(3)	1.811(7)	C(51)-P(3)	1.825(7)
C(57)-P(4)	1.822(5)	C(63)-P(4)	1.854(9)
C(69)-P(4)	1.813(7)	C(75)-O(3)	1.246(11)
C(75)-O(4)	1.239(10)	C(41)-C(40)	1.395(6)
C(39)-C(40)	1.395(6)	C(42)-C(41)	1.395(5)
C(43)-C(42)	1.395(6)	C(44)-C(43)	1.395(6)
C(39)-C(44)	1.395(5)	C(47)-C(46)	1.395(8)
C(45)-C(46)	1.395(7)	C(48)-C(47)	1.395(7)
C(49)-C(48)	1.395(7)	C(50)-C(49)	1.395(8)
C(45)-C(50)	1.395(7)	C(53)-C(52)	1.395(8)
C(51)-C(52)	1.395(6)	C(54)-C(53)	1.395(6)
C(55)-C(54)	1.395(6)	C(56)-C(55)	1.395(8)
C(51)-C(56)	1.395(6)	C(59)-C(58)	1.395(5)
C(57)-C(58)	1.395(6)	C(60)-C(59)	1.395(5)
C(61)-C(60)	1.395(6)	C(62)-C(61)	1.395(5)
C(57)-C(62)	1.395(5)	C(65)-C(64)	1.395(11)
C(63)-C(64)	1.395(13)	C(64')-C(64)	1.369(26)
C(65')-C(64)	1.841(27)	C(66')-C(64)	2.290(31)
C(68')-C(64)	2.035(22)	C(66)-C(65)	1.395(13)
C(64')-C(65)	2.202(25)	C(65')-C(65)	1.579(27)
C(66')-C(65)	1.403(31)	C(67')-C(65)	1.912(28)
C(67)-C(66)	1.395(13)	C(65')-C(66)	1.939(24)
C(66')-C(66)	0.685(27)	C(67')-C(66)	1.027(26)
C(68')-C(66)	2.284(21)	C(68)-C(67)	1.395(11)
C(66')-C(67)	1.499(28)	C(67')-C(67)	0.738(29)

C(68')-C(67)	1.608(22)	C(63)-C(68)	1.395(13)
C(64')-C(68)	2.265(24)	C(67')-C(68)	1.623(28)
C(68')-C(68)	0.857(21)	C(64')-C(63)	1.419(22)
C(67')-C(63)	2.288(28)	C(68')-C(63)	1.229(20)
C(65')-C(64')	1.410(32)	C(66')-C(65')	1.342(34)
C(67')-C(66')	1.387(34)	C(68')-C(67')	1.431(32)
C(71)-C(70)	1.395(8)	C(69)-C(70)	1.395(8)
C(72)-C(71)	1.395(8)	C(73)-C(72)	1.395(8)
C(74)-C(73)	1.395(8)	C(69)-C(74)	1.395(8)
C(76)-C(75)	1.510(13)		

Table 6-8 Complex **(3)**, bond angles (°).

P(2)-Ag(1)-P(1)	129.7(2)	O(1)-Ag(1)-P(1)	114.7(2)
O(1)-Ag(1)-P(2)	113.0(2)	O(2)-Ag(1)-P(1)	106.1(2)
O(2)-Ag(1)-P(2)	114.6(2)	O(2)-Ag(1)-O(1)	53.4(2)
C(37)-Ag(1)-P(1)	112.0(2)	C(37)-Ag(1)-P(2)	117.8(2)
C(37)-Ag(1)-O(1)	26.5(2)	C(37)-Ag(1)-O(2)	26.9(2)
C(1)-P(1)-Ag(1)	116.2(3)	C(7)-P(1)-Ag(1)	113.8(3)
C(7)-P(1)-C(1)	103.4(3)	C(13)-P(1)-Ag(1)	112.7(2)
C(13)-P(1)-C(1)	105.8(3)	C(13)-P(1)-C(7)	103.6(3)
C(19)-P(2)-Ag(1)	107.6(3)	C(25)-P(2)-Ag(1)	118.3(2)
C(25)-P(2)-C(19)	103.2(3)	C(31)-P(2)-Ag(1)	115.8(2)
C(31)-P(2)-C(19)	104.3(3)	C(31)-P(2)-C(25)	106.0(3)
C(37)-O(1)-Ag(1)	91.6(5)	C(37)-O(2)-Ag(1)	92.1(5)
C(1)-C(2)-C(3)	120.0(5)	C(4)-C(3)-C(2)	120.0(5)
C(5)-C(4)-C(3)	120.0(5)	C(6)-C(5)-C(4)	120.0(5)
C(1)-C(6)-C(5)	120.0(5)	C(2)-C(1)-P(1)	122.8(5)
C(6)-C(1)-P(1)	117.1(4)	C(6)-C(1)-C(2)	120.0(5)
C(7)-C(8)-C(9)	120.0(4)	C(10)-C(9)-C(8)	120.0(4)
C(11)-C(10)-C(9)	120.0(5)	C(12)-C(11)-C(10)	120.0(4)
C(7)-C(12)-C(11)	120.0(4)	C(8)-C(7)-P(1)	117.5(4)
C(12)-C(7)-P(1)	122.4(4)	C(12)-C(7)-C(8)	120.0(5)

C(13)-C(14)-C(15)	120.0(4)	C(16)-C(15)-C(14)	120.0(4)
C(17)-C(16)-C(15)	120.0(5)	C(18)-C(17)-C(16)	120.0(4)
C(13)-C(18)-C(17)	120.0(4)	C(14)-C(13)-P(1)	122.2(4)
C(18)-C(13)-P(1)	117.5(4)	C(18)-C(13)-C(14)	120.0(5)
C(19)-C(20)-C(21)	120.0(5)	C(22)-C(21)-C(20)	120.0(5)
C(23)-C(22)-C(21)	120.0(5)	C(24)-C(23)-C(22)	120.0(5)
C(19)-C(24)-C(23)	120.0(5)	C(20)-C(19)-P(2)	116.7(4)
C(24)-C(19)-P(2)	123.0(4)	C(24)-C(19)-C(20)	120.0(5)
C(25)-C(26)-C(27)	120.0(4)	C(28)-C(27)-C(26)	120.0(4)
C(29)-C(28)-C(27)	120.0(4)	C(30)-C(29)-C(28)	120.0(4)
C(25)-C(30)-C(29)	120.0(4)	C(26)-C(25)-P(2)	122.6(4)
C(30)-C(25)-P(2)	117.3(4)	C(30)-C(25)-C(26)	120.0(4)
C(31)-C(32)-C(33)	120.0(5)	C(34)-C(33)-C(32)	120.0(4)
C(35)-C(34)-C(33)	120.0(5)	C(36)-C(35)-C(34)	120.0(5)
C(31)-C(36)-C(35)	120.0(4)	C(32)-C(31)-P(2)	117.0(4)
C(36)-C(31)-P(2)	122.9(4)	C(36)-C(31)-C(32)	120.0(5)
O(1)-C(37)-Ag(1)	61.9(4)	O(2)-C(37)-Ag(1)	60.9(4)
O(2)-C(37)-O(1)	122.7(7)	C(38)-C(37)-Ag(1)	173.9(4)
C(38)-C(37)-O(1)	119.8(6)	C(38)-C(37)-O(2)	117.5(7)
P(4)-Ag(2)-P(3)	124.0(2)	O(3)-Ag(2)-P(3)	125.4(2)
O(3)-Ag(2)-P(4)	109.5(2)	O(4)-Ag(2)-P(3)	118.5(2)
O(4)-Ag(2)-P(4)	101.9(2)	O(4)-Ag(2)-O(3)	52.7(3)
C(75)-Ag(2)-P(3)	127.3(2)	C(75)-Ag(2)-P(4)	106.4(2)
C(75)-Ag(2)-O(3)	26.4(2)	C(75)-Ag(2)-O(4)	26.4(2)
C(39)-P(3)-Ag(2)	113.1(2)	C(45)-P(3)-Ag(2)	112.3(3)
C(45)-P(3)-C(39)	105.9(3)	C(51)-P(3)-Ag(2)	117.5(2)
C(51)-P(3)-C(39)	103.6(3)	C(51)-P(3)-C(45)	103.2(3)
C(57)-P(4)-Ag(2)	120.6(2)	C(63)-P(4)-Ag(2)	115.3(4)
C(63)-P(4)-C(57)	104.5(4)	C(69)-P(4)-Ag(2)	104.7(3)
C(69)-P(4)-C(57)	102.6(3)	C(69)-P(4)-C(63)	107.9(5)
C(75)-O(3)-Ag(2)	95.7(5)	C(75)-O(4)-Ag(2)	89.2(6)
C(39)-C(40)-C(41)	120.0(4)	C(42)-C(41)-C(40)	120.0(4)
C(43)-C(42)-C(41)	120.0(4)	C(44)-C(43)-C(42)	120.0(4)
C(39)-C(44)-C(43)	120.0(4)	C(40)-C(39)-P(3)	117.3(3)
C(44)-C(39)-P(3)	122.7(4)	C(44)-C(39)-C(40)	120.0(4)
C(45)-C(46)-C(47)	120.0(5)	C(48)-C(47)-C(46)	120.0(5)
C(49)-C(48)-C(47)	120.0(6)	C(50)-C(49)-C(48)	120.0(5)

C(45)-C(50)-C(49)	120.0(5)	C(46)-C(45)-P(3)	122.9(5)
C(50)-C(45)-P(3)	117.0(4)	C(50)-C(45)-C(46)	120.0(6)
C(51)-C(52)-C(53)	120.0(4)	C(54)-C(53)-C(52)	120.0(4)
C(55)-C(54)-C(53)	120.0(5)	C(56)-C(55)-C(54)	120.0(4)
C(51)-C(56)-C(55)	120.0(4)	C(52)-C(51)-P(3)	117.2(4)
C(56)-C(51)-P(3)	122.8(4)	C(56)-C(51)-C(52)	120.0(5)
C(57)-C(58)-C(59)	120.0(4)	C(60)-C(59)-C(58)	120.0(4)
C(61)-C(60)-C(59)	120.0(4)	C(62)-C(61)-C(60)	120.0(4)
C(57)-C(62)-C(61)	120.0(4)	C(58)-C(57)-P(4)	121.9(3)
C(62)-C(57)-P(4)	118.1(3)	C(62)-C(57)-C(58)	120.0(4)
C(63)-C(64)-C(65)	120.0(9)	C(64')-C(64)-C(65)	105.6(13)
C(64')-C(64)-C(63)	61.8(12)	C(65')-C(64)-C(65)	56.4(10)
C(65')-C(64)-C(63)	92.5(11)	C(65')-C(64)-C(64')	49.5(12)
C(66')-C(64)-C(65)	35.2(9)	C(66')-C(64)-C(63)	88.5(10)
C(66')-C(64)-C(64')	77.0(13)	C(66')-C(64)-C(65')	35.9(9)
C(68')-C(64)-C(65)	89.0(8)	C(68')-C(64)-C(63)	36.3(6)
C(68')-C(64)-C(64')	86.4(12)	C(68')-C(64)-C(65')	90.3(10)
C(68')-C(64)-C(66')	67.1(9)	C(66)-C(65)-C(64)	120.0(8)
C(64')-C(65)-C(64)	36.8(8)	C(64')-C(65)-C(66)	101.0(10)
C(65')-C(65)-C(64)	76.2(11)	C(65')-C(65)-C(66)	81.1(12)
C(65')-C(65)-C(64')	39.7(10)	C(66')-C(65)-C(64)	109.9(15)
C(66')-C(65)-C(66)	28.3(11)	C(66')-C(65)-C(64')	79.7(14)
C(66')-C(65)-C(65')	53.1(15)	C(67')-C(65)-C(64)	91.6(10)
C(67')-C(65)-C(66)	31.5(8)	C(67')-C(65)-C(64')	85.5(11)
C(67')-C(65)-C(65')	85.9(12)	C(67')-C(65)-C(66')	46.4(13)
C(67)-C(66)-C(65)	120.0(8)	C(65')-C(66)-C(65)	53.6(10)
C(65')-C(66)-C(67)	92.3(10)	C(66')-C(66)-C(65)	76.5(26)
C(66')-C(66)-C(67)	85.0(26)	C(66')-C(66)-C(65')	23.9(25)
C(67')-C(66)-C(65)	103.2(17)	C(67')-C(66)-C(67)	31.0(15)
C(67')-C(66)-C(65')	103.1(16)	C(67')-C(66)-C(66')	106.5(28)
C(68')-C(66)-C(65)	79.4(7)	C(68')-C(66)-C(67)	44.1(6)
C(68')-C(66)-C(65')	80.9(9)	C(68')-C(66)-C(66')	91.3(25)
C(68')-C(66)-C(67')	25.8(15)	C(68)-C(67)-C(66)	120.0(9)
C(66')-C(67)-C(66)	27.1(11)	C(66')-C(67)-C(68)	108.6(13)
C(67')-C(67)-C(66)	45.8(20)	C(67')-C(67)-C(68)	94.0(23)
C(67')-C(67)-C(66')	66.9(22)	C(68')-C(67)-C(66)	98.7(11)
C(68')-C(67)-C(68)	32.2(8)	C(68')-C(67)-C(66')	101.0(14)

C(68')-C(67)-C(67')	62.9(22)	C(63)-C(68)-C(67)	120.0(8)
C(64')-C(68)-C(67)	99.4(8)	C(64')-C(68)-C(63)	36.8(7)
C(67')-C(68)-C(67)	27.0(10)	C(67')-C(68)-C(63)	98.3(12)
C(67')-C(68)-C(64')	90.6(12)	C(68')-C(68)-C(67)	87.7(15)
C(68')-C(68)-C(63)	60.7(15)	C(68')-C(68)-C(64')	87.1(15)
C(68')-C(68)-C(67')	61.6(17)	C(64)-C(63)-P(4)	114.6(7)
C(68)-C(63)-P(4)	125.0(7)	C(68)-C(63)-C(64)	120.0(8)
C(64')-C(63)-P(4)	105.8(11)	C(64')-C(63)-C(64)	58.2(12)
C(64')-C(63)-C(68)	107.2(13)	C(67')-C(63)-P(4)	159.0(7)
C(67')-C(63)-C(64)	77.0(9)	C(67')-C(63)-C(68)	44.6(8)
C(67')-C(63)-C(64')	95.2(12)	C(68')-C(63)-P(4)	125.8(10)
C(68')-C(63)-C(64)	101.5(12)	C(68')-C(63)-C(68)	37.5(9)
C(68')-C(63)-C(64')	127.8(14)	C(68')-C(63)-C(67')	33.4(10)
C(65)-C(64')-C(64)	37.6(7)	C(68)-C(64')-C(64)	79.2(11)
C(68)-C(64')-C(65)	77.3(8)	C(63)-C(64')-C(64)	60.0(11)
C(63)-C(64')-C(65)	80.6(11)	C(63)-C(64')-C(68)	36.1(7)
C(65')-C(64')-C(64)	83.0(16)	C(65')-C(64')-C(65)	45.6(11)
C(65')-C(64')-C(68)	87.4(14)	C(65')-C(64')-C(63)	112.9(17)
C(65)-C(65')-C(64)	47.4(7)	C(66)-C(65')-C(64)	79.4(10)
C(66)-C(65')-C(65)	45.3(7)	C(64')-C(65')-C(64)	47.6(12)
C(64')-C(65')-C(65)	94.8(17)	C(64')-C(65')-C(66)	113.9(16)
C(66')-C(65')-C(64)	90.6(17)	C(66')-C(65')-C(65)	56.7(16)
C(66')-C(65')-C(66)	11.9(13)	C(66')-C(65')-C(64')	120.6(21)
C(65)-C(66')-C(64)	34.9(8)	C(66)-C(66')-C(64)	92.2(27)
C(66)-C(66')-C(65)	75.2(26)	C(67)-C(66')-C(64)	92.4(14)
C(67)-C(66')-C(65)	112.7(19)	C(67)-C(66')-C(66)	68.0(22)
C(65')-C(66')-C(64)	53.5(15)	C(65')-C(66')-C(65)	70.2(18)
C(65')-C(66')-C(66)	144.2(37)	C(65')-C(66')-C(67)	117.8(22)
C(67')-C(66')-C(64)	77.0(17)	C(67')-C(66')-C(65)	86.5(20)
C(67')-C(66')-C(66)	45.2(20)	C(67')-C(66')-C(67)	29.3(13)
C(67')-C(66')-C(65')	122.3(25)	C(66)-C(67')-C(65)	45.3(12)
C(67)-C(67')-C(65)	125.5(24)	C(67)-C(67')-C(66)	103.2(27)
C(68)-C(67')-C(65)	103.9(14)	C(68)-C(67')-C(66)	130.1(19)
C(68)-C(67')-C(67)	59.0(19)	C(63)-C(67')-C(65)	69.6(9)
C(63)-C(67')-C(66)	108.5(18)	C(63)-C(67')-C(67)	91.0(22)
C(63)-C(67')-C(68)	37.1(7)	C(66')-C(67')-C(65)	47.1(14)
C(66')-C(67')-C(66)	28.2(14)	C(66')-C(67')-C(67)	83.8(24)

C(66')-C(67')-C(68)	102.4(18)	C(66')-C(67')-C(63)	88.8(17)
C(68')-C(67')-C(65)	93.0(16)	C(68')-C(67')-C(66)	135.9(23)
C(68')-C(67')-C(67)	89.8(25)	C(68')-C(67')-C(68)	31.8(9)
C(68')-C(67')-C(63)	28.2(9)	C(68')-C(67')-C(66')	116.7(22)
C(66)-C(68')-C(64)	67.8(7)	C(67)-C(68')-C(64)	99.3(10)
C(67)-C(68')-C(66)	37.1(6)	C(68)-C(68')-C(64)	106.0(15)
C(68)-C(68')-C(66)	88.4(14)	C(68)-C(68')-C(67)	60.1(13)
C(63)-C(68')-C(64)	42.2(7)	C(63)-C(68')-C(66)	100.9(11)
C(63)-C(68')-C(67)	116.1(13)	C(63)-C(68')-C(68)	81.8(15)
C(67')-C(68')-C(64)	85.6(14)	C(67')-C(68')-C(66)	18.2(10)
C(67')-C(68')-C(67)	27.3(11)	C(67')-C(68')-C(68)	86.5(18)
C(67')-C(68')-C(63)	118.4(17)	C(69)-C(70)-C(71)	120.0(6)
C(72)-C(71)-C(70)	120.0(6)	C(73)-C(72)-C(71)	120.0(5)
C(74)-C(73)-C(72)	120.0(6)	C(69)-C(74)-C(73)	120.0(6)
C(70)-C(69)-P(4)	115.6(5)	C(74)-C(69)-P(4)	124.4(5)
C(74)-C(69)-C(70)	120.0(5)	O(3)-C(75)-Ag(2)	57.9(5)
O(4)-C(75)-Ag(2)	64.4(5)	O(4)-C(75)-O(3)	122.2(8)
C(76)-C(75)-Ag(2)	171.6(5)	C(76)-C(75)-O(3)	118.7(7)
C(76)-C(75)-O(4)	119.0(8)		

Table 6-9 Complex **(3)**, selected non-bonded distances (Å).

Intramolecular:	C(6)-Ag(1)	3.750	C(1)-Ag(1)	3.631
Intermolecular:	C(9)-Ag(1a)	3.802		

Key to symmetry operations relating designated atoms to reference atoms at (x,y,z):

(a) -x,-y,-z

A4.2 Structural data for complex (12), $AgO_2CC_3F_7(PPh_3)_2$

A crystal of approximate dimensions 0.02 x 0.02 x 0.01 mm was used for data collection.

Crystal data: $C_{40}H_{30}F_7O_2P_2Ag$, M = 845.45, Triclinic , a = 13.160(5), b = 13.251(4), c = 13.613(4) Å , α = 97.29(3), β = 109.15(3), γ = 118.20(2)°, U = 1859.6(11) Å^3, space group P-1 (No.2), Z = 2, D_c = 1.510 gcm^{-3}, (mMo-K_a) = 0.697 mm^{-1}, F(000) = 852. Crystallographic measurements were made at 293(2)° K on a CAD4 automatic four-circle diffractometer in the range 2.03<q<23.92°. Data (6102 reflections) were corrected for Lorentz and polarization but not for absorption.

In the final least squares cycles all atoms were allowed to vibrate anisotropically. Hydrogen atoms were included at calculated positions where relevant.

The solution of the structure (SHELX86) [366] and refinement (SHELX93) [367] converged to a conventional [i.e. based on 4130 with Fo>4s(Fo)] $R1$ = 0.0437 and $wR2$ = 0.1145. Goodness of fit = 0.936. The max. and min. residual densities were 0.785 and -0.509eÅ^{-3} respectively. The asymmetric unit (shown in Figure 3-7), along with the labelling scheme used was produced using ORTEX. [368] Final fractional atomic co-ordinates and isotropic thermal parameters, bond distances and angles are presented in the following tables. Tables of anisotropic temperature factors are available as supplementary data.

Table 6-10 Complex **(12)**, crystal data and structure refinement.

Identification code	95KCM5
Empirical formula	$C_{40}H_{30}F_7O_2P_2Ag$
Formula weight	845.45
Temperature	293(2)°K
Wavelength	0.70930 Å
Crystal system	Triclinic
Space group	P-1(No.2)
Unit cell dimensions	a = 13.160(5)Å α= 97.29(3)°
	b = 13.251(4)Å β = 109.15(3)°
	c = 13.613(4)Å γ = 118.20(2)°
Volume	1859.6(11) $Å^3$
Z	2
Density (calculated)	1.510 Mg/m^3
Absorption coefficient	0.697 mm^{-1}
F(000)	852
Crystal size	0.02 x 0.02 x 0.01 mm
Thcta range for data collection	2.03 to 23.92°
Index ranges	-15<=h<=0; -13<=k<=15; -14<=l<=15
Reflections collected	6102
Independent reflections	5814 [R(int) = 0.0165]
Refinement method	Full-matrix least-squares on F^2
Data / restraints / parameters	5808 / 0 / 470
Goodness-of-fit on F2	0.936
Final R indices [I>2σ(I)]	R1 = 0.0437 wR2 = 0.1145
R indices (all data)	R1 = 0.0840 wR2 = 0.1483
Largest diff. peak and hole	0.785 and -0.509 $eÅ^{-3}$
Weighting scheme	calc $w=1/[\sigma^2(Fo^2)+(0.0946P)^2+3.0203P]$ where
	$P=(Fo^2+2Fc^2)/3$
Extinction coefficient	0.0019(8)

Table 6-11 Complex **(12)**, atomic coordinates (x 10^4) and equivalent isotropic displacement parameters ($Å^2$ x 10^3).

U(eq) is defined as one third of the trace of the orthogonalized Uij tensor.

Atom	x	y	z	U(eq)
Ag(1)	1571(1)	2804(1)	2306(1)	54(1)
P(1)	897(1)	3791(1)	3342(1)	47(1)
P(2)	1824(1)	1123(1)	2475(1)	49(1)
F(1)	3899(6)	4487(7)	154(6)	157(3)
F(2)	2201(5)	4350(5)	-754(4)	126(2)
F(3)	4934(6)	6527(7)	1591(5)	180(3)
F(4)	2977(9)	6390(6)	1361(8)	183(4)
F(5)	4363(9)	7998(6)	830(8)	209(4)
F(6)	2600(12)	6557(11)	-411(10)	283(7)
F(7)	4445(9)	6563(8)	-299(7)	198(4)
O(1)	3317(5)	4270(6)	1905(5)	117(2)
O(2)	1377(5)	3414(4)	598(4)	82(1)
C(1)	974(5)	5152(5)	3121(4)	49(1)
C(2)	662(6)	5197(6)	2063(5)	63(2)
C(3)	691(7)	6210(7)	1869(6)	81(2)
C(4)	1032(7)	7164(6)	2720(7)	78(2)
C(5)	1349(7)	7122(6)	3758(6)	72(2)
C(6)	1320(6)	6118(5)	3966(5)	62(2)
C(7)	1940(5)	4317(5)	4815(4)	49(1)
C(8)	3262(6)	4959(5)	5149(5)	64(2)
C(9)	4116(7)	5374(6)	6249(6)	76(2)
C(10)	3657(7)	5133(6)	7016(5)	75(2)
C(11)	2363(7)	4510(6)	6702(5)	74(2)
C(12)	1490(6)	4093(5)	5591(5)	59(1)
C(13)	-723(5)	2789(5)	3195(4)	53(1)
C(14)	-1603(6)	3120(6)	3025(5)	66(2)
C(15)	-2832(6)	2289(7)	2896(7)	84(2)
C(16)	-3201(7)	1151(7)	2928(6)	87(2)
C(17)	-2326(7)	826(6)	3105(7)	88(2)

C(18)	-1102(6)	1626(6)	3226(6)	68(2)
C(19)	3198(5)	1540(5)	3743(4)	54(1)
C(20)	3532(6)	2395(6)	4698(5)	70(2)
C(21)	4552(8)	2732(7)	5668(5)	85(2)
C(22)	5276(8)	2260(8)	5723(6)	91(2)
C(23)	4972(8)	1425(8)	4797(7)	96(2)
C(24)	3929(7)	1048(6)	3818(6)	75(2)
C(25)	2057(5)	407(5)	1404(4)	52(1)
C(26)	3075(6)	1166(6)	1208(5)	69(2)
C(27)	3369(7)	669(8)	470(6)	83(2)
C(28)	2636(8)	-556(8)	-96(6)	83(2)
C(29)	1612(7)	-1294(6)	76(5)	70(2)
C(30)	1300(6)	-837(5)	819(5)	59(1)
C(31)	451(5)	-89(5)	2569(5)	52(1)
C(32)	535(6)	-379(6)	3516(5)	67(2)
C(33)	-558(8)	-1227(7)	3589(7)	88(2)
C(34)	-1738(8)	-1798(7)	2697(9)	94(2)
C(35)	-1828(7)	-1513(6)	1755(7)	86(2)
C(36)	-758(6)	-662(6)	1689(6)	71(2)
C(37)	2528(7)	4077(6)	989(6)	63(2)
C(38)	3093(7)	4758(7)	281(6)	76(2)
C(39)	3712(13)	6112(10)	708(9)	162(6)
C(40)	3717(17)	6918(12)	294(22)	244(12)

Table 6-12 Complex **(12)**, bond lengths (Å) and angles (°).

Ag(1)-P(2)	2.430(2)	Ag(1)-P(1)	2.436(2)
Ag(1)-O(1)	2.495(5)	P(1)-C(7)	1.823(5)
Ag(1)-O(2)	2.532(5)	P(1)-C(13)	1.824(6)
P(1)-C(1)	1.828(5)	P(2)-C(31)	1.822(6)
P(2)-C(19)	1.822(6)	P(2)-C(25)	1.828(5)
F(1)-C(38)	1.322(9)	F(3)-C(39)	1.435(14)
F(2)-C(38)	1.333(8)	F(4)-C(39)	1.64(2)
F(5)-C(40)	1.22(2)	O(1)-C(37)	1.232(8)

F(6)-C(40)	1.27(2)	O(2)-C(37)	1.201(8)
F(7)-C(40)	1.62(2)	C(1)-C(6)	1.378(8)
C(1)-C(2)	1.380(8)	C(4)-C(5)	1.353(10)
C(2)-C(3)	1.386(9)	C(5)-C(6)	1.381(8)
C(3)-C(4)	1.375(10)	C(7)-C(12)	1.371(8)
C(7)-C(8)	1.392(8)	C(10)-C(11)	1.368(10)
C(8)-C(9)	1.382(9)	C(11)-C(12)	1.401(9)
C(9)-C(10)	1.368(10)	C(13)-C(14)	1.385(8)
C(13)-C(18)	1.388(8)	C(16)-C(17)	1.372(11)
C(14)-C(15)	1.393(9)	C(17)-C(18)	1.383(9)
C(15)-C(16)	1.361(11)	C(19)-C(24)	1.381(8)
C(19)-C(20)	1.395(8)	C(23)-C(24)	1.375(10)
C(20)-C(21)	1.366(9)	C(25)-C(26)	1.380(8)
C(21)-C(22)	1.355(11)	C(25)-C(30)	1.392(8)
C(22)-C(23)	1.368(11)	C(26)-C(27)	1.386(9)
C(27)-C(28)	1.369(10)	C(31)-C(32)	1.377(8)
C(28)-C(29)	1.358(10)	C(31)-C(36)	1.386(8)
C(29)-C(30)	1.383(8)	C(32)-C(33)	1.391(10)
C(33)-C(34)	1.370(11)	C(37)-C(38)	1.534(9)
C(34)-C(35)	1.367(12)	C(38)-C(39)	1.505(14)
C(35)-C(36)	1.368(9)	C(39)-C(40)	1.27(2)

P(2)-Ag(1)-P(1)	129.28(5)	C(7)-P(1)-C(13)	104.7(2)
P(2)-Ag(1)-O(1)	108.3(2)	C(7)-P(1)-C(1)	103.4(2)
P(1)-Ag(1)-O(1)	112.8(2)	C(13)-P(1)-C(1)	105.3(2)
P(2)-Ag(1)-O(2)	121.62(12)	C(7)-P(1)-Ag(1)	109.1(2)
P(1)-Ag(1)-O(2)	107.14(13)	C(13)-P(1)-Ag(1)	114.4(2)
O(1)-Ag(1)-O(2)	51.3(2)	C(1)-P(1)-Ag(1)	118.6(2)
C(31)-P(2)-C(25)	106.6(3)	C(19)-P(2)-C(31)	103.9(3)
C(19)-P(2)-Ag(1)	113.0(2)	C(19)-P(2)-C(25)	103.1(3)
C(31)-P(2)-Ag(1)	110.7(2)	C(4)-C(3)-C(2)	120.6(6)
C(25)-P(2)-Ag(1)	118.3(2)	C(5)-C(4)-C(3)	120.0(6)
C(37)-O(1)-Ag(1)	91.4(4)	C(4)-C(5)-C(6)	120.2(6)
C(37)-O(2)-Ag(1)	90.4(4)	C(1)-C(6)-C(5)	120.5(6)
C(6)-C(1)-C(2)	119.5(5)	C(12)-C(7)-C(8)	119.2(5)
C(6)-C(1)-P(1)	122.5(4)	C(12)-C(7)-P(1)	123.5(4)
C(2)-C(1)-P(1)	118.0(4)	C(8)-C(7)-P(1)	117.3(4)

C(1)-C(2)-C(3)	119.2(6)	C(9)-C(8)-C(7)	120.8(6)
C(9)-C(10)-C(11)	120.4(6)	C(10)-C(9)-C(8)	119.6(6)
C(10)-C(11)-C(12)	120.4(6)	C(17)-C(18)-C(13)	120.5(6)
C(7)-C(12)-C(11)	119.6(6)	C(24)-C(19)-C(20)	117.6(6)
C(14)-C(13)-C(18)	118.5(6)	C(24)-C(19)-P(2)	123.6(4)
C(14)-C(13)-P(1)	123.2(5)	C(20)-C(19)-P(2)	118.7(5)
C(18)-C(13)-P(1)	118.3(4)	C(21)-C(20)-C(19)	120.8(6)
C(13)-C(14)-C(15)	119.6(6)	C(22)-C(21)-C(20)	120.8(7)
C(16)-C(15)-C(14)	121.8(7)	C(21)-C(22)-C(23)	119.5(7)
C(15)-C(16)-C(17)	118.6(7)	C(25)-C(26)-C(27)	119.4(6)
C(16)-C(17)-C(18)	120.9(7)	C(28)-C(27)-C(26)	120.9(7)
C(22)-C(23)-C(24)	120.6(7)	C(29)-C(28)-C(27)	119.4(6)
C(23)-C(24)-C(19)	120.5(6)	C(28)-C(29)-C(30)	121.5(6)
C(26)-C(25)-C(30)	119.8(5)	C(29)-C(30)-C(25)	119.0(6)
C(26)-C(25)-P(2)	116.4(4)	C(32)-C(31)-C(36)	118.0(6)
C(30)-C(25)-P(2)	123.8(4)	C(32)-C(31)-P(2)	123.0(5)
C(34)-C(33)-C(32)	119.5(7)	C(36)-C(31)-P(2)	118.6(5)
C(35)-C(34)-C(33)	119.6(7)	C(31)-C(32)-C(33)	121.2(7)
C(34)-C(35)-C(36)	121.0(7)	F(2)-C(38)-C(37)	111.7(6)
C(35)-C(36)-C(31)	120.6(7)	C(39)-C(38)-C(37)	114.4(8)
O(2)-C(37)-O(1)	126.9(6)	C(40)-C(39)-F(3)	113.4(11)
O(2)-C(37)-C(38)	117.4(6)	C(40)-C(39)-C(38)	136.2(14)
O(1)-C(37)-C(38)	115.7(6)	F(3)-C(39)-C(38)	102.8(11)
F(1)-C(38)-F(2)	102.7(7)	C(40)-C(39)-F(4)	87(2)
F(1)-C(38)-C(39)	111.6(9)	F(3)-C(39)-F(4)	102.8(9)
F(2)-C(38)-C(39)	106.9(7)	C(38)-C(39)-F(4)	108.6(8)
F(1)-C(38)-C(37)	108.9(6)	F(5)-C(40)-F(7)	112(2)
F(5)-C(40)-C(39)	123(2)	C(39)-C(40)-F(7)	82.5(13)
F(5)-C(40)-F(6)	113.3(14)	F(6)-C(40)-F(7)	110(2)
C(39)-C(40)-F(6)	112(2)		

Table 6-13 Complex **(12)**, anisotropic displacement parameters ($Å^2 \times 10^3$).

The anisotropic displacement factor exponent takes the form:

$-2\pi^2 [h^2 a^* 2 U11 + ... + 2 h k a^* b^* U12]$

Atom	U11	U22	U33	U23	U13	U12
Ag(1)	65(1)	58(1)	56(1)	24(1)	34(1)	39(1)
P(1)	53(1)	52(1)	44(1)	16(1)	23(1)	33(1)
P(2)	52(1)	48(1)	49(1)	14(1)	22(1)	29(1)
F(1)	143(5)	195(6)	215(7)	107(5)	146(5)	98(5)
F(2)	133(4)	114(4)	66(3)	32(3)	33(3)	30(3)
F(3)	89(4)	195(7)	124(5)	62(5)	1(3)	15(4)
F(4)	251(8)	139(5)	270(9)	95(6)	219(8)	112(6)
F(5)	224(8)	73(4)	262(10)	25(5)	102(8)	45(5)
F(6)	231(10)	266(12)	262(12)	35(9)	-35(9)	181(10)
F(7)	217(8)	179(7)	202(8)	36(6)	162(7)	73(6)
O(1)	69(3)	164(6)	110(4)	89(4)	36(3)	51(4)
O(2)	65(3)	83(3)	69(3)	18(2)	35(2)	19(3)
C(1)	51(3)	57(3)	52(3)	23(3)	27(3)	34(3)
C(2)	72(4)	70(4)	58(4)	26(3)	28(3)	45(3)
C(3)	102(5)	113(6)	73(4)	61(4)	50(4)	76(5)
C(4)	101(5)	74(4)	100(5)	49(4)	60(5)	61(4)
C(5)	91(5)	64(4)	80(5)	26(3)	44(4)	51(4)
C(6)	80(4)	66(4)	61(3)	26(3)	38(3)	49(3)
C(7)	57(3)	49(3)	51(3)	19(2)	24(3)	35(3)
C(8)	57(4)	62(4)	61(4)	15(3)	23(3)	28(3)
C(9)	57(4)	70(4)	71(4)	12(3)	10(3)	29(3)
C(10)	84(5)	72(4)	53(4)	13(3)	9(3)	48(4)
C(11)	94(5)	77(4)	54(4)	27(3)	32(4)	49(4)
C(12)	61(4)	68(4)	54(3)	24(3)	25(3)	38(3)
C(13)	56(3)	59(3)	40(3)	8(2)	20(3)	33(3)
C(14)	61(4)	70(4)	71(4)	20(3)	29(3)	40(3)
C(15)	54(4)	91(5)	104(6)	22(4)	35(4)	40(4)
C(16)	62(4)	78(5)	99(6)	10(4)	45(4)	23(4)
C(17)	90(5)	60(4)	111(6)	23(4)	58(5)	32(4)
C(18)	69(4)	60(4)	84(4)	22(3)	42(4)	37(3)

C(19)	51(3)	53(3)	50(3)	13(3)	17(3)	28(3)
C(20)	74(4)	74(4)	56(4)	11(3)	25(3)	41(4)
C(21)	90(5)	94(5)	50(4)	11(4)	20(4)	47(5)
C(22)	76(5)	117(6)	61(4)	27(4)	13(4)	50(5)
C(23)	84(5)	129(7)	84(5)	31(5)	21(4)	78(5)
C(24)	77(4)	82(4)	64(4)	15(3)	20(3)	52(4)
C(25)	57(3)	57(3)	48(3)	17(3)	22(3)	36(3)
C(26)	66(4)	63(4)	65(4)	11(3)	31(3)	29(3)
C(27)	74(5)	100(6)	81(5)	30(4)	47(4)	45(4)
C(28)	97(6)	109(6)	65(4)	19(4)	42(4)	70(5)
C(29)	78(4)	69(4)	57(4)	4(3)	22(3)	45(4)
C(30)	60(3)	53(3)	56(3)	13(3)	21(3)	30(3)
C(31)	54(3)	54(3)	59(3)	18(3)	28(3)	35(3)
C(32)	70(4)	65(4)	69(4)	26(3)	31(3)	38(3)
C(33)	102(6)	83(5)	110(6)	57(5)	71(5)	50(5)
C(34)	72(5)	77(5)	148(8)	52(5)	62(6)	40(4)
C(35)	60(4)	69(4)	117(6)	34(4)	32(4)	31(4)
C(36)	60(4)	71(4)	76(4)	25(3)	26(3)	34(3)
C(37)	63(4)	69(4)	70(4)	30(3)	38(3)	38(4)
C(38)	65(4)	86(5)	83(5)	44(4)	40(4)	37(4)
C(39)	164(11)	96(8)	105(8)	44(6)	24(8)	8(8)
C(40)	150(13)	82(9)	371(30)	48(13)	-1(17)	56(9)

Table 6-14 Complex **(12)**, hydrogen coordinates (x 10^4) and isotropic displacement parameters ($Å^2$ x 10^3).

Atom	x	y	z	U(eq)
H(2)	435(6)	4555(6)	1486(5)	76
H(3)	477(7)	6245(7)	1158(6)	97
H(4)	1046(7)	7839(6)	2581(7)	94
H(5)	1586(7)	7771(6)	4333(6)	86
H(6)	1535(6)	6093(5)	4681(5)	74
H(8)	3573(6)	5110(5)	4626(5)	77
H(9)	4998(7)	5815(6)	6466(6)	91
H(10)	4229(7)	5394(6)	7754(5)	90
H(11)	2060(7)	4363(6)	7231(5)	88
H(12)	610(6)	3666(5)	5380(5)	71
H(14)	-1375(6)	3892(6)	2998(5)	79
H(15)	-3417(6)	2519(7)	2785(7)	101
H(16)	-4028(7)	605(7)	2833(6)	104
H(17)	-2559(7)	56(6)	3144(7)	106
H(18)	-528(6)	1384(6)	3328(6)	82
H(20)	3055(6)	2739(6)	4673(5)	84
H(21)	4752(8)	3293(7)	6299(5)	102
H(22)	5975(8)	2502(8)	6385(6)	110
H(23)	5476(8)	1108(8)	4829(7)	115
H(24)	3715(7)	458(6)	3202(6)	90
H(26)	3558(6)	2002(6)	1568(5)	82
H(27)	4074(7)	1175(8)	358(6)	99
H(28)	2837(8)	-880(8)	-594(6)	100
H(29)	1111(7)	-2124(6)	-315(5)	84
H(30)	595(6)	-1353(5)	926(5)	70
H(32)	1336(6)	0(6)	4119(5)	80
H(33)	-488(8)	-1406(7)	4238(7)	106
H(34)	-2473(8)	-2375(7)	2733(9)	112
H(35)	-2629(7)	-1905(6)	1149(7)	103
H(36)	-843(6)	-465(6)	1047(6)	85

A4.3 Structural data for complex (21), Ag(hfac)(PPh_3)

A crystal of approximate dimensions 0.4 x 0.3 x 0.2 mm was used for data collection.

Crystal data: $C_{23}H_{16}O_2F_6PAg$, M = 577.2 monoclinic, a = 11.175(4), b = 17.457(3), c = 11.260(3)Å, β= 101.14(2) , U = 2155.0 $Å^3$, space group $P2_1/c$, Z = 4, D_c = 1.78 gcm^{-3}, μ(Mo-K_α) = 10.7 cm^{-1}, F(000) = 1144. Data were measured at 170 K on a CAD4 automatic four-circle diffractometer in the range $2 \geq 3 \geq 24^\circ$. 3698 reflections were collected of which 2848 were unique with $I \geq 2\sigma(I)$. Data were corrected for Lorentz and polarization but not for absorption. The structure was solved by Patterson methods and refined using the SHELX [364, 365] suite of programs. In the final least squares cycles all atoms were allowed to vibrate anisotropically. Hydrogen atoms were included at calculated positions except in the instance of H211 (attached to C21) which was located in an advanced Difference Fourier and refined at a distance of 0.98 Å from the parent atom. Final residuals after 10 cycles of least squares were R = 0.0407, R_w= 0.0459, for a weighting scheme of $w = 2.1494/[\sigma^2(F) + 0.001252(F)^2]$. Max. final shift/esd was 0.000. The max. and min. residual densities were 0.51 and -0.66 $eÅ^{-3}$ respectively. Final fractional atomic coordinates and isotropic thermal parameters, bond distances, angles and least square plane calculations are presented in the following tables. Tables of anisotropic temperature factors are available as supplementary data. The asymmetric unit is shown in Figure 4-10, along with the labelling scheme used.

Table 6-15 Complex **(21)**, fractional atomic co-ordinates ($x10^4$) and equivalent isotropic temperature factors ($Å^2 x10^3$).

	x	y	z	U
Ag(1)	2409	329	4808	26
P(1)	961(1)	1319(1)	4529(1)	19
F(1)	5751(3)	-1879(2)	6285(3)	39(1)
F(2)	4252(4)	-2467(2)	5257(4)	67(1)
F(3)	4080(4)	-1894(2)	6918(4)	76(2)
F(4)	-5988(3)	742(3)	7610(3)	68(2)
F(5)	4168(4)	-847(3)	1315(3)	65(2)
F(6)	-4996(3)	-238(2)	8277(3)	50(1)
O(1)	3411(3)	-699(2)	5621(3)	25(1)
O(2)	3578(3)	114(2)	3324(3)	27(1)
C(1)	18(4)	1185(3)	3024(4)	21(1)
C(2)	608(4)	1120(3)	2042(4)	24(2)
C(3)	-44(5)	939(3)	909(4)	29(2)
C(4)	-1292(5)	798(3)	743(4)	30(2)
C(5)	-1881(4)	855(3)	1711(4)	28(2)
C(6)	-1236(4)	1060(3)	2850(4)	21(1)
C(7)	-102(4)	1412(3)	5559(4)	20(1)
C(8)	-835(4)	2061(3)	5539(4)	21(1)
C(9)	-1630(4)	2128(3)	6341(4)	24(1)
C(10)	-1702(4)	1540(3)	7155(4)	28(2)
C(11)	-992(4)	893(3)	7167(4)	27(1)
C(12)	-192(4)	829(3)	6372(4)	24(1)
C(13)	1658(4)	2266(2)	4572(4)	19(1)
C(14)	1419(4)	2796(3)	3631(4)	21(1)
C(15)	2028(4)	3494(3)	3745(4)	25(1)
C(16)	2848(4)	3674(3)	4777(4)	27(2)
C(17)	3078(4)	3151(3)	5727(4)	28(2)
C(18)	2500(4)	2444(3)	5628(4)	24(1)
C(19)	4546(5)	-1843(3)	5919(5)	33(2)
C(20)	4147(4)	-1113(3)	5202(4)	24(1)
C(21)	4644(4)	-1015(3)	4166(4)	26(2)

C(22)	4307(4)	-421(3)	3316(5)	26(2)
C(23)	4878(5)	-443(3)	2177(5)	34(2)

Table 6-16 Complex **(21)**, anisotropic temperature factors (Å x10^3).

	U_{11}	U_{22}	U_{33}	U_{23}	U_{13}	U_{12}
Ag(1)	25	23	31	1	8	9
P(1)	18(1)	17(1)	23(1)	2	7	3
F(1)	29(2)	46(2)	38(2)	7(1)	0(1)	14(1)
F(2)	75(3)	24(2)	82(3)	6(2)	-35(2)	-1(2)
F(3)	69(3)	80(3)	94(3)	62(2)	56(2)	48(2)
F(4)	49(2)	107(3)	57(2)	22(2)	34(2)	44(2)
F(5)	77(3)	86(3)	37(2)	-24(2)	24(2)	-30(2)
F(6)	51(2)	62(2)	42(2)	12(2)	24(2)	-2(2)
O(1)	25(2)	24(2)	29(2)	1(1)	11(1)	4(1)
O(2)	27(2)	27(2)	30(2)	2(1)	10(1)	2(2)
C(1)	23(2)	15(2)	25(2)	-2(2)	8(2)	-2(2)
C(2)	23(2)	21(2)	30(2)	1(2)	10(2)	1(2)
C(3)	38(3)	24(3)	29(3)	-4(2)	15(2)	0(2)
C(4)	38(3)	26(3)	24(2)	-2(2)	2(2)	-4(2)
C(5)	23(2)	23(3)	35(3)	2(2)	3(2)	-3(2)
C(6)	23(2)	17(2)	23(2)	2(2)	7(2)	1(2)
C(7)	17(2)	19(2)	23(2)	-5(2)	2(2)	-3(2)
C(8)	22(2)	17(2)	24(2)	2(2)	5(2)	-2(2)
C(9)	17(2)	27(3)	27(2)	-9(2)	4(2)	-2(2)
C(10)	25(2)	35(3)	27(3)	-10(2)	12(2)	-12(2)
C(11)	35(3)	26(3)	22(2)	3(2)	6(2)	-9(2)
C(12)	29(2)	17(2)	24(2)	-2(2)	3(2)	-6(2)
C(13)	18(2)	14(2)	28(2)	-2(2)	11(2)	0(2)
C(14)	16(2)	25(3)	22(2)	-2(2)	1(2)	-1(2)
C(15)	25(2)	25(3)	25(2)	4(2)	5(2)	-4(2)

C(16)	23(2)	28(3)	31(3)	-1(2)	10(2)	-7(2)
C(17)	22(2)	38(3)	23(2)	-4(2)	3(2)	-3(2)
C(18)	21(2)	27(3)	26(2)	3(2)	9(2)	4(2)
C(19)	28(3)	32(3)	39(3)	10(2)	7(2)	8(2)
C(20)	21(2)	21(2)	28(2)	-3(2)	3(2)	-3(2)
C(21)	18(2)	29(3)	34(3)	-1(2)	7(2)	4(2)
C(22)	14(2)	35(3)	30(3)	-3(2)	6(2)	-3(2)
C(23)	32(3)	46(3)	25(3)	-2(2)	6(2)	9(2)

The temperature factor exponent takes the form:

$-2\ (U.h.a^* + \ldots + 2U.h.k.a^*.b^*)$

Table 6-17 Complex **(21)**, hydrogen fractional atomic co-ordinates ($x10^4$) and isotropic temperature factors ($Å^2\ x10^3$).

	x	y	z	U
H(21)	1474(4)	1198(3)	2157(4)	35(4)
H(31)	361(5)	911(3)	232(4)	35(4)
H(41)	-1741(5)	660(3)	-43(4)	35(4)
H(51)	-2740(4)	753(3)	1595(4)	35(4)
H(61)	-1655(4)	1115(3)	3514(4)	35(4)
H(81)	-788(4)	2464(3)	4970(4)	35(4)
H(91)	-2124(4)	2579(3)	6335(4)	35(4)
H(101)	-2247(4)	1584(3)	7713(4)	35(4)
H(112)	-1055(4)	484(3)	7722(4)	35(4)
H(121)	301(4)	377(3)	6383(4)	35(4)
H(141)	833(4)	2681(3)	2910(4)	35(4)
H(151)	1874(4)	3854(3)	3089(4)	35(4)
H(161)	3263(4)	4158(3)	4845(4)	35(4)
H(171)	3640(4)	3281(3)	6456(4)	35(4)
H(181)	2677(4)	2080(3)	6277(4)	35(4)
H(211)	5285(35)	-1381(24)	4105(46)	35(4)

Table 6-18 Complex **(21)**, bond lengths (Å).

P(1)-Ag(1)	2.346(3)	O(1)-Ag(1)	2.218(5)
O(2)-Ag(1)	2.341(5)	C(1)-P(1)	1.829(6)
C(7)-P(1)	1.821(7)	C(13)-P(1)	1.824(6)
C(19)-F(1)	1.331(7)	C(19)-F(2)	1.324(7)
C(19)-F(3)	1.330(7)	C(23)-F(5)	1.331(7)
C(20)-O(1)	1.253(6)	C(22)-O(2)	1.240(7)
C(2)-C(1)	1.398(7)	C(6)-C(1)	1.394(7)
C(3)-C(2)	1.378(8)	C(4)-C(3)	1.392(8)
C(5)-C(4)	1.382(8)	C(6)-C(5)	1.391(7)
C(8)-C(7)	1.396(7)	C(12)-C(7)	1.386(7)
C(9)-C(8)	1.389(7)	C(10)-C(9)	1.390(8)
C(11)-C(10)	1.379(8)	C(12)-C(11)	1.387(8)
C(14)-C(13)	1.393(7)	C(18)-C(13)	1.401(7)
C(15)-C(14)	1.389(8)	C(16)-C(15)	1.370(8)
C(17)-C(16)	1.392(8)	C(18)-C(17)	1.387(8)
C(20)-C(19)	1.529(9)	C(21)-C(20)	1.396(8)
C(22)-C(21)	1.412(8)	C(23)-C(22)	1.539(9)
H(21)-C(2)	0.960	H(31)-C(3)	0.960
H(41)-C(4)	0.960	H(51)-C(5)	0.960
H(61)-C(6)	0.960	H(81)-C(8)	0.960
H(91)-C(9)	0.960	H(101)-C(10)	0.960
H(112)-C(11)	0.960	H(121)-C(12)	0.960
H(141)-C(14)	0.960	H(151)-C(15)	0.960
H(161)-C(16)	0.960	H(171)-C(17)	0.960
H(181)-C(18)	0.960	H(211)-C(21)	0.973(20)

Table 6-19 Complex **(21)**, bond angles (°).

O(1)-Ag(1)-P(1)	158.7(1)	O(2)-Ag(1)-P(1)	119.2(2)
O(2)-Ag(1)-O(1)	81.8(2)	C(1)-P(1)-Ag(1)	106.8(2)
C(7)-P(1)-Ag(1)	119.9(2)	C(7)-P(1)-C(1)	105.7(3)
C(13)-P(1)-Ag(1)	112.6(2)	C(13)-P(1)-C(1)	107.8(3)
C(13)-P(1)-C(7)	103.3(3)	C(20)-O(1)-Ag(1)	128.9(4)
C(22)-O(2)-Ag(1)	125.8(4)	C(2)-C(1)-P(1)	117.9(4)
C(6)-C(1)-P(1)	122.2(4)	C(6)-C(1)-C(2)	119.4(5)
C(3)-C(2)-C(1)	120.3(5)	C(4)-C(3)-C(2)	120.1(5)
C(5)-C(4)-C(3)	119.9(5)	C(6)-C(5)-C(4)	120.3(5)
C(5)-C(6)-C(1)	119.8(5)	C(8)-C(7)-P(1)	121.1(4)
C(12)-C(7)-P(1)	119.6(4)	C(12)-C(7)-C(8)	119.3(5)
C(9)-C(8)-C(7)	120.4(5)	C(10)-C(9)-C(8)	119.5(5)
C(11)-C(10)-C(9)	120.4(5)	C(12)-C(11)-C(10)	120.1(5)
C(11)-C(12)-C(7)	120.3(5)	C(14)-C(13)-P(1)	124.3(4)
C(18)-C(13)-P(1)	115.9(4)	C(18)-C(13)-C(14)	119.8(5)
C(15)-C(14)-C(13)	119.5(5)	C(16)-C(15)-C(14)	121.1(5)
C(17)-C(16)-C(15)	119.6(5)	C(18)-C(17)-C(16)	120.5(5)
C(17)-C(18)-C(13)	119.4(5)	F(2)-C(19)-F(1)	105.2(5)
F(3)-C(19)-F(1)	105.9(5)	F(3)-C(19)-F(2)	109.0(6)
C(20)-C(19)-F(1)	112.1(5)	C(20)-C(19)-F(2)	111.9(5)
C(20)-C(19)-F(3)	112.3(5)	C(19)-C(20)-O(1)	115.3(5)
C(21)-C(20)-O(1)	129.7(5)	C(21)-C(20)-C(19)	114.9(5)
C(22)-C(21)-C(20)	124.1(5)	C(21)-C(22)-O(2)	129.5(6)
C(23)-C(22)-O(2)	113.9(5)	C(23)-C(22)-C(21)	116.6(5)
C(22)-C(23)-F(5)	109.6(5)	H(21)-C(2)-C(1)	119.9(4)
C(3)-C(2)-H(21)	119.8(4)	H(31)-C(3)-C(2)	120.0(4)
C(4)-C(3)-H(31)	119.8(4)	H(41)-C(4)-C(3)	120.0(4)
C(5)-C(4)-H(41)	120.1(4)	H(51)-C(5)-C(4)	119.7(4)
C(6)-C(5)-H(51)	120.0(4)	H(61)-C(6)-C(1)	120.2(3)
H(61)-C(6)-C(5)	120.0(4)	H(81)-C(8)-C(7)	119.8(4)
C(9)-C(8)-H(81)	119.8(4)	H(91)-C(9)-C(8)	120.2(4)
C(10)-C(9)-H(91)	120.3(4)	H(101)-C(10)-C(9)	119.8(4)
C(11)-C(10)-H(101)	119.8(4)	H(112)-C(11)-C(10)	120.1(4)

C(12)-C(11)-H(112)	119.9(4)	H(121)-C(12)-C(7)	119.8(4)
H(121)-C(12)-C(11)	119.9(4)	H(141)-C(14)-C(13)	120.2(3)
C(15)-C(14)-H(141)	120.2(4)	H(151)-C(15)-C(14)	119.4(4)
C(16)-C(15)-H(151)	119.5(4)	H(161)-C(16)-C(15)	120.2(4)
C(17)-C(16)-H(161)	120.2(4)	H(171)-C(17)-C(16)	119.6(4)
C(18)-C(17)-H(171)	119.8(4)	H(181)-C(18)-C(13)	120.3(4)
H(181)-C(18)-C(17)	120.2(4)	H(211)-C(21)-C(20)	113.3(32)
C(22)-C(21)-H(211)	122.6(32)		

Table 6-20 Complex **(21)**, selected non-bonded distances (Å).

Intramolecular:

C(1)-Ag(1)	3.366	C(2)-Ag(1)	3.638
H(21)-Ag(1)	3.331	C(7)-Ag(1)	3.616
C(12)-Ag(1)	3.779	H(121)-Ag(1)	3.211
C(13)-Ag(1)	3.482	C(18)-Ag(1)	3.803
H(181)-Ag(1)	3.461	C(20)-Ag(1)	3.158
C(21)-Ag(1)	3.599	C(22)-Ag(1)	3.227
C(2)-P(1)	2.774	H(21)-P(1)	2.845
C(6)-P(1)	2.830	H(61)-P(1)	2.947
C(8)-P(1)	2.808	H(81)-P(1)	2.905
C(12)-P(1)	2.780	H(121)-P(1)	2.863
C(14)-P(1)	2.853	H(141)-P(1)	2.984
C(18)-P(1)	2.743	H(181)-P(1)	2.803
F(2)-F(1)	2.109	F(3)-F(1)	2.124
O(1)-F(1)	3.298	C(20)-F(1)	2.375
C(21)-F(1)	2.891	H(211)-F(1)	2.561
F(3)-F(2)	2.161	O(1)-F(2)	3.274
C(20)-F(2)	2.366	C(21)-F(2)	2.887
H(211)-F(2)	2.681	O(1)-F(3)	2.573
C(20)-F(3)	2.378	F(6)-F(4)	2.096
O(2)-F(5)	2.990	C(21)-F(5)	3.164

C(22)-F(5)	2.348	O(2)-O(1)	2.986
C(19)-O(1)	2.355	C(21)-O(1)	2.399
C(22)-O(1)	2.996	C(20)-O(2)	2.990
C(21)-O(2)	2.400	C(23)-O(2)	2.335
H(21)-C(1)	2.052	C(3)-C(1)	2.408
C(4)-C(1)	2.783	C(5)-C(1)	2.410
H(61)-C(1)	2.052	C(7)-C(1)	2.910
C(13)-C(1)	2.953	C(14)-C(1)	3.227
H(141)-C(1)	2.777	H(31)-C(2)	2.035
C(4)-C(2)	2.400	C(5)-C(2)	2.773
C(6)-C(2)	2.411	C(13)-C(2)	3.494
C(14)-C(2)	3.458	H(141)-C(2)	2.890
C(3)-H(21)	2.033	H(31)-H(21)	2.335
H(41)-C(3)	2.048	C(5)-C(3)	2.401
C(6)-C(3)	2.779	C(4)-H(31)	2.047
H(41)-H(31)	2.350	H(51)-C(4)	2.036
C(6)-C(4)	2.406	C(5)-H(41)	2.040
H(51)-H(41)	2.339	H(61)-C(5)	2.047
C(6)-H(51)	2.047	H(61)-H(51)	2.350
C(7)-C(6)	3.129	C(8)-C(6)	3.450
C(7)-H(61)	2.653	C(8)-H(61)	2.822
H(81)-C(7)	2.050	C(9)-C(7)	2.416
C(10)-C(7)	2.778	C(11)-C(7)	2.405
H(121)-C(7)	2.041	C(13)-C(7)	2.858
C(18)-C(7)	3.408	H(91)-C(8)	2.047
C(10)-C(8)	2.399	C(11)-C(8)	2.770
C(12)-C(8)	2.401	C(13)-C(8)	3.200
C(9)-H(81)	2.043	H(91)-H(81)	2.349
C(13)-H(81)	2.874	H(101)-C(9)	2.044
C(11)-C(9)	2.402	C(12)-C(9)	2.777
C(10)-H(91)	2.049	H(101)-H(91)	2.351
H(112)-C(10)	2.037	C(12)-C(10)	2.396
C(11)-H(101)	2.034	H(112)-H(101)	2.336
H(121)-C(11)	2.042	C(12)-H(112)	2.042
H(121)-H(112)	2.343	H(141)-C(13)	2.052
C(15)-C(13)	2.404	C(16)-C(13)	2.783
C(17)-C(13)	2.408	H(181)-C(13)	2.060

H(151)-C(14)	2.039	C(16)-C(14)	2.402
C(17)-C(14)	2.775	C(18)-C(14)	2.417
C(15)-H(141)	2.048	H(151)-H(141)	2.343
H(161)-C(15)	2.030	C(17)-C(15)	2.388
C(18)-C(15)	2.774	C(16)-H(151)	2.024
H(161)-H(151)	2.326	H(171)-C(16)	2.045
C(18)-C(16)	2.413	C(17)-H(161)	2.050
H(171)-H(161)	2.349	H(181)-C(17)	2.046
C(18)-H(171)	2.042	H(181)-H(171)	2.348
C(21)-C(19)	2.467	H(211)-C(19)	2.482
H(211)-C(20)	1.992	C(22)-C(20)	2.480
C(23)-C(21)	2.511	C(22)-H(211)	2.102
C(23)-H(211)	2.686		

Intermolecular:

F(4)-Ag(1a)	3.391	F(1)-Ag(1b)	3.747
C(6)-Ag(1c)	3.985	H(61)-Ag(1c)	3.354
C(7)-Ag(1c)	3.955	C(10)-Ag(1c)	3.934
C(11)-Ag(1c)	3.261	H(112)-Ag(1c)	3.279
C(12)-Ag(1c)	3.273	H(121)-Ag(1c)	3.304
C(20)-Ag(1b)	4.087	C(21)-Ag(1b)	3.485
H(211)-Ag(1b)	3.208	C(22)-Ag(1b)	3.869
C(23)-Ag(1b)	4.096	H(121)-P(1c)	3.354
O(2)-F(1b)	3.182	C(13)-F(1b)	3.295
C(18)-F(1b)	3.326	C(17)-F(1d)	3.367
H(171)-F(1d)	2.518	C(9)-F(2c)	3.183
H(91)-F(2c)	2.694	F(5)-F(2e)	3.184
H(171)-F(3d)	2.852	F(5)-F(4c)	2.164
C(21)-F(4c)	2.764	H(211)-F(4c)	2.485
C(22)-F(4c)	2.384	C(23)-F(4c)	1.323
C(15)-F(4f)	3.070	H(151)-F(4f)	2.646
C(16)-F(4f)	3.149	H(161)-F(4f)	2.807
F(6)-F(5c)	2.119	H(41)-F(5g)	2.830
H(101)-F(5c)	2.892	O(1)-F(6h)	3.271
O(2)-F(6c)	2.629	H(51)-F(6i)	2.715
C(22)-F(6c)	2.380	C(23)-F(6c)	1.311

H(161)-F(6j)	2.785	C(6)-O(1c)	3.300
H(61)-O(1c)	2.463	C(22)-O(1b)	3.253
C(11)-O(2c)	3.335	C(20)-O(2b)	3.260
H(121)-C(1c)	2.847	H(112)-C(2c)	2.848
C(17)-H(21k)	2.866	H(112)-C(3c)	3.054
H(81)-C(3k)	3.040	C(15)-H(31k)	2.926
C(16)-H(31k)	3.009	H(91)-C(5k)	2.771
H(121)-C(6c)	2.790	H(91)-C(6k)	2.981
H(141)-C(8l)	2.980	C(20)-C(9c)	3.490
H(141)-C(9l)	2.989	C(21)-C(10c)	3.460
C(22)-C(10c)	3.460	C(15)-C(12l)	3.483
H(151)-C(12l)	2.765	H(211)-C(18b)	3.062
C(22)-C(20b)	3.439		

Key to symmetry operations relating designated atoms to reference atoms at (x,y,z):

(a) -1.0+x,y,z
(b) 1.0-x,-y,1.0-z
(c) -x,-y,1.0-z
(d) 1.0-x,0.5+y,1.5-z
(e) x,-0.5-y,-0.5+z
(f) 1.0+x,0.5-y,-0.5+z
(g) -x,-y,-z
(h) 1.0+x,y,z
(i) -1.0-x,-y,1.0-z
(j) -x,0.5+y,1.5-z
(k) x,0.5-y,0.5+z
(l) x,0.5-y,-0.5+z

Table 6-21 Complex **(21)**, least square plane calculations.

Plane 1 : Ag-O2-C22-C21-C20-O1

Atom	Distance from plane (Å)
P1	-0.192
Ag1	-0.013
O2	0.007
C22	0.001
C21	0.002
C20	-0.021
O1	0.027

Plane 2 : P-Ag-O2-C22-C21-C20-O1

Atom	Distance from plane (Å)
P1	-0.054
Ag1	0.058
O2	0.032
C22	-0.012
C21	-0.032
C20	-0.038
O1	0.046

A4.4 Structural data for complex (24), {2-(dimethylaminomethyl)phenyl}silver(I)

A crystal of approximate dimensions 0.2 x 0.2 x 0.1 mm was used for data collection.

Crystal data: $C_9H_{12}AgN$, M = 242.07, Triclinic , a = 12.110(3), b = 12.301(4), c = 13.182(4) Å , α = 88.60(2), β = 86.84(2), γ = 65.40(2)°, U = 1782.7(9) Å^3, space group P-1 (No. 2), Z = 8, D_c = 1.804 gcm^{-3}, (mMo-K_a) = 2.195 mm^{-1}, F(000) = 960. Crystallographic measurements were made at 170(2)° K on a CAD4 automatic four-circle diffractometer in the range 2.35<q<22.00°. Data (4646 reflections) were corrected for Lorentz and polarization and also for linear crystal decay (24%) but not for absorption. The asymmetric unit was infact a tetramer as expected. In the final least squares cycles all atoms were allowed to vibrate anisotropically except for C13 and C24. Anisotropic refinement of these 2 carbons would have resulted in unsatisfactory thermal parameters, so they were refined isotropically. Hydrogen atoms were included at calculated positions where relevant. The solution of the structure (SHELX86) [366] and refinement (SHELX93) [367] converged to a conventional [i.e. based on 2295 with Fo>4s(Fo)] $R1$ = 0.0496 and $wR2$ = 0.1108. Goodness of fit = 1.068. The max. and min. residual densities were 1.486 and -0.793eÅ^{-3} respectively. The asymmetric unit (shown in Figure 5-10), along with the labelling scheme used was produced using ORTEX. [368] Final fractional atomic co-ordinates and isotropic thermal parameters, bond distances, angles and least square plane calculations are presented in the following tables. Tables of anisotropic temperature factors are available as supplementary data.

Table 6-22 Complex **(24)**, crystal data and structure refinement.

Identification code	95KCM4
Empirical formula	$C_9 H_{12} Ag N$
Formula weight	242.07
Temperature	170(2)°K
Wavelength	0.70930 Å
Crystal system	Triclinic
Space group	P-1
Unit cell dimensions	a = 12.110(3)Å α = 88.60(2)°
	b = 12.301(4)Å β = 86.84(2)°
	c = 13.182(4)Å γ = 65.40(2)°
Volume	1782.7(9) $Å^3$
Z	8
Density (calculated)	1.804 Mg/m^3
Absorption coefficient	2.195 mm^{-1}
F(000)	960
Crystal size	0.2 x 0.2 x 0.1 mm
Theta range for data collection	2.35 to 22.00°.
Index ranges	0<=h<=13; -12<=k<=14; -15<=l<=15
Reflections collected	4646
Independent reflections	4391 [R(int) = 0.0403]
Refinement method	Full-matrix least-squares on F^2
Data / restraints / parameters	3495 / 0 / 389
Goodness-of-fit on F^2	1.068
Final R indices [$I>2\sigma(I)$]	R1 = 0.0496 wR2 = 0.1108
R indices (all data)	R1 = 0.1265 wR2 = 0.1619
Largest diff. peak and hole	1.486 and -0.793 $eÅ^{-3}$
Weighting scheme	calc $w=1/[\sigma^2(Fo^2)+(0.0730P)^2+3.2034P]$ where
	$P=(Fo^2+2Fc^2)/3$
Extinction coefficient	0.0003(2)
Extinction expression	$Fc^*=kFc[1+0.001xFc^2\lambda^3/\sin(2\theta)]^{-1/4}$

Table 6-23 Complex **(24)**, atomic coordinates (x 10^4) and equivalent isotropic displacement parameters ($Å^2$ x 10^3).

U(eq) is defined as one third of the trace of the orthogonalized Uij tensor.

Atom	x	y	z	U(eq)
Ag(1)	3789(1)	7133(1)	3591(1)	23(1)
Ag(2)	2545(1)	8973(1)	2317(1)	24(1)
Ag(3)	1272(1)	7901(1)	1403(1)	24(1)
Ag(4)	2489(1)	6082(1)	2716(1)	23(1)
N(1)	2069(10)	10395(9)	3806(8)	23(3)
N(2)	2946(10)	9644(10)	592(8)	30(3)
N(3)	468(10)	5944(9)	3093(9)	29(3)
N(4)	4403(9)	4110(9)	2640(8)	25(3)
C(1)	4488(13)	8406(12)	3038(11)	31(4)
C(2)	5517(11)	7980(11)	2358(9)	22(3)
C(3)	6313(12)	8520(12)	2297(9)	28(3)
C(4)	6115(12)	9503(13)	2864(10)	32(4)
C(5)	5102(12)	9950(12)	3541(10)	31(4)
C(6)	4296(13)	9444(12)	3632(10)	26(4)
C(7)	3192(12)	9914(11)	4347(10)	25(3)
C(8)	1065(13)	10415(13)	4481(11)	37(4)
C(9)	1831(14)	11593(12)	3397(11)	39(4)
C(10)	553(11)	9792(12)	1628(9)	22(3)
C(11)	-432(11)	10291(12)	2319(10)	29(3)
C(12)	-1228(13)	11529(12)	2271(11)	35(4)
C(13)	-1043(13)	12257(13)	1566(10)	32(3)
C(14)	-78(13)	11774(11)	869(11)	35(4)
C(15)	731(13)	10561(12)	896(12)	28(4)
C(16)	1787(12)	10049(11)	142(10)	27(3)
C(17)	3940(13)	8706(13)	-45(11)	46(4)
C(18)	3287(13)	10621(13)	757(10)	32(3)
C(19)	1815(12)	6020(11)	1080(10)	26(3)
C(20)	2745(13)	5513(12)	341(10)	32(4)

C(21)	2840(16)	4502(13)	-193(11)	46(4)
C(22)	2092(19)	3967(14)	38(13)	62(6)
C(23)	1134(15)	4453(13)	766(12)	43(4)
C(24)	977(13)	5510(13)	1331(11)	27(4)
C(25)	0(13)	6015(12)	2103(12)	42(4)
C(26)	823(13)	4753(12)	3539(12)	38(4)
C(27)	-375(12)	6831(13)	3790(12)	43(4)
C(28)	3156(11)	5917(11)	4378(9)	19(3)
C(29)	2279(12)	6444(12)	5158(9)	24(3)
C(30)	2113(13)	5818(14)	5969(11)	35(4)
C(31)	2798(14)	4583(15)	6018(11)	41(4)
C(32)	3638(13)	4039(13)	5246(10)	30(4)
C(33)	3896(12)	4659(11)	4438(10)	17(3)
C(34)	4893(11)	4050(11)	3650(10)	28(4)
C(35)	5306(13)	4045(13)	1847(11)	40(4)
C(36)	4036(13)	3152(12)	2524(11)	36(4)

Table 6-24 Complex **(24)**, bond lengths (Å) and angles (°).

Ag(1)-C(1)	2.162(14)	Ag(2)-N(1)	2.539(10)
Ag(1)-C(28)	2.167(12)	Ag(2)-Ag(3)	2.748(2)
Ag(1)-Ag(4)	2.729(2)	Ag(3)-C(10)	2.140(13)
Ag(1)-Ag(2)	2.732(2)	Ag(3)-C(19)	2.172(12)
Ag(2)-C(1)	2.403(14)	Ag(3)-Ag(4)	2.743(2)
Ag(2)-C(10)	2.416(12)	Ag(4)-C(28)	2.351(12)
Ag(2)-N(2)	2.493(11)	Ag(4)-C(19)	2.362(12)
Ag(4)-N(4)	2.563(10)	Ag(4)-N(3)	2.544(11)
N(1)-C(8)	1.46(2)	C(1)-C(2)	1.41(2)
N(1)-C(7)	1.46(2)	C(1)-C(6)	1.44(2)
N(1)-C(9)	1.47(2)	C(2)-C(3)	1.38(2)
N(2)-C(16)	1.44(2)	C(3)-C(4)	1.36(2)
N(2)-C(18)	1.45(2)	C(4)-C(5)	1.39(2)
N(2)-C(17)	1.50(2)	C(5)-C(6)	1.36(2)

N(3)-C(25)	1.44(2)	C(6)-C(7)	1.50(2)
N(3)-C(27)	1.45(2)	C(10)-C(11)	1.39(2)
N(3)-C(26)	1.46(2)	C(19)-C(24)	1.42(2)
N(4)-C(36)	1.44(2)	C(20)-C(21)	1.40(2)
N(4)-C(35)	1.45(2)	C(21)-C(22)	1.34(2)
N(4)-C(34)	1.48(2)	C(22)-C(23)	1.40(2)
C(10)-C(15)	1.41(2)	C(23)-C(24)	1.45(2)
C(11)-C(12)	1.43(2)	C(24)-C(25)	1.45(2)
C(12)-C(13)	1.35(2)	C(28)-C(29)	1.39(2)
C(13)-C(14)	1.38(2)	C(28)-C(33)	1.43(2)
C(14)-C(15)	1.40(2)	C(31)-C(32)	1.37(2)
C(15)-C(16)	1.50(2)	C(32)-C(33)	1.39(2)
C(19)-C(20)	1.39(2)	C(33)-C(34)	1.50(2)
C(29)-C(30)	1.36(2)	C(30)-C(31)	1.40(2)

C(1)-Ag(2)-C(10)	173.0(4)	Ag(4)-Ag(1)-Ag(2)	82.76(5)
C(1)-Ag(2)-N(2)	101.0(4)	C(28)-Ag(1)-Ag(2)	128.1(3)
C(1)-Ag(1)-C(28)	171.0(5)	C(1)-Ag(1)-Ag(2)	57.4(4)
C(1)-Ag(1)-Ag(4)	132.8(4)	C(28)-Ag(1)-Ag(4)	56.0(3)
C(10)-Ag(2)-N(2)	77.5(4)	C(1)-Ag(2)-Ag(3)	138.5(3)
C(1)-Ag(2)-N(1)	76.7(4)	C(10)-Ag(2)-Ag(3)	48.4(3)
C(10)-Ag(2)-N(1)	98.0(4)	N(2)-Ag(2)-Ag(3)	87.3(2)
N(2)-Ag(2)-N(1)	119.1(3)	N(1)-Ag(2)-Ag(3)	133.8(2)
C(1)-Ag(2)-Ag(1)	49.3(3)	Ag(1)-Ag(2)-Ag(3)	97.41(6)
C(10)-Ag(2)-Ag(1)	136.0(3)	C(10)-Ag(3)-C(19)	173.4(4)
N(2)-Ag(2)-Ag(1)	135.8(3)	C(10)-Ag(3)-Ag(4)	129.2(3)
N(1)-Ag(2)-Ag(1)	88.5(2)	C(19)-Ag(3)-Ag(4)	56.0(3)
C(19)-Ag(3)-Ag(2)	128.9(3)	C(10)-Ag(3)-Ag(2)	57.7(3)
Ag(4)-Ag(3)-Ag(2)	82.21(5)	N(3)-Ag(4)-Ag(1)	136.4(2)
C(28)-Ag(4)-C(19)	173.1(4)	N(4)-Ag(4)-Ag(1)	89.0(2)
C(28)-Ag(4)-N(3)	99.5(4)	C(28)-Ag(4)-Ag(3)	136.6(3)
C(19)-Ag(4)-N(3)	77.0(4)	C(19)-Ag(4)-Ag(3)	49.7(3)
C(28)-Ag(4)-N(4)	77.8(4)	N(3)-Ag(4)-Ag(3)	86.5(3)
C(19)-Ag(4)-N(4)	98.4(4)	N(4)-Ag(4)-Ag(3)	136.9(3)
N(3)-Ag(4)-N(4)	117.0(3)	Ag(1)-Ag(4)-Ag(3)	97.59(5)
C(28)-Ag(4)-Ag(1)	49.8(3)	C(8)-N(1)-C(7)	109.6(10)
C(19)-Ag(4)-Ag(1)	136.4(3)	C(8)-N(1)-C(9)	111.5(11)

C(7)-N(1)-C(9)	110.7(10)	C(18)-N(2)-Ag(2)	105.6(7)
C(8)-N(1)-Ag(2)	113.6(7)	C(17)-N(2)-Ag(2)	115.2(8)
C(7)-N(1)-Ag(2)	103.1(7)	C(25)-N(3)-C(27)	112.8(11)
C(9)-N(1)-Ag(2)	108.0(8)	C(25)-N(3)-C(26)	111.7(11)
C(16)-N(2)-C(18)	111.7(11)	C(27)-N(3)-C(26)	109.5(12)
C(16)-N(2)-C(17)	112.1(11)	C(25)-N(3)-Ag(4)	103.3(8)
C(18)-N(2)-C(17)	108.9(11)	C(27)-N(3)-Ag(4)	115.6(8)
C(16)-N(2)-Ag(2)	103.2(8)	C(2)-C(1)-Ag(1)	117.3(10)
C(26)-N(3)-Ag(4)	103.4(8)	C(6)-C(1)-Ag(1)	120.5(10)
C(36)-N(4)-C(35)	109.8(11)	C(2)-C(1)-Ag(2)	116.7(9)
C(36)-N(4)-C(34)	110.2(11)	C(6)-C(1)-Ag(2)	102.2(9)
C(35)-N(4)-C(34)	110.5(10)	Ag(1)-C(1)-Ag(2)	73.3(4)
C(36)-N(4)-Ag(4)	108.2(8)	C(3)-C(2)-C(1)	120.7(12)
C(35)-N(4)-Ag(4)	115.1(8)	C(4)-C(3)-C(2)	121.5(12)
C(34)-N(4)-Ag(4)	102.8(7)	C(3)-C(4)-C(5)	119.2(13)
C(2)-C(1)-C(6)	116.9(12)	C(15)-C(10)-Ag(2)	98.8(9)
C(6)-C(5)-C(4)	121.5(13)	Ag(3)-C(10)-Ag(2)	73.9(4)
C(5)-C(6)-C(1)	120.2(14)	C(10)-C(11)-C(12)	120.8(13)
C(5)-C(6)-C(7)	122.6(12)	C(13)-C(12)-C(11)	121.4(14)
C(1)-C(6)-C(7)	117.2(11)	C(12)-C(13)-C(14)	118.5(14)
N(1)-C(7)-C(6)	111.9(10)	C(13)-C(14)-C(15)	121.8(14)
C(11)-C(10)-C(15)	117.1(13)	C(14)-C(15)-C(10)	120(2)
C(11)-C(10)-Ag(3)	117.1(10)	C(14)-C(15)-C(16)	121.3(14)
C(15)-C(10)-Ag(3)	122.0(10)	Ag(3)-C(19)-Ag(4)	74.3(4)
C(11)-C(10)-Ag(2)	116.6(8)	C(19)-C(20)-C(21)	120(2)
C(10)-C(15)-C(16)	118.3(13)	C(22)-C(21)-C(20)	121(2)
N(2)-C(16)-C(15)	113.4(11)	C(21)-C(22)-C(23)	121(2)
C(20)-C(19)-C(24)	121.2(12)	C(22)-C(23)-C(24)	120(2)
C(20)-C(19)-Ag(3)	116.4(10)	C(19)-C(24)-C(25)	122.4(12)
C(24)-C(19)-Ag(3)	118.5(10)	C(19)-C(24)-C(23)	116.6(13)
C(20)-C(19)-Ag(4)	114.3(9)	C(25)-C(24)-C(23)	121.0(13)
C(24)-C(19)-Ag(4)	99.4(9)	N(3)-C(25)-C(24)	111.3(12)
C(29)-C(28)-C(33)	118.0(12)	C(29)-C(30)-C(31)	119.8(13)
C(29)-C(28)-Ag(1)	114.3(9)	C(32)-C(31)-C(30)	118.6(14)
C(33)-C(28)-Ag(1)	122.1(9)	C(31)-C(32)-C(33)	123.5(14)
C(29)-C(28)-Ag(4)	117.6(9)	C(32)-C(33)-C(28)	117.2(12)
C(33)-C(28)-Ag(4)	101.0(8)	C(32)-C(33)-C(34)	122.1(12)

Ag(1)-C(28)-Ag(4)	74.2(4)	C(28)-C(33)-C(34)	120.7(12)
C(30)-C(29)-C(28)	122.8(13)	N(4)-C(34)-C(33)	111.3(10)

Table 6-25 Complex **(24)**, anisotropic displacement parameters ($Å^2 \times 10^3$).

The anisotropic displacement factor exponent takes the form:

$-2\pi^2 [h^2 a^* 2 U11 + ... + 2 h k a^* b^* U12]$

	U11	U22	U33	U23	U13	U12
Ag(1)	30(1)	15(1)	25(1)	4(1)	-6(1)	-9(1)
Ag(2)	31(1)	16(1)	24(1)	2(1)	-10(1)	-7(1)
Ag(3)	32(1)	12(1)	25(1)	2(1)	-8(1)	-6(1)
Ag(4)	31(1)	15(1)	24(1)	4(1)	-8(1)	-9(1)
N(1)	37(7)	8(6)	20(6)	3(5)	0(5)	-7(5)
N(2)	39(7)	31(7)	20(6)	1(5)	-1(5)	-16(6)
N(3)	30(7)	19(7)	37(7)	-7(6)	-3(6)	-7(6)
N(4)	18(6)	15(6)	37(7)	1(5)	-11(5)	-1(5)
C(1)	36(9)	21(8)	35(9)	11(7)	-11(7)	-10(7)
C(2)	26(8)	19(8)	15(7)	-4(6)	3(6)	-3(7)
C(3)	23(8)	39(9)	13(7)	4(7)	-4(6)	-5(7)
C(4)	18(8)	41(9)	34(9)	6(7)	-6(7)	-9(7)
C(5)	36(9)	25(8)	34(9)	1(7)	-23(7)	-14(7)
C(6)	33(9)	27(9)	23(8)	14(7)	-27(7)	-14(8)
C(7)	40(9)	10(7)	21(7)	7(6)	-16(7)	-6(6)
C(8)	43(9)	30(9)	34(9)	-2(7)	4(7)	-12(8)
C(9)	50(10)	19(8)	39(10)	-3(7)	-9(8)	-5(7)
C(10)	26(8)	29(8)	15(7)	-7(6)	-11(6)	-14(7)
C(11)	11(7)	33(9)	34(9)	7(7)	-9(6)	0(7)
C(12)	28(8)	20(8)	38(9)	-12(7)	-3(7)	11(7)
C(14)	63(11)	10(8)	30(9)	15(7)	-18(8)	-11(7)

C(15)	30(9)	18(8)	40(10)	-12(7)	-15(8)	-11(7)
C(16)	36(9)	10(7)	32(9)	13(7)	-13(8)	-6(7)
C(17)	42(10)	43(10)	39(10)	-1(8)	-13(8)	-4(8)
C(18)	40(9)	45(10)	19(8)	5(7)	-3(7)	-26(8)
C(19)	43(9)	7(7)	19(8)	9(6)	-16(7)	1(7)
C(20)	40(9)	30(9)	17(8)	-3(7)	-1(7)	-4(7)
C(21)	82(13)	14(8)	24(9)	-10(7)	-2(8)	-2(9)
C(22)	113(17)	15(9)	43(11)	-2(8)	-33(12)	-6(11)
C(23)	67(12)	22(9)	40(10)	-1(8)	-25(9)	-15(8)
C(25)	43(10)	18(8)	62(12)	5(8)	-7(9)	-12(8)
C(26)	31(9)	29(9)	58(11)	19(8)	-12(8)	-16(7)
C(27)	19(8)	34(9)	71(12)	-4(9)	1(8)	-6(7)
C(28)	31(8)	21(8)	7(7)	-4(6)	0(6)	-12(7)
C(29)	32(8)	28(8)	15(7)	-3(6)	-2(6)	-14(7)
C(30)	41(9)	47(11)	25(9)	-13(8)	5(7)	-26(9)
C(31)	58(11)	60(12)	20(8)	5(8)	-10(8)	-38(10)
C(32)	46(9)	37(9)	21(8)	7(7)	-11(7)	-28(8)
C(33)	21(8)	5(7)	20(8)	-5(6)	0(6)	0(6)
C(34)	16(8)	10(8)	47(10)	6(7)	-9(7)	6(6)
C(35)	34(9)	44(10)	31(9)	-5(7)	-2(7)	-6(8)
C(36)	41(9)	22(8)	40(9)	2(7)	-26(7)	-5(7)

Table 6-26 Complex **(24)**, hydrogen coordinates (x 10^4) and isotropic displacement parameters ($Å^2$ x 10^3).

Atom	x	y	z	U(eq)
H(2)	5660(11)	7328(11)	1945(9)	27
H(3)	7000(12)	8208(12)	1859(9)	33
H(4)	6650(12)	9870(13)	2801(10)	38
H(5)	4976(12)	10609(12)	3939(10)	37

H(7A)	3196(12)	9273(11)	4793(10)	30
H(7B)	3225(12)	10537(11)	4765(10)	30
H(8A)	326(13)	10732(13)	4124(11)	55
H(8B)	980(13)	10909(13)	5059(11)	55
H(8C)	1228(13)	9617(13)	4706(11)	55
H(9A)	2506(14)	11550(12)	2957(11)	58
H(9B)	1725(14)	12130(12)	3948(11)	58
H(9C)	1106(14)	11881(12)	3021(11)	58
H(11)	-575(11)	9812(12)	2819(10)	35
H(12)	-1889(13)	11841(12)	2736(11)	43
H(13)	-1557(13)	13068(13)	1551(10)	38
H(14)	41(13)	12263(11)	366(11)	42
H(16A)	1739(12)	9383(11)	-201(10)	32
H(16B)	1729(12)	10653(11)	-365(10)	32
H(17A)	4698(13)	8460(13)	280(11)	68
H(17B)	4007(13)	9031(13)	-703(11)	68
H(17C)	3750(13)	8029(13)	-118(11)	68
H(18A)	4063(13)	10319(13)	1057(10)	48
H(18B)	2687(13)	11196(13)	1205(10)	48
H(18C)	3335(13)	10996(13)	120(10)	48
H(20)	3303(13)	5843(12)	201(10)	39
H(21)	3432(16)	4197(13)	-717(11)	55
H(22)	2212(19)	3263(14)	-292(13)	75
H(23)	595(15)	4099(13)	889(12)	51
H(25A)	-494(13)	6845(12)	1939(12)	50
H(25B)	-515(13)	5586(12)	2108(12)	50
H(26A)	1131(13)	4739(12)	4198(12)	57
H(26B)	1444(13)	4174(12)	3108(12)	57
H(26C)	129(13)	4565(12)	3605(12)	57
H(27A)	-20(12)	6746(13)	4436(12)	65
H(27B)	-1114(12)	6719(13)	3871(12)	65
H(27C)	-552(12)	7616(13)	3524(12)	65
H(29)	1788(12)	7258(12)	5122(9)	29
H(30)	1545(13)	6209(14)	6490(11)	42
H(31)	2686(14)	4140(15)	6564(11)	49
H(32)	4059(13)	3211(13)	5261(10)	37
H(34A)	5455(11)	4428(11)	3621(10)	34

H(34B)	5339(11)	3220(11)	3840(10)	34
H(35A)	5548(13)	4686(13)	1928(11)	59
H(35B)	4966(13)	4111(13)	1195(11)	59
H(35C)	6001(13)	3294(13)	1891(11)	59
H(36A)	3438(13)	3200(12)	3051(11)	54
H(36B)	4730(13)	2400(12)	2569(11)	54
H(36C)	3694(13)	3217(12)	1873(11)	54

Table 6-27 Complex **(24)**, plane calculations (Ag1-Ag2-Ag3-Ag4).

Atom	Distance from plane (Å)
Ag1	-0.014
Ag2	0.014
Ag3	-0.014
Ag4	0.014

Distance to Ag1-Ag2-Ag3-Ag4 plane (Å)

C1	-0.827
C10	0.951
C19	-0.938
C28	0.966

Angles to Ag1-Ag2-Ag3-Ag4 plane (°)

Ag1-Ag4-C28	32.7(4)
Ag1-Ag2-C1	27.0(5)
Ag2-Ag3-C10	31.9(3)
Ag3-Ag4-C19	31.6(5)

A4.5 Structural data for complex (25), $[Ag(PPh_3)]_4(Me_2(O)SiOSi(O)Me_2)_2$

A crystal of approximate dimensions 0.2 x 0.2 x 0.8 mm was used for data collection.

Crystal data: $C_{40}H_{42}O_3P_2Si_2Ag_2.3(C_7H_8).2(H_2O)$, $M = 1217.1$ triclinic, $a = 13.160(4)$, $b = 13.345(4)$, $c = 17.445(4)$Å, $\alpha = 88.36(2)$, $\beta = 80.81(2)$, $\gamma = 67.88(2)$, $U = 2800.1$ Å^3, space group P-1 (No.2), $Z = 2$, $D_c = 1.44$ gcm^{-3}, μ(Mo-K$_\alpha$) = 8.40 cm^{-1}, F(000) = 1256. Data were measured at 170 K on a CAD4 automatic four-circle diffractometer in the range $2 \geq 3\theta \geq 24^\circ$. 4970 reflections were collected of which 2664 were unique with $I \geq 3\sigma(I)$. Data were corrected for Lorentz and polarization but not for absorption. The structure was solved by Patterson methods and refined using the SHELX [364, 365] suite of programs. Data quality and refinement values were impeded by 2 obstacles. Firstly, the crystals were not of exceptionally high quality. Secondly, the sample selected was not of ideal size. However, crystal mounting in a sealed capillary prior to transfer onto the diffractometer was a particularly precarious task due to rapid solvent loss. Attempts to apply an empirical absorption correction (despite a low μ value) did not improve convergence.

The asymmetric unit was seen to consist of one half of a dimer close to an inversion centre, along with 3 toluene molecules and two water entities. In the final least squares cycles the Ag, P and Si atoms were allowed to vibrate anisotropically. (Anisotropic refinement of the other remaining atoms only served to yield unsatisfactory thermal parameters for some atoms). Hydrogen atoms were included at calculated positions where relevant except in the case of the water molecules. Refinement was conducted in 2 blocks, one for the organometallic, and one for the solvent molecules. Final residuals after 20 cycles of blocked matrix least squares were R

= 0.0750, R_w = 0.0766, for a weighting scheme of $w = 6.6522/[\sigma^2(F) + 0.000502(F)^2]$. Max. final shift/esd was 0.000. The max. and min. residual densities were 0.45 and -0.36 eÅ^{-3} respectively. Final fractional atomic coordinates and isotropic thermal parameters, bond distances and angles are presented in the following tables. Tables of anisotropic temperature factors are available as supplementary data. The asymmetric unit is shown in Figure 5-12, along with the labelling scheme used.

Table 6-28 Complex **(25)**, fractional atomic co-ordinates (x10^4).

	x	y	z
Ag(1)	958(2)	5914(2)	3668(1)
Ag(2)	955(2)	3883(2)	4828(1)
P(1)	2507(6)	2501(5)	5059(3)
P(2)	1381(6)	7098(5)	2867(3)
Si(1)	326(7)	3936(6)	3051(4)
Si(2)	-1486(7)	4047(6)	4428(3)

Table 6-29 Complex **(25)**, anisotropic temperature factors (Å $x10^3$).

	U_{11}	U_{22}	U_{33}	U_{23}	U_{13}	U_{12}
Ag(1)	33(2)	20(1)	19(1)	6(1)	-7(1)	-16(2)
Ag(2)	27(2)	18(1)	20(1)	1(1)	-8(1)	-9(2)
P(1)	27(5)	14(4)	16(3)	3(3)	-5(3)	-7(5)
P(2)	30(5)	21(4)	20(3)	3(3)	-7(3)	-15(5)
Si(1)	32(6)	20(5)	21(4)	-3(3)	-2(4)	-10(6)
Si(2)	22(6)	20(5)	20(3)	-5(3)	-1(3)	-11(5)

Table 6-30 Complex **(25)**, hydrogen fractional atomic co-ordinates ($x10^4$) and isotropic temperature factors (Å^2 $x10^3$).

	x	y	z	U
O(1)	978(15)	4418(13)	3521(8)	25(4)
O(2)	-969(13)	4461(11)	5040(7)	8(3)
O(3)	-929(14)	4178(13)	3534(8)	23(4)
C(2)	1398(13)	7586(9)	1254(8)	32(6)
C(3)	1682(13)	7256(9)	471(8)	39(7)
C(4)	2102(13)	6157(9)	262(8)	48(7)
C(5)	2236(13)	5388(9)	836(8)	45(7)
C(6)	1952(13)	5718(9)	1618(8)	20(5)
C(1)	1533(13)	6818(9)	1828(8)	20(5)
C(8)	3304(12)	7575(11)	2467(7)	25(6)
C(9)	4344(12)	7535(11)	2578(7)	32(6)
C(10)	4809(12)	7009(11)	3214(7)	38(6)
C(11)	4234(12)	6523(11)	3738(7)	25(5)
C(12)	3193(12)	6562(11)	3626(7)	25(5)
C(7)	2728(12)	7088(11)	2991(7)	21(5)

C(14)	762(10)	9195(11)	3169(8)	23(5)
C(15)	-18(10)	10255(11)	3244(8)	36(6)
C(16)	-1087(10)	10479(11)	3085(8)	25(5)
C(17)	-1375(10)	9643(11)	2852(8)	39(7)
C(18)	-594(10)	8584(11)	2777(8)	31(6)
C(13)	474(10)	8359(11)	2936(8)	13(5)
C(20)	4817(13)	2167(11)	4738(7)	23(5)
C(21)	5713(13)	2326(11)	4284(7)	43(7)
C(22)	5550(13)	2958(11)	3630(7)	35(6)
C(23)	4490(13)	3431(11)	3430(7)	49(7)
C(24)	3593(13)	3272(11)	3884(7)	32(6)
C(19)	3756(13)	2639(11)	4538(7)	20(5)
C(26)	3467(11)	1334(10)	6323(6)	20(5)
C(27)	3600(11)	1236(10)	7102(6)	18(5)
C(28)	3014(11)	2108(10)	7627(6)	28(6)
C(29)	2295(11)	3077(10)	7372(6)	32(6)
C(30)	2162(11)	3175(10)	6593(6)	18(5)
C(25)	2748(11)	2304(10)	6068(6)	25(5)
C(32)	3494(12)	665(12)	4224(8)	23(5)
C(33)	3552(12)	-357(12)	4009(8)	27(6)
C(34)	2708(12)	-713(12)	4321(8)	42(7)
C(35)	1806(12)	-48(12)	4847(8)	33(6)
C(36)	1747(12)	974(12)	5062(8)	20(5)
C(31)	2592(12)	1330(12)	4750(8)	32(6)
C(37)	1059(24)	2557(20)	2893(13)	33(6)
C(38)	151(23)	4454(21)	2067(12)	33(6)
C(39)	-1243(23)	2676(20)	4546(12)	29(6)
C(40)	-3034(22)	4836(20)	4499(12)	27(6)
C(42)	6231(12)	4622(10)	2120(8)	38(6)
C(43)	7261(12)	4155(10)	2367(8)	33(6)
C(44)	7960(12)	3098(10)	2127(8)	38(6)
C(45)	7629(12)	2508(10)	1640(8)	43(7)
C(46)	6599(12)	2975(10)	1393(8)	39(6)
C(41)	5900(12)	4032(10)	1634(8)	29(6)
C(47)	4814(29)	4530(28)	1368(16)	67(9)
C(49)	2624(17)	3761(14)	9242(10)	60(8)
C(50)	3744(17)	3524(14)	9274(10)	71(9)

C(51)	4247(17)	2862(14)	9849(10)	63(8)
C(52)	3631(17)	2437(14)	10392(10)	56(8)
C(53)	2512(17)	2675(14)	10361(10)	68(9)
C(48)	2009(17)	3337(14)	9786(10)	83(11)
C(54)	938(40)	3542(43)	9739(26)	160(20)
C(56)	5700(15)	-1049(15)	7857(9)	39(6)
C(57)	4710(15)	-1229(15)	8012(9)	50(7)
C(58)	3885(15)	-658(15)	8622(9)	57(8)
C(59)	4049(15)	93(15)	9077(9)	66(9)
C(60)	5039(15)	273(15)	8922(9)	59(8)
C(55)	5864(15)	-298(15)	8312(9)	48(7)
C(61)	6915(32)	-134(31)	8118(18)	85(11)
O(4)	828(54)	692(49)	448(30)	290(25)
O(5)	-262(44)	-193(41)	648(22)	222(18)
H(51)	1110(13)	8343(9)	1398(8)	80
H(41)	1590(13)	7785(9)	77(8)	80
H(31)	2297(13)	5929(9)	-277(8)	80
H(21)	2525(13)	4632(9)	692(8)	80
H(61)	2045(13)	5189(9)	2013(8)	80
H(81)	2983(12)	7937(11)	2029(7)	80
H(91)	4740(12)	7869(11)	2217(7)	80
H(101)	5525(12)	6982(11)	3291(7)	80
H(111)	4554(12)	6161(11)	4176(7)	80
H(121)	2797(12)	6228(11)	3987(7)	80
H(141)	1498(10)	9041(11)	3278(8)	80
H(151)	180(10)	10830(11)	3404(8)	80
H(161)	-1624(10)	11208(11)	3137(8)	80
H(171)	-2110(10)	9798(11)	2743(8)	80
H(181)	-793(10)	8009(11)	2617(8)	80
H(201)	4929(13)	1732(11)	5189(7)	80
H(211)	6443(13)	2000(11)	4422(7)	80
H(221)	6167(13)	3067(11)	3318(7)	80
H(231)	4378(13)	3866(11)	2980(7)	80
H(241)	2864(13)	3597(11)	3747(7)	80
H(261)	3870(11)	734(10)	5961(6)	80
H(271)	4094(11)	569(10)	7278(6)	80
H(281)	3105(11)	2040(10)	8164(6)	80

H(291)	1892(11)	3677(10)	7734(6)	80
H(301)	1668(11)	3843(10)	6417(6)	80
H(321)	4075(12)	910(12)	4009(8)	80
H(331)	4173(12)	-815(12)	3647(8)	80
H(341)	2748(12)	-1416(12)	4173(8)	80
H(351)	1225(12)	-293(12)	5062(8)	80
H(361)	1127(12)	1431(12)	5424(8)	80
H(371)	665(24)	2262(20)	2607(13)	80
H(372)	1138(24)	2214(20)	3383(13)	80
H(373)	1782(24)	2431(20)	2601(13)	80
H(381)	867(23)	4329(21)	1765(12)	80
H(382)	-287(23)	5217(21)	2104(12)	80
H(383)	-219(23)	4086(21)	1821(12)	80
H(391)	-1564(23)	2433(20)	4168(12)	80
H(392)	-1574(23)	2574(20)	5058(12)	80
H(393)	-457(23)	2266(20)	4475(12)	80
H(401)	-3399(22)	4785(20)	5013(12)	80
H(402)	-3319(22)	4542(20)	4126(12)	80
H(403)	-3168(22)	5581(20)	4395(12)	80
H(421)	5750(12)	5350(10)	2286(8)	80
H(431)	7489(12)	4562(10)	2702(8)	80
H(441)	8669(12)	2777(10)	2296(8)	80
H(451)	8111(12)	1780(10)	1475(8)	80
H(461)	6372(12)	2569(10)	1058(8)	80
H(471)	4714(29)	4020(28)	1040(16)	80
H(472)	4789(29)	5162(28)	1081(16)	80
H(473)	4231(29)	4732(28)	1810(16)	80
H(491)	2278(17)	4217(14)	8847(10)	80
H(501)	4167(17)	3816(14)	8900(10)	80
H(511)	5017(17)	2698(14)	9870(10)	80
H(521)	3978(17)	1982(14)	10788(10)	80
H(531)	2088(17)	2383(14)	10735(10)	80
H(541)	637(40)	3194(43)	10153(26)	80
H(542)	890(40)	3269(43)	9249(26)	80
H(543)	523(40)	4309(43)	9784(26)	80
H(561)	6268(15)	-1442(15)	7437(9)	80
H(571)	4597(15)	-1746(15)	7698(9)	80

H(581)	3204(15)	-782(15)	8728(9)	80
H(591)	3481(15)	486(15)	9497(9)	80
H(601)	5152(15)	790(15)	9236(9)	80
H(611)	6926(32)	398(31)	8471(18)	80
H(612)	6983(32)	111(31)	7596(18)	80
H(613)	7523(32)	-805(31)	8158(18)	80

Table 6-31 Complex **(25)**, bond lengths (Å).

Ag(2)-Ag(1)	3.336(6)	P(2)-Ag(1)	2.246(9)
O(1)-Ag(1)	2.010(21)	P(1)-Ag(2)	2.262(8)
O(1)-Ag(2)	2.368(16)	O(2)-Ag(2)	2.321(18)
Ag(2)-Ag(2a)	3.090(6)	C(19)-P(1)	1.817(20)
C(25)-P(1)	1.832(15)	C(31)-P(1)	1.626(20)
C(1)-P(2)	1.825(17)	C(7)-P(2)	1.816(21)
C(13)-P(2)	1.651(15)	O(1)-Si(1)	1.578(25)
O(3)-Si(1)	1.647(21)	C(37)-Si(1)	1.733(27)
C(38)-Si(1)	1.849(25)	O(2)-Si(2)	1.568(20)
O(3)-Si(2)	1.649(17)	C(39)-Si(2)	1.746(30)
C(40)-Si(2)	1.893(28)	C(3)-C(2)	1.395(20)
C(1)-C(2)	1.395(19)	C(4)-C(3)	1.395(17)
C(5)-C(4)	1.395(19)	C(6)-C(5)	1.395(20)
C(1)-C(6)	1.395(17)	C(9)-C(8)	1.395(25)
C(7)-C(8)	1.395(22)	C(10)-C(9)	1.395(18)
C(11)-C(10)	1.395(22)	C(12)-C(11)	1.395(25)
C(7)-C(12)	1.395(18)	C(15)-C(14)	1.395(18)
C(13)-C(14)	1.395(24)	C(16)-C(15)	1.395(21)
C(17)-C(16)	1.395(24)	C(18)-C(17)	1.395(18)
C(13)-C(18)	1.395(21)	C(21)-C(20)	1.395(24)
C(19)-C(20)	1.395(23)	C(22)-C(21)	1.395(18)
C(23)-C(22)	1.395(23)	C(24)-C(23)	1.395(24)
C(19)-C(24)	1.395(18)	C(27)-C(26)	1.395(18)
C(25)-C(26)	1.395(17)	C(28)-C(27)	1.395(16)

C(29)-C(28)	1.395(17)	C(30)-C(29)	1.395(18)
C(25)-C(30)	1.395(16)	C(33)-C(32)	1.395(24)
C(31)-C(32)	1.395(18)	C(34)-C(33)	1.395(25)
C(35)-C(34)	1.395(18)	C(36)-C(35)	1.395(24)
C(31)-C(36)	1.395(25)	C(43)-C(42)	1.395(22)
C(41)-C(42)	1.395(24)	C(44)-C(43)	1.395(17)
C(45)-C(44)	1.395(24)	C(46)-C(45)	1.395(22)
C(41)-C(46)	1.395(17)	C(47)-C(41)	1.476(39)
C(50)-C(49)	1.395(33)	C(48)-C(49)	1.395(30)
C(51)-C(50)	1.395(25)	C(52)-C(51)	1.395(30)
C(53)-C(52)	1.395(33)	C(48)-C(53)	1.395(25)
C(54)-C(48)	1.346(60)	C(57)-C(56)	1.395(31)
C(55)-C(56)	1.395(30)	C(58)-C(57)	1.395(21)
C(59)-C(58)	1.395(30)	C(60)-C(59)	1.395(31)
C(55)-C(60)	1.395(21)	C(61)-C(55)	1.466(51)

Key to symmetry operations relating
designated atoms to reference atoms
at (x,y,z):

(a) -x,1.0-y,1.0-z

Table 6-32 Complex **(25)**, bond angles (°).

P(2)-Ag(1)-Ag(2)	167.0(2)	O(1)-Ag(1)-Ag(2)	44.5(4)
O(1)-Ag(1)-P(2)	134.2(4)	P(1)-Ag(2)-Ag(1)	124.2(3)
O(1)-Ag(2)-Ag(1)	36.5(5)	O(1)-Ag(2)-P(1)	114.9(5)
O(2)-Ag(2)-Ag(1)	93.3(4)	O(2)-Ag(2)-P(1)	142.1(4)
O(2)-Ag(2)-O(1)	91.7(6)	C(19)-P(1)-Ag(2)	111.6(6)
C(25)-P(1)-Ag(2)	117.6(5)	C(25)-P(1)-C(19)	104.5(9)
C(31)-P(1)-Ag(2)	113.3(8)	C(31)-P(1)-C(19)	103.6(8)
C(31)-P(1)-C(25)	105.0(8)	C(1)-P(2)-Ag(1)	116.4(7)
C(7)-P(2)-Ag(1)	109.3(6)	C(7)-P(2)-C(1)	103.8(8)

C(13)-P(2)-Ag(1)	117.1(7)	C(13)-P(2)-C(1)	100.2(8)
C(13)-P(2)-C(7)	109.0(9)	O(3)-Si(1)-O(1)	110.1(10)
C(37)-Si(1)-O(1)	109.3(14)	C(37)-Si(1)-O(3)	110.6(14)
C(38)-Si(1)-O(1)	115.9(14)	C(38)-Si(1)-O(3)	106.7(12)
C(38)-Si(1)-C(37)	104.1(12)	O(3)-Si(2)-O(2)	111.2(11)
C(39)-Si(2)-O(2)	110.4(12)	C(39)-Si(2)-O(3)	107.4(10)
C(40)-Si(2)-O(2)	112.3(11)	C(40)-Si(2)-O(3)	106.2(10)
C(40)-Si(2)-C(39)	109.2(15)	Ag(2)-O(1)-Ag(1)	99.0(7)
Si(1)-O(1)-Ag(1)	133.7(9)	Si(1)-O(1)-Ag(2)	113.3(11)
Si(2)-O(2)-Ag(2)	116.0(7)	Si(2)-O(3)-Si(1)	137.1(11)
C(1)-C(2)-C(3)	120.0(12)	C(4)-C(3)-C(2)	120.0(13)
C(5)-C(4)-C(3)	120.0(13)	C(6)-C(5)-C(4)	120.0(12)
C(1)-C(6)-C(5)	120.0(13)	C(2)-C(1)-P(2)	125.4(11)
C(6)-C(1)-P(2)	114.1(11)	C(6)-C(1)-C(2)	120.0(13)
C(7)-C(8)-C(9)	120.0(13)	C(10)-C(9)-C(8)	120.0(15)
C(11)-C(10)-C(9)	120.0(16)	C(12)-C(11)-C(10)	120.0(13)
C(7)-C(12)-C(11)	120.0(15)	C(8)-C(7)-P(2)	121.9(11)
C(12)-C(7)-P(2)	118.1(13)	C(12)-C(7)-C(8)	120.0(16)
C(13)-C(14)-C(15)	120.0(14)	C(16)-C(15)-C(14)	120.0(16)
C(17)-C(16)-C(15)	120.0(12)	C(18)-C(17)-C(16)	120.0(14)
C(13)-C(18)-C(17)	120.0(16)	C(14)-C(13)-P(2)	120.5(12)
C(18)-C(13)-P(2)	119.5(14)	C(18)-C(13)-C(14)	120.0(12)
C(19)-C(20)-C(21)	120.0(13)	C(22)-C(21)-C(20)	120.0(15)
C(23)-C(22)-C(21)	120.0(16)	C(24)-C(23)-C(22)	120.0(13)
C(19)-C(24)-C(23)	120.0(15)	C(20)-C(19)-P(1)	125.5(11)
C(24)-C(19)-P(1)	114.5(13)	C(24)-C(19)-C(20)	120.0(16)
C(25)-C(26)-C(27)	120.0(11)	C(28)-C(27)-C(26)	120.0(11)
C(29)-C(28)-C(27)	120.0(12)	C(30)-C(29)-C(28)	120.0(11)
C(25)-C(30)-C(29)	120.0(11)	C(26)-C(25)-P(1)	123.1(10)
C(30)-C(25)-P(1)	116.9(10)	C(30)-C(25)-C(26)	120.0(12)
C(31)-C(32)-C(33)	120.0(16)	C(34)-C(33)-C(32)	120.0(13)
C(35)-C(34)-C(33)	120.0(16)	C(36)-C(35)-C(34)	120.0(16)
C(31)-C(36)-C(35)	120.0(13)	C(32)-C(31)-P(1)	122.4(15)
C(36)-C(31)-P(1)	117.5(11)	C(36)-C(31)-C(32)	120.0(16)
C(41)-C(42)-C(43)	120.0(12)	C(44)-C(43)-C(42)	120.0(16)
C(45)-C(44)-C(43)	120.0(15)	C(46)-C(45)-C(44)	120.0(12)
C(41)-C(46)-C(45)	120.0(16)	C(46)-C(41)-C(42)	120.0(15)

C(47)-C(41)-C(42)	120.0(18)	C(47)-C(41)-C(46)	120.0(20)
C(48)-C(49)-C(50)	120.0(17)	C(51)-C(50)-C(49)	120.0(20)
C(52)-C(51)-C(50)	120.0(21)	C(53)-C(52)-C(51)	120.0(17)
C(48)-C(53)-C(52)	120.0(20)	C(53)-C(48)-C(49)	120.0(21)
C(54)-C(48)-C(49)	119.8(27)	C(54)-C(48)-C(53)	120.2(29)
C(55)-C(56)-C(57)	120.0(15)	C(58)-C(57)-C(56)	120.0(20)
C(59)-C(58)-C(57)	120.0(20)	C(60)-C(59)-C(58)	120.0(15)
C(55)-C(60)-C(59)	120.0(20)	C(60)-C(55)-C(56)	120.0(20)
C(61)-C(55)-C(56)	117.6(19)	C(61)-C(55)-C(60)	122.4(23)

Table 6-33 Complex **(25)**, selected non-bonded distances (Å).

Intramolecular:

Si(1)-Ag(1)	3.303	C(6)-Ag(1)	3.587
C(1)-Ag(1)	3.467		

Intermolecular:

Ag(2)-Ag(1a)	3.274	Si(2)-Ag(1a)	3.506
O(2)-Ag(1a)	2.296		

Key to symmetry operations relating
designated atoms to reference atoms
at (x,y,z):

(a) -x,1.0-y,1.0-z

APPENDIX FIVE *Instrumentation*

Infra-red spectrometry

Infra-red spectra were recorded as nujol (liquid paraffin) or hexachlorobutadiene mulls between KBr plates. Measurements were taken using a Nicolet 510P fourier transform spectrometer within the range 4000-400 cm^{-1} with a medium slit width and a peak resolution of 4.0 cm^{-1}.

Microanalysis

Carbon, hydrogen and nitrogen were analysed for using a Carlo-Erba Strumentazione E.A. mod 1106 microanalyser operating at 500°C. Results were calibrated against an acetanilide {$PhNHC(O)CH_3$} standard.

^1H, $^{13}C\{^1H\}$ Nuclear Magnetic Resonance spectroscopy

Proton and carbon-13 NMR spectra were recorded using either Jeol JNM-GX-270FT (270 MHz) or Jeol EX-400 (400 MHz) fourier transform spectrometers using $SiMe_4$ as an internal reference.

^{19}F, ^{29}Si, ^{31}P Nuclear Magnetic Resonance spectroscopy

Fluorine, silicon and phosphorus NMR spectra were recorded on a Jeol EX400 (400 MHz) fourier transform spectrometer. Chemical shifts [$\delta(^{19}F)$] are relative to $CFCl_3$. In the case of ^{29}Si spectra, the solution of the compound under investigation was doped with $Cr(acac)_3$ to increase relation of the nuclei. Chemical shifts [$\delta(^{29}Si)$] for the silicon spectra are relative to $SiMe_4$. Chemical shifts [$\delta(^{31}P)$] for the phosphorus spectra are relative to 85% H_3PO_4.

^{109}Ag Nuclear Magnetic Resonance spectroscopy

Silver-109 NMR spectra were recorded on a Jeol EX400 (400 MHz) fourier transform spectrometer. Experiments were run as DEPT experiments at an observational frequency of 18.45 MHz. A pulse width of 25 microseconds was used with an acquisition time of 0.744 and a pulse delay of 10.0 seconds. Observable resonances were typically detected after 500-1000 scans.

FAB(LSIMS) Mass spectrometry

Fast Atom Bombardment (Liquid Secondary Ion Mass Spectrometry) experiments were carried out by the EPSRC Mass Spectrometry Service at the University College of Swansea. FAB(LSIMS) spectra were carried out on a VG AutoSpec instrument using a Caesium ion bombardment at 25kV. Samples were dissolved in a 3-nitrobenzyl alcohol (NOBA) matrix typically with the aid of a CH_2Cl_2 co-solvent.

Thermal Gravimetric Analysis and Differential Scanning Calorimetry

TGA and DSC experiments were carried out at atmospheric pressure in either air-, nitrogen- or helium-purged atmospheres, from room temperature to 850°C at a ramp rate of 25°Cmin^{-1}.

Scanning Electron Microscopy

Samples were examined by SEM using a JEOL 6310 scanning electron microscope operating at an accelerating voltage of 5, 10 or 15 kV. Coatings under investigation were not sputter coated although a path to ground was provided by means of silver dag or electrically conducting putty.

Energy Dispersive X-ray Spectroscopy

Film thickness estimates using EDXS techniques were performed on a JEOL Superprobe instrument operating at an accelerating voltage of 5 kV with a beam current of 5 x 10^{-8}A. X-ray counts (typically over 200 seconds) from sample films were compared against a solid silver standard.

Conductivity measurements

Sheet resistance was measured over a 25 mm square. Silver 'dag' busbar contacts were painted on the sample and resistance measured using a digital volt-meter.

Reflectance measurements

Reflection spectra at near-normal incidence were measured on a Hitachi U-3410 spectrophotometer over the range 295-2600 nm in 5 nm steps. Calibration was against Rhodium standard mirrors. Reflectance is quoted at $\lambda = 550$ nm corresponding to the peak in the eye response curve for both the coated surface and the film-glass interface (as observed through the glass). The assessment area (corresponding to the beam size) was a rectangle of approximately 11 by 4 mm.

APPENDIX SIX *Film Growth Equipment and Procedures*

A6.1 Design and Construction of CVD Film Growth Apparatus

The CVD apparatus utilised in this project has been assembled as a general screening rig for use with this and other projects. The entire system consists of a horizontal cold wall reactor with associated gas-lines, electrical heater controls, gas-distribution via a manifold and flowmeters and an additional aerosol assisted delivery system. A schematic representing the major components of this film growth system is shown in Figure 6-5. Screening tests for this project have exclusively utilised the nebuliser line due to the difficulty in performing conventional CVD with silver precursors at atmospheric pressure.

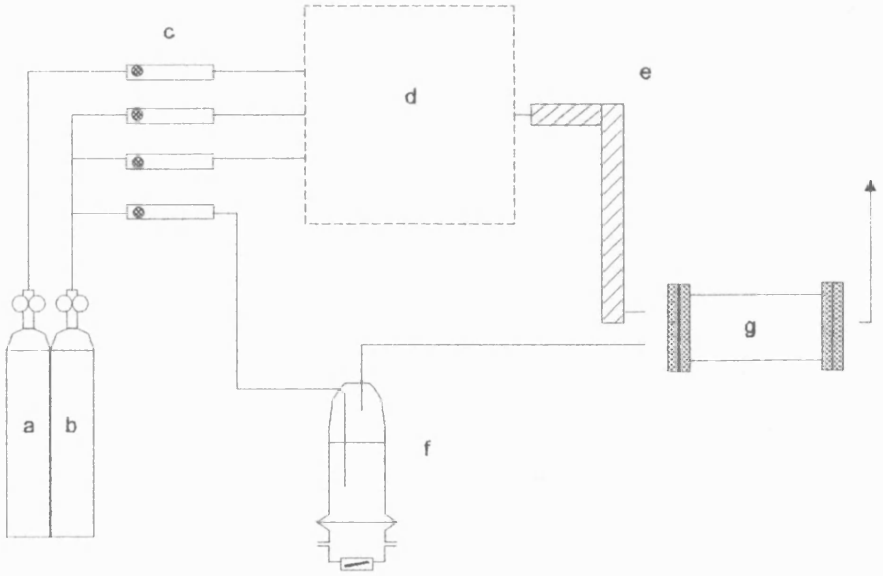

Figure 6-5 Schematic representation of the CVD system used in this study, a - O_2 supply, b - N_2 supply, c - gas manifold and flowmeters, d - heated bubbler assembly, e - heated gas line, f - ultrasonic nebuliser, g - CVD reactor.

The ultrasonic nebuliser is of a dual chamber design, i.e. ultrasonic waves are transmitted from the transducer, via liquid medium into the chamber where nebulisation takes place. In the case of this apparatus, the piezzoelectric transducer is positioned in the lower water-filled chamber so as to transmit ultrasound though the water into the upper nebulising chamber. The two chambers are divided by means of a taught plastic (solvent resistant) sheet fixed in place by means of a sealant. The distance between the piezzoelectric transducer and the sheet is approximately 3-4 cm. The water in the lower chamber is constantly replaced to allow for cooling of the transducer.

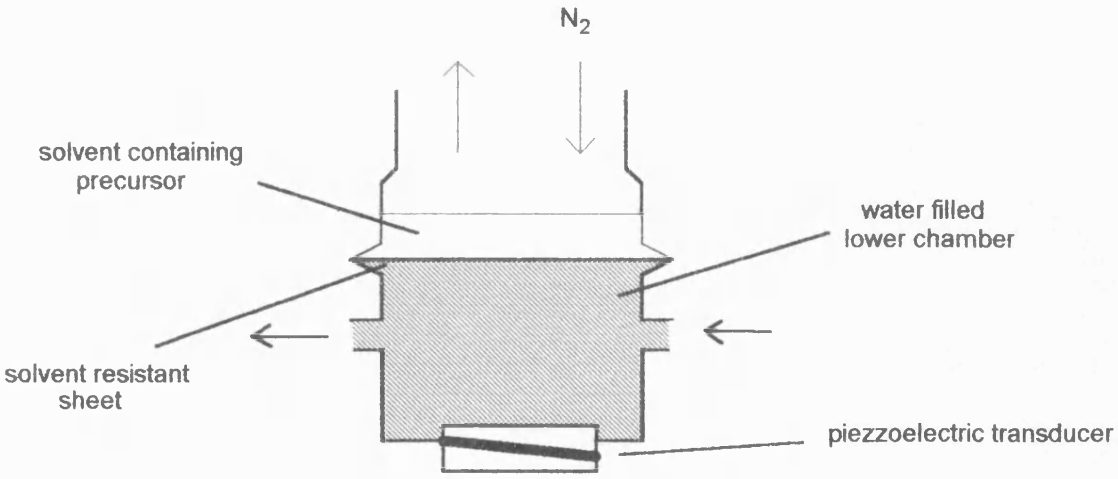

Figure 6-6 Schematic of the ultrasonic nebuliser.

A solution of the precursor (both THF and toluene were found to be satisfactorily nebulised) is placed in the upper chamber. On activation of the nebuliser, the solution in the upper chamber fountains to generate an aerosol of fine droplets of the solution. This aerosol is simply swept out of the nebuliser and into the CVD reactor by a slow nitrogen flow. A number of other

research groups developing aerosol delivery techniques have gently heated the aerosol, by means of a heated gas line, while en route to the CVD reactor but this has not been attempted in this work.

The CVD reactor itself is of a horizontal, cold wall design. After passing through a baffle to promote laminar flow, the aerosol is passed directly into the CVD chamber (8 mm high, 40 mm wide, 300 mm long) of which the base is the heated substrate (Figure 6-7). The ceiling tile and walls being silica. The substrate is positioned upon a large graphite susceptor which is heated by three cartridge heaters. The temperature of the graphite block is maintained by a Watlow series 965 controller which monitors the temperature by means of thermocouples inside the block. The graphite susceptor is held inside a large silica tube (330 mm long, 100 mm diameter) suspended between stainless steel flanges upon which many of the electrical and gas line fittings are fixed. Air-tight seals between the silica and flanges are provided for by 'Viton' O-rings.

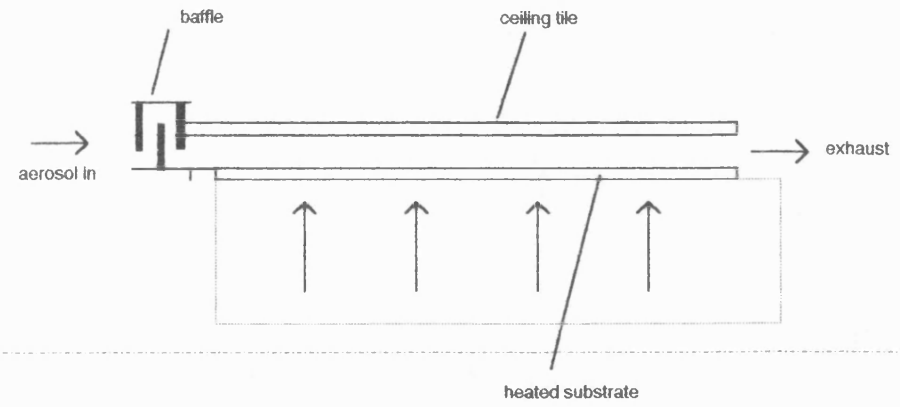

Figure 6-7 Schematic of the CVD reactor chamber

A6.2 Substrate Preparation Procedures

All glass substrates were subject to the same preparation prior to film growth. Before insertion into the reactor, the glass was handled as little as possible. When being handled, the glass was picked up by handling the glass outside of the deposition area. To ensure a clean substrate surface, the following substrate preparation was used.

1. Using polythene gloves, the glass was washed thouroughly with tap water and detergent. The glass was rinsed and allowed to drain.
2. Once completely dry, the glass was rinsed with isopropyl alcohol (IPA) to ensure the surface was free of grease. The substrate was allowed to drain.
3. After the glass was completely dry, the substrate was subject to a final rinse with distilled water and again allowed to drain dry.

Only recently prepared substrates were used for film growth experiments, i.e. those prepared within 24 hours. In addition, substrate surfaces which had come into contact with un-gloved hands could not be satisfactorily cleaned and were discarded.

APPENDIX SEVEN

Table 6-34 Reflectance data

Compound	Coating side		Glass side	
	λ = 550 nm	λ = 750 nm	λ = 550 nm	λ = 750 nm
(2)	1.1	7.4	20.7	16.4
(3)	17.5	16.1	6.5	6.9
(4)	49.7	41.6	30.6	25.2
(6)	0.7	2.4	42.8	38.9
(7)	22.2	16.8	9.7	9.8
(9)	46.6	45.3	31.1	22.5
(10)	17.6	12.8	7.3	9.7
(11)	0.5	1	42.5	43
(12)	6.8	6	8.1	9
(13)	4.9	7	29.8	28
(14)	45.9	46	34.9	33
(15)	18.1	58	36.5	39
(16)	20.4	23	19.8	18
(17)	12.9	11.0	10.9	10.1
(18)	12.2	10.5	10.5	9.8
(19)	19.4	25.3	19.8	9.8
(20)	62.5	82.5	70.3	71.5
(21)	0.3	0.9	18.0	13.5
(22)	64.7	101.1	85.3	85.3
(23)	51.4	80.1	30.0	34.0

[a] the glass substrate demonstrated a reflectivity of 11.6 and 9.0 % at 550 and 750 nm respectively

APPENDIX EIGHT *Numerical Index of Compounds*

(1) AgO_2CCH_3

(2) $AgO_2CCH_3.(PMe_3)_2$

(3) $AgO_2CCH_3.(PPh_3)_2$

(4) $AgO_2CCH_3.(PPh_3)_3$

(5) AgO_2C^tBu

(6) $AgO_2C^tBu.(PMe_3)_2$

(7) $AgO_2C^tBu.(PPh_3)_2$

(8) $AgO_2C\text{-}Me_3C_6H_2$

(9) $AgO_2C\text{-}Me_3C_6H_2.(PMe_3)_2$

(10) $AgO_2C\text{-}Me_3C_6H_2.(PPh_3)_2$

(11) $AgO_2CC_3F_7$

(12) $AgO_2CC_3F_7.(PPh_3)_2$

(13) $AgO_2CC_6F_{13}$

(14) $AgO_2CC_6F_{13}.(PPh_3)_2$

(15) $AgO_2CC_7F_{15}$

(16) $AgO_2CC_7F_{15}.(PPh_3)_2$

(17) $Ag(acac)(PPh_3)$

(18) $Ag(dpm)(PPh_3)$

(19) $[Ag(fod)]_3(PPh_3)_5$

(20) $Ag(tfac)(PPh_3)$

(21) $Ag(hfac)(PPh_3)$

(22) $Ag(hfacNhex)(PPh_3)$

(23) $Ag(hfacNchex)(PPh_3)$

(24) {2-(dimethylaminomethyl)phenyl}silver(I)

(25) $[Ag(PPh_3)]_4\{Me_2(O)SiOSi(O)Me_2\}_2$

REFERENCES

1 'Mirrors', B. Schweig, Pelham book, London (1973)

2 'Deposition Technologies for Films and Coatings : Developments and Applications', Edited by R.F. Bunshah, Chapter 10 by Morton Schwartz, Noyes, New Jersey (1982)

3 J.R. Pitts, T.M. Thomas, A.W. Czanderna, *Solar Energy Materials*, **11** (4), 261-271 (1984)

4 C. Kennedy, R. Goggin, *Solar Energy Materials and Solar Cells*, **33** (2), 183-197 (1994)

5 A.F. Rubira, J.D. Rancourt, M.L.Caplan, A.K.St Clair, A.T.Taylor, *Chem. Mater.*, **6**, 2351-2358 (1994)

6 'Thin Film Physics', O.S. Heavens, Methuen and Co. Ltd., London (1970)

7 'Thin films', K.D. Leaver, B.N. Chapman, Wykeham, London (1971)

8 'Sol-gel Science, the Physics and Chemistry of Sol-gel Processing', C.J. Brinker, G.W. Scherer, Academic Press, New York (1990)

9 R. Latz, B. Ocker, R. Schneider, Ger.Offen. DE 4,239,355 (1994) through *Chem. Abs.* **121**:41242r (1994)

10 S. Koch, V. Rondeau, J. Brochot, O. Guiselin, Eur. Pat. Appl. EP 611,213 (1994) through *Chem. Abs.* **121**:185520 (1994)

11 O. Guiselin, J. Brochot, P. Petit, Eur. Pat. Appl. EP 638,528 (1995) through *Chem. Abs.* **122**:194970x

12 'The Chemistry of Metal CVD', Eds. T.T. Kodas, M.J. Hampden-Smith, Chapter 1 'Introduction' by R. Jairath, A. Jain, R.D. Tolles, M.J. Hampden-Smith, T.T. Kodas, VCH, Weinheim (1994)

13 S. Shingubara, Y. Nakasaki, H. Kaneko, *Appl. Phys. Lett.*, **58** (1), 42-44 (1991)

14 J.R. Creighton, J.E. Parmeter, *Critical Reviews in Solid State and Materials Sciences*, **18** (2), 175-238 (1993)

15 'The Chemistry of Metal CVD', Eds. T.T. Kodas, M.J. Hampden-Smith, Chapter 6 'Chemical Vapour Deposition of Gold and Silver' by T.H. Baum, P.B. Comita, VCH, Weinheim (1994)

16 S.F. Wang, J.P. Dougherty, W. Huebner, J.G. Pepin, *J. Am. Ceram. Soc.*, 77 (12), 3051-3072 (1994)

17 N. Marechal, Y. Pauleau, S. Paidassi, *Surf. Coat. Technol.*, **54**, 320-323 (1992)

18 J.M. Zhang, B.W. Wessels, L.M. Tonge, T.J. Marks, *Appl. Phys. Lett.*, **56** (10), 976-978 (1990)

19 M.J. Shapiro, W.J. Lackey, J.A. Hanigofsky, D.N. Hill, W.B. Carter, E.K. Barefield, *J. Alloys and Compounds*, **187**, 331-349 (1992)

20 S. Jin, R.C. Sherwood, T.H. Tiefel, G.W. Kammlott, R.A. Fastnacht, M.E. Davis, S.M. Zahurak, *Appl. Phys. Lett.* , **52** (19), 1628-1630 (1988)

21 P.M. Jeffries, S.R. Wilson, G.S. Girolami, *J. Organomet. Chem.*, **449**, 203-209 (1993)

22 C.A. Chang, *Appl. Phys. Lett.* , **52** (11), 924-926 (1988)

23 J.H. Miller Jr, S.L. Holder, J.D. Hunn, G.N. Holder, *Appl. Phys. Lett.*, **54** (22), 2256-2258 (1989)

24 B. Dwir, M. Affronte, D. Pavuna, *Appl. Phys. Lett.*, **55** (4), 399-401 (1989)

25 J.A. Deluca, P.L. Karas, J.E. Tkaczyk, P.J. Bednarczyk, M.F. Garbauskas, C.L. Briant, D.B. Sorensen, *Physica C*, **205** (1-2), 21-31 (1993)

26 C.L. Briant, J.A. Deluca, P.L. Karas, M.F. Garbauskas, J.A. Sutcliff, A. Goyal, D. Kroeger, *Journal of Materials Research*, **10** (4), 823-842 (1995)

27 Y.F. Ren, Z.T. Zeng, J. Meng, P. He, *Solid State Communications*, **75** (8), 625-627 (1990)

28 'Recent developments in the Adiabatic Engine', SAE SP-738, Society of Automotive Engineers , 'Developments of advanced high temperature liquid lubricants', pp 37-49, by P. Sutor, W. Bryzik, Warrendale, PA (1988)

29 C. Dellacorte, *Surf. Coat. Technol.*, **36** (1-2), 87-97 (1988)

30 R.A. Erck, A. Erdimir, G.R. Fenske, *Surf. Coat. Technol.*, **43/44**, 577-587 (1990)

31 C. Dellacorte, S.V. Pepper, F.C. Honecy, *Surf. Coat. Technol.*, **52**, 31-37 (1992)

32 N. Marechal, Y. Pauleau, E. Quesnel, P. Juliet, A. Ronzaud, C. Zimmerman, *Surf. Coat. Technol.*, **68/69**, 416-421 (1994)

33 M.C. Jeng, Y.L. Soong, *Surf. Coat. Technol.*, **57**, 145-150 (1993)

34 D. Wu, R.A. Outlaw, R.L. Ash, *J. Appl. Phys.*, **74** (8), 4990-4994 (1993)

35 Z.Y. Li, H. Maeda, K. Kusakabe, S. Morooka, H. Anzai, S. Akiyama, *J. Membrane Science*, **78**, 247-254 (1993)

36 J. Shu, B.P.A. Grandjean, A. van Neste, S. Kaliaguine, *Can. J. Chem. Engineering*, **69** (5), 1036-1060 (1991)

37 L.K.L. Dean, K.L. Busch, *Organic Mass Spectrometry*, **24**, 733-736 (1989)

38 A. Vogler, C. Quett, H. Kunkely, *Ber. Bungsenges. Phys. Chem.*, **92**, 1486-1492 (1988)

39 Y.-F. Lu, M. Takai, S. Nagamoto, K. Kato, S. Namba, *Appl. Phys.*, **A54**, 51-56 (1992)

40 Y. Yonezawa, Y. Konishi, H. Hada, K. Yamamoto, H. Ishida, *Thin Solid Films*, **218**, 109-121 (1992)

41 Y.-F. Lu, M. Takai, T. Shiokawa, Y. Aoyagi, *Jpn. J. Appl. Phys.*, **33**, L1313-L1315 (1994)

42 'Deposition technologies for films and coatings: developments and applications', Ed. R.F. Bunshah, Chapter 4 'Evaporation' by R.F. Bunshah, Noyes, New Jersey (1982)

43 'Deposition technologies for films and coatings: developments and applications', Ed. R.F. Bunshah, Chapter 5 'Sputtering' by J.A. Thornton, Noyes, New Jersey (1982)

44 'Thin film processes', Eds. J.L. Vossen, W. Kern, Part II "Physical methods of film deposition" various authors, Academic Press, New York (1978)

45 W.E. Sawyer, A. Mann, US Pat. 229,335 (1880)

46 L. Mond, C. Langer, F. Quinke, *J. Chem. Soc.*, **57**, 749-753 (1890)

47 'Vapor deposition', Eds. C.F. Powell, J.H. Oxley, J.M. Blocher Jr., John Wiley, New York (1966)

48 M.E. Coltrin, R.J. Kee, J.A. Miller, *J. Electrochem. Soc.*, **133** (6), 1206-1213 (1986)

49 J.M. Jasinski, B.S. Meyerson, B.A. Scott, *Annu. Rev. Phys. Chem.*, **38**, 109-140 (1987)

50 M.E. Coltrin, R.J. Kee, J.A. Miller, *J. Electrochem. Soc.*, **131** (2), 425-434 (1984)

51 G.B. Stringfellow in 'Mechanisms of reactions of organometallic compounds with surfaces' Ed. D. Cole-Hamilton, NATO advanced study institute (1990)

52 'The surface scientist's guide to organometallic chemistry', M.R. Albert, Y.T. Yates Jr., American Chemical Society, Washington DC (1987)

53 G.D.T. Spiller, P. Akhter, J.A. Venables, *Surface Science*, **131** (2-3), 517-533 (1983)

54 T.C. Nason, PhD Thesis, Rensselaer Polytech. Inst., Troy, NY, 1992, 137pp (Eng), through *Diss. Abstr. Int. B*, **54** (1), 307 (1993) or *Chem. Abstr.* 121:70613t (1994)

55 Th. Hartel, U. Struber, J. Kuppers, *Thin Solid Films*, **229**, 163-170 (1993)

56 'Microelectronics Processing : Chemical Engineering Aspects', Ed. D.W. Hess, K.F. Jensen, Chapter 5 'Chemical Vapour Deposition' by K.F. Jensen, ACS, Washington (1989)

57 J.T. Spencer, *Progress in Inorganic Chemistry*, **41**, 145-237 (1994)

58 V. Hlavacek, J.J. Thiart, D. Orlicki, *Journal de Physique IV, Colloque C5, supplement au Journal de Physique II,* **5**, 3-44 (1995)

59 A. Jain, T.T. Kodas, R. Jairath, M.J. Hampden-Smith, *J. Vac. Sci. Technol. B*, **11**(6), 2107-2113 (1993)

60 'Deposition technologies for films and coatings: developments and applications', Ed. R.F. Bunshah, Chapter 9 'PECVD' by T.D. Bonifield, Noyes, New Jersey (1982)

61 'Microelectronics Processing: Chemical Engineering Aspects', Eds. D.W. Hess, K.F. Jensen, Chapter 8 'Plasma enhanced etching and deposition' by D.W. Hess, D.B. Graves, ACS, Washington (1989)

62 R. Marriott, D.A.V. Morton, M. Rampling, 'Developments in droplet-to-particle synthesis of powders', in press

63 C.M. Whitehouse, J.B. Fenn, S. Shen, C. Smith, US Patent 5,306,412 (1994) and references therein

64 A. Gurav, T.T. Kodas, T. Pluym, Y. Xiong, *Aerosol Science and Technology*, **19**, 411-452 (1993)

65 'The Chemistry of Metal CVD', Eds. T.T. Kodas, M.J. Hampden-Smith, Chapter 9 'Overview of metal CVD' by T.T. Kodas, M.J. Hampden-Smith, VCH, Weinheim (1994)

66 J.C. Evans, R.D. Gillard, R.J. Lancashire, P.H. Morgan, *J. Chem. Soc., Dalton Trans.*, 1277-1281 (1980)

67 H.F. Priest, *Inorg. Synth.*, **3** , 176 (1950) through 'Inorganic Reactions and Methods', Vol. 4, Ed. Zuckerman, Published by VCH Publishers Inc.

68 B. Standke, M. Jansen, *Angew. Chemie., Int. Ed. Eng.*, **24**, 118-119 (1985)

69 B. Standke, M. Jansen, *Angew. Chemie., Int. Ed. Eng.*, **25**, 77-78 (1986)

70 A.I. Popov, Y.M. Kiselev, *Zhur. neorg. Khim.*, **33** (4), 965-970 (1988) through 'Inorganic Reactions and Methods', Vol. 4, Ed. Zuckerman, Published by VCH Publishers Inc.

71 for example Y.S. -Yan, L.Q. -Hui, S.M. -Chang, H.X. -Yun, *Inorg. Chem.*, **33**, 1251-1252 (1994)

72 'Comprehensive Coordination Chemistry', Eds. G. Wilkinson, R.D. Gillard, J.A. McCleverty, Volume 5, Chapter 54 'Silver' by R.J. Lancashire, Pergamon Press, Oxford (1987)

73 W. Levason, M.D. Spicer, *Coord. Chem. Rev.*, **76**, 45-120 (1987)

74 H.N. Po, *Coord. Chem. Rev.*, **20**, 171-195 (1976)

75 J.A. McMillan, *Chem. Rev.*, **62**, 65-80 (1962)

76 'Advanced Inorganic Chemistry', 5th Edition, F.A. Cotton and G. Wilkinson, Wiley Interscience, New York (1988)

77 R.B. Corey, K. Pestrecov, *Z. Kristallogr.*, **89**, 528 (1934) through *Chem. Abstr.* **29**:6122^{5} (1934)

78 L.E. Orgel, *J. Chem. Soc.*, 4186-4190 (1958)

79 J.L. Hoard, *Z. Kristallogr.*, **84**, 231-255 (1933)

80 E. Straritzky, *Anal. Chem.*, **28**, 419-420 (1956)

81 O.H. Ellestad, P. Klaeboe, E.E. Tucker, J. Songstad, *Acta Chemica Scand.*, **26**, 3579-3592 (1972)

82 L.J. Baker, G.A. Bowmaker, D. Camp, Effendy, P.C. Healy, H. Schmidbaur, O. Steigelmann, A.H. White, *Inorg. Chem.*, **31** (17), 3656-3662 (1992)

83 M. Munakata, S. Kitagawa, N. Ujimaru, M. Nakamura, M. Maekawa, H. Matsuda, *Inorg. Chem.*, **32**, 826-832 (1993)

84 M.N. Ikhan, R.J. Staples, C. King, J.P. Fackler, R.E.P. Winpenny, *Inorg. Chem.*, **32**, 5800-5807 (1993)

85 G.A. Bowmaker, Effendy, J.V. Hanna, P.C. Healy, B.W. Skelton, A.H. White, *J. Chem. Soc., Dalton Trans.*, 1387-1397 (1993)

86 A. Cassel, *Acta Cryst.*, **B35**, 174-177 (1979)

87 B.K. Teo, J.C. Calabrese, *J. Am. Chem. Soc.*, **97** (5), 1256-1257 (1975)

88 C.S.W. Harker, E.R.T. Tiekink, *J. Coord. Chem.*, **21**, 287-293 (1990)

89 E.W. Ainscough, A.M. Brodie, S.L. Ingham, J.M. Waters, *J. Chem. Soc., Dalton Trans.*, 215-220 (1994)

90 H. Adams, N.A. Bailey, D.E. Fenton, C. Fukuhara, P.C. Hellier, P.D. Hempstead, *J. Chem. Soc., Dalton Trans.*, 729-730, (1992)

91 A.J. Amoroso, J.C. Jeffery, P.L. Jones, J.A. McCleverty, E.Psillakis, M.D. Ward, *J. Chem. Soc., Chem. Comm.*, 1175-1176 (1995)

92 A.J. Blake, G. Reid, M. Schroder, *J. Chem. Soc., Chem. Comm.*, 1074-1076 (1992)

93 R.J.H. Voorhoeve, J.W. Merewether, *J. Electrochem. Soc.: Solid State Science and Tech.*, **119** (3), 364-368 (1972)

94 Anonymous, *Research Disclosure*, 26343, March 1986

95 C. Oehr, H. Suhr., *Appl. Phys.*, **A49**, 691-696 (1989)

96 T.H. Baum, C.E. Larson, S.K. Reynolds, US Patent 5,096,737 (1992)

97 W. Lin, T.H. Warren, R.G. Nuzzo, G.S. Girolami, *J. Am. Chem. Soc.*, **115**, 11644-11645 (1993)

98 N.H. Dryden, J.J. Vittal, R.J. Puddephatt, *Chem. Mater.*, **5**, 765-766 (1993)

99 Z. Yuan, N.H. Dryden, J.J. Vittal, R.J. Puddephatt, *Chem Mater.*, **7**, 1696-1702 (1995)

100 S. Serghini-Monim, Z. Yuan, K. Griffiths, P.R. Norton, R.J. Puddephatt, *J. Am. Chem. Soc.*, **117**, 4030-4036 (1995)

101 Z. Yuan, N.H. Dryden, X. Li, J.J. Vittal, R.J. Puddephatt, *J. Mater. Chem.*, **5** (2), 303-307 (1995)

102 C.Y. Xu, M.J. Hampden-Smith, T.T. Kodas, *Advanced Materials*, **6** (10), 746-748 (1994)

103 C.Y. Xu, M.J. Hampden-Smith, T.T. Kodas, *Chem. Mater.*, **7**, 1539-1546 (1995)

104 N.J. Bruce, N.G. Murray, *Tetrahedron*, **27**, 5323 (1971)

105 J. Kleinberg, *Chem. Rev.*, 381-390 (1947)

106 C. Oldham, *Progress in Inorganic Chemistry*, **10**, 223 (1968)

107 D.S. Sagatys, G. Smith, R.C. Bott, D.E. Lynch, C.H.L. Kennard, *Polyhedron*, **12** (6), 709-713 (1993) and references therein

108 'Metal carboxylates', R.C. Mehrotra, R. Bohra, Chapter 3 'Physicochemical Properties', 3.9 'Decarboxylation Reactions', pp 145-151, Academic Press, London (1983)

109 E.K. Fields, S. Meyerson, *J. Org. Chem.*, **41** (6), 916-920 (1976)

110 A.D. Kirshenbaum, A.G. Streng, M. Hauptschein, *J. Am. Chem. Soc.*, **75**, 3141-3145 (1953)

111 S.K. Adams, D.A. Edwards, R. Richards, *Inorganica Chimica Acta*, **12** , 163-166 (1975)

112 K.L. Busch, R.G. Cooks, R.A. Walton, K.V. Wood, *Inorg. Chem.*, **23**, 4093-4097 (1984)

113 G.D. Roberts, E. White, *Organic Mass Spectrometry*, **16** (12), 546-550 (1981)

114 X.-M. Chen, T.C.W. Mak, *Polyhedron* **10** (14), 1723-1726 (1991)

115 X.-M.Chen, T.C.W.Mak, *J. Chem. Soc., Dalton Trans.*, 1219-1222 (1991)

116 W.-Y. Huang, L. Lu, X.-M. Chen, T.C.W. Mak, *Polyhedron*, **10** (23/24), 2687-2691 (1991)

117 D.D. Wu, T.C.W. Mak, *J. Chem. Soc., Dalton Trans.*, 2671-2678 (1995)

118 T.C.W. Mak, W.H. Yip, X.M. Chen, *Inorganica Chimica Acta*, **203** (1), 97-99 (1993)

119 X.M. Chen, T.C.W. Mak, *Aust. J. Chem.*, **44** (12), 1783-1787 (1991)

120 B.T. Usubaliev, E.M. Movsumov, I.R. Amiraslanov, A.I. Akhmedov, A.A. Musaev, Kh.S. Mamedov, *Zh. Strukt. Khim.*, **22** (1), 98-103 (1981) (Eng)

121 T.C.W. Mak, W.-H. Yip, C.H.L. Kennard, G. Smith, E.J. O'Reilly, *Aust. J. Chem.*, **41**, 683-691 (1988)

122 C.B. Acland, H.C. Freeman, *J. Chem. Soc., Chem. Commun.*, 1016-1017 (1971)

123 J.K. Mohana Rao, M.A. Viswanitra, *Acta Cryst.*, **B28**, 1484-1496 (1972)

124 T.C.W. Mak, W.-H. Tip, C.H.L. Kennard, G. Smith, E.J. O'Reilly, *Aust. J. Chem.*, **39**, 541-546 (1986)

125 V.N. Kolesnikov, V.N. Baumer, *Vestn. Khar'kov Un-ta, Khimiya*, **127** (6), 38-41 (1975) (Russ) through *Chem. Abstr.* **84**:172478n (1975)

126 D.Y. Namov, A.V. Virovets, N.V. Podberezskaya, E.V. Boldyreva, *Acta Cryst.*, **C51**, 60-62 (1995)

127 F. Charbonnier, R. Faure, H. Loiseleur, *Rev. Chim. Miner.*, **18** (3), 245-253 (1981)

128 G. Smith, D.S. Sagatys, C.A. Campbell, D.E. Lynch, C.H.L. Kennard, *Aust. J. Chem.*, **43**, 1707-1712 (1990)

129 F. Charbonnier, R. Faure, M. Petit-Ramel, *Eur. J. Solid State Inorg. Chem.*, **t29**, 93-100 (1992)

130 D.S. Sagatys, G. Smith, D.E. Lynch, C.H.L. Kennard, *J. Chem. Soc., Dalton Trans.*, 361-364 (1991)

131 G. Smith, A.N. Reddy, K.A. Byriel, C.H.L. Kennard, *J. Chem. Soc., Dalton Trans.*, 3565-3570 (1995)

132 I.R. Amiraslanov, B.T. Usubaliev, G.N. Nadzhafov, A.A. Musaev, E.M. Movsumov, Kh.S. Mamedov, *Zh. Strukt. Khim.*, **21** (5), 112-118 (1980) (Russ) through *Chem. Abs.* **94**:112828y (1981)

133 F. Charbonnier, M. Petit-Ramel, R. Faure, H. Loiseleur, *Rev. Chim. Miner.*, **t21**, 601-610 (1984) (French)

134 T.C.W. Mak, W.-H. Yip, C.H.L. Kennard, G. Smith, E.J. O'Reilly, *J. Chem. Soc.,Dalton Trans.*, 2353-2356 (1988)

135 W.-H. Chan, T.C.W. Mak, W.-H. Yip, C.H.L. Kennard, G. Smith, E.J. O'Reilly, *Aust. J. Chem.*, **40**, 1161-1168 (1987)

136 J.P. Deloume, R. Faure, H. Loiseleur, *Acta Cryst.*, **B33**, 2709-2712 (1977) (French)

137 N.J. Calos, C.H.L. Kennard, T.C.W. Mak, G. Smith, *Aust. J. Chem.*, **42**, 2047-2050 (1989)

138 G. Smith, A.N. Reddy, K.A. Byriel, C.H.N. Kennard, *Polyhedron*, **13** (15/16), 2425-2430 (1994)

139 D.M.L. Goodgame,T.E. Muller, D.J. Williams, *Polyhedron*, **11** (12), 1513-1516 (1992)

140 F. Jaber, F. Charbonnier, R. Faure, *Acta Cryst.*, **C50**, 1444-1447 (1994)

141 P. Coggon, A.T. McPhail, *J. Chem. Soc., Chem. Commun.*, 91-92 (1972)

142 G.W. Hunt, T.C. Lee, E.L. Amma, *Inorg. Nucl. Chem. Letters*, **10**, 909-913 (1974)

143 G. Smith, C.H.L. Kennard, T.C.W. Mak, *Z. Kristallogr.*, **184** (3-4), 275-280 (1988) (Eng)

144 F. Jaber, F. Charbonnier, R. Faure, *Eur. J. Solid State Inorg. Chem.*, **t32**, 25-33 (1995)

145 A. Michaelodes, S. Skoulika, V. Kiritsis, A. Aubry, *J. Chem. Soc., Chem. Commun.*, 1415-1416 (1995)

146 G. Smith, A.N. Reddy, K.A. Byriel, C.H.L. Kennard, *Aust. J. Chem.*, **47**, 1179-1183 (1994)

147 D.W. Hartley, G. Smith, D.S. Sagatys, C.H.L. Kennard, *J. Chem. Soc., Dalton Trans.*, 2735-2738 (1991)

148 D.A. Edwards, M. Longley, *J. Inorg. Nucl. Chem.*, **40**, 1599-1601 (1978)

149 C. Oldham, W.F. Sandford, *J. Chem. Soc., Dalton Trans.*, 2068-2070 (1977)

150 E.L. Muetterties, C.W. Alegranti, *J. Am. Chem. Soc.*, **92** (13), 4114-4115 (1970)

151 V.M. Hedrich, H. Hartl, *Acta Cryst.*, **C39**, 533-536 (1983) (Ger)

152 A.F.M.J. van der Ploeg, G. van Koten, A.L.Spek, *Inorg. Chem.*, **18** (4), 1052-1060 (1979)

153 E.T. Blues, M.G.B. Drew, B. Femi-Onadeko, *Acta Cryst.*, **B33**, 3965-3967 (1977)

154 G.A. Bowmaker, Effendy, J.V. Hanna, P.C. Healy, G.J. Millar, B.W. Skelton, A.H. White, *J. Phys. Chem.*, **99** (12), 3909-3917 (1995)

155 B. Femi-Onadeko, *Z. Kristallogr.*, **152**, 159-160 (1980)

156 S.P. Neo, Z.-Y. Zhou, T.C.W. Mak, T.S.A. Hor, *Inorg. Chem.*, **34**, 520-523 (1995)

157 T.S.A. Hor, S.P. Neo, C.S. Tan, T.C.W. Mak, K.W.P. Leung, R.-J. Wang, *Inorg. Chem.*, **31**, 4510-4516 (1992)

158 G. Ferguson, R. McCrindle, M. Parvez, *Acta Cryst.*, **C40**, 354-356 (1984)

159 J. Powell, M. Horvath, A. Lough, *J. Organomet. Chem.*, **456**, C27-C28 (1993)

160 H.E. Donley, U.S.Patent 3,528,845 (1970)

161 'Metal Carboxylates', R.C. Mehrotra, R. Bohra, Chapter 3 'Physicochemical properties', Section 3.1 'Vibrational Spectra', Academic Press, London (1983)

162 'Infrared and Raman Spectra of Inorganic and Coordination Compounds' 3rd Edition, K. Nakamoto, John Wiley and Sons, New York (1978)

163 A.I. Grigorev, *Russ. J. Inorg. Chem.*, **8**, 409 (1963)

164 D.A. Edwards, R.N. Hayward, *Can. J. Chem.*, **46**, 3443-3446 (1968)

165 G.B. Deacon, F. Huber, R.J. Phillips, *Inorganica Chimica Acta*, **104**, 41-45 (1985)

166 R.G. Goel, P. Pilon, *Inorg. Chem.*, **17** (10), 2876-2879 (1978)

167 M.G.B. Drew, A.H. Othman, D.A. Edwards, R. Richards, *Acta Crystallogr.*, **B31**, 2695-2697 (1975)

168 D.F. Evans, J.N. Tucker, G.C. De Villardi, *J. Chem. Soc., Chem. Commun.*, 205-206 (1975)

169 A. Dambska, A. Janowski, *Org. Magn. Reson.*, **13**, 122 (1980)

170 E. Szlyk, I. Lakomska, A. Grodzicki, *Thermochimica Acta*, **223**, 207-212 (1993)

171 E. Szlyk, I. Lakomska, A. Grodzicki, *Polish J. Chem.*, **68**, 1529-1534 (1994)

172 M.J. Ballie, D.H. Brown, K.C. Moss, D.W.A. Sharp, *J. Chem. Soc. (A)*, 3110-3114 (1968)

173 R.G. Griffin, J.D. Ellett, M. Mehring, J.G. Bullitt, J.S. Waugh, *J. Chem. Phys.*, **57** (5), 2147-2155 (1972)

174 A.E. Blakeslee, J.L. Hoard, *J. Am. Chem. Soc.*, **78**, 3029-3033 (1956)

175 E.C. Alyea, G. Ferguson, A. McAlees, R. McCrindle, R. Myers, P.Y. Siew, S.A. Dias, *J. Chem. Soc., Dalton Trans.*, 481-490 (1981)

176 'High Resolution Nuclear Magnetic Resonance Spectroscopy', J.W. Emsley, J. Feeney, L.H. Sutcliffe, Pergamon Press, Oxford (1966)

177 E.L. Muetterties, C.W. Alegranti, *J. Am. Chem. Soc.*, **94** (18), 6386-6391 (1972)

178 'Mass Spectrometry of Organic Compounds', Eds. H. Budzikiewicz, C. Djerassi, D.H. Williams, p 647

179 T.J. Wenzel, T.C. Bettes, J.E. Sadlowski, R.E. Sievers, *J. Am. Chem. Soc.*, **102**, 5903-5904 (1980)

180 T.J. Wenzel, R.E. Sievers, *Anal. Chem.*, **53**, 393-399 (1981)

181 T.J. Wenzel, R.E. Sievers, *J. Am. Chem. Soc.*, **104** (2), 382-388 (1982)

182 T.J. Wenzel, R.E. Sievers, *Anal. Chem.*, **54** (9), 1602-1606 (1982)

183 for example M.L. Green, R.A. Levy, *J. Met.*, **37** (6), 63-71 (1985)

184 for example S. Motojima, S. Kuri, T. Hattori, *J. Less-Common Metals*, **124**, 193-204 (1986)

185 for example J.P. Lu, P.W. Chu, R. Raj, H. Gysling, *Thin Solid Films*, **208** (2), 172-176 (1992)

186 for example J.T. Harding, V.R. Fry, R.H. Tuffias, R.B. Caplan, AFRPL TR-86-099 (1987)

187 for example N.H. Dryden, R. Kumar, E.C. Ou, M. Rashidi, S. Roy, P.R. Norton, R.J. Puddephatt, J.D. Scott, *Chem. Mater.*, **3**, 677-685 (1991)

188 for example H.-K. Shin, K. M. Chi, J. Farkas, M.J. Hampden-Smith, T.T. Kodas, E.N. Duesler, *Inorg. Chem.*, **31**, 424-431 (1992)

189 for example M. Hoshino, *Gold Bull.*, **27**, 2 (1994)

190 G.T. Morgan, H.W. Moss, *J. Chem. Soc.*, **105**, 189-201 (1914)

191 'Metal β-diketonates and allied derivatives', R.C. Mehrotra, R. Bohra, D.P. Gaur, Chapter 2 'Oxygen-bonded β-diketonato complexes', Academic Press, London (1978)

192 E.A Mazurenko, A.I. Gerasimchuk, *Journal de Physique IV, Colloque C5, supplement au Journal de Physique II*, **5**, C5-547-551 (1995)

193 V.A. Bogdanov, A.I. Gerasimchuk, E.A. Mazurenko, *J. Koord. Khimii.*, **10**, 1346-1352 (1984) through reference 250 (new 192)

194 E.A. Mazurenko, J.N. Bublik, S.V. Volkov, *Ukr. Khim. Jour.*, **7**, 591-596 (1979) through reference 250 (new192)

195 J.V.Nef, *Liebigs Ann. Chem.*, **277**, 68-78 (1893)

196 I.Wakeshima, H.Ohgi, I.Kijima, *Synth. React. Inorg. Met. -Org. Chem.*, **23** (9), 1507-1513 (1993)

197 D. Gibson, PhD Thesis, Victoria University of Manchester (1967)

198 D. Gibson, B.F.G. Johnson, J. Lewis, *J. Chem. Soc. (A)*, 367-369 (1970)

199 W. Partenheimer, E.H. Johnson, *Inorg. Chem.*, **11** (11), 2840-2841 (1972)

200 W. Partenheimer, E.H. Johnson, *Inorg. Synth.*, **16**, 117-119 (1976)

201 W. Partenheimer, E.H. Johnson, *Inorg. Chem.*, **12** (6), 1274-1278 (1973)

202 C.Y. Xu, T.S. Corbitt, M.J. Hampden-Smith, T.T. Kodas, E.N. Duesler, *J. Chem. Soc., Dalton Trans.*, 2841-2849 (1994)

203 C.Y. Xu, M.J. Hampden-Smith, T.T. Kodas, E.N. Duesler, A.L. Rheingold, G.Yap, *Inorg. Chem.*, **34**, 4767-4773 (1995)

204 A. Bailey, T.S. Corbitt, M.J. Hampden-Smith, E.N. Duesler, T.T. Kodas, *Polyhedron*, **12** (14), 1785-1792 (1993)

205 G. Doyle, K.A. Eriksen, D. Van Engen, *Organometallics*, **4**, 830-835 (1985)

206 P. Doppelt, T.H. Baum, L. Ricard, *Inorg. Chem.*, **35** (5), 1286-1291 (1996)

207 W.H. Watson, C.T. Lin, *Inorg. Chem.*, **5**, 1074-1077 (1966)

208 J. Fornies, R. Navarro, M. Tomas, E.P. Urriolabeitia, *Organometallics*, **12**, 940-943 (1993)

209 K.M. Chi, H.-K. Shin, M.J. Hampden-Smith, E.N. Duesler, T.T. Kodas, *Polyhedron*, **10** (19), 2293-2299 (1991)

210 S.K. Mitra, *J. Indian Chem. Soc.*, **10**, 71-74 (1933) through *Chem. Abstr.* **27**:3914 (1933)

211 'Metal β-diketonates and allied derivatives', R.C. Mehrotra, R. Bohra, D.P. Gaur, Chapter 4 'Metal thio-β-diketonates - an introduction', Academic Press, London (1978)

212 S.H.H. Chaston, S.E. Livingstone, *Aust. J. Chem.*, **20**, 1065-1077 (1967)

213 T. Honjo, S. Shima, *Bull. Chem. Soc. Jpn.* **57**, 293-294 (1984)

214 D.L. Schulz, B.J. Hinds, D.A. Neumayer, C.L. Stern, T.J. Marks, *Chem. Mater.*, **5**, 1605-1617 (1993)

215 T.J. Marks, *Pure & Appl. Chem.*, **67** (2), 313-318 (1995)

216 H.-K. Shin, M.J. Hampden-Smith, T.T. Kodas, A.L. Rheingold, *J. Chem. Soc., Chem. Commun.*, 217-219 (1992)

217 L. Simeral, G.E. Maciel, *J. Phys. Chem.*, **77**, 1590-1593 (1973)

218 S. Pinchas, B.L. Silver, I. Laulicht, *J. Chem. Phys.*, **46**, 1506-1510 (1967)

219 K. Nakamoto, Y. Morimoto, A.E. Martell, *J. Phys. Chem.*, **66**, 346-348 (1962)

220 'Vogel's textbook of practical organic chemistry' Fourth Edition, A.I. Vogel, B.S. Furniss, Longman, London (1978)

221 'Spectroscopic methods in organic chemistry', Fourth Edition, D.H. Williams, I. Fleming, McGraw-Hill, London (1987)

222 Z. Yuan, N.H. Dryden, J.J. Vittal, R.J. Puddephatt, *Can. J. Chem.*, **72**, 1605-1609 (1994)

223 H.-K. Shin, M.J. Hampden-Smith, E.N. Duesler, T.T. Kodas, *Can. J. Chem.*, **70**, 2954-2966 (1992)

224 'Comprehensive Organometallic Chemistry' Eds. E.W. Abel, F.G.A. Stone, G. Wilkinson, Chapter 14 'Copper and Silver' by G. van Koten, J.G. Noltes, Pergamon Press, Oxford (1982) and 'Comprehensive Organometallic Chemistry II - A review of the literature 1982-1994', Eds.

E.W. Abel, F.G.A. Stone, G. Wilkinson, Volume 2, Chapter 2 'Copper and Silver' by G. van Koten, S.L. James, J.T.B.H. Jastrzebski, Pergamon Press, Oxford (1995)

225 T. Kauffmann, C. Neiteler, S. Robbe, *Chem. Ber.*, **125**, 2409-2418 (1992)

226 H. Westmijze, H. Kleijn, P. Vermeer, *J. Organometal. Chem.*, **172**, 377-383 (1979)

227 H. Westmijze, H. Kleijn, P. Vermeer, *Tetrahedron Lett.*, 3327-3328 (1979)

228 H. Kleijn, H. Westmijze, J. Meijer, P. Vermeer, *J. Organometal. Chem.*, **192**, 275-281 (1980)

229 H. Westmijze, H. Kleijn, H.J.T. Bos, P. Vermeer, *J. Organometal. Chem.*, **199**, 293-297 (1980)

230 H. Kleijn, H. Westmijze, J. Meijer, P. Vermeer, *J. Organometal. Chem.*, **206**, 257-264 (1981)

231 A. Erbil, U.S. Patent 4,880,670 (1989)

232 M.J. Hampden-Smith, T.T. Kodas, M. Paffett, J.D. Farr, H.-K. Shin, *Chem. Mater.*, **2** (6), 636-639 (1990)

233 D.B. Beach, F.K. LeGoues, C.K. Hu, *Chem. Mater.*, **2** (3), 216-219 (1990)

234 E. Feurer, H. Suhr, *Appl. Phys. A*, **44** (2), 171-175 (1987)

235 T.H. Baum, E.E. Marinero, C.R. Jones, *Appl. Phys. Lett.*, **49** (18), 1213-1215 (1986)

236 A.D. Dubner, A. Wagner, *J. Appl. Phys.*, **65** (9), 3636-3643 (1989)

237 G.M. Shedd, H. Lezec, A.D. Dubner, J. Melngailis, *J. Appl. Phys.*, **49** (23), 1584-1586 (1986)

238 R.J. Puddephatt, I. Trennicht, *J. Organometal. Chem.*, **319** (1), 129-137 (1987)

239 R.D. Sanner, J.H. Satcher, M.W. Droege, *Organometallics*, **8** (6), 1498-1506 (1989)

240 D.R. Biswas, C. Ghosh, R.L. Layman, *J. Electrochem. Soc.*, **130**, 234-236 (1983)

241 J.A.T. Norman, B.A. Muratore, P.N. Dyer, D.A. Roberts, A.K. Hochberg, *Mater. Sci. Eng. B*, **17** (1-3), 87-92 (1993)

242 H. Schmidbaur, M. Bergfeld, *Inorg. Chem.*, **5**, 2069-2070 (1966)

243 G.W. Roland, A.I. Braginski, *Adv. Cryog. Eng.*, **22**, 347 (1977)

244 N.M. Rutherford, C.E. Larson, R.L. Jackson, *Mater. Res. Soc. Symp. Proc.*, **131**, 439 (1989)

245 G.J.M. Dormans, *J. Cryst. Growth*, **108** (3-4), 806-816 (1991)

246 for example B.E. Bent, R.G. Nuzzo, L.H. Dubois, *J. Am. Chem. Soc.*, **111** (5), 1634-1644 (1989)

247 E.M. Meyer, S. Gambarotta, C. Floriani, A. Chiesi-Villa, C. Guastini, *Organometallics*, **8**, 1067-1079 (1989)

248 S. Gambarotta, C. Floriani, A. Chiesi-Villa, C. Guastini, *J. Chem. Soc., Chem. Commun.*, 1087-1089 (1983)

249 A.J. Leusink, G. van Koten, J.G. Noltes, *J. Organomet. Chem.*, **56**, 379-390 (1973)

250 H.K.Hofstee, Thesis, Univ. Utrecht (1978)

251 K.K. Sun, W.T. Miller, *J. Am. Chem. Soc.*, **92** (23), 6985-6987 (1970)

252 G. Coasta, A. Camus, *Gazz. Chim. Ital.*, **86**, 77-86 (1956) through *Chem. Abstr.* **50**:12719 (1956)

253 M.C. Gimeno, P.G. Jones, A. Laguna, M.D. Villacampa, *J. Chem. Soc., Dalton Trans.*, 805-810 (1995)

254 H. Schmidbaur, *Inorg. Synth.*, **18**, 136-143 (1978)

255 H. Schmidbaur, J. Adlkofer, W. Bucher, *Angew. Chemie., Int. Ed. Eng.*, **12** (5), 415-416 (1973)

256 R. Usón, A. Laguna, A. Usón, P.G. Jones, K. Meyer-Bäse, *J. Chem. Soc., Dalton Trans.*, 341-345 (1988) and references therein

257 S. Wang, J.P. Fackler, T.F. Carlson, *Organometallics*, **9**, 1973-1975 (1990) and references therein

258 A.J. Ardnengo, H.V. Rasika Dias, J.C. Calabrese, F. Davidson, *Organometallics*, **12**, 3405-3409 (1993)

259 G.Buckton, *Ann.*, **109**, 225 (1859)

260 J.A. Wanklyn, L. Carius, *Ann.*, **120**, 70 (1861)

261 E. Krause, M. Schmitz, *Ber. Deutsch. Chem. Ges.*, **52**, 2159-2164 (1919)

262 G. van Koten, J.G. Noltes, *J. Am. Chem. Soc.*, **101**, 6593-6599 (1979)

263 A.J. Leusink, G. van Koten, J.W. Marsman, J.G. Noltes, *J. Organomet. Chem.*, **55**, 419-425 (1973)

264 G. van Koten, C.A. Schaap, J.T.B.H. Jastrzebski, J.G. Noltes, *J. Organomet. Chem.*, **186**, 427-445 (1980)

265 G. van Koten, J.T.B.H. Jastrzebski, C.H. Stam, N.C. Niemann, *J. Am. Chem. Soc.*, **106**, 1880-1881 (1984)

266 R.R. Burch, J.C. Calabrese, *J. Am. Chem. Soc.*, **108**, 5359-5360 (1986) and references therein

267 W.T. Miller, R.H. Snider, R.J. Hummel, *J. Am. Chem. Soc.*, **91** (23), 6532-6534 (1969)

268 B.L. Dyatkin, B.I. Martynov, L.G. Martynova, N.G. Kizim, S.R. Sterlin, Z.A. Stumbrevichute, L.A. Federov, *J. Organomet. Chem.*, **57**, 423-433 (1973)

269 C.D.M. Beverwijk, G.J.M. van der Kerk, A.J. Leusink, J.G. Noltes, *Organometallic Chem. Rev.*, **5** (2), 215-280 (1970)

270 A.N. Nesmeyanov, B.A. Sazonova, N.S. Sazonova, *Dokl. Akad. Nauk SSSR*, **176**, 598-601 (1967), *Proc. Acad. Sci. USSR*, **176**, 843-846 (1967)

271 'Methoden der Organischen Chemie', Ed. E.Muller, Band XIII/1, p.763, 'Methoden zur Herstellung und Umwandlung von Organosilber - Verbindungen', G. Bahr, P. Burba, Houben-Weyl, Georg Thieme Verlag, Stuttgart (1970)

272 H.K. Hofstee, Thesis, Univ. Utrecht (1978)

273 R.A. Papasergio, C.L. Raston, A.H. White, *J. Chem. Soc., Chem. Commun.*, 612-613 (1984)

274 R.A. Papasergio, C.L. Raston, A.H. White, *J. Chem. Soc., Dalton Trans.*, 3085-3091 (1987)

275 C. Eaborn, P.B. Hitchcock, J.D. Smith, A.C. Sullivan, *J. Chem. Soc., Chem. Commun.*, 870-871 (1984)

276 F. Glockling, D. Kingston, *J. Chem. Soc.*, 3001-3004 (1959)

277 R.E. Banks, R.N. Haszeldine, D.R. Taylor, G. Webb, *Tetrahedron Lett.*, 5215-5216 (1970)

278 H.K. Hofstee, J. Boersma, G.J.M. van der Kerk, *J. Organomet. Chem.*, **168**, 241-249 (1978)

279 E.J. Fernández, A. Laguna, A. Mendìa, *Inorganica Chimica Acta*, **223**, 161-164 (1994)

280 A.N. Nesmeyanov, N.N. Sedova, Y.T. Struchkov, V.G. Adrianov, E.N. Stakheeva, V.A. Sazonova, *J. Organomet. Chem.*, **153**, 115-122 (1978)

281 R. Lingnau, J. Strahle, *Angew. Chemie., Int. Ed. Eng.*, **27** (3), 436 (1988)

282 A. Haaland, K. Rypdal, H.P. Verne, W. Scherer, W.R. Thiel, *Angew. Chemie., Int. Ed. Eng.*, **33** (23/24), 2443-2445 (1994)

283 M.D. Janssen, M. Herres, A.L. Spek, D.M. Grove, H. Lang, G. van Koten, *J. Chem. Soc., Chem. Commun.*, 925-926 (1995)

284 P.W.R. Corfield, H.M.M. Shearer, *Acta Cryst.*, **20**, 502-508 (1966)

285 C. Brasse, P.R. Raithby, M. Rennie, C.A. Russell, A. Steiner, D.S. Wright, *Organometallics*, **15**, 639-644 (1996)

286 D.B. Beach, J.M. Jasinski, U.S.Patent 4,948,623 (1990)

287 C.D.M. Beverwijk, G.J.M. van der Kerk, *J. Organomet. Chem.*, **43**, C11-C12 (1972)

288 O. Wennerstrom, *Acta Chemica. Scand.*, **25**, 2341-2349 (1971)

289 J.T.B.H. Jastrzebski, G. van Koten, M. Konijn, C.H. Stam, *J. Am. Chem. Soc.*, **104**, 5490-5492 (1982)

290 C.J. Moulton, B.L. Shaw, *J. Chem. Soc., Dalton Trans.*, 1020-1024 (1976)

291 D.M. Grove, G. van Koten, P. Mul, R. Zoet, J.G.M. van der Linden, J. Legters, J.E.J. Schmitz, N.W. Murrall, A.J. Welch, *Inorg. Chem.*, **27**, 2466-2473 (1988)

292 H. Rimml, L.M. Venanzi, *J. Organomet. Chem.*, **259**, C6-C7 (1983)

293 D.M. Grove, G. van Koten, J.N. Louwen, J.G. Noltes, A.L. Spek, H.J.C. Ubbels, *J. Am. Chem. Soc.*, **104**, 6609-6616 (1982)

294 G. van Koten, *Pure & Appl. Chem.*, **61** (10), 1681-1694 (1989)

295 D.K. Coggin, P.E. Fanwick, M.A. Green, *J. Chem. Soc., Chem. Commun.*, 1127-1129 (1993)

296 A.H. Cowley, R.A. Jones, M.A. Mardones, J. Ruiz, J.L. Atwood, S.G. Bott, *Angew. Chemie., Int. Ed. Eng.*, **29** (10), 1150-1151 (1990)

297 A.H. Cowley, F.P. Gabbai, D.A. Atwood, C.J. Carrano, L.M. Mokry, M.R. Bond, *J. Am. Chem. Soc.*, **116**, 1559-1560 (1994)

298 H. Schumann, U. Hartmann, W. Wassermann, A. Dietrich, F.H. Gorlitz, L. Pohl, M. Hostalek, *Chem. Ber.*, **123**, 2093-2099 (1990)

299 G. van Koten, J.T.B.H. Jastrzebski, J.G. Noltes, A.L. Spek, J.C. Schoone, *J. Organomet. Chem.*, **148**, 233-245 (1978)

300 D.A. Atwood, A.H. Cowley, R.D. Schluter, M.R. Bond, C.J. Carrano, *Inorg. Chem.*, **34** (8), 2186-2189 (1995)

301 H. Schmidbaur, J. Adlkofer, A. Shiotan, *Chem. Ber.*, **105**, 3389-3396 (1972) (Ger)

302 B.J. Brisdon, M.F. Mahon, K.C. Molloy, P.J. Schofield, *J. Organomet. Chem.*, **436**, 11-22 (1992)

303 M.R. Churchill, C.H. Lake, S-H. Chao, O.T. Beachley, *J. Chem. Soc., Chem. Commun.*, 1577-1578 (1993)

304 X. Zhou, H. Ma, X. Huang, X. You, *J. Chem. Soc., Chem. Commun.*, 2483-2484 (1995)

305 G.B. Ansell, *J. Chem. Soc. (B)*, 443-446 (1971)

306 G.B. Ansell, W.G. Finnegan, *J. Chem. Soc., Chem. Commun.*, 1300 (1969)

307 G.B. Ansell, W.G. Finnegan, *J. Chem. Soc., Chem. Commun.*, 960-961 (1969)

308 J.A.J. Jarvis, R. Pearce, M.F. Lappert, *J. Chem. Soc., Dalton Trans.*, 999-1003 (1977), T. Greiser, E. Weiss, *Chem. Ber.*, **109** (9), 3142-3146 (1976) (Ger) through *Chem. Abstr.* **85**:170093e (1976) and H. Hope, P.P. Power, *Inorg. Chem.*, **23**, 936-937 (1984)

309 M.B. Hursthouse, M. Motevalli, M. Sanganee, A.C. Sullivan, *J. Chem. Soc., Chem. Commun.*, 1709-1710 (1991)

310 A.K. McMullen, T.D. Tilley, A.L. Rheingold, S.J. Geib, *Inorg. Chem.*, **28**, 3772-3774 (1989)

311 J. Emsly, 'The elements', Oxford University Press, (1989)

312 J. Kronenbitter, U. Scheizer, A. Schwenk, *Z. Naturforsch*, **35A** (3), 319-328 (1980) (Eng)

313 'NMR of newly accessible nuclei, Vol 2', Ed. Pierre Laszlo, Chapter 12 'Silver-109' by P.M.Henrichs, Academic Press, London (1983)

314 C. Brevard, G.C. van Stein, G. van Koten, *J. Am. Chem. Soc.*, **103** (22), 6746-6748 (1981)

315 E. Brun, J. Oesler, H.H. Staub, C.G. Telschow, *Phys. Rev.*, **93** (1), 172-173 (1954)

316 P.B. Sogo, C.D. Jeffries, *Phys. Rev.*, **93** (1) , 174-175 (1954)

317 A. Abragam, J.M. Winter, *Compt. Rend.*, **249**, 1633-1634 (1959) through *Chem. Abstr.*, **54** : 18058g (1960)

318 A. Schwenk, *J. Magn. Resonance*, **5** (3), 376-389 (1971)

319 C.W. Burges, R. Koschmieder, W. Sahm, A. Schwenk, *Z. Naturforsch*, **28A** (11), 1753-1758 (1973) through *Chem. Abstr.*, **80** : 76352p (1974)

320 K. Jucker, W. Sahm, A. Schwenk, *Z. Naturforsch*, **31A** (12), 1532-1538 (1976)

321 A.K. Rahimi, A.I. Popov, *Inorg. Nucl. Chem. Letters*, **12**, 703-707 (1976)

322 A.K. Rahimi, A.I. Popov, *J. Magn. Res.*, **36** (3), 351-358 (1979) through *Chem. Abstr.*, **92** : 67307y (1980)

323 P.M. Henrichs, J.J.H. Ackerman, G.E. Maciel, *J. Am. Chem. Soc.*, **99** (8), 2544-2548 (1977)

324 P.M. Henrichs, S. Sheard, J.J.H. Ackerman, G.E. Maciel, *J. Am. Chem. Soc.*, **101** (12), 3222-3228 (1979)

325 for example for phosphine complexes; 'NMR-16 Basic Principles and Progress' Eds. P. Diehl, E. Fluck, R. Kosfeld, '^{31}P and ^{13}C NMR of Transition Metal Phosphine Complexes' by P.S. Pregosin, R.W. Kunz, Springer-Verlag, Berlin (date)

326 for example for phosphite complexes; I.J. Colquhoun, W. McFarlane, *J. Chem. Soc., Chem. Commun.*, 145-147 (1980)

327 G.C. van Stein, H. van der Poel, G. van Koten, A.L. Spek, A.J.M. Duisenberg, S. Pregosin, *J. Chem. Soc., Chem. Commun.,*, 1016-1018 (1980)

328 G. van Koten, J.G. Noltes, *J. Organomet. Chem.*, **82**, C53-C55 (1974)

329 Y. Yamamoto, H. Schmidbaur, *J. Organomet. Chem.*, **96**, 133-138 (1975)

330 Y. Yamamoto, H. Schmidbaur, *J. Organomet. Chem.*, **97**, 479-486 (1975)

331 P.K. Hurlburt, J.J. Rack, S.F. Dec, O.P. Anderson, S.H. Strauss, *Inorg. Chem.*, **32**, 373-374 (1993)

332 S.S.D. Brown, P.J. McCarthy, I.D. Salter, P.A. Bates, M.B. Hursthouse, I.J. Colquhoun, W. McFarlane, M. Murray, *J. Chem. Soc., Dalton Trans.*, 2787-2796 (1988)

333 S.S.D. Brown, I.D. Salter, V. Sik, I.J. Colquhoun, W. McFarlane, P.A. Bates, M.B. Hursthouse, M. Murray, *J. Chem. Soc., Dalton Trans.*, 2177-2185 (1988)

334 A.F.M.J. van der Ploeg, G. van Koten, C. Brevard, *Inorg. Chem.*, **21** (7), 2878-2881 (1982)

335 K. Endo, K. Matsushita, K. Deguchi, K. Yamamoto, S. Suzuki, K. Futaki, *Chem. Letters*, 1497-1500 (1982)

336 K. Endo, K. Yamamoto, K. Matsushita, K. Deguchi, K. Kanda, H. Nakatsuji, *J. Magn. Reson.*, **65**, 268-281 (1985)

337 J.R. Black, N.R. Champness, W. Levason, G. Reid, *J. Chem. Soc., Dalton Trans.*, 3439-3445 (1995)

338 C. Brevard, G.C. van Stein, G. van Koten, *J. Am. Chem. Soc.*, **103** (22), 6746-6748 (1981)

339 C. Brevard, R. Schimpf, *J. Magnetic Reson.*, **47** (3), 528-534 (1982)

340 G.C. van Stein, G. van Koten, C. Brevard, *J. Organomet. Chem.*, **226** (2), C27-C30 (1982)

341 G.C. van Stein, G. van Koten, K. Vrieze, A.L. Spek, E.A. Klop, C. Brevard, *Inorg. Chem.*, **24** (19), 1367-1375 (1985)

342 G.C. van Stein, G. van Koten, K. Vrieze, C. Brevard, A.L. Spek, *J. Am. Chem. Soc.*, **106** (16), 4486-4492 (1984)

343 S.J. Berners-Price, C. Brevard, A. Pagelot, P.J. Sadler, *Inorg. Chem.*, **24**, 4278-4281 (1985)

344 R.J. Goodfellow in 'NMR and the periodic table', Eds R.K. Harris, B.E. Mann, Academic Press (1978)

345 R.J. Goodfellow in Chapter 21 of 'Multinuclear NMR', Ed J. Mason, Plenum Press (1987)

346 B.E. Mann in 'The Cinderella Nuclei', *Annual Reports on NMR Spectroscopy*, **23**, 141-207 (1991)

347 M. Barber, R.S. Bordoli, R.D. Sedgwick, A.N. Tyler, *J. Chem. Soc., Chem. Commun.*, 325-327 (1981)

348 C. Fenselau, R.J. Cotter, *Chem. Rev.*, **87**, 501-512 (1987)

349 'Inorganic Mass Spectrometry', Edited by F. Adams, R. Gijbels, R. van Grieken, Chapter 4 'Secondary Ion Mass Spectrometry' by A. Lodding, pp 125-172, John Wiley & Sons, New York (1988)

350 P.K. Chu, *Materials Chemistry and Physics*, **38** (3), 203-223 (1994)

351 R.P.H. Garten, H.W. Werner, *Analytica Chimica Acta*, **297** (1-2), 3-14 (1994)

352 R. Levisetti, J.M. Chabala, J. Li, K.L. Gavrilov, R. Mogilevsky, K.K. Soni, *Scanning Microscopy*, 7 (4), 1161-1172 (1993)

353 R.W. Odom, *Applied Spectroscopy Reviews*, **29** (1), 67-116 (1994)

354 J.M. Miller, *Advances in Inorganic Chemistry and Radiochemistry*, **28**, 1-27 (1984)

355 S.A. Martin, C.E. Costello, K. Biemann, *Anal. Chem.*, **54** (13), 2362-2368 (1982)

356 M.V. Martinezdiaz, T. Torres, W. Schafer, *Inorganica Chimica Acta*, **219** (1-2), 85-92 (1994)

357 K.B. Yatsimirsky, V.G. Golovafy, V.P. Shabelnikov, P.N. Grabovy, *J. Teoreticheskaya I - Eksperimentalnaya Khimiya* (Russ), **30** (1), 50-54 (1994)

358 M.I. Bruce, M.J. Liddell, *J. Organomet. Chem.*, **427**, 263-274 (1992)

359 L.D. Letter, R.G. Cooks, R.A. Walton, *Inorganica Chimica Acta*, **115** (1), 55-63 (1986)

360 A.J. Canty, R. Colton, *Inorganica Chimica Acta*, **220**, 99-105 (1994)

361 A.M. Bond, R. Colton, Y.A. Mah, J.C. Traeger, *Inorg. Chem.*, **33** (12), 2548-2554 (1994)

362 'Fundamentals of Energy Dispersive X-Ray Analysis', J.C.Russ, Butterworths & Co., London (1984)

363 'Quantitative Electron-Probe Microanalysis' 2nd Edition, V.D. Scott, G. Love, S.J.B. Reed, Ellis Horwood, New York (1995)

364 G.M. Sheldrick, SHELX 86, a computer program for crystal structure determination, University of Gottingen, 1986

365 G.M. Sheldrick, SHELX 76, a computer program for crystal structure determination, University of Cambridge, 1976

366 G.M. Sheldrick, *Acta Cryst.*, **A46**, 467-473 (1990)

367 G.M. Sheldrick, *J. Appl. Cryst.*, 1995 (in preparation)

368 P. McArdle, *J. Appl. Cryst.*, **27**, 438 (1994)